



Kent Academic Repository

Lilley, Rebecca (2020) *An Investigation into the Multifunctional Nature of Renal Pericytes*. Doctor of Philosophy (PhD) thesis, University of Kent,.

Downloaded from

<https://kar.kent.ac.uk/84487/> The University of Kent's Academic Repository KAR

The version of record is available from

This document version

UNSPECIFIED

DOI for this version

Licence for this version

CC BY-NC (Attribution-NonCommercial)

Additional information

Versions of research works

Versions of Record

If this version is the version of record, it is the same as the published version available on the publisher's web site. Cite as the published version.

Author Accepted Manuscripts

If this document is identified as the Author Accepted Manuscript it is the version after peer review but before type setting, copy editing or publisher branding. Cite as Surname, Initial. (Year) 'Title of article'. To be published in *Title of Journal*, Volume and issue numbers [peer-reviewed accepted version]. Available at: DOI or URL (Accessed: date).

Enquiries

If you have questions about this document contact ResearchSupport@kent.ac.uk. Please include the URL of the record in KAR. If you believe that your, or a third party's rights have been compromised through this document please see our [Take Down policy](https://www.kent.ac.uk/guides/kar-the-kent-academic-repository#policies) (available from <https://www.kent.ac.uk/guides/kar-the-kent-academic-repository#policies>).

An Investigation into the Multifunctional Nature of Renal Pericytes

Rebecca Lilley

A thesis submitted in partial fulfilment of the
requirements of the University of Kent and
the University of Greenwich for the degree
of Doctor of Philosophy

Abstract

Emerging evidence shows vascular resident pericytes are multifunctional, with involvement in inflammation and immune cell infiltration in addition to their well characterised functions in angiogenesis and the regulation of vascular stability and perfusion. Similar to pericytes from animal models, cultured human pericytes are able to produce inflammatory mediators, and renal pericytes show active involvement in the recruitment and direction of immune cells. This has big implications for the treatment of renal disease, where loss of pericytes and marked inflammation are associated with poor patient outcomes. However, the nature of this pericyte-mediated inflammation varies between animals and humans, and tissue culture does not always accurately reflect *in vivo* behaviour. Further still, the means by which inflammatory involvement of pericytes is identified may be misattributed; with a known overlap in cell-surface molecule expression between pericytes and macrophage (MΦ). Proper identification of pericytes and thus their multifunctionality is imperative.

The hypothesis behind this investigation is that renal pericytes in *in situ* kidney slices reflect *in vivo* physiology and are multifunctional, distinguishable from MΦ, and involved in renal inflammation. The utilisation of both rodent and murine *in situ* “live” kidney slices will enable investigations into this phenomenon by enabling use of co-labelling with overlapping pericyte (NG2 and PDGFR-β) and MΦ (CD163 and F4/80) markers, maintaining *in vivo* cellular communications, and visualisation of notable cell morphology. Overall, this thesis presents data to support kidney slices accurately modelling *in vivo* vascular physiology and thus other pericyte-mediated functions. Furthermore, this data supports renal pericytes exhibiting multifunctionality, notably in a cell-surface molecule-specific manner that is conserved across species. While not investigated in this thesis it is hoped these findings may translate to human physiology providing novel therapeutic targets against the progression of renal disease.

Declaration

I certify that this work has not been accepted in substance for any degree and is not concurrently being submitted for any degree other than that of Doctor of Philosophy being studied at Universities of Greenwich and Kent. I also declare that this work is the result of my own investigations except where otherwise identified by references and that I have not plagiarised the work of others.

Signed:

Rebecca Lilley

July 2020

Word Count: 64 568

Acknowledgements

Thanks pals, we crushed it.

1.3.2.1	A subset of NG2 ⁺ pericytes are derived from macrophages	40
1.3.3	Pericytes as non-professional immune cells.	40
1.3.3.1	Are these pericytes acting as immune cells or perivascular macrophages?.....	41
1.4	Pericytes and macrophage converge on the renal medulla.	42
1.4.1	Renal Pericytes co-ordinate inflammation in the kidney.....	43
1.4.1.1	NG2 and PDGFR- β , though not other pericyte markers are reportedly expressed by immune cells.....	47
1.5	Species specific differences in behaviour can influence translatability. ..	47
1.5.1	Cross-species and Cross-organ pericyte immune functionality is conserved, in a species dependent manner.....	49
1.6	Summary and aims.	49
2	General Methodology.	51
2.1	Tissue preparation and slicing.....	51
2.2	Viability of C57BL/6J live kidney slices.....	51
2.3	C57BL/6J pericyte characteristics.	52
2.4	Functional experiments and video analysis.	54
2.5	Immunohistochemical staining of Sprague-Dawley and C57BL/6J kidney slices with pericyte and macrophage markers.	56
2.6	Statistics	61
3	A rodent live kidney slice model to investigate the multifunctional nature of renal pericytes.....	62
3.1	Introduction	62
3.2	Methods:.....	64
3.2.1	Immunohistochemical staining of Sprague-Dawley kidney slices.....	64
3.2.2	Statistics.	65
3.3	Results:.....	65
3.3.1	Vasa recta pericytes are identifiable via immunohistochemical staining with PDGFR- β	65
3.3.2	CD68 and CD163 expression is regionally specific in rodent kidney slices. 66	
3.3.3	PDGFR- β ⁺ pericytes are larger and more abundant than NG2 ⁺ pericytes.....	70
3.3.4	In control tissue, few CD163 ⁺ macrophages are present spatially close to vasa recta NG2 ⁺ and PDGFR- β ⁺ pericytes.....	72
3.3.5	Pericytes in contact with CD163 ⁺ macrophages are constricted in healthy tissue.	75

3.3.6	Exposure of live tissue to cytokines, and duration of incubation in control tissue sections, influences CD163 ⁺ macrophage presence in the renal medulla.	76
3.3.6.1	Cytokine stimulation did not influence contact between CD163 ⁺ macrophage and NG2 ⁺ pericytes.	78
3.3.7	Cytokine stimulation differentially altered PDGFR- β ⁺ and NG2 ⁻ -labelled pericyte densities.	80
3.3.8	Cytokine stimulation differentially altered PDGFR- β ⁺ -labelled and NG2 ⁺ -labelled pericyte covered vasa recta diameters.	82
3.3.9	Cytokine stimulation, but not CD163 ⁺ macrophage cellular contact, influenced NG2 ⁺ pericyte soma size.	85
3.3.10	Stimulation of kidney slices with pro-inflammatory cytokines TNF- α and IL-1 β does not induce CD163 expression in NG2 ⁺ pericytes but does in few PDGFR- β ⁺ pericytes.	86
3.4	Discussion:	89
3.4.1	PDGFR- β ⁺ pericyte covered vasa recta have larger diameters and are more numerous than those covered by NG2 ⁺ pericytes.	90
3.4.1.1	Vasa recta PDGFR- β ⁺ pericytes bear morphological differences to NG2 ⁺ pericytes.	92
3.4.2	In control kidney tissue there are few CD163 ⁺ macrophages, which primarily reside in the medulla.	93
3.4.3	CD163 ⁺ macrophage and pericytes may actively communicate to regulate vasa recta diameter.	94
3.4.4	Stimulation of tissue with TNF- α and IL-1 β increase the number of CD163 ⁺ macrophages in the medulla.	95
3.4.5	TNF- α and IL-1 β stimulation significantly reduce NG2 ⁺ pericyte density in both medullary regions.	96
3.4.6	TNF- α and IL-1 β differentially affect PDGFR- β ⁺ and NG2 ⁺ pericyte contractility and morphology.	97
3.4.7	A small number of PDGFR- β ⁺ pericytes were co-labelled with anti-CD163.	98
4	Establishment of a murine live kidney slice model.	100
4.1	Introduction.	100
4.2	Methods.	101
4.2.1	C57BL/6J tissue slicing.	101
4.2.2	Viability of C57BL/6J live kidney slices.	102
4.2.3	Determination of C57BL/6J NG2 ⁺ pericyte density and pericyte characteristics.	102

4.2.4	Functional experiments and video analysis	103
4.2.5	Statistics	103
4.3	Results.....	104
4.3.1	C57BL/6J kidney slices are viable, with pericytes clearly identifiable. 104	
4.3.2	NG2 ⁺ pericytes are clearly labelled in C57BL/6J kidney slices.....	105
4.3.3	C57BL/6J renal pericytes are functionally responsive, and vasoactive agents affect vasa recta diameter <i>in situ</i>	107
4.3.3.1	Responsiveness of murine pericytes <i>in situ</i> to endogenous vasoactive compounds varies from those in the rat.	109
4.3.3.1.1	Angiotensin-II	109
4.3.3.1.2	Adenosine-5'-triphosphate and noradrenaline.....	111
4.3.3.1.3	Endothelin-1	113
4.3.3.1.4	Prostaglandin E ₂ and bradykinin	114
4.3.3.2	Superfusion of C57BL/6J slices with exogenous compounds demonstrates pericyte-mediated vasoactivity.	115
4.4	Discussion.	118
4.4.1	C57BL/6J kidney slices are viable.	118
4.4.2	C57BL/6J NG2 ⁺ pericyte morphology is comparable to the rat whilst vasa recta capillaries are smaller.....	119
4.4.3	C57BL/6J renal pericyte-mediated responsiveness is less frequent than the SD model.	120
4.4.4	C57BL/6J renal pericytes are vasoactive, and contractility reflects known species differences in vascular reactivity	121
4.4.4.1	Angiotensin II-mediated constriction of DVR-pericytes is conserved across species.	122
4.4.4.2	Bradykinin is contractile at high concentrations at C57 DVR pericytes.....	123
4.4.4.3	Adenosine-5'-triphosphate and BzATP suggest DVR pericytes- contractility is mediated at least in part by P2X ₇	124
4.4.4.4	The activity of noradrenaline (NA) and tyramine in the mouse further suggest species-related differences to both NA and ATP	125
4.4.4.5	In the mouse, the DVR pericyte responsiveness to endothelin-1 differs from that described in the literature.....	127
4.4.4.6	Prostaglandin E ₂ , and associated exogenous drugs, have comparable pericyte-mediated activity in both species.	128
4.4.5	There is benefit to developing and characterising a cross-species model. 130	

5	The use of a murine live slice model to investigate the multifunctional nature of renal pericytes.....	132
5.1	Introduction.....	132
5.2	5.2 Methods:.....	134
5.2.1	5.2.1 DIC video analysis.....	134
5.2.2	5.2.2 Immunohistochemical experiments.....	134
5.2.3	Statistics.....	135
5.3	Results:.....	136
5.3.1	TNF- α , but not IL-1 β induces a significant pericyte-mediated vasoconstriction of vasa recta.....	136
5.3.2	PDGFR- β and CD68 expression in the C57BL/6J mouse kidney is similar to that observed in the Sprague-Dawley rat model.....	136
5.3.3	Vasa recta capillaries where pericytes are in contact with F4/80 ⁺ macrophages are constricted.....	139
5.3.4	NG2 ⁺ -labelled pericytes and F4/80 ⁺ -labelled macrophages have a close spatial relationship in the OM.	143
5.3.5	A small population of cells were positive for both F4/80 and either PDGFR- β or NG2.	146
5.3.6	Incubations with cytokines increased the outer medullary (OM) F4/80 ⁺ macrophages presence and reduced both PDGFR- β ⁺ and NG2 ⁺ pericyte density.	147
5.3.7	IL-1 β , not TNF- α , retained F4/80 ⁺ macrophages near NG2 ⁺ pericytes in both the OM and IM.	152
5.3.8	154
5.3.9	TNF- α - and IL-1 β -induced, pericyte-mediated vasoconstriction, is potentiated by macrophage contact in NG2 ⁺ , but not PDGFR- β ⁺ pericytes... ..	154
5.3.10	Presence of F4/80 ⁺ macrophages, not cytokine stimulation has potential to influence PDGFR- β ⁺ pericyte morphology	157
5.3.11	Pro-inflammatory cytokine stimulation does not appear to encourage cellular co-expression of F4/80 and NG2 ⁺ , but does for F4/80 and PDGFR- β	159
5.4	Discussion	163
5.4.1	5.4.1 Murine PDGFR- β ⁺ pericyte covered vasa recta have larger diameters and are more numerous than those covered by NG2 ⁺ pericytes.. ..	163
5.4.2	5.4.2 F4/80 ⁺ macrophages and pericytes may actively communicate to regulate vasa recta diameter.....	164
5.4.3	The differential acute activity of TNF- α and IL-1 β appears to be conserved between mice and rats, whilst reflecting species differences.	165

5.4.3.1	In the mouse, TNF- α and IL-1 β differentially affect PDGFR- β^+ and NG2 $^+$ pericyte contractility, whilst not affecting the morphology of either. .	165
5.4.4	Dormant monocytes when activated migrate towards NG2 $^+$ pericytes in the outer medulla.	166
5.4.5	IL-1 β , but not TNF- α , significantly influences distances between NG2 $^+$ pericytes and F4/80 $^+$ macrophages.....	168
5.4.6	The pericyte-mediated constriction of vasa recta capillaries induced by macrophages may be orchestrated by NG2 $^+$ not NG2 $^-$ pericytes.	168
5.4.7	A small population of cells co-label with anti-PDGFR- β and anti-F4/80, with both pericyte and macrophage morphology	170
	Interestingly in the kidney it has	170
6	General Discussion	172
6.1	Pericytes as a multifunctional class of cell?	172
6.2	Renal pericytes are contractile in a species-specific manner.....	173
6.3	The kidney slice models can be used to further investigate the multifunctionality of renal pericytes.	174
6.4	PDGFR- β^+ and NG2 $^+$ pericytes represent different renal populations of pericytes, likely correlating to AVR and DVR coverage.	175
6.5	Renal pericytes and macrophages seemingly communicate.....	176
6.6	Macrophages and NG2 $^+$ pericytes may communicate via RhoA/ROCK signalling.....	177
6.7	PDGFR- β co-labels with CD163 and F4/80.	178
6.8	Expression of NG2 by macrophage-derived pericytes may occur at a later stage of investment into the endothelial wall.	179
6.9	Future work.....	180
	References	185
	Appendix 1:	217

List of Figures

Figure 1.1 Schematic showing the gross architecture of the mammalian kidney.	16
Figure 1.2 Anatomy of the renal vasculature.	18
Figure 1.3 A schematic illustrating counter-current multiplication and counter-current exchange.	20
Figure 1.4 A schematic showing the effect Tubulo-vascular crosstalk and medullary blood flow on solute excretion and local oxygenation.	22
Figure 1.5 Known markers for renal pericyte identification.	26
Figure 1.6 Schematic showing the diversity of pericytes around the microvasculature network of the renal medulla.	28
Figure 1.7 A schematic illustrating cell type pericytes reportedly differentiate into...	33
Figure 1.8 Renal NG2+/PDGFR-β+ pericyte distribution in the cortex and outer medulla of healthy young adult mice.	35
Figure 1.9 NG2-dependent extravasation of polymorphonuclear leukocytes (PMN).	38
Figure 1.10 . In healthy mammalian kidneys immune cells have preponderance in the medulla.	44
Figure 1.11 Proposed co-ordination of the immune response at the vasa recta capillaries by pericytes.	46
Figure 2.1 Distribution of NG2 ⁺ pericytes in a region of interest (ROI) from mouse tissue.	59
Figure 3.1 Platelet derived growth factor receptor-β (PDGFR-β) ⁺ , CD68 ⁺ , and CD163 ⁺ positive staining in the Sprague-Dawley rat.	67
Figure 3.2 Morphologies of CD163 ⁺ macrophage (MΦ).	69
Figure 3.3 Features of neural-glial-2 (NG2) ⁺ pericyte and CD163 ⁺ macrophage (MΦ) distribution.	70
Figure 3.4 Both platelet derived growth factor receptor-β (PDGFR-β) ⁺ vessel diameter, and fluorescent staining is significantly greater than neural-glial-2 (NG2) ⁺ staining in the outer and inner medulla.	73
Figure 3.5 The effect of pro-inflammatory cytokines TNF-α and IL-1β on the spatial arrangement of neural-glial-2 (NG2) ⁺ pericytes and CD163 ⁺ macrophages (MΦ). ...	78
Figure 3.6 Effects of pro-inflammatory cytokine stimulation on CD163 ⁺ macrophage (MΦ) and neural-glial-2 (NG2) ⁺ pericyte density in the outer (OM) and inner (IM) medulla.	81
Figure 3.7 Effects of pro-inflammatory cytokine stimulation on CD163 ⁺ macrophage (MΦ) and platelet derived growth factor receptor-β (PDGFR-β) ⁺ pericyte density in the outer (OM) and inner (IM) medulla.	82

Figure 3.8 The effect of pro-inflammatory cytokines TNF- α and IL-1 β and CD163 ⁺ macrophage (M Φ) presence on neural-glia-2 (NG2) ⁺ or platelet derived growth factor receptor- β (PDGFR- β) ⁺ pericyte-regulated vasa recta diameter.	84
Figure 3.9 Co-expression of platelet derived growth factor receptor- β (PDGFR- β) ⁺ with CD163 ⁺ on vascular resident cells in the renal medulla bearing morphological similarities to PDGFR- β ⁺ pericytes.	88
Figure 4.1 Viability of kidney slices from C57BL/6J mice.....	104
Figure 4.2 Identification of NG2 ⁺ pericytes in the C57BL/6J renal medulla.	105
Figure 4.3 Pericytes in the C57BL/6J preparation only constrict in the presence of an agonist.....	108
Figure 4.4 Angiotensin-II (Ang-II) evoked constriction of <i>in situ</i> vasa recta is of a lower magnitude than in the Sprague-Dawley (SD) model.....	110
Figure 4.5 Adenosine-5'-triphosphate (ATP) and noradrenaline (NA) needed marked increase in concentration to stimulate vasoactivity of C57BL/6J <i>in situ</i> vasa recta capillaries.	112
Figure 4.6 Endothelin-1 (ET-1) evoked a significantly greater, pericyte-mediate, constriction in the C57BL/6J mouse.....	113
Figure 4.7 Prostaglandin E ₂ (PGE ₂) and Bradykinin (BK) needed marked increase in concentration to stimulate vasoactivity of C57BL/6J <i>in situ</i> vasa recta capillaries. .	115
Figure 4.8 Stimulating or attenuating the release of endogenous compounds in C57BL/6J kidney slices.....	117
Figure 4.9 Interspecies differences between SD (a) and C57 (b) pericyte density..	120
Figure 5.1 Superfusion of C57BL/6J murine kidney slices with TNF- α , but not IL-1 β , caused a pericyte-mediated constriction of vasa recta capillaries.	137
Figure 5.2 Platelet derived growth factor receptor- β (PDGFR- β) ⁺ and CD68 ⁺ positive staining in the C57BL/6J mouse.....	138
Figure 5.3 The regional densities of pericytes and macrophage (M Φ) in the outer (OM) and inner medulla (IM).	140
Figure 5.4 The effect of F4/80 ⁺ M Φ on vasa recta diameter and their spatial relationship with neural-glia-2 (NG2) ⁺ pericytes.....	142
Figure 5.5 Features of neural-glia 2 (NG2) ⁺ pericyte and F4/80 ⁺ macrophage (M Φ) morphology	144
Figure 5.6 Features of platelet derived growth factor receptor- β (PDGFR- β) ⁺ pericyte and F4/80 ⁺ macrophage (M Φ) morphology.	145
Figure 5.7 Co-expression of neural-glia-2 (NG2) and F4/80 on perivascular cells.	147
Figure 5.8 Co-expression of platelet derived growth factor receptor- β (PDGFR- β) and F4/80 on perivascular cells.	148

Figure 5.9 Effects of pro-inflammatory cytokine stimulation on F4/80 ⁺ macrophage (MΦ) and neural-glial 2 (NG2) ⁺ -labelled pericyte density in the outer (OM) and inner (IM) medulla.....	150
Figure 5.10 Effects of pro-inflammatory cytokine stimulation on F4/80 ⁺ macrophage (MΦ) and platelet derived growth factor receptor-β (PDGFR-β) ⁺ -labelled pericyte density in the outer (OM) and inner (IM) medulla.	151
Figure 5.11 The effect of pro-inflammatory cytokines TNF-α and IL-1β on the spatial arrangement between neural-glial-2 (NG2) ⁺ pericytes and F4/80 ⁺ macrophage (MΦ).	153
Figure 5.12 The effect of pro-inflammatory cytokines TNF-α and IL-1β and MΦ presence on vasa recta diameter.	156
Figure 5.13 Differential effect of F4/80 ⁺ macrophage (MΦ) presence on neural-glial-2 (NG2) ⁺ or platelet derived growth factor receptor-β (PDGFR-β) ⁺ pericytes in the outer medulla (OM).	158
Figure 5.14 Morphology of perivascular neural-glial-2 (NG2) ⁻ , F4/80 ⁺ cells is comparable to NG2 ⁺ pericytes, irrespective of cytokine treatment in the renal medulla.	160
Figure 5.15 Co-expression of platelet derived growth factor receptor-β (PDGFR-β) and F4/80 on non-vascular resident cells in the renal medulla.	161
Figure 5.16 Co-expression of platelet derived growth factor receptor-β (PDGFR-β) ⁺ with F4/80 ⁺ on vascular resident cells in the renal medulla bearing morphological similarities to PDGFR-β ⁺ pericytes.	162
Figure 6.1 Proposed co-ordination of the immune response at the vasa recta capillaries by NG2 ⁺ and NG2 ⁻ pericytes.....	181

List of Tables

Table 1.1 Vasoactive agonists that evoke a pericyte-mediated change in DVR diameter.....	25
Table 2.1 Concentration of agonists used for functional experiments.....	53
Table 2.2 Antibody dilutions table.	57
Table 3.1 Characteristics of platelet derived growth factor receptor- β (PDGFR- β) ⁺ and neural-glia 2 (NG2) ⁺ pericytes in the renal medulla.....	71
Table 3.2 Characteristics of renal platelet derived growth factor receptor- β (PDGFR- β) ⁺ and neural-glia 2 (NG2) ⁺ pericytes in contact with CD163 ⁺ macrophages (M Φ). 74	
Table 3.3 CD163 ⁺ Macrophage (M Φ), platelet derived growth factor receptor- β (PDGFR- β) ⁺ , and neural-glia-2 (NG2) ⁺ pericyte quantification after TNF- α and IL-1 β stimulation.	77
Table 3.4 Effect of TNF- α and IL-1 β stimulation, and CD163 ⁺ macrophage (M Φ) presence on vasa recta diameter encircled by neural-glia-2 (NG2) ⁺ or platelet derived growth factor receptor- β (PDGFR- β) ⁺ pericytes.....	83
Table 3.5 Effect of TNF- α and IL-1 β stimulation, and CD163 ⁺ macrophage (M Φ) presence neural-glia-2 (NG2) ⁺ or platelet derived growth factor receptor- β (PDGFR- β) ⁺ pericyte soma size.....	85
Table 4.1 Summary of C57BL/6J NG2 ⁺ pericyte characteristics.	106
Table 5.1 Characteristics of platelet derived growth factor receptor- β (PDGFR- β) ⁺ and neural-glia 2 (NG2) ⁺ pericytes in the renal medulla.	139
Table 5.2 Characteristics of renal platelet derived growth factor receptor- β (PDGFR- β) ⁺ and neural-glia 2 (NG2) ⁺ pericytes in contact with F4/80 ⁺ macrophages (M Φ). 141	
Table 5.3 F4/80 ⁺ Macrophage (M Φ), platelet derived growth factor receptor- β (PDGFR- β) ⁺ , and neural-glia-2 (NG2) ⁺ pericyte quantification after TNF- α and IL-1 β stimulation	149
Table 5.4 The spatial relationship between F4/80 ⁺ Macrophage (M Φ) and neural-glia-2 (NG2) ⁺ pericytes after TNF- α and IL-1 β stimulation.....	152
Table 5.5 Effect of TNF- α and IL-1 β stimulation, and F4/80 ⁺ macrophage (M Φ) presence on vasa recta diameter encircled by neural-glia-2 (NG2) ⁺ or platelet derived growth factor receptor- β (PDGFR- β) ⁺ pericytes.....	155
Table 5.6 Effect of TNF- α and IL-1 β stimulation, and F4/80 ⁺ macrophage (M Φ) presence on neural-glia-2 (NG2) ⁺ or platelet derived growth factor receptor- β (PDGFR- β) ⁺ pericyte soma size.	157

1 GENERAL INTRODUCTION.

1.1 The kidney.

The kidneys are highly-specialised organs located outside the peritoneal cavity, responsible for a multitude of homeostatic processes in the body including: regulation of body fluid, glucose, pH, and electrolytes; the regulation of local and systemic blood pressure (BP) via the production of an array of vasoactive agents; the filtration and purification of blood; the activation of vitamin D; and the removal of waste products via the production of urine (Martini et al., 2012). In humans to efficiently perform these duties kidneys receive approximately 20% of the cardiac output and handling approximately 170 L of blood per day (Epstein, 1997). Consequently, kidneys are highly vascularised, with a diverse regional vascular structure to perform its many tasks.

Mammalian kidneys consist of 2 major regions; the cortex and the medulla. The medulla is further subdivided into: the outer medulla (OM), having both outer (OSOM) and inner stripes (ISOM); and the inner medulla (IM) (Shaw et al., 2018) (**Figure 1.1**). Filtration begins in the cortex via the passage of blood into the nephrons. Each nephron is comprised of a renal corpuscle (a Bowman's Capsule and a glomerulus) with an associated tubule. Adult human kidneys have approximately 800,000-1 million nephrons each, which constitute the tubular compartment of the kidney. These nephrons are either cortical, who's Loop of Henle (LoH) is confined to the OM, or juxtamedullary, who's LoH extend deep into the medulla. Juxtamedullary nephrons are the predominant type and all nephrons are perfused by an extensive vascular network to meet their metabolic requirements (Am et al., 2013; Kriz, and Kaissling, 2013), described in more detail below in **section 1.1.2**.

The glomerulus is where the filtration process is initiated in the nephron, before entry of filtrate into the Bowman's space. Glomeruli are small looping bundles of capillaries or "capillary tufts", that are surrounded by podocytes, supported by contractile mesangial cells, and work together with endothelial cells to form a functional unit (Schlondorff, and Banas, 2009). These tufts are permeable to water and small or uncharged molecules, such as glucose, NaCl and urea, with both the hydrostatic and osmotic pressure differential providing the force behind the ultrafiltration of blood. The rate at which this filtration occurs is known as the glomerular filtration rate (GFR) and is highly dependent upon upstream blood flow (BF) through the afferent arteriole (AA); described in more detail in **section 1.1.2**).

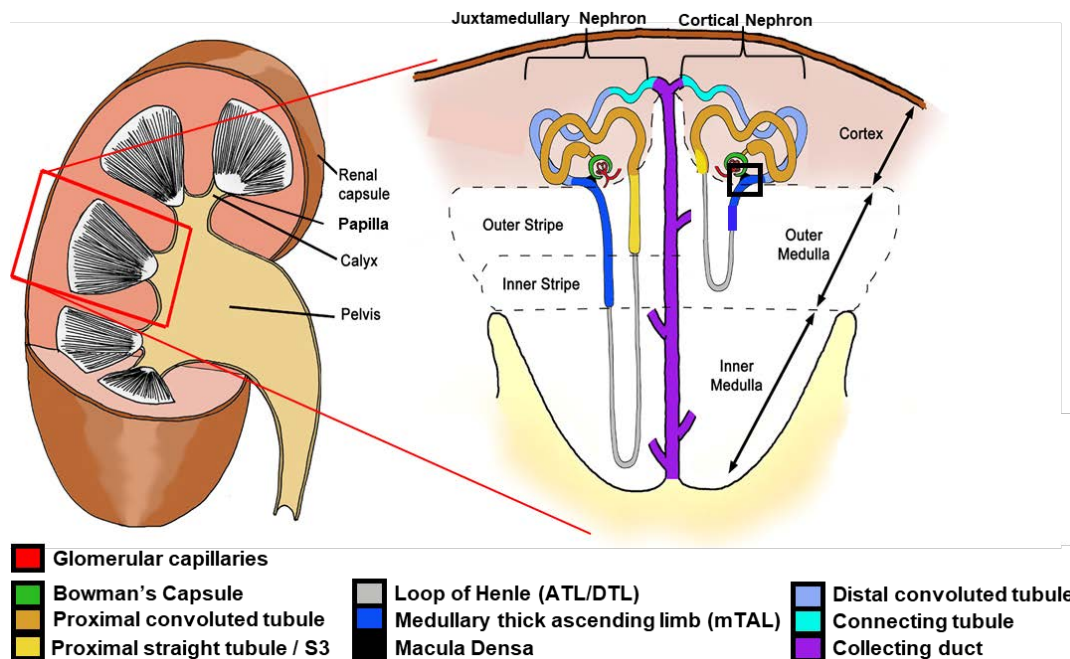


Figure 1.1 Schematic showing the gross architecture of the mammalian kidney.

Kidneys are comprised of the outer fibrous capsule layer externally. Internally, there is a peripheral region called the cortex and internal pyramidal regions called the medulla (red box). The medulla can be further divided into the outer stripe of the outer medulla, the inner stripe of the outer medulla, and the inner medulla. Nephrons, and their various segments, are found within the cortex and medulla, and are comprised of a glomerulus and associated tubule. Blood flows through the glomerular capillaries, with the filtrate collecting in the Bowman's capsule and subsequently passing through all tubule segments, being modified as it passes. Urine drains from the collecting duct at the papillary tip of the medulla into the calices and subsequently flows through the renal pelvis, transmitting urine to the bladder via the ureter. Nephrons can be classified as either: juxtamedullary, descending deep into the medulla; or cortical, with only the descending thin limb of Henle (DTL), ascending thin limb of Henle (ATL), and mTAL present in the medulla. The tubule is subdivided into proximal segments, the Loop of Henle, and distal segments (see colour key). The black box highlights the juxtaglomerular apparatus which is involved in tubuloglomerular feedback (Davidson, 2009).

1.1.1 The tubular compartment

Once in the Bowman's Space, the glomerular filtrate begins its passage along the tubule. The tubular segments consist of; the proximal tubule (convoluted; PCT, and straight; PST/ S3) immediately post Bowman's Capsule, the Loop of Henle, the distal tubule (convoluted; DCT, and straight; DST or medullary thick ascending limb (mTAL)), and finally a connecting tubule (CT) passing filtrate into the collecting duct (CD; **Figure 1.1**). As filtrate passes along the nephron it is continuously being altered. Overall the solute secretion remains fairly constant (Hall, 2010), it is the reabsorption of water that influences urine concentration. The DCT and the CD are impermeable to water except in the presence of anti-diuretic hormone (ADH), which stimulates the translocation of aquaporin-2 (AQP-2) to the cell membrane and subsequent movement of tubular fluid into the hyperosmotic medullary interstitium to be collected taken up by the ascending vasa recta (AVR) and producing a concentrated urine output (Sands, and Layton,

2014). Each section of the nephron, and the subsequent cell types present, are adapted for the filtration, reabsorption and secretion of solutes or waste products to produce a concentrated urine (Martini et al., 2012).

Perfusion of the glomerulus is autoregulated by the juxtaglomerular apparatus (JGA). The JGA consists of the juxtaglomerular cells, the mesangium, and the macula densa, residing between the terminal pole of the AA and the mTAL and form a feedback unit (Peti-Peterdi, and Harris, 2010). The mTAL segment of the nephron communicates to the AA via purinergic signalling through the JGA in response to fluctuations in tubular NaCl concentration. This autoregulatory mechanism, known as tubuloglomerular feedback (TGF), modulates AA perfusion and the GFR (Peti-Peterdi, and Harris, 2010; Marsh et al., 2019). TGF exists to regulate glomerular perfusion (Palmer et al., 2013), to both protect the glomerular capillaries from excessive pressure, and preserve flow rate through the nephron and regulate solute excretion. These are autoregulatory processes confined to the microvasculature, with possibilities for further cortical nephron-to-vascular crosstalk to occur (Pallone, and Cao, 2013). This highlights the importance of communication between the tubular and vascular network for renal function.

1.1.2 The vascular compartment

In order to efficiently filter the blood, as well meeting the metabolic needs of the tubules, the structure of the vascular compartment is highly complex and varied. Blood enters the kidney through the renal artery, which undergoes several structural divisions before blood passes through the glomerular tuft. It is at the corticomedullary border where the vascular network begins to then change quite drastically comparative to other tissues. The divisions of the renal artery that arise at this border are known as arcuate arteries. These give rise to the interlobular arteries, which ascend radially within the cortex, and diverge into numerous afferent arterioles (AA; **Figure 1.2(a)**). Individual AA split into the glomerular tuft inside the Bowman's capsule. These glomerular capillaries subsequently coalesce into the efferent arteriole (EA), as opposed to a venule, leaving the Bowman's Space (Pallone et al., 2003b). Cortical EA become the cortical capillary plexus and perfuse the tubular segments in this region before ultimately re-joining with the arcuate vein, juxtamedullary EA descend into the renal medulla. It is important to note tubules are not perfused by capillaries that arise from the EA of their parent glomerulus (Chou et al., 1990).

Comparative to the cortex that is rich in arteries, the medulla is perfused solely by the microvasculature arising from juxtamedullary EA. These EA split into descending vasa

recta (DVR) capillaries in the OSOM. DVR coalesce to form cone-shaped vascular bundles in the ISOM. In these bundles, few central DVR descend into the IM (Pallone et al., 1990), whilst peripheral DVR branch off and give rise to the interbundle capillary plexus which perfuse the highly metabolically active tubular segments in the OM (Pallone et al., 2003b). Most DVR join the capillary plexus within the ISOM and as such perfusion of the IM by DVR is very limited (**Figure 1.2(a)**). In the IM DVR become dispersed with nephron segments, with few reaching the papillary tip. All DVR ultimately join a capillary plexus, but that of the IM is less dense than that in the ISOM, converging to become AVR, which run in parallel and counterflow to the DVR (**Figure 1.2(b)**).

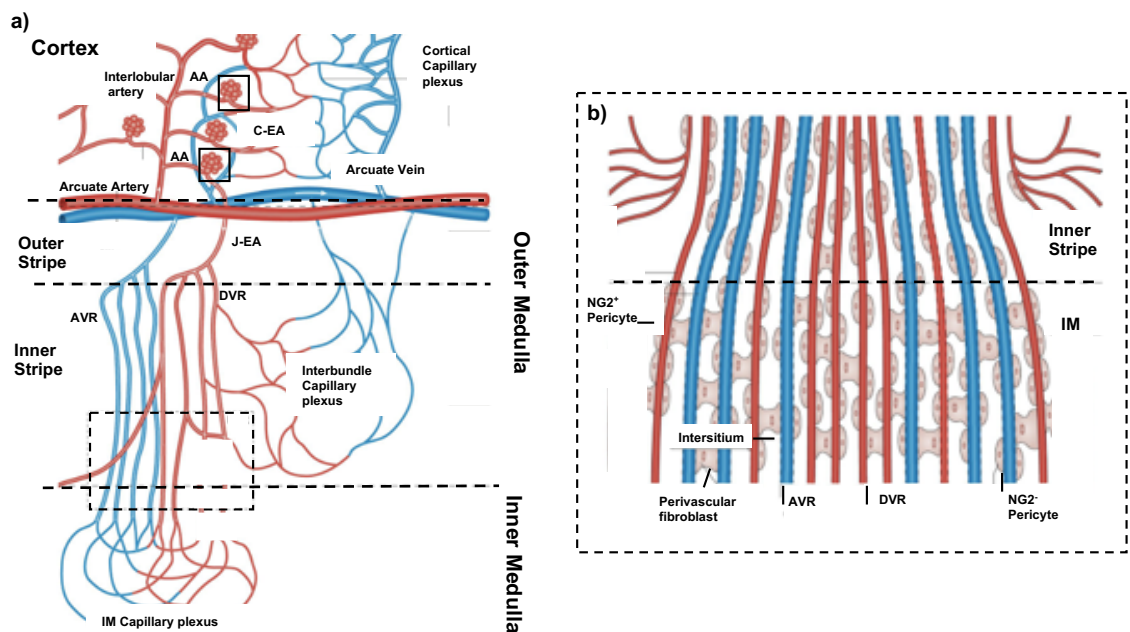


Figure 1.2 Anatomy of the renal vasculature.

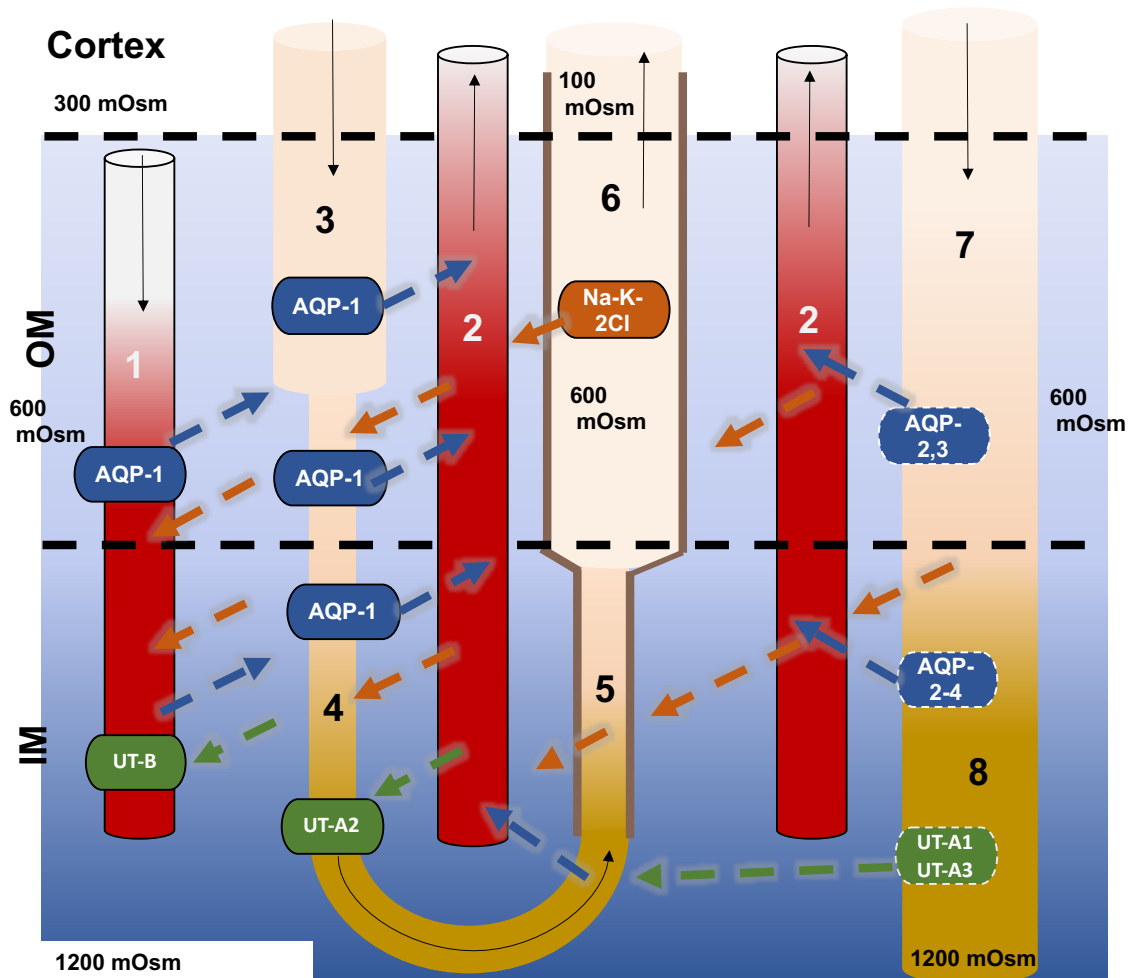
(a) The renal artery divides into the arcuate arteries along the corticomedullary border; the border of the cortex and the outer stripe of the outer medulla (OSOM). These give rise to interlobular arteries that feed the glomeruli and subsequently branch into the peritubular capillary network. Individual afferent arterioles (AA) split into the glomerular tuft (black box), which then coalesce into the efferent arterioles (EA). Cortical EA (C-EA) become the cortical capillary plexus before ultimately re-joining with the arcuate vein. Juxtamedullary EA (J-EA) provide the medullary blood flow, branching into the descending vasa recta (DVR) in the OSOM, forming cone-shaped bundles in the inner stripe of the outer medulla (ISOM). DVR on the periphery of the vascular bundles branch off in the ISOM to form the interbundle capillary plexus which perfuse the metabolically active tubular segments in this region. Most DVR leave the vascular bundles in the ISOM, the remaining DVR in the centre of the bundle descend into the inner medulla (IM) with few reaching the papillary tip (Figure 1). These IM-DVR form a sparser IM-capillary plexus, which converge to become the ascending vasa recta (AVR). AVR drain the medulla and ascend to ultimately re-join the arcuate vein and ultimately the remaining renal venous architecture. The dashed box highlights a vascular bundle (b) demonstrating a longitudinal view. DVR (red, solid border) have a continuous endothelium and are covered with NG2⁺ pericytes. AVR (blue, dashed border) are fenestrated, slightly larger and more abundant, and covered with NG2⁻ pericytes. The interstitium contains perivascular fibroblasts. [Shaw et al, 2018].

AVR are the draining vessels of the medulla, reabsorbing water, whilst also being a primary source of oxygenated blood to the tubules due to O₂ shunting (Pallone et al., 2003b). AVR are fenestrated, larger in diameter, and covered in neural-gial 2 (NG2)-pericytes, whereas the DVR have a narrower continuous endothelium, and encircled by NG2+ pericytes (**Figure 1.2(b)**). Once the AVR breach the IM, some join the centre of the vascular bundles whilst the remaining AVR do not and ascend straight to the OSOM. At the corticomedullary border, AVR empty deoxygenated blood into the arcuate veins and the remaining venous architecture to leave the kidney. The overall structure and regional variation of the microcirculation arising from the arcuate artery can be seen in **Figure 1.2(a)**. Helping maintain renal homeostasis and effective urine concentration is highly dependent on the microvascular architecture and subsequent regional regulation of BF.

1.1.3 Regional regulation of renal blood flow is needed to facilitate urine concentration.

Even as total RBF remains constant, within the kidney there is marked regional variation in perfusion. Given the size and function of the cortex, the distribution of blood flow is significantly higher in this region; cortical nephrons comprise ~85% of nephrons (Martini et al., 2012) and thus the majority of the blood that enters the kidney remains within the cortical vasculature. Blood flow in the cortex (CBF), and thus the GFR, is regulated by TGF and the myogenic response (MR) (Just, 2007). The MR is a Ca²⁺-dependent contractile response of smooth muscle to the stretch induced by an increase in perfusion pressure to maintain GFR. TGF occurs due to reasons described above (**section 1.1.1**), with fluctuations in tubular [NaCl] or perfusion activating this mechanism. TGF acts to increase parent glomerular capillary pressure and thus GFR in response to low tubular perfusion and [NaCl] via renin release from juxtaglomerular cells and PGE₂-mediated AA dilation (Peti-Peterdi, and Harris, 2010). TGF acts to decrease GFR in response to increased tubular perfusion and [NaCl] via ATP release from the macula densa eliciting an A₁ receptor dependent vasoconstriction of AA, and a reduction in renin release (Peti-Peterdi, and Harris, 2010). TGF is a slower mechanism than the MR (Mitrou, and Cupples, 2014) but both act to regulate CBF and maintain the GFR.

The medulla receives a small percentage of RBF, equating to less than 10% of the cortical BF (Cowley, 2008). The medullary BF (MBF) has to satisfy the conflicting demands of preserving the microenvironment, whilst maintaining adequate O₂ and nutrient delivery to the metabolically active mTAL (Sands, and Layton, 2009; Mattson, 2003). As filtrate flows through the medullary LoH to the CD, the exchange of NaCl, urea and water with the medullary interstitium and vasa recta generates a corticomedullary NaCl and urea concentration gradient; a progressive



- | | |
|---|---|
| 1 Descending vasa recta (DVR) | 5 Ascending thin limb (ATL) |
| 2 Ascending vasa recta (AVR) | 6 Medullary thick ascending limb (mTAL) |
| 3 Proximal straight tubule (PST) | 7 Outer medullary collecting duct (OMCD) |
| 4 Descending thin limb (DTL) | 8 Inner medullary collecting duct (IMCD) |

Figure 1.3 A schematic illustrating counter-current multiplication and counter-current exchange.

The mTAL actively reabsorbs NaCl (orange) through the apical Na-K-2Cl cotransporter. Flow is constant through the tubule, and the DTL reaches equilibrium with the interstitium via aquaporin (AQP)-1-mediated water (blue) efflux. The OMCD is impermeable to urea (*green*), whilst the IMCD express vasopressin-regulated urea transporter (UT)-A1 (dashed border) and UT-A3, enabling passive movement of urea out of the CD. This increases the IMCD NaCl concentration and thus NaCl passively diffuses from the CD into the interstitium. Water is reabsorbed across the CD by regionally expressed AQP-3-4, and vasopressin regulated-AQP-2. Resultantly, the NaCl concentration of the ATL is higher, and the urea concentration is lower than the interstitium, urea will passively diffuse into the ATL and NaCl will be passively reabsorbed from the ATL. Reabsorbed NaCl keeps adding to new inflow into the DTL thus multiplying the concentration. DVR reach equilibrium with the interstitium via passive and AQP-1-mediated water efflux and NaCl diffusion, with UT-B facilitated urea reabsorption in the IM. The solute concentration of the AVR is higher than the DVR and the interstitium and as such NaCl and urea are passively shunted from the AVR to the DVR or DTL (UT-A2), and water is collected by the AVR, effectively trapping NaCl and urea in the interstitium. Increasing concentration of blood (*red*), tubular (*yellow*), or interstitial fluid (*light-dark blue*) is indicated by the darkening gradient in structures. Segments are numbered according to key. Direction of flow is indicated by black arrows (Dantzler et al., 2011; Sands, and Layton, 2014).

increase in osmolality from the cortex to the innermost IM and papillary tip (Shaw et al., 2018), summarised in **Figure 1.3**.

NaCl exchange of the LoH is facilitated by its hair pin arrangement, and the variable permeability of tubular segments. The mTAL is impermeable to water and actively reabsorbs NaCl via the apical Na-K-2Cl cotransporter. As the DTL is permeable to water, filtrate here quickly reaches osmotic equilibrium, with water drained by the AVR. As flow is continuous through the tubule, hyperosmotic fluid from the DTL flows into the mTAL, where again NaCl is actively reabsorbed, concentrating the medullary interstitium further. NaCl reabsorbed from mTAL is additive to the new inflow of NaCl into the DTL thereby “multiplying” the concentration as this process repeats itself (Hall, 2010).

Unlike NaCl, urea cycles between the IMCD and the IM LoH in the presence of antidiuretic hormone (ADH), with cortical and OM tubular segments always poorly permeable to urea. High concentrations of ADH upregulates expression of aquaporin (AQP)-2 water channels and the rapid reabsorption of water from the cortical connecting tubule, as well as the entirety of the CD, resulting in a concentrated tubular fluid. Urea can only diffuse out of the IMCD with ADH-induced expression of urea transporter (UT)-A1 and UT-A3, passing into the interstitium and cycles back into the IM LoH, which are always permeable to this solute, thus creating a corticomedullary urea concentration gradient.

Together these processes result in a urea concentration in the interstitium that is higher than in the ATL and mTAL, and a NaCl concentration in the ATL and mTAL higher than in the interstitium, with the AVR draining away water. NaCl will then tend to diffuse out whilst urea will tend to diffuse into the corresponding tubular segments. If the permeability of the ATL and mTAL to NaCl is sufficiently high and to urea sufficiently low, the interstitium will be concentrated (Sands, and Layton, 2014), with counter-current exchange between the vasa recta preserving this concentration gradient.

The osmolality of the blood within the DVR equilibrates with that of the medullary interstitium; solutes diffuse passively down their concentration gradient into the blood, with urea transport facilitated by UTB on the IM. Some, but not all, DVR are poorly permeable to NaCl, so equilibrium here is reached via AQP-1-mediated water efflux in these DVR (Pallone et al., 2003a). The AVR, with a greater flow rate and osmolality, collects the water and deposits solutes into the interstitium, maintaining the osmolality of the blood and trapping NaCl and urea in the interstitium (Evans, and Cowley, 2015), whilst preserving perfusion of the IM albeit at the cost of low O₂ tensions (**Figure 1.3**).

1.1.3.1 Generation of the corticomedullary concentration gradient results in a low medullary oxygen tension.

Overall, the hairpin arrangements of the LoH and the vasa recta effectively trap solutes in the interstitium and enable the production of a concentrated urine (**Figure 1.3**) (Pallone et al., 2003a). However, this structural arrangement results in low O_2 availability in the medulla. The partial pressure of O_2 (PO_2) in the medulla is between 10-20 mmHg (Brezis et al., 1991), and whilst not low for capillaries, the OM is a highly metabolically active region and O_2 is not evenly released from the capillaries (Leonhardt, and Landes, 1963). O_2 is shunted from the DVR to the AVR, resultantly delivering O_2 poor blood to the medulla (Leonhardt, and Landes, 1963; Brezis, 2005). This O_2 delivery would be influenced by changes in MBF.

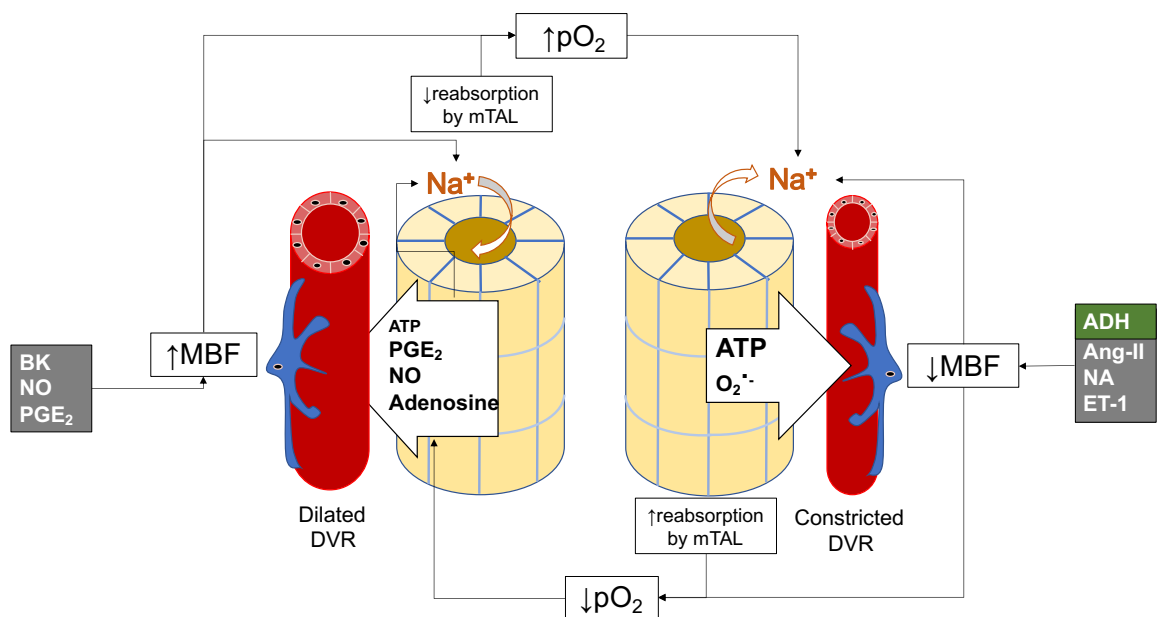


Figure 1.4 A schematic showing the effect Tubulo-vascular crosstalk and medullary blood flow on solute excretion and local oxygenation.

Signalling molecules released from the medullary thick ascending limb (mTAL; yellow tubes) directly (white arrows) or by other renal cells directly (grey boxes) can act at pericytes to either increase (↑) or decrease (↓) medullary blood flow (MBF) in response to (↓) low or high (↑) oxygen tension (pO_2). High concentration adenosine 5'-triphosphate (ATP, bold) or superoxide ($O_2^{\cdot-}$) produced by the mTAL can diffuse across to the pericytes (blue cells) on the descending vasa recta (DVR) to cause a pericyte-mediated constriction and thereby reduce MBF to reabsorb more solute (Na^+). Circulating angiotensin-II (Ang-II), antidiuretic hormone (ADH), noradrenaline (NA), and endothelin-1 (ET-1) from vascular or other renal sources can also constrict pericytes to reduce MBF. The increased metabolic activity of the mTAL and reduced MBF reduces the pO_2 . Hypoxia induced adenosine, or compensatory production of prostaglandin E2 (PGE2), nitric oxide (NO), or low concentration ATP from the mTAL can buffer the vasoconstrictor effects, dilate pericytes and thus increase MBF. This reduces reabsorption of Na^+ , reducing the metabolic demand of the mTAL. Bradykinin (BK), NO, and PGE2 from other renal sources can also increase MBF to the same effect. This in turn increases the pO_2 . This increase in pO_2 can also increase Na^+ reabsorption by enabling mTAL metabolically and thus continued communication between the pericytes on the DVR and mTAL are necessary to maintain pO_2 and Na^+ balance (Cowley, 2008; Kriz, and Kaissling, 2013; Dickhout et al., 2002; Neuhofer, and Beck, 2005).

ADH acts via vasopressin receptor 2 (V2) to regulate the permeability of the tubular segments to NaCl and urea. Interestingly, ADH CAN also influence MBF via V1a activity (Evans, and Cowley, 2015; Davenport, 2008; Nakanishi et al., 1995; Turner, and Pallone, 1997), but with potentially different outcomes. ADH contracting central DVR would reduce IMBF, provide more time for the AVR to reach equilibrium with the interstitium, enhancing counter-current exchange and reabsorption of water, whilst increasing perfusion of peripheral DVR and therefore O₂ supply to the mTAL. Constriction of peripheral DVR would encourage blood flow to the IM via the central DVR, inducing pressure-natriuresis and NaCl excretion (Cowley, 2008). Increasing IMBF comes at the risk of reducing counter-current exchange interstitial solute washout, whereas reducing IMBF enhances counter-current exchange at the risk of reduced nutrient supply and waste clearance from this IM (Sands, and Layton, 2014). Interestingly, a regional difference of ADH activity has been noted; ADH, reduces IMBF to a greater extent than OMBF or CBF (Neuhofer, and Beck, 2005; Nakanishi et al., 1995), suggesting ADH preferentially constricts central DVR to increase the reabsorption of water.

Preservation of the corticomedullary gradient, whilst meeting the metabolic needs of the parenchyma, demonstrates importance of regionally regulated BF in the kidney. As stated in section 1.1.1, nephrons are not perfused by their parent glomerulus-derived capillaries (Chou et al., 1990); thus if regulation of MBF was controlled by the AA, nephrons and the surrounding microenvironment are at risk of a metabolism-perfusion mismatch. Summarily, it is the DVR that provide BF to the medulla (**Figure 1.2**) and therefore within the DVR potential exists to regulate MBF (Evans, and Cowley, 2015), and such control must exist outside of upstream autoregulatory mechanisms. The evidence would suggest that MBF is autoregulated by tubule-vascular feedback between mTAL and pericytes on the DVR (**Figure 1.4**).

1.1.3.2 Autoregulation of MBF.

Mechanisms behind the autoregulation of CBF are well characterised (**Section 1.1.3**), yet autoregulatory mechanisms for MBF remain controversial despite data illustrating this process (Kennedy-Lydon et al., 2013). A recent study, using an *in vivo* Microfil technique to visualise the renal vascular architecture demonstrated angiotensin-II (Ang-II) differentially effects cortical and medullary BF, with preferential reduction of IMBF (Fan et al., 2019). Much like the data for ADH (Evans, and Cowley, 2015), this illustrates autoregulation at the level of the OM DVR. As there are no arteries present

in the medulla, all BF is provided by the extensive capillary network. In place of vascular smooth muscle, capillaries are enwrapped by spatially separated contractile pericytes (Shaw et al., 2018; Peppiatt-Wildman, 2013). Evidence in the rodent brain (Hall et al., 2014; Peppiatt et al., 2006), retina (Peppiatt et al., 2006), lungs (Kerker et al., 2006; Speyer et al., 1999), kidneys (Silldorff et al., 1995; Crawford et al., 2012; Crawford et al., 2011; Zhang et al., 2005; Cowley Jr, and O'connor, 2013) and murine pancreas (Almaça et al., 2018) demonstrate regulation of the microcirculation by pericytes.

Human and rodent kidney sections show contractile filaments α -smooth muscle actin (α -SMA) and desmin localised around the vascular bundles (Colvin, 2019; Wei et al., 2015; Park et al., 1997a). From the late 1980's studies have demonstrated that endogenously synthesised vasoactive substances and their corresponding receptors converge around the medullary vasculature, modulating medullary blood flow and therefore O₂ supply (Neuhofer, and Beck, 2005; Pallone, and Silldorff, 2001; Cowley et al., 1995; Brezis et al., 1991), with key agonists and receptors summarised in **Table 1.1**. These agents also act specifically at contractile DVR pericytes with no downstream arteriolar signalling feasible due to vivisection (Silldorff et al., 1995; Zhang et al., 2004; Zhang et al., 2005; Sendeski et al., 2013; Crawford et al., 2012; Crawford et al., 2011; Cowley Jr, and O'connor, 2013)

Not only are renal pericytes contractile, but data supports their role in autoregulation via communications with the other cell types present. In DVR that have been isolated with the adjacent mTAL segment, the tubular epithelium buffers Ang-II-evoked pericyte-mediated vasoconstriction via NO-crosstalk (Cowley Jr, and O'connor, 2013). Further still Crawford *et al*, have shown that manipulation of live kidney slices with exogenous manipulators of endogenous BF exert their vasoactivity specifically via pericytes, further demonstrating communications between renal parenchyma and pericytes (Crawford et al., 2011; Crawford et al., 2012). The activity of specific agonists on pericytes of the DVR are discussed in more detail in **Chapter 4 section 4.4.4**.

Table 1.1 Vasoactive agonists that evoke a pericyte-mediated change in DVR diameter.

Agonist	Source of agonist	Receptor location	References
Adenosine	mTAL	A ₁ : DVR, LoH and CD. A _{2a} : CD. A _{2b} : LoH	(Billet et al., 2007; Pallone et al., 1998b; Crawford et al., 2011)
Ang-II	EdC	AT ₁ : OMDVR, interstitial cells and CD (constrict) AT ₂ : renal arteries (dilate)	(Weinstein, 2013; Crawford et al., 2012; Zhang et al., 2004; Ruan et al., 1999; Sasamura et al., 1994)
ADH	hypothalamus	V _{1a} : vSM, glomerulus, pericytes, medullary vasculature, ATL and OMCD V ₂ : CD	(Davenport, 2008; Cowley, 2008; Nakanishi et al., 1995; Turner, and Pallone, 1997)
ATP	mTAL, CD, EdC, RBCs	P2: DVR, LoH and CD	(Crawford et al., 2011; Menzies et al., 2015; Crawford et al., 2013; Shirley et al., 2013)
Bradykinin	CD, Interstitial fluid	B ₂ R: vSM, EdC, CT, CCD, pericytes	(Rhinehart et al., 2002; Ma et al., 1994; Staruschenko, 2012; Pallone et al., 1998a)
ET-1	EdC and CD	ET-1a: EdC, OM vasa recta ET-1b: EA	(Crawford et al., 2012; Silldorff et al., 1995; Schildroth et al., 2011)
NA	sympathetic nerves	α ₁ : OM vasa recta	(Crawford et al., 2012; Crawford et al., 2013)
NO	PST, mTAL, CD, MΦ (medulla)	diffuses through biological membranes	(Mohaupt et al., 1994; Crawford et al., 2012; Dickhout et al., 2002; Cowley Jr, and O'connor, 2013)
PGE₂	mTAL, CD, ISC, MΦ	EP ₂ : PST and OM vasa recta, IM. EP ₃ : OM>IM EP ₄ : CD, OM vasa recta	(Hume, and Gordon, 1983; Meurer et al., 2018; Silldorff et al., 1995; Crawford et al., 2012)

Ang-II; Angiotensin II, **ADH**; Antidiuretic Hormone, **ATL**; Ascending Thin Limb, **ATP**: Adenosine-5'-triphosphate, **CD**; Collecting Duct, **CCD**; Cortical Collecting Duct, **CT**; Connecting Tubule, **DVR**; Descending Vasa Recta, **EA**; Efferent Arteriole, **EdC**; Endothelial cells, **ET-1**; Endothelin-1, **ISC**; Interstitial Cells. **LoH**; Loop of Henle, **MΦ**; Macrophage, **mTAL**; Medullary Thick Ascending Limb, **NA**; noradrenaline, **NO**; nitric oxide, **OMCD**; Outer Medullary Collecting Duct, **OM**; Outer Medulla, **PGE₂**; prostaglandin E₂, **PST**; Proximal Straight Tubule, **RBC**; Red Blood Cells **vSMC**; Vascular Smooth Muscle Cell.

1.2 Pericytes.

Pericytes embody a multifunctional population of perivascular cells present in every capillary bed in the body (Harrell et al., 2018). These are spatially separated cells, embedded in the basement membrane on the abluminal side of the endothelium (Díaz-Flores et al., 2009) that are notable for their characteristic “bump-on-a-log” cellular morphology (Attwell et al., 2016), with numerous claw-like processes that are circumferential around and longitudinal along the capillary wall (Bergers, and Song, 2005). Pericytes are primarily defined by this proximity to endothelial cells (EdC), their characteristic morphology, their cell-surface molecule expression, and their functionality (Shaw et al., 2018).

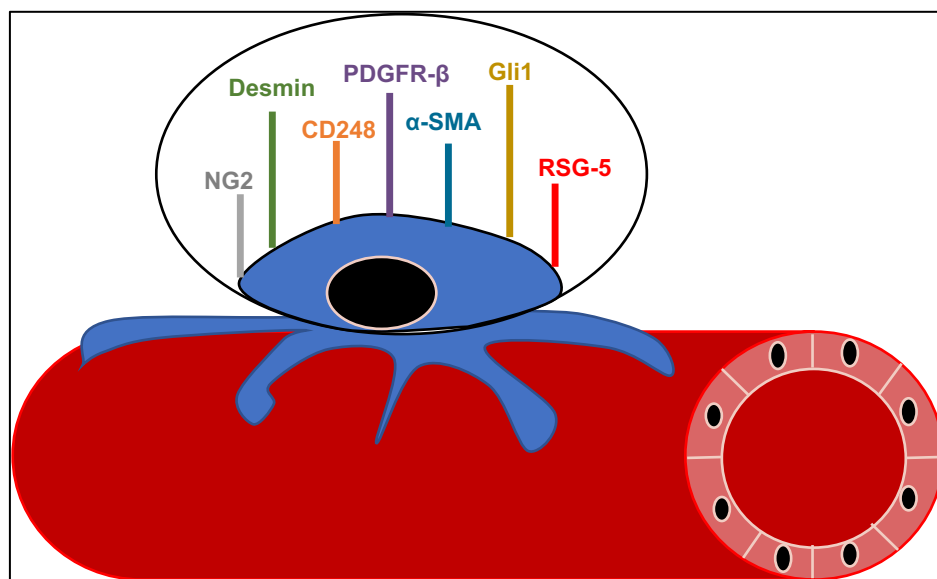


Figure 1.5 Known markers for renal pericyte identification.

Pericytes are a known heterogeneous cell-type and as such multiple markers, although no pan-specific marker, has been found, pericytes in the kidney are identified by expression of cell-surface protein expression such as platelet-derived growth factor receptor β (PDGFR β): a widely used marker, receptor with tyrosin kinase activity, involved in pericytes proliferation, recruitment investment, and maturation of the vasculature ; neural-glial antigen-2 (NG2): membrane chondroitin sulfate proteoglycan, another commonly used pericyte marker, NG2 is involved in pericyte recruitment to tumour vasculature as well as angiogenesis; α -smooth muscle actin (α -SMA) and desmin: structural proteins providing the contractile machinery and thereby enabling regulation of vessel diameter; CD248: a Type I transmembrane protein important for PDGFR- β -mediated signalling and is upregulated in disease; Gli1: zinc finger protein, involved in pericyte-mediated modulation of fibrosis and vital for maintenance of the peritubular capillary; and RSG-5: a GTPase- activating protein, expressed on activated angiogenic pericytes (Harrell et al., 2018; Smith et al., 2012; Am et al., 2013).

Organs with high metabolic needs and need for tightly regulated BF have higher pericyte densities; in the retina the ratio of EdC:pericytes is approximately 1:1, whereas in skeletal muscle it is much closer to 100:1 (Armulik et al., 2011; Smith et al., 2012), Renal pericytes are comprised of mesangial, peritubular and vasa recta pericytes,

constituting 30% of the renal tissue population (Ferland-McCollough et al., 2016). There is a correspondingly high EdC: pericyte ratio of approximately 2.5:1, with neural-glial-2 (NG2)⁺ pericytes covering 62 ± 23% of the renal vasculature (Smith et al., 2015). However, difficulties arise in identifying pericytes as their morphology and receptor expression patterns vary significantly along the capillary bed, expression patterns which identify functionally differing sub-populations. A summary of identifying-markers used for renal pericytes are summarised in **Figure 1.5**. Further discussion of the most commonly used markers platelet derived growth factor receptor-β (PDGFR-β), the proteoglycan NG2, and α-SMA (Attwell et al., 2016; Shaw et al., 2018; Am et al., 2013; Smith et al., 2012) is presented below in **Section 1.2.1.1**

1.2.1 Pericytes are a highly heterogenous population of cell.

Pericytes are a heterogenous class of cell, yet across tissues there are conserved functions. Primarily pericytes; regulate blood flow, provide and maintain the structural support and integrity of the endothelium (Lemos et al., 2016), are involved in angiogenic processes (Stapor et al., 2014; Betsholtz et al., 2005; Bergers, and Song, 2005; Díaz-Flores et al., 2009), and have an emerging role in inflammation. Specific examples of immune-pathogenic roles of pericytes are discussed further below in **section 1.3**. Further to this, pathogenically pericytes contribute to fibrosis in multiple organs (Birbrair et al., 2014) including: the liver (Iwaisako et al., 2014); cardiac and skeletal muscle (Murray et al., 2017); and in the kidney (Rojas et al., 2012; Kramann et al., 2017); as well as directly contributing to localised ischaemia and vessel rarefaction (Hall et al., 2014; Kramann et al., 2017), and tumorigenesis (Huang et al., 2011; You et al., 2014; Lu, and Shenoy, 2017). However, as described above (**Section 1.2**) there is inherent difficulty in determining behaviours that are pericyte-mediated.

Pericytes do not have an entirely specific identifying-marker, and not all markers are useful as receptor expression is dynamic and there is regional variation in protein expression dependent where upon the vascular tree they reside (Murfee et al., 2005) and developmental or pathologic states (Armulik et al., 2011). That considered, the best described cell-surface proteins for the identification of pericytes are PDGFR-β, NG2, and α-SMA (Attwell et al., 2016; Shaw et al., 2018; Am et al., 2013; Smith et al., 2012). These, and other known renal-pericyte identifying cell surface proteins are shown in **Figure 1.5**. Further discussion of pericyte distribution and morphology will primarily focus on expression of PDGFR-β, NG2 and α-SMA (**Section 1.2.1.1-1.2.1.1.1**).

1.2.1.1 NG2 and PDGFR- β expression varies along the capillary network.

PDGFR- β appears to be the broadest pericyte-identifying marker (Winkler et al., 2010; Dore-duffy, and Esen, 2018; Crisan et al., 2008), whilst non-specific, (Bergers, and Song, 2005; Díaz-Flores et al., 2009), identifying macrophage (Inaba et al., 1993; de Parseval et al., 1993), T-cells (Daynes et al., 1991), and NK-cells (Gersuk et al., 1991). All NG2⁺ pericytes are considered to co-express PDGFR- β (Dore-duffy, and Esen, 2018; Crisan et al., 2008; Castellano et al., 2018), in pericytes cultured from the CNS a minimum of 97% of pericytes express PDGFR β , while 50–80% express the proteoglycan NG2. In the lung all pericytes were PDGFR- β ⁺, and 60% of them expressed NG2 (Barron et al., 2016). A similar finding has been observed in human tissue; in the umbilical cord, all pericytes expressed PDGFR- β , but varied in NG2 and α -SMA expression depending on location along the vascular tree (Montemurro et al., 2011). This appears consistent with other tissues. α -SMA expression is restricted to the pre/post-capillary pericytes vs “true” mid-capillary pericytes (Nehls, and Drenckhahn, 1991). NG2 expression distinguishes three subsets of human pericytes, associated with: capillaries (NG2⁺/ α -SMA⁻), venules (NG2⁻/ α -SMA⁺) and arterioles (NG2⁺/ α -SMA⁺) (Crisan et al., 2012) (**Figure 1.6**). This pattern of expression has been observed in the rodent ureteric microvascular network (Burdyga, and Borysova, 2014), the murine CNS (Grant et al., 2017; Hartmann et al., 2015), and the rodent mesentery (Murfee et al., 2005).

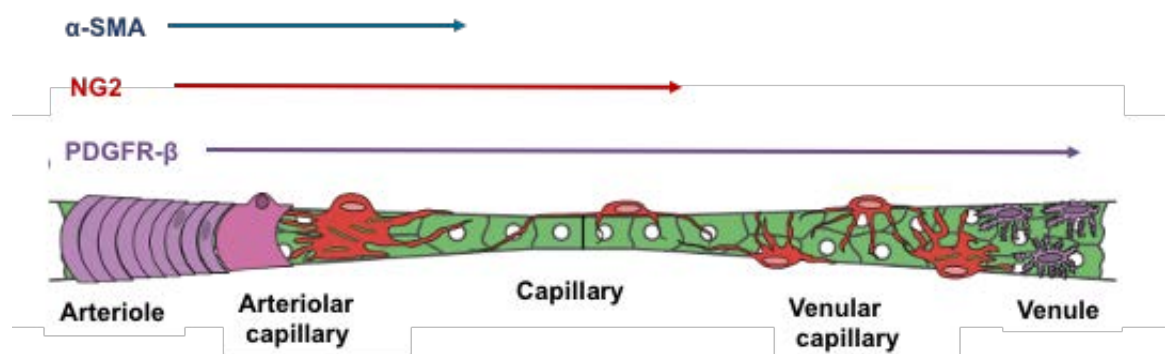


Figure 1.6 Schematic showing the diversity of pericytes around the microvasculature network of the renal medulla.

Differences presented here are both morphological and in expression of proteins α -SMA, PDGFR- β , and NG2. Only the red cells between the arteriolar capillary and venular capillary are pericytes. Arrows indicate expression limits of the corresponding protein (Hartmann et al., 2015).

Unlike the use of PDGFR- β to identify renal pericytes, the use of NG2 in adult tissues has been contested. Reportedly only 3% of mature pericytes express NG2 in the healthy adult rodent renal cortex (Lin et al., 2008; Rojas et al., 2012), yet adult murine kidneys show NG2⁺ pericytes with a marked regional distribution, with an approximately 6-fold difference in presence between the cortex and the medulla (Stefanska et al., 2015). Crawford *et al* reported a density of 12.4 \pm 1.2 NG2⁺ pericytes per 100 μm^2 in the adult rodent OM (Crawford et al., 2012) and as such it is possible a focus in the renal cortex where NG2⁺ pericytes are demonstrably less populated is a confounding factor with the low percentages reported.

Expression of α -SMA by pericytes is also debated, yet a recent paper has suggested this contractile protein is influenced by fixation method used in the tissue (Alarcon-Martinez et al., 2018). Medullary pericytes of chickens have shown to express contractile proteins desmin and vimentin (Fuxe et al., 2011; Fujimoto, and Singer, 1987), with rodent, chicken, and murine medullary pericytes expressing α -SMA (Park et al., 1997a; Stefanska et al., 2015). Interestingly, in the murine renal medulla NG2⁺/PDGFR- β ⁺ pericytes express α -SMA (Stefanska et al., 2015) whereas PDGFR- β ⁺/NG2⁻ pericytes show minimal expression of this contractile protein (Wang et al., 2017). This suggests renal NG2⁻ pericytes are α -SMA⁻, unlike other tissues such as the murine cremaster muscle where venular capillary pericytes are NG2⁻/ α -SMA⁺ (Proebstl et al., 2012). **Figure 1.6** illustrates the cell-surface molecule diversity of pericytes of the renal microvascular network in light of this finding. Why this difference exists in the kidney remains unclear, but possibly pertains to the unique architecture of the vasa recta and the counterflow arrangement (Pallone et al., 1998b). Overall, the arteriolar-restriction of NG2 expression appears to be a conserved feature of pericytes across different tissues and species (Díaz-Flores et al., 2009; Kumar et al., 2017; Burdyga, and Borysova, 2014; Murfee et al., 2005; Crisan et al., 2008; Fuxe et al., 2011), and taken together suggests the pericyte subpopulation which regulate MBF are likely PDGFR- β ⁺/NG2⁺/ α -SMA⁺ encircling the DVR, with PDGFR- β ⁺/NG2⁻/ α -SMA⁻ pericytes reside on the AVR, and potentially offers a means of discrimination between pericyte subtypes.

1.2.1.2 Pericyte morphology correlates with NG2 and PDGFR- β expression.

Zimmerman was the first to describe pericyte variation according to their location along blood vessels as: arteriolar, true-capillary, and venular (Zimmermann, 1923). Along

with regional expression of cell-surface molecules discussed above, there also appears to be a heterogeneity in morphology along the vascular tree (**Figure 1.6**) (Zimmermann, 1923). Arteriolar pericytes that are NG2⁺/α-SMA⁺ have thick cell bodies with circular branches that overlap or attach to each other, forming a complicated and dense meshwork over the arteriolar capillary. True-capillary pericytes are NG2⁺/α-SMA⁻ with highly elongated longitudinal processes and soma, with short circumferential processes. Arteriolar contractile pericytes also appear to have a smaller soma morphology (Kutcher et al., 2007; Kolyada et al., 2003), with true-capillary α-SMA⁻ pericytes (soma and processes) 3-4x larger than arteriolar pericytes (Borysova et al., 2013). Venular pericytes cover the abluminal surface of postcapillaries and are PDGFR-β⁺/NG2⁻ and stellate shaped (Díaz-Flores et al., 2009; Kumar et al., 2017; Burdyga, and Borysova, 2014; Murfee et al., 2005; Crisan et al., 2008; Fuxe et al., 2011).

Comparative to the vSMC of arterioles that also express NG2 and PDGFR-β (Stefanska et al., 2016), it is the pericytes characteristic morphology that enables their identification. Unfortunately, specific measurements of pericyte soma size, despite visual morphological differences, are not readily reported. If the contractile population of pericytes that consistently express NG2 are determined to have a smaller cellular morphology consistently, these characteristics together may enable accurate identification of the sub-population of pericytes which reside on the DVR and regulate MBF, and consequently any other alternative functions of these NG2⁺ pericytes.

1.2.1.1.1 NG2 and PDGFR-β are more suitable identifying markers than others.

Pericyte expressed NG2 proteoglycan is involved recruitment of pericytes pericyte-EdC network formation and mediates communications between them to maintain vascular stability (You et al., 2014). As an identifying molecule, NG2 readily identifies medullary pericytes in both rat, mouse, and porcine kidneys (Crawford et al., 2012; Stefanska et al., 2015; Castellano et al., 2018). During angiogenesis, sprouting endothelial cells express PDGF-B and recruit pericytes via PDGF-B/PDGFR-β signalling (Trost et al., 2016) thus pericyte PDGFR-β expression is necessary for the investment of pericytes into the endothelial tube to finish angiogenesis and provide structural support (Bergers, and Song, 2005). PDGFR-β is expressed by all pericytes and has extensively been used for pericyte identification (**Section 1.2.1.1**).

Use of the other proteins presented in **Figure 1.5** for identifying renal pericytes believe specific functions and distinguish further subpopulations. Regulator of G protein signalling protein 5 (RGS-5)-expression is restricted to pericytes and vSMC (Adams et al., 2000) and co-labelling with PDGFR- β (Cho et al., 2003; Berger et al., 2005). It is an indicator of actively angiogenic renal pericytes for both embryonic vascularisation (Cho et al., 2003) and pathological angiogenesis associated with renal cell carcinoma (Berger et al., 2005). However, RGS-5 is not expressed in healthy adult renal tissue unlike NG2 and PDGFR- β (Stefanska et al., 2015) and as such unlikely to broadly identify pericytes.

Zinc finger protein “Gli1” expression represents a sub-population of PDGFR- β^+ pericytes (Grgic et al., 2014), and fate tracing showed their loss induces capillary rarefaction and PST injury (Kramann et al., 2017). Gli1 contributes to capillary stability and Gli1 $^+$ pericytes seemingly contribute to the pathogenesis of fibrosis. Much like NG2 $^+$ pericytes, Gli1 $^+$ pericytes are most abundant in the renal OM (Kramann et al., 2017). Given the density of pericytes in the OM it would be interesting to further probe the expression pattern of renal Gli1 $^+$ pericytes, yet Gli1 $^+$ pericytes in the lung do not co-express NG2 despite over 60% of lung pericytes expressing NG2 (Barron et al., 2016), and only identifies a very small population of PDGFR- β^+ pericytes (Kramann et al., 2015). Further work is needed to characterise Gli1 $^+$ pericytes prior to its use in identifying pericyte multifunctionality.

CD248 is expressed by the mesangium and renal pericytes. When assessing the degree of co-expression, it was found some, but not all, of cellular CD248 expression correlated with PDGFR- β , NG2, and α -SMA expression. The authors concluded CD248 identifies a subset of pericytes not commonly identified by the above markers based upon the location and morphology (Smith et al., 2015). Functionally, CD248 appears to modulate fibrosis by enhancing PDGF-signalling. In CD248 $^{-/-}$ mice there was reduced fibrotic scarring, and reduced numbers of α -SMA $^+$ and NG2 $^+$ pericytes comparative to wild type controls after unilateral ureteral obstruction. Unlike NG2 and PDGFR- β (Tanaka et al., 2017; Proebstl et al., 2012; Alon, and Nourshargh, 2013), CD248 $^+$ pericytes do not appear to influence the inflammatory response as no difference in CD45, CD3, or F4/80 staining was observed (Smith et al., 2015), whilst NG2 $^+$ and PDGFR- β^+ pericytes appear extensively involved in inflammation, discussed in greater detail below in **section 1.4.1**.

What can be seen here is that these less common pericyte identifying-markers, whilst useful for specific subtypes or activation states, are unlikely to identify most pericytes.

Comparatively, NG2 and PDGFR- β are more reliably expressed and are regularly used to identify renal pericytes.

1.2.2 Novel pericyte-mediated activities can be organ specific, yet there remain conserved behaviours across tissues.

It is known that pericytes have organ-specific functions. In skeletal muscle, type-2 nestin⁺/NG2⁺ pericytes contribute to muscle formation and regeneration (Birbrair et al., 2015), and in both the skin and skeletal muscle, "type-1" nestin⁻/NG2⁺ pericytes contribute to fat accumulation (Birbrair et al., 2015). In the liver, pericytes store 80% of the body's total vitamin A (Sato et al., 2003). In a mouse model of skin-regeneration, NG2⁺/PDGFR- β ⁺ pericytes promote epithelial proliferation, differentiation, and tissue regeneration without any angiogenic behaviours, by modifying the surrounding ECM, demonstrating a role for co-ordinating wound healing (Paquet-Fifield et al., 2009). α -SMA⁺/NG2⁺/PDGFR- β ⁺ pericytes are involved in adipogenesis during murine development (Tang et al., 2008), and in the rodent inguinal fat pad in response to thermal lesion (Richardson et al., 1982). This is also true for the kidney; PDGFR- β ⁺ pericytes contribute to the production of erythropoietin (Shih et al., 2018), and human NG2⁺ foetal renal pericytes produce renin (Stefanska et al., 2016). Summarily, duties enacted by different organs are often conducted, in part, by pericytes. Yet the expression of cell-surface proteins PDGFR- β and NG2 remain consistent suggesting it is the organs the pericytes reside which influences some behaviours, whilst other features remain conserved.

This describes organ-specific behaviours of pericytes, yet pericytes do exhibit conserved behaviours. Along with regulation of BF (**section 1.2.1.2.1**), pericytes also seemingly possess conserved progenitor properties. Vascular cells have a slow turnover, and secondary colonies of single-sorted CD34⁺/CD31⁻ pericytes conserve a mesenchymal phenotype *in vitro* (Campagnolo et al., 2010). NG2⁺/PDGFR- β ⁺/CD146⁺ human pericytes isolated from various tissues including the placenta, skeletal muscle, pancreas, retina, and adipose tissue, show multipotency *in vivo* (Crisan et al., 2009). Adult pericytes are reportedly able to differentiate into ECs, vSMC, neural cells, and Macrophages (M Φ) (Orekhov et al., 2014; Dore-duffy, and Esen, 2018; Díaz-Flores et al., 2009). A summary of the multipotency of pericytes can be seen in **Figure 1.7**, but further comment is beyond the scope of this study.

What is to be taken away is that receptor expression, the varied morphology of pericytes, and the tissues in which they reside together can indicate what the functionality of the particular subpopulations of pericytes (Attwell et al., 2016), yet in all tissues pericytes multifunctionality appears consistently, primarily when identifying pericytes with NG2 and PDGFR- β .

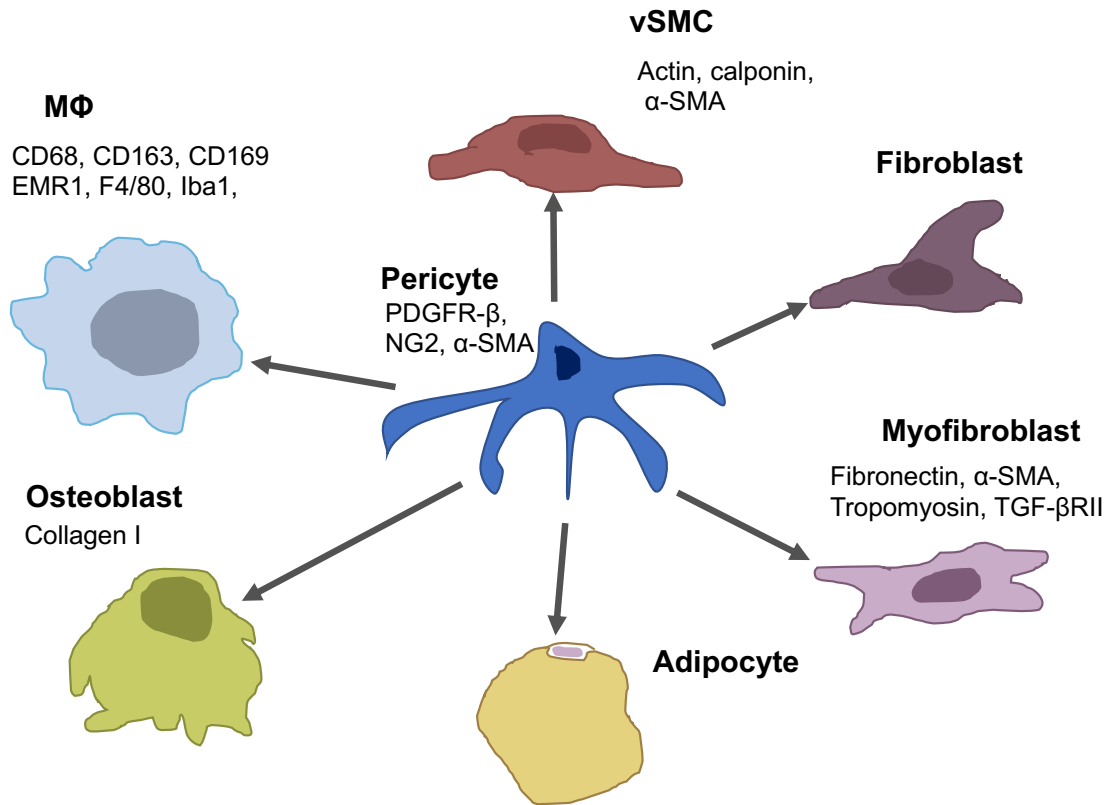


Figure 1.7 A schematic illustrating cell type pericytes reportedly differentiate into. Cell types and the key identifying cell-surface markers used to determine the multipotency of pericytes have been highlighted. M Φ = macrophage. (Orekhov et al., 2014)

1.2.3 Inconsistent experimental methods in identifying pericytes may confound findings.

One of the most extensively investigated, and controversial, multipotent behaviours of pericytes is that they are considered a source of myofibroblasts. Data has shown communications between the endothelium and PDGFR- β^+ pericytes encourages fibrosis; inhibiting PDGF-signalling and vascular endothelial growth factor (VEGF)-signalling attenuates fibrosis and vessel rarefaction (Lin et al., 2011). How pericytes are involved does seem to vary. Birbriar *et al*, found nestin $^-$ pericytes contribute to collagen production in fibrosis (Birbriar et al., 2014) whilst NG2 $^+$ pericyte contribution to collagen production varies between tissues, although all NG2 $^+$ pericytes congregate

around the fibrotic area (Birbrair et al., 2014; Dulauroy et al., 2012; Soderblom et al., 2013) These studies suggest two potential mechanisms by which pericytes may contribute to fibrosis: by directly producing collagen (Grgic et al., 2014), or by first differentiating into α -SMA⁺ myofibroblasts that are responsible for the expansion of fibrotic tissue via the production of collagen (Kisseleva, and Brenner, 2008). What these studies show is subtype-dependent involvement of pericytes in fibrosis. Consistent use of well characterised pericyte-identifying markers here has been key for elucidating their fibrotic involvement.

This is highlighted by a recent study, which suggested pericytes do not contribute to fibrosis. However, the marker used for tracing pericytes and their subsequent fibrotic involvement, Tbx18 (Guimarães-Camboa et al., 2017) was not the most suitable choice. Whilst Tbx18 co-labels with PDGFR- β ⁺ perivascular cells in the heart, brain, skeletal muscle, and adipose tissue it does not label any pericytes in the liver, intestines, or the kidney (Campagnolo et al., 2018). Given the high pericyte density of the kidney (Crawford et al., 2012; Lin et al., 2008), the fact Tbx18 does not identify pericytes in this organ would suggest Tbx18 is not a pan-pericyte marker. Consistent use of pericyte-identification necessary and accumulating evidence points at pericytes as a source of myofibroblast progenitors (Lin et al., 2011; Grgic et al., 2014; Kisseleva, and Brenner, 2008; Birbrair et al., 2014; Dulauroy et al., 2012; Soderblom et al., 2013; Iwaisako et al., 2014). With respect to renal pericytes, another key consideration is their regional distribution in the kidney.

1.2.3.1 There is a highly varied regional distribution of renal pericytes.

Renal pericytes are present throughout the microvasculature of the kidney with the greatest density in the OM (**Figure 1.8**). As described above (**Section 1.2.1**) the cell-surface protein expression pattern varies along the vascular bed. However, a focus in the cortex may not best represent the activities of all renal pericytes.

In a unilateral ureteric obstruction (UUO) injury model LeBleu *et al*, found 5% of renal myofibroblasts were sourced via the epithelial-mesenchymal transition, 10% came from EdC-mesenchymal transition, and 50% came from residential fibroblasts (LeBleu et al., 2013), with an accumulation but no active involvement of PDGFR- β ⁺ or NG2⁺ pericytes in the cortex. However, another lab using a different method to induce UUO (Duffield et al., 2005), *coll1a1* expressing PDGFR- β ⁺/ α -SMA⁺ cortical pericytes are the primary source of fibrosis in the renal cortex (Lin et al., 2008). Whilst the different

methods to induce renal injury might influence cell types responsible for fibrosis, as observed in the liver (Iwaisako et al., 2014), the limited pericyte involvement measured above may have also resulted from a focus in the renal cortex.

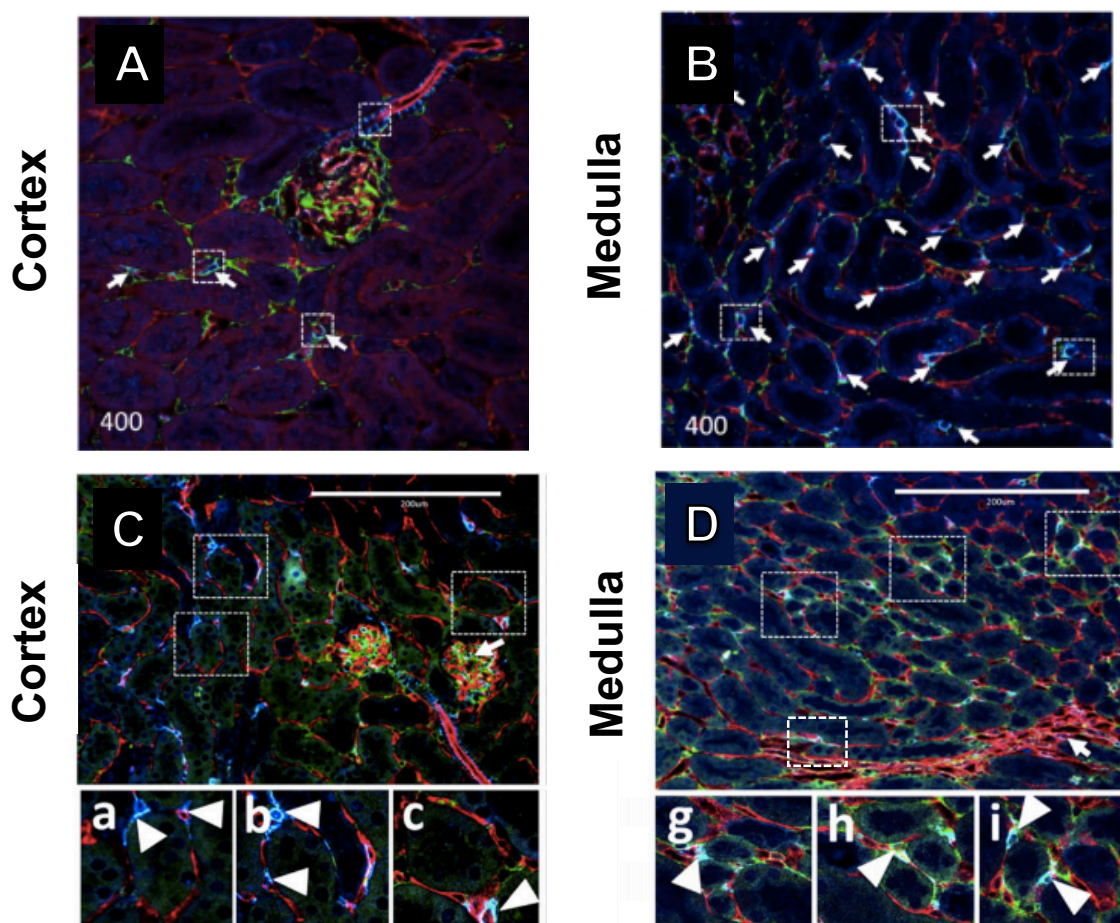


Figure 1.8 Renal NG2⁺/PDGFR-β⁺ pericyte distribution in the cortex and outer medulla of healthy young adult mice.

Young adult C57BL/6J kidney slices were triple stained with NG2 (blue), PDGFR-β (green), and CD31 (red) to identify pericytes and the endothelium. (A-B) Double positive cells that are indicated with white arrows are pericytes, whilst double-positive cells that are highlighted only with a hatched box in (A) are afferent arteriolar vascular smooth muscle cells. Cells indicated with an arrow and box show the pericyte soma. Pericytes in the outer medulla were far more numerous than in the cortex. (C) the white arrow highlights a glomerular tuft, with hatched box regions highlighting pericytes. These pericytes are shown in higher power images (a-c), showing pericytes supporting peritubular capillaries. (D) in the outer medulla, vasa recta can be seen (white arrow), as can NG2⁺/PDGFR⁺ pericytes. (g-i) show high power images of hatched boxed in (D). (C-D) also show pericytes are more numerous in the outer medulla than the cortex. Arrow heads highlight pericyte soma. PDGFR-β⁺ staining is more abundant than NG2⁺ staining. Scale bars are 200 μm. Data taken from (Stefanska et al., 2015).

When the renal medulla has been investigated, fibrotic scarring is most abundant at the corticomedullary junction and around the vascular bundles in the ISOM (Strupler et al., 2008; Shaw et al., 2018). Further still, studies that include the medulla in analysis, and use PDGFR-β and NG2, have consistently identified pericyte

involvement in the progression of fibrosis. Fate tracing *in vivo* that renal pericytes (FoxD1⁺/ PDGFR- β ⁺/ CD73⁺) demonstrated differentiation into myofibroblasts (Humphreys et al., 2010) and found collagen producing *col1 α 1*-eGFP-L10a⁺ pericytes actually have the highest density in the OM (Grgic et al., 2014). Using flow cytometry with digestion of the whole kidney, another lab who used both UUO and a folic acid-induced kidney injury model found that PDGFR- β ⁺ pericytes secrete complement and contribute to the progression of fibrosis via upregulation of α -SMA, fibronectin, and *col1 α 1* in both disease models (Xavier et al., 2017) although potential difference between models are not discussed. Consistency in the identification of pericytes and their microanatomical location are clearly important considerations in elucidating conserved pericyte-mediated activities.

1.3 A novel emerging conserved behaviour of NG2⁺ and PDGFR- β ⁺ pericytes involves coordination and involvement in the immune response.

The lack of a specific pan-pericyte marker makes investigations into the multifunctional nature of pericytes difficult and makes data analysis complicated. From the literature PDGFR- β and NG2 are optimal for use in identifying pericytes, although expression of these proteins is influenced by different factors (Morita et al., 2014). A more complete profile of pericytes might aid in their identification, such as objective metrics like soma size, as discussed above (**Section 1.2.1.2**). However, it is also important to determine whether it is pericytes responsible as opposed to a pericyte-derived cell type. Much of the data relating to the multifunctionality of pericytes derives from tissue culture (**section 1.3.3**), which do not belie the complexity of the functions or distribution of cells *in vivo* (Vickers, and Fisher, 2005; Bach et al., 1996). Further still, *ex vivo* or *in vitro* analysis of extracted cell suspensions can oversimplify both M Φ and pericyte populations (Gordon, and Plüddemann, 2017), with a varied morphology and stark microheterogeneity, and therefore not wholly reflect the cellular distribution (Gordon et al., 2014) or functionality (Stapor et al., 2014) *in situ* or *in vivo*. Cultured cells can dedifferentiate and lose functionality leading to variation in data generated comparative to *in vivo* observations (Elberg et al., 2008)). *In vitro* work also does not offer the advantage of maintaining cell-cell interactions and the complex structural integrity that better mimic *in vivo* behaviours, whilst tissues slices, like the rodent kidney slice model (Crawford et al., 2012), maintain these communications.

Studies in the kidney *in vivo* have shown that both pericytes and immune cells contribute to tubulointerstitial fibrosis, and are heavily implicated in its progression

(Xavier et al., 2017; Kurts et al., 2013). Inflammation is a key feature in the pathogenesis of renal disease, regardless of whether the insult is primarily induced by the immune response, the innate immune system is involved in injury (Weisheit et al., 2015). However, with recent evidence suggesting that an emerging conserved pericyte-mediated activity is co-ordination of the immune response and may themselves act as immune cells, with the overlap of protein expression between pericytes and immune cells shown in **Figure 1.7**, the question becomes which cell populations are actually responsible for propagating and directing the innate immune response.

1.3.1 Pericytes as coordinators of immune function.

As potential mediators of inflammation, not only do pericytes occupy an optimal physical location between the interstitium and the blood stream residing along the capillary wall (Stark et al., 2018; Lapenna et al., 2018; Navarro et al., 2016), there is evidence demonstrating pericyte presence is necessary for inflammation. Pericytes of the kidney (PDGFR- β^+) and in tumour models (NG2 $^+$) can directly recruit inflammatory M Φ via VEGFR2 and PDGF- β signalling, and cytokines IL-33, macrophage migration-inhibitory factor (MIF) and CCL2 (Lin et al., 2011; Yang et al., 2016). It is NG2 $^+$ pericytes on arteriolar capillaries of the cremaster muscle and ear that express and store the chemoattractant MIF to recruit polymorphonuclear leukocytes (PMN; Ly6G $^+$) and mediate PMN transmigration and activity post extravasation via ICAM-1, MAC-1 and LFA-1 (Stark et al., 2012; Proebstl et al., 2012) interactions with the NG2 proteoglycan (Alon, and Nourshargh, 2013).

However, PMN migrate out into the interstitium via NG2 $^-$ pericytes on the venular capillaries. This venular extravasation was observed with microspheres in the murine trachea, where they only extravasate out via venular specific PECAM-1, with no capillary involvement (Fuxe et al., 2011), and has been experimentally demonstrated *in vivo* (Proebstl et al., 2012; Wang et al., 2012). PMN migrate out through the low expression regions where there are reduced matrix proteins α -SMA and Collagen IV, with direct contact between PMN and pericytes causing a α -SMA $^+$ /NG2 $^-$ pericyte-mediated relaxation (Wang et al., 2012), creating sites for further PMN to extravasate (Proebstl et al., 2012). Some of these extravasated PMN are then further “instructed” by arteriolar NG2 $^+$ pericytes to migrate towards the inflammatory stimulus via ICAM-1, MAC-1 and LFA-1 (Alon, and Nourshargh, 2013) (**Figure 1.9**). This data suggests subpopulations of pericytes co-ordinate differing stages of immune cell infiltration; with

arteriolar NG2⁺ pericytes necessary for recruitment, whilst venular NG2⁻ pericyte involvement in PMN extravasation. However, data shows perivascular MΦ (PVM) are also involved in this process (discussed in **section 1.3.3.1**).

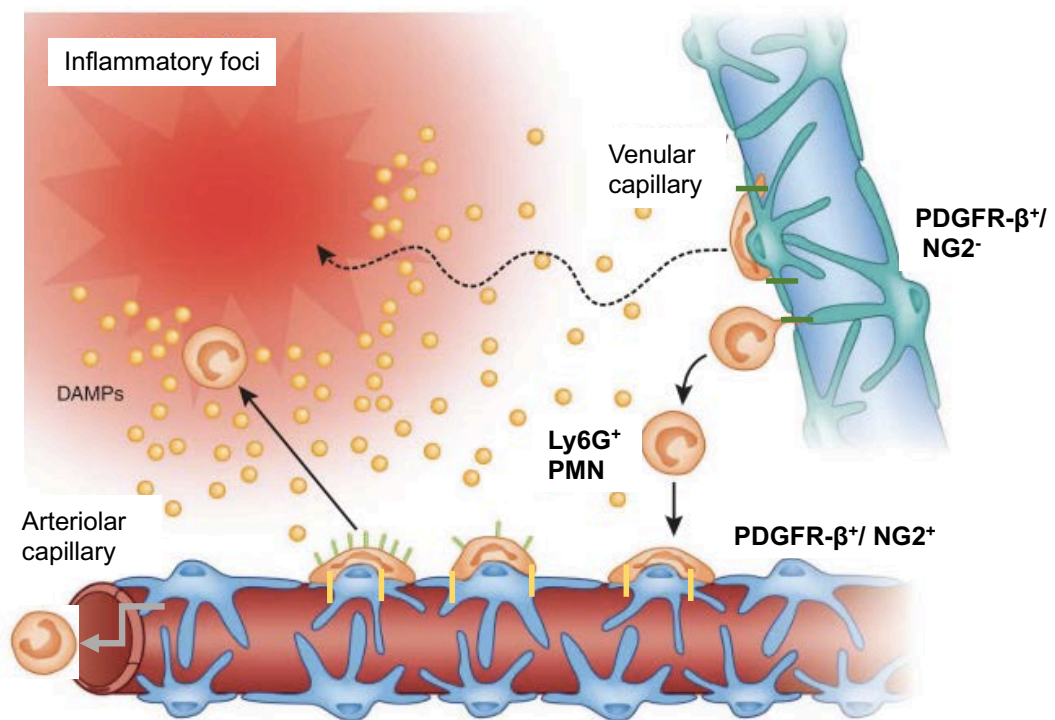


Figure 1.9 NG2-dependent extravasation of polymorphonuclear leukocytes (PMN).

Pericyte cell surface protein expression varies dependent upon where along the capillary network they reside. Along the arteriolar capillary, NG2⁺/PDGFR-β⁺ pericytes (*blue*) attract circulating Ly6G⁺ PMN via MIF, IL-33, IL-6, and CCL2 (grey arrow). These PMN travel along the capillary network and extravasate via venular capillary NG2⁻/PDGFR-β⁺ pericytes (*turquoise*). Direct cell-cell contact between PMN and NG2⁻/PDGFR-β⁺ encourages these pericytes to dilate, express PECAM-1 (dark green bars), and thereby enable PMN to extravasate out of low expression regions where there are reduced matrix proteins (shown as less pericyte coverage). After migrating into the interstitial space and crawling on NG2⁻/PDGFR-β⁺ pericytes, some PMN migrate directly to the inflammatory foci (dashed arrow) whilst a fraction of PMN are attracted by NG2⁺/PDGFR-β⁺ pericytes. Secretion of MIF, ICAM-1, MAC-1 and LFA-1 by these pericytes (yellow bars) render the recruited leukocytes highly sensitized (light green bars) and “instruct” these PMN, which then have the capacity for highly directional migration through the interstitial space toward the inflammatory foci. DAMP, damage-associated molecular pattern. (Alon, and Nourshargh, 2013).

1.3.2 Angiogenesis and vessel stability require macrophages and pericytes.

Angiogenesis is a well characterised pericyte-mediated activity (Stapor et al., 2014). EdC from pre-existing vessels secrete proteases like matrix metalloproteinases-9 (MMP-9) to degrade basement membrane and invade the surrounding extracellular matrix (ECM) (Bergers, and Song, 2005). These EdC form a migration column of

proliferatory and migratory cells that assemble into a simple capillary network, guided by tip EdC (Bergers, and Song, 2005) and pericytes (Kang et al., 2019; Nicosia, 2009). As the new capillary sprout is formed, the EdC adhere to one another and cease proliferating. EdC secrete PDGF-BB to recruit PDGFR- β^+ pericytes to stabilise this new endothelial tube (Tanaka, and Nangaku, 2013). This pericyte-EdC contact is required for tissue inhibitor of matrix metalloproteinases-3 (TIMP-3)-mediated stabilisation of new vessels, dependent on pericyte-expressed NG2 (Hesp et al., 2017; Cuervo et al., 2017; You et al., 2014). TIMP-3 inhibits pro-angiogenic molecules MMP-9, MMP-2, and VEGF-A activity at the VEGF receptor-2 (Saunders et al., 2006), inducing matrix-bridging protein production to stabilise the newly formed basement membrane (Stratman et al., 2009), arresting EdC growth (Durham et al., 2014). Investment of pericytes resolves angiogenesis, achieving EdC quiescence and maturation of the vessel in a GTPase-dependent manner (Kutcher et al., 2007). To maintain homeostasis in adult vascular beds, pericytes are constantly secreting potent pro- and anti-angiogenic factors to maintain stability of the capillary (Schrimpf et al., 2012). Interestingly *in vivo* data suggests pericyte-M Φ interaction is necessary for angiogenesis to occur, with M Φ -pericyte interactions occurring well before vessel maturation (Rajantie et al., 2004).

Developmentally renal M Φ promote endothelial connections and proliferation frequently associating with the capillaries developing PTC (Munro et al., 2019; Puranik et al., 2018). Direct adherence of M Φ to EdC directs EdC tube and neovessel formation (Munro, and Hughes, 2017). In an aortic ring model, at atmospheric O₂ neovessels formed of EdC tubes were coated with pericytes and surrounded by M Φ (Aplin, and Nicosia, 2016). subsequent depletion of these M Φ inhibited neovessel formation (Nicosia, 2009). This, in line with the above *ex vivo* data suggest pericytes and M Φ together are required for angiogenesis. In adult tissues, perivascular macrophage (PVM; Mrc1⁺) are frequently associated with the capillary, interacting with pericytes to regulate the endothelial barrier and permeability (He et al., 2016). In the cochlear duct, communication of residential M Φ (F4/80⁺) with NG2⁺ pericytes is essential to maintain vascular integrity, regulating the tight junctions proteins VE-cadherin and ZO-1 (Neng et al., 2013). What can be seen is that pericytes and M Φ communicate and collaborate to maintain the microvasculature, therefore it is feasible they may communicate to regulate other physiological functions.

1.3.2.1 A subset of NG2⁺ pericytes are derived from macrophages

As mentioned above (**section 1.2.2**) pericytes reportedly differentiate into MΦ, but it has also been found that some pericytes derive from MΦ. In both the embryonic skin and brain genetic fate mapping studies have shown that 27% of NG2⁺ pericytes were derived from MΦ. Although these pericytes did not continue to express CD11b or F4/80, around 13% of all pericytes had originated from CD11b⁺ cells (Yamazaki et al., 2017), with transforming growth factor (TGF)-β encouraging myeloid progenitors differentiation into NG2⁺ pericytes (Yamazaki et al., 2017). In the developing midbrain CD31⁺/F4/80⁺ cells transdifferentiated into pericytes expressing NG2, PDGFR-β or desmin (Komuro et al., 2017). This differentiation of MΦ into pericytes has also been observed in adult animals.

In a subcutaneous matrigel plug model, pericyte-MΦ interactions occurred well before vessel maturation, with the appearance of CD31⁺ EdC signifying the onset of perfusion. In this study, a small population of NG2⁺ pericytes were derived from F4/80⁺ MΦ, and when EdC populated blood vessels were perfused, 10% of these cells remained co-expressing NG2 and F4/80 (Tigges et al., 2008). In the murine ear, subpopulations of VEGF-induced angiogenic cells were NG2⁺, CD11b⁺, and CD45⁺, with a small population of NG2⁺ cells co-expressing CD11b or CD45 (Rajantie et al., 2004). Taken together this suggests a shared lineage of F4/80⁺ MΦ and a subpopulation of NG2⁺ pericytes. These MΦ-derived pericytes may not lose their immune-activities, and MΦ that adhere to the developing endothelium may become pericytes.

1.3.3 Pericytes as non-professional immune cells.

Outside of the emergent role of pericytes in co-ordinating the immune response (**Section 1.3.1**), data shows pericytes across tissues acting as “non-professional” immune cells; non-immune cells which show capacity for immunogenicity and phagocytosis (Hamada et al., 2019). In the lung, following LPS-stimulation pericyte-like PDGFR-β⁺ cells act as immune sentinels expressing IL-6, chemokine (C-X-C motif) ligand-1, chemokine (C-C motif) ligand 2/ monocyte chemoattractant protein-1, and ICAM-1 *in vivo* (Hung et al., 2017). In the liver, pericytes act as antigen-presenting cells, recruiting Natural Killer T-cells (Winau et al., 2007), as well as inactivating T-cells in the human and murine kidney by inhibiting antigen-specific activation of chemokine recruited cells (Poerber, and Tellides, 2012). In disease models, NG2⁺/PDGFR-β⁺

tumour pericytes secrete high levels of IL-33, MIF and CCL2 recruiting F4/80⁺ tumour associated MΦ (Yang et al., 2016). CNS PDGFR-β⁺ pericytes sense inflammation in a CCL2 dependent manner (Duan et al., 2018), and secrete a panel of pro- and anti-inflammatory mediators (Lin et al., 2008; Hung et al., 2017) as well as demonstrating phagocytotic capabilities (Balabanov et al., 1996). Pericytes of the kidney (PDGFR-β⁺) directly recruit inflammatory MΦ (Lin et al., 2011). Renal mesangial cells (Schreiner, 1992) have shown phagocytic potential, co-labelling with CD68; a marker of phagocytic cells (Beranek, 2005). However, overlap in receptor expression might also mean that PVM may have been mis-identified as pericytes.

1.3.3.1 Are these pericytes acting as immune cells or perivascular macrophages?

Described above is pericyte-mediated direction of inflammatory cells (**section 1.3.1**). However, some of the reports of pericyte-mediated immune activity may be confounded by their developmental origin and the co-expression of pericyte- and MΦ-associated markers as evidence shows PVM involvement in these processes. In the heart, skin, and intestine post ischaemia-reperfusion injury (IRI) PVM are necessary for PMN recruitment and extravasation, with ICAM-1-mediated neutrophil adherence and extravasation are markedly reduced in their absence (Li et al., 2016; Abtin et al., 2014; Chen et al., 2004)..PVM are not necessarily solely pro-inflammatory however as in the kidney, CD169⁺ PVM show to be protective post-IRI. CD169⁺ PVM homeostatically suppress basal ICAM-1 expression by EdC, acting as anti-inflammatory MΦ population and promoting tissue repair post-IRI (Karasawa et al., 2015). Much like with pericytes, there appears to be differing roles for subpopulations of PVM, but they remain key regulators of the inflammation and tissue homeostasis.

With reports of the immunoactivity of pericytes – the population of MΦ they may overlap with would be PVM given their vascular residence. Clarity over which cell type; PVM or pericytes, is important to define. Whilst argued that PVM and pericytes can be distinguished on the basis of morphology, location and phenotype (Fabriek et al., 2005b) the definitions proposed for both are overlapping; PVM-identifying criteria are “making direct contact with the abluminal surface of the vasculature, or within 15 μm” (Lapenna et al., 2018); somewhat similar to pericytes “spatially isolated cells with a bump-on-a-log morphology present on the outside of capillaries, both on straight parts of the capillaries and at capillary branch points” (Attwell et al., 2016). However,

morphology is not always a key consideration for the primary identification of pericytes, instead designating functions based on markers that are co-expressed.

F4/80 is not the only M Φ -identifying marker to be co-expressed by pericytes (**section 1.3.2.1, Figure 1.7**). Other classic M Φ markers such as CD163 and CD68 in the rodent CNS and skeletal muscle are reportedly expressed by pericytes (Graeber et al., 1989; Balabanov et al., 1996; Rustenhoven et al., 2016; Pieper et al., 2014; Thomas, 1999). And much like PDGFR- β and NG2-expression by pericytes being encourage by osmotic stimulation (Morita et al., 2014), MHC-II is expressed by porcine brain pericytes after stimulation with interferon- γ (Pieper et al., 2014). Interestingly, this co-expression of M Φ markers by pericytes is seemingly further conserved across species as both CD68 and MHC-II have reported expression on hepatic pericytes in mice and humans (Winau et al., 2007). Human CNS NG2⁺ pericytes express CD68 and CD11c (Pouly et al., 1999), and more recently, Iba1⁺/NG2⁺ perivascular cells have been (Smirkin et al., 2009; Özen et al., 2014). Whilst these cells were determined by investigators to be pericytes, given the definitions above they may well be PVM. As NG2 expression by F4/80⁺ M Φ is dynamic (Moransard et al., 2011), pericyte expression of M Φ proteins also appears dynamic (Pieper et al., 2014). NG2 is upregulated in response to TGF- β (Moransard et al., 2011), where it encourages M Φ -pericyte differentiation, or pericyte-M Φ differentiation (Orekhov et al., 2014; Doreddy, and Esen, 2018; Díaz-Flores et al., 2009; Leaf et al., 2016). PDGFR- β also reportedly labels human immune cells (Inaba et al., 1993; de Parseval et al., 1993) so boundaries between these cells are blurred.

Under basal conditions in the kidney, residential M Φ predominate in the OM, much like pericyte, in humans and animals (see **section 1.4**). This abundance of both cell types could mean that direct pericyte-immune functions in the kidney could be misattributed to pericyte, or that they are interacting. Experimental evidence suggests communication between M Φ and pericytes in the OM.

1.4 Pericytes and macrophage converge on the renal medulla.

With the above sections (**1.2-1.3**) considered, it is interesting to note that pericytes and M Φ are most dense in the OM. Whilst there have been no reports of PVM on the vasa recta, there is convergence of M Φ around in OM in humans (CD163⁺ and CD14⁺) (Colvin, 2019; Berry et al., 2017) and in mice (F4/80⁺ or CD169⁺) (Hume, and Gordon, 1983; Karasawa et al., 2015; Clements et al., 2013) under basal conditions, primarily

around the vascular bundles. In humans and mice, these medullary M Φ are notably more active with their phagocytic and secretory behaviour with the hypersalinity stimulated M Φ producing more IL-6, IL-8, and TNF- α (Berry et al., 2017). Tissue resident perivascular F4/80⁺ M Φ in the renal cortex actively patrol the microvascular environment located between the endothelium and the basement membrane of tubules, (Stamatiades et al., 2016) but ultimately the density of pericytes (**Figure 1.8**) and M Φ (**Figure 1.10**) are greatest in the OM.

Both damage to and the low O₂ availability in the medulla encourages immune cell recruitment; M Φ migrate via CXCR₄/CXCL₁₂ and CCR₂/CCL₂ dependent chemotaxis (Berry et al., 2017; Ceradini, and Gurtner, 2005). In various rodent models of AKI, immune cell infiltration is present in early observations; residential macrophages (M Φ ; CX₃CR₁⁺) migrate within an hour of ischaemic injury (Basile et al., 2012), and in a murine ischaemia reperfusion model of AKI, IL-6 producing residential F4/80⁺ M Φ are specifically located adjacent to the vascular bundles 4-hours post reperfusion (Kielar et al., 2005). Furthermore, in rodent models of AKI circulating T-cells (CD28⁺) and infiltrating M Φ (CD68⁺) are present in this region within 3-4-hours, occluding the AVR (Ysebaert et al., 2004). The NG2-expression dependent, pericyte-mediated PMN recruitment (**section 1.3.1**) is seemingly reflected in these findings,;the recruitment of PMN is potentially co-ordinated by DVR NG2⁺ pericytes and residential M Φ , whilst the PMN extravasation involves NG2⁻ pericytes on the AVR. The evidence of renal pericytes being directly involved in the propagation of the immune response is ever growing.

1.4.1 Renal Pericytes co-ordinate inflammation in the kidney.

In the kidney there is a wealth of evidence showing involvement of renal pericytes in key stages of inflammation. In both humans and mice, samples from AKI patients show FoxD₁⁺ pericytes activate the NLRP3 inflammasome, leading to IL-1 β and IL-18 secretion, signalling which is both propagated and amplified by pericyte TLR-2/4 and MyD88-activation (Leaf et al., 2016). Interestingly, after ischaemic damage, F4/80⁺ M Φ migrate to vascular bundles to recruit inflammatory cells via production of IL-6 (Kielar et al., 2005), yet, Leaf *et al*, have recently found pericytes had significantly higher expression of IL-6 compared with EdC, epithelial cells and even M Φ in mouse kidneys following IRI (Leaf et al., 2016) suggesting perhaps pericytes recruiting PMN with IL-6 secretion. Vascular adhesion molecule VAP-1 and the generation of a H₂O₂ gradient, is mediated by PDGFR- β ⁺ pericytes to enhances PMN infiltration (Tanaka et al., 2017),

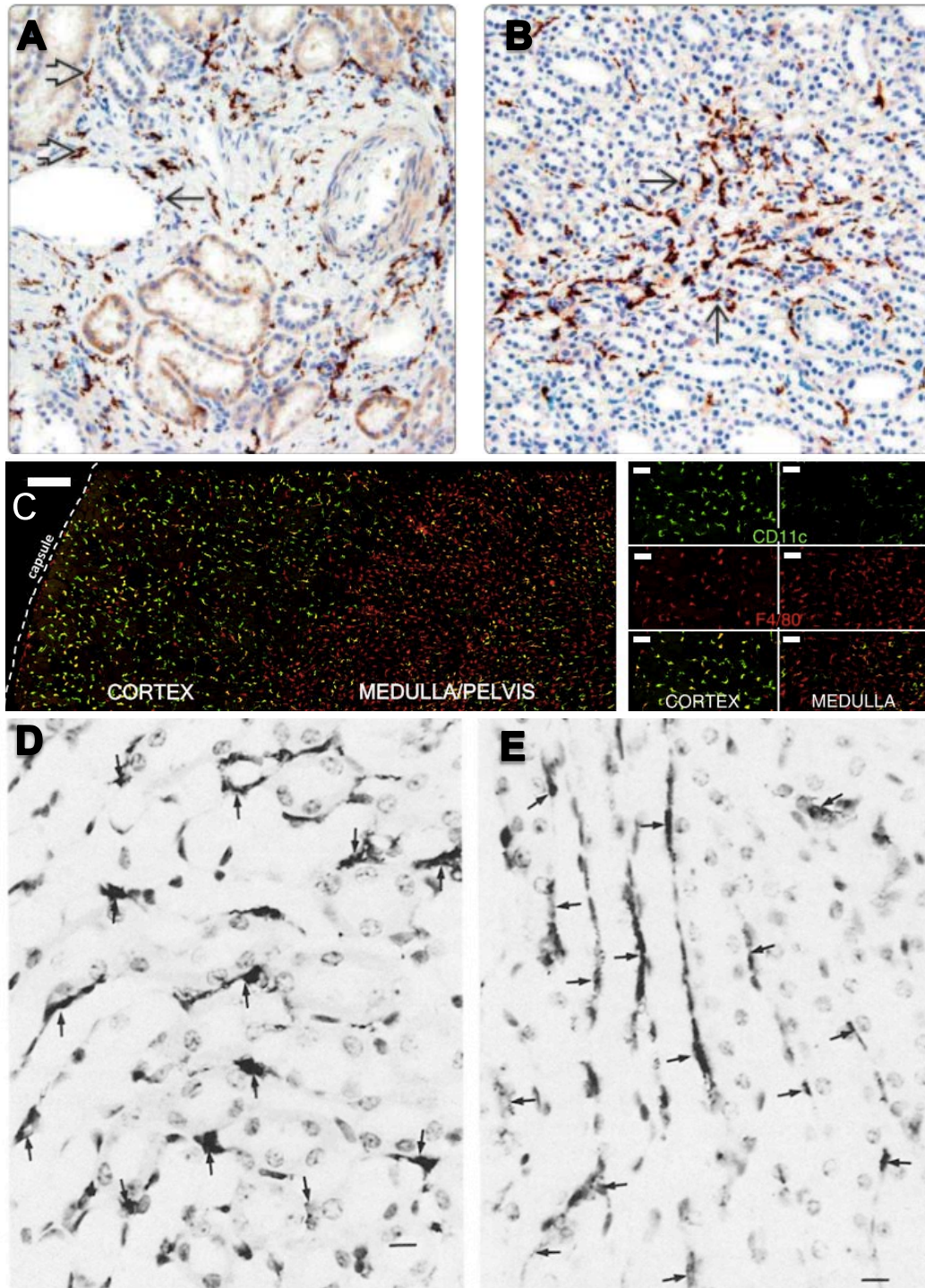


Figure 1.10 . In healthy mammalian kidneys immune cells have preponderance in the medulla.

(A-B) show CD163⁺ residential MΦ distribution in the (A) cortex and (B) medulla. In both regions the MΦ are apposite capillaries, with the greatest density along the vascular bundles in the outer medulla. open black arrows show apposition to venules, and black arrows show apposition to vascular bundles. Data Taken from (Colvin, 2019). (C) Shows a low magnification image of a healthy C57BL/6J kidney slice showing CD11c(*green*) and F4/80 (*red*) in the cortex and medulla, with the combined density greatest in the medulla. Scale bar is 300µm on low magnification, and 50µm on high magnification images on the right. Data taken from (Berry et al., 2017) (D-E) Shows higher magnification of outer medullary F4/80 staining as a healthy cross-section (D) through the medullary rays and (E) longitudinally through medullary rays highlighting numerous F4/80⁺ macrophage (MΦ) surrounding the capillaries and tubules in a C57BL/6J kidney. Black arrows highlight F4/80⁺ cells. Scale bar is 10µm. Data taken from (Hume, and Gordon, 1983).

assisted by CD169⁺ PVM (Karasawa et al., 2015), further suggesting specific pericyte involvement. In addition to this, in the absence of PDGFR- β ⁺ pericytes, early indicators of inflammation; the increased presence of F4/80⁺ M Φ , and expression of IL-6 and TNF- α , are not detected (Lemos et al., 2016).

In a unilateral ureteric obstruction (UUO) murine model PDGFR- β ⁺ pericytes secrete complement factor C1q (Xavier et al., 2017), which instructs the progression of innate to adaptive immunity (Hosszu et al., 2010). Recruitment of immune cells is not the only reported immune activity of pericytes as further recent data from show aspects of pericyte-mediated antigen presentation or inactivation of T-cells in both mice and humans (Liu et al., 2018). In acute T-cell mediated rejection of renal allografts in humans, INF- γ -stimulated (α -SMA⁺) pericytes express Indoleamine-pyrrole 2,3-dioxygenase (IDO1), a memory T-cell inhibitory protein (Liu et al., 2018). Interestingly, as inhibition of T-cells is anti-inflammatory, these studies suggest further pericyte-subpopulation-mediated inflammation, though this requires further study.

Pericytes are spatially close to residential immune cells in both basal and pathogenic settings, and it has been suggested this proximity is indicative of cell-cell communication (**section 1.3.1**). In a rodent model of acute brain injury, PDGFR- β ⁺ perivascular cells have a close spatial relationship with allograft inflammatory factor 1 (Iba1)⁺ M Φ , with increased cell-to-cell contact post injury encouraging fibrosis (Riew et al., 2018). It has been found using knock-in mice with PDGFR- β mutations, that genes encoding immune factors are upregulated by increased PDGFR- β signalling (Olson, and Soriano, 2011). In the human kidney it has also been proposed that cell-cell contact between M Φ and pericyte-derived myofibroblasts encourage fibrosis (Campanholle et al., 2013), with a close spatial and temporal relationship between CD163⁺ and CD204⁺ M Φ and fibroblasts during healing (Eardley et al., 2008; Nikolic-Paterson et al., 2014). It is possible that coupled with the increased density in the OM, pericyte-M Φ cell-cell contact is potentially indicative of communication, this is how MRP14⁺ PMN instruct α -SMA⁺/NG2⁻ pericytes to dilate and thereby extravasate (Wang et al., 2012). An interpretation of this renal data, in line with what was discussed in **section 1.3.1** is summarised in **Figure 11**. However, it is important to consider the reported co-expression of PDGFR- β , NG2, F4/80, and CD163, amongst other markers (**section 1.3.3.1**).

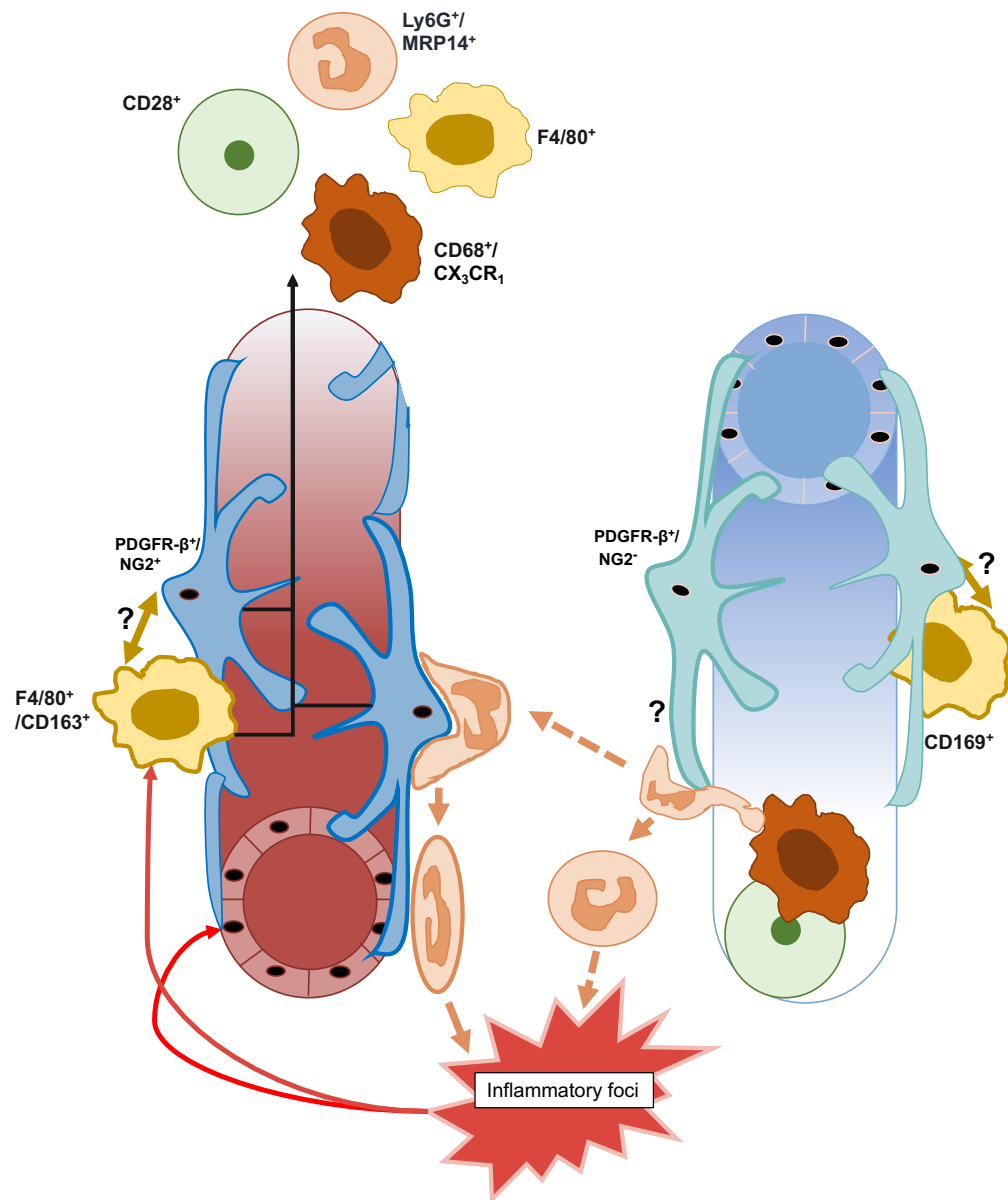


Figure 1.11 Proposed co-ordination of the immune response at the vasa recta capillaries by pericytes.

The inflammatory foci stimulates both residential macrophage (MΦ; *yellow*) and NG2⁺/PDGFR-β⁺ pericytes (*blue*) on the DVR to communicate (dark yellow arrow) secrete pro-inflammatory mediators IL-1β, TNF-α, IL-6, MIF, IL-33 and CCL2 (black arrows) to recruit more immune cells including more MΦ, infiltrating MΦ (*orange*), T-cells (*green*) and polymorphonuclear leukocytes (*peach*). These immune cells travel along the vasa recta and towards a H₂O₂ concentration gradient generated by NG2⁺/PDGFR-β⁺ pericytes (*turquoise*) on the AVR, that have detached from the endothelium. PMN can pass through the destabilised endothelial cell layer, as well as communicate directly via cell-cell contact with NG2⁻ pericytes to dilate the capillary and migrate into the interstitial space via PECAM-1 mediated transmigration (thick border), at areas of low matrix protein expression. Infiltrating MΦ and T-cells also extravasate via the AVR which can lead to congestion and blockage of the AVR. If the process is the same across tissues some immune cells can amble to the inflammatory foci (peach dashed arrows), whereas a small population will be instructed by the NG2⁺ pericytes on the DVR expressing ICAM-1, MIF, MAC-1, and LFA-1 (thick border), sensitising them and directing them directly to the inflammation (solid peach arrow) in an NG2-dependent manner. MΦ also express ICAM-1 (thick border) and are necessary for both recruitment (DVR; F4/80⁺ mouse; CD163⁺ human) and enabling extravasation (AVR; CD169⁺). Gradients indicates a chemotactic gradient on the DVR (red), and expression of matrix proteins α-SMA and Collagen IV as well as H₂O₂ concentration gradient on the AVR (*blue*). A “?” Highlights unclear proposed communications between cells.

1.4.1.1 NG2 and PDGFR- β , though not other pericyte markers are reportedly expressed by immune cells

Pericyte subpopulations identified with niche markers do not appear to have any overlapping expression. Although spatially close, PDGFR- β^+ eGFP- L10a⁺pericytes, do not co-stain with macrophage marker F4/80 or T-cell marker CD3 (Ferland-McCollough et al., 2016). Gli1⁺ pericytes often come into close contact with F4/80⁺ M Φ , though co-expression does not occur in the OM (Fabian et al., 2012), and CD248⁺ pericytes do not appear to influence the inflammatory response as no difference in CD45, CD3, or F4/80 staining was observed (Smith et al., 2015). However, both anti-NG2 and PDGFR- β appear to label M Φ (**section 1.3.3.1**) so caution is needed, and further identifying criteria are necessary to discriminate between pericytes and M Φ . The notable characteristic pericyte “bump-on-a-log” morphology (Peppiatt et al., 2006) may be useful in this instance concurrently with antibody labelling.

1.5 Species specific differences in behaviour can influence translatability.

Use of a valid model is important when trying to address specific research questions. However, equally useful is seeing what is conserved across species, whilst considering the species-specific physiology. Despite plentiful data showing species-dependent differences in responsiveness (Boswell et al., 2014; Steven et al., 2017), translating findings across species can be confounded by such differences (Natoli et al., 2013; Ellenbroek, and Youn, 2016) or the use of inconsistent experimental methods (Steven et al., 2017), affecting interpretation of the data. For example, in septic shock models with multiple different; methods to induce disease, set experimental time-points for data acquisition, and different strains and species used, it is difficult to accurately characterise the response to disease. However, when these are considered species-independent pathways can be identified *i.e.* conserved behaviours across species, which aids translatability to humans (Steven et al., 2017).

Even within the same animal, tissue-variation might confound data; LPS stimulated VCAM-1 and ICAM-1 varies between the heart, mesentery, brain and small intestine within the same animal (Henninger et al., 1997). Methodology is a key consideration, in the kidney not using comparable M Φ marker CD68, and instead opting for F4/80 in the mouse, led to conflicting results over glomerular M Φ infiltration between mice, and what was measured in rats and humans (CD68⁺) (Masaki et al., 2003). Lack of

investigations into inter-species heterogeneity, or assuming between species findings will be conserved in a “like-for-like”-manner *i.e.* findings in the rat will be identical to findings in the mouse, has likely led to erroneous conclusions. As such, the use of the same methods in different species allows more holistic interpretation of data (Vandamme, 2014), and gives better generalisation to the findings.

If a novel model performs in a way that the literature suggests it should it demonstrates predictive validity of the model and thus data generated (Denayer et al., 2014). Data generated in differing rat and mouse models are often used to corroborate findings using the assumption that physiology is similar, if not equivalent, between them (Downs, 2011), yet evidence demonstrates they are markedly different in vascular profiles and responsiveness (Russell, and Watts, 2000; Cholewa et al., 2005; Hedemann et al., 2004; Zhao et al., 2009; Boswell et al., 2014), disease pathogenesis (Natoli et al., 2013; Ellenbroek, and Youn, 2016), susceptibility to disease (Neuhofer, and Beck, 2005; Hartner et al., 2003), inflammatory gene induction (Schroeter et al., 2003), receptor pharmacology (Sabolic et al., 2011; Schildroth et al., 2011; Russell, and Watts, 2000; Wiley, and Davenport, 2004), and enzyme activity (Martignoni et al., 2006), to name a few examples. This highlights that translation of models between species is not straightforward, and why species differences require consideration.

Data on the physiological response of a mouse or a rat model can only be understood in keeping with the frame of reference of the animal’s physiology. However, probing such differences can aid in translatability. By acknowledging and understanding these differences, they can be used as a frame of reference for comparative pathophysiology (Radermacher, and Haouzi, 2013). For example, use of 2-butoxyethanol in both species depleted vitamin E and increased ROS-production. However, rats have a significantly higher basal vitamin E level than mice, and as such mice were more sensitive to the ROS damage (Siesky et al., 2002). Subsequently, translating these findings to humans, it was concluded that humans would be resistant to ROS-induced damage following 2-butoxyethanol given the basal levels of vitamin E are 100x higher than that of the mouse (Cunningham, 2002). This allows both insight into the pathomechanisms of 2-butoxyethanol and translatability to humans.

For a better understanding of comparative physiology, it is beneficial to determine conserved behaviours whilst considering species differences. Interestingly, investigations into pericyte-mediated regulation of DVR have been conducted in both humans and rats, and show active regulation of vasa recta diameter by pericytes (Sendeski et al., 2013; Zhang et al., 2004; Crawford et al., 2012). In chapter 4, it is also demonstrated that murine pericytes, in a species-dependent manner, regulate the

DVR; this is a conserved behaviour of renal pericytes (discussed in more detail **chapter 4, section 4.4.**). Immune activity of pericytes is also present across species.

1.5.1 Cross-species and Cross-organ pericyte immune functionality is conserved, in a species dependent manner.

Discussed above in **sections 1.3 and 1.4** is the conserved inflammatory multifunctionality of pericytes present in human and animal models. Another consideration is that the immunogenicity of human pericytes appears to vary from that observed in animal models; rodent and porcine in vitro models secrete pro-inflammatory cytokines TNF- α , IL-1 β , and IFN γ , where human pericytes do not (Rustenhoven et al., 2017). Yet human CNS pericytes do secrete monocyte chemoattractant protein-1 (MCP-1) and interferon inducible protein 10 (IP-10/ CXCL10), which could increase immune cell recruitment (Jansson et al., 2014). Human placental NG2⁺ pericytes express CXCL1, CXCL8, MIF, CCL2, forming a structural and chemotactic microenvironment to traffic PMN in response to ATP and LPS (Stark et al., 2012), much like human renal pericytes (Leaf et al., 2016). As such, the inter-species nature of pericyte-mediated immune activity may be different in line with species-specific physiology *i.e.* CD8⁺/CD4⁺ T-cells express functional GABA-A receptors, but the subtype profile varies between mice, rats, and humans (Mendu et al., 2012), yet GABA is involved in T-cell modulation in all species (Bjurström et al., 2009). If immune functionality is conserved across animal models and enables elucidation of how pericytes are multifunctional these findings could hopefully translate across and inform human physiology and as such provide novel therapeutic targets to prevent the associated complications and progression of renal disease.

1.6 Summary and aims.

In the kidney, it has been observed that human DVR pericytes are contractile (Sendeski et al., 2013), and that renal M Φ across species congregate around the vasa recta (Colvin, 2019; Berry et al., 2017; Hume, and Gordon, 1983; Karasawa et al., 2015), with both human and mouse pericytes post-AKI showing inflammatory activation (Leaf et al., 2016). The trans-species trends in function and cellular distribution of both cell types having predominance in the OM is suggestive of a conserved cellular dynamics and function. As discussed in **section 1.4**, it appears pericyte-mediated direction of inflammation is conserved across tissues but ultimately

the relationships between pericytes and M Φ in the kidney warrants further investigation and delineation. However, given that the proteins used to identify M Φ (F4/80, CD68, CD163 etc.) in the above studies show spatial overlap (Karasawa et al., 2015), and reportedly co-label with markers expressed by pericytes (NG2⁺ and PDGFR- β ⁺) (Graeber et al., 1989; Balabanov et al., 1996; Komuro et al., 2017; Tigges et al., 2008; Rajantie et al., 2004), accurate identification of cells is essential in order to support this line of investigation.

The aims are as follows:

Chapter 3: The overall aim of this chapter is to assess the use of using rodent kidney slices in investigating the multifunctional nature of renal medullary pericytes by:

- i. Determining the suitability of anti-PDGFR- β for identifying pericytes the rodent live kidney slice model.
- ii. Determining the suitability of anti-CD163 and anti-CD68 for the identification of residential macrophage (M Φ) in the rodent live kidney slice model.
- iii. Determining any overlap in cellular expression with M Φ (anti-CD163) and pericyte (anti-NG2 and anti-PDGFR- β) markers.
 - a) Determine if co-expression can be encouraged in an emulated inflammatory environment with cytokines TNF- α and IL-1 β .
- iv. Characterise the spatial relationship between M Φ and pericytes.
 - a) Characterise any functional consequence of close proximity by measuring vasa recta diameter.

Chapter 4: Given the limitations from the rodent model in chapter 3, the overall aim is this chapter is establishing a companion kidney slice model using murine tissue, by:

- i. Characterising NG2⁺ pericyte density and morphology in murine kidney slices
- ii. Characterising the vasoactive responsiveness of murine pericytes on the vasa recta capillaries using endogenously produced vasoactive mediators.

Chapter 5: With the newly established murine live kidney slice model, the aim here is to assess use this tissue in investigating the multifunctional nature of renal medullary pericytes by:

- i. Performing acute superfusion experiments on murine kidney slices with TNF- α and IL-1 β
- ii. Repeating the aims as listed under the chapter 3 subsection above, using anti-F4/80 in place of anti-CD163.

2 GENERAL METHODOLOGY.

2.1 Tissue preparation and slicing

Experiments using either 9-week-old male C57BL/6J mice (C57) or 200-225g male Sprague-Dawley rats (SD; Charles River UK Ltd, Margate, UK) were conducted in accordance with United Kingdom Home Office Scientific Procedures Act (1968). This age of C57 was chosen as an approximate age-match to the weight of the SD used in the live rodent kidney slice model (Crawford et al., 2012). Animals were killed by cervical dislocation, kidneys isolated, the renal capsule was removed, and kidneys were placed in ice cold physiological saline solution (PSS) bubbled with 95% O₂/ 5% CO₂ for preparation for slicing. PSS contained (mM): NaCl (100), KCl (5), NaH₂PO₄ (0.24), Na₂HPO₄ (0.96), Na acetate (10), CaCl₂ (1), MgSO₄ (1.2), glucose (5), NaHCO₃ (25) and Na pyruvate (5) (Sigma-Aldrich Ltd, Dorset, UK). PSS pH was determined using a Hanna bench pH 209 meter (Hanna Instruments, Bedfordshire, UK) and adjusted to 7.4 using 0.1 M NaOH or 95% O₂/ 5% CO₂. Kidneys from either C57 mice or SD rats were fixed on an ice-cold slicing block and sliced using a Leica VT 1200 S vibrating microtome (Leica, Germany). To expose the renal medulla, the outer cortical dome region of the mouse and rat kidney was removed (1.2 cm and 3.5 cm respectively, from the exposed surface) after which 200-µm thick slices were cut serially. Descriptions of differences between rodent and murine kidney slice properties are presented in **Chapter 4 section 4.3.1**. Post slicing, kidney slices were kept for up to 4-hours in a holding chamber containing PSS bubbled with 95% O₂/ 5% CO₂ at room temperature (25°C) before experimentation.

2.2 Viability of C57BL/6J live kidney slices

To ascertain viability of cells within C57 kidney slices, slices were incubated at room temperature (25°C) for 20 mins with: 20 µM propidium iodide (PI; Sigma-Aldrich Ltd.), a red fluorescent nuclear and chromosome stain only able to permeate dead cells via damaged membranes; and 5 µM Hoechst 33342 (Hoechst; Invitrogen Ltd. UK), a blue fluorescent nuclear stain that binds to dsDNA in all cells. Both fluorescent compounds were made up in PSS bubbled with 95% O₂/ 5% CO₂ (1). After incubations, slices were washed with PSS for 5-minutes three times and then subsequently fixed for 15-minutes with 4% PFA (made in 0.1 M phosphate buffered saline, PBS, Sigma-Aldrich Ltd.).

Post-fixation slices were washed three times in 0.1 M PBS for 10-minutes each then mounted using Citifluor (Agar Scientific Ltd, Stanstead) and stored at 4°C in the dark prior to imaging.

Images were acquired from both the inner (IM) and outer medulla (OM) of stained slices, using a Carl Zeiss LSM 800 confocal microscope with a Plan-Apochromat 63x oil immersion lens (Carl Zeiss Ltd, Oberkochen, Germany) using immersion oil (#518F, Carl Zeiss Ltd, Oberkochen, Germany). At least 6 randomly selected regions of interest (ROIs) in the IM and OM were visualized. For visualization: PI was excited at with the argon laser line 561 nm, and emission detected by a at 566-697 nm; and Hoechst was excited at with the ultraviolet laser line 405 nm, with emission detected at 410-508 nm. Differential interference contrast (DIC) images of were also obtained using the transmitted light field, to see if the parenchyma was alive reference tubular and vascular structures. Stained (Hoechst alone; all cells) and co-stained (Hoechst and PI; dead cells only) cells were quantified using the cell counter plugin in the open-source image processing FIJI software (2) so the overall percentage of live cells in the kidney slices could be calculated with Equation 2.1.

$$\text{Live cells} = \left(\frac{(\#Hoechst^+ \text{ cells}) - (\#Hoechst^+ \text{ and PI}^+ \text{ cells})}{\#Hoechst^+ \text{ cells}} \right) * 100$$

Equation 2.1 Calculation for the percentage of live cells in murine kidney slices.

2.3 C57BL/6J pericyte characteristics.

Nerual-glia 2 (NG2)⁺-positive pericyte density in the SD kidney slice model has previously been established (1), so the NG2+ve pericyte density and morphology were determined in the C57 model (murine). For primary identification of NG2-positive pericytes on the murine vasa recta (n=4 animals, 2-3 slices per animal), live kidney slices were first incubated for 45-minutes with Alexa Fluor 488-conjugated isolectin B₄ (IB₄; i21411, Invitrogen Ltd.), prepared using PSS bubbled with 95% O₂/ 5% CO₂ at a concentration of 50 µg/mL at room temperature (25°C). IB₄ labels alpha-D-galactosyl residues expressed by the endothelial cells of non-primates, selectively staining murine renal capillaries (Laitinen, 1987) . After incubation, slices were given a 15-minute wash in PSS and fixed using 4% PFA. After fixation, three 10-minute washes with PBS (0.1 M; Sigma-Aldrich) were performed, then slices were permeabilised using 0.1% Triton-X 100 (Sigma-Aldrich Ltd, Dorset, UK) solution made in 0.1 M PBS for 10-minutes. Subsequently, non-selective binding of antibodies to structures in slices was blocked with a 2-hour incubation in 10% donkey serum, 90% 0.1% Triton-X 100/ 0.1

M PBS solution (DS-Triton) at room temperature before an overnight incubation with anti-NG2 primary antibody (rabbit; 1:200; AB5320, Millipore UK Ltd, Watford, UK), diluted in 10% DS-Triton, at 4°C.

Table 2.1 Concentration of agonists used for functional experiments.

Compound	Concentration	Compound	Concentration
A438079	10 µM	IL-1β	10 ng/mL
Ang-II	1 nM	Indomethacin	30 µM
	10 nM	NA	10 nM
	50 nM		30 nM
	100 nM		100 nM
	300 nM		300 nM
ATP	100 µM	PGE₂	1 µM
	1 mM		10 µM
	2 mM		100 µM
	3 mM	PSS + ET-1	10 nM
Bradykinin	1 µM	SNAP	10 µM
	10 µM		100 µM
	100 µM	TNF-α	10 ng/mL
BzATP	10 µM	Tyramine	100 nM
ET-1	1 nM		1 µM
	3 nM		10 µM
	5 nM		30 µM
	10 nM		100 µM

Ang-II; Angiotensin II, **ATP**: Adenosine-5'-triphosphate, **BzATP**; 2'(3')-O-(4-Benzoylbenzoyl) Adenosine5'-triphosphate **ET-1**; Endothelin-1, **IL-1β**; interleukin 1β, **NA**; noradrenaline, **PGE₂**; prostaglandin E₂, **PSS**; Physiological saline solution, **SNAP**; (S)-Nitroso-*N*-acetylpenicillamine, **TNF-α**; tumour necrosis factor-α.

The anti-NG2 primary antibody was probed using donkey-anti-rabbit conjugated with Alexa Fluor-555 secondary antibody (donkey, 1:200, A-31572, Invitrogen Ltd.), diluted in DS-Triton, via a 2-hour incubation. Post incubation, slices were washed in three times in PBS 0.1 M for 10-minutes then mounted using Citifluor (Agar Scientific Ltd, Stanstead) and stored at 4°C in the dark.

For analysis, both the IM and OM of stained slices were imaged using a Carl Zeiss LSM 800 confocal microscope with a Plan-Apochromat 63x oil immersion lens (Carl Zeiss Ltd, Oberkochen, Germany) using immersion oil (#518F, Carl Zeiss Ltd, Oberkochen, Germany). For visualization: Alexa Fluor-488 was excited with the argon laser 488 nm line and detected at 490-570 nm and Alexa Fluor-555 was excited with the argon laser line 514 nm, excited at 561 nm, and detected at 566-697 nm DIC bright field images were acquired alongside the fluorescence. Images were processed in the open-source FIJI software (2). For NG2⁺ pericyte density calculations, $\geq 4 \times 100 \mu\text{m}^2$ regions in both the IM and OM of every kidney slice were selected at random for comparison with the original rodent model for comparison (Crawford et al., 2012). In these regions, NG2⁺ pericyte soma size was calculated, by: measuring soma height, by measuring top-to-bottom from the side of the cell adjacent to the vasa recta wall; and soma width, the length of the pericyte running along the vessel. Pericyte process length along the IB₄-labelled vasculature (longitudinal), and around the vasculature (circumferential) were also measured as described previously (Crawford et al., 2012). IB₄-labelled vasa recta capillary diameter was measured at: a pericyte site, defined as the segment of the vessel underneath the pericyte soma and surrounded by circumferential processes; and at a non-pericyte site, defined as a segment of the vasa recta capillary with no observable pericyte soma. Values obtained were compared between the OM and IM as described in **Section 2.6**. Processes were not used for calculating overall pericyte size due to difficulty in discriminating between processes from different pericytes. Any subsequent comments of pericyte size relate solely to the soma.

2.4 Functional experiments and video analysis.

A single live C57 kidney slice was secured in a 1.25mL bath chamber on the stage of an upright Olympus microscope (model BX51WI, Olympus microscopy, Essex, UK) using a purpose-built platinum slice anchor. The slice was continuously perfused ($\sim 2.5\text{mL min}^{-1}$) with PSS bubbled with 95% O₂/ 5% CO₂ and maintained at room temperature ($\sim 25^\circ\text{C}$). Differential interference contrast (DIC) images of pericytes on

subsurface vasa recta capillaries (identified by their 'bump on a log' morphology; (Peppiatt et al., 2006)) were recorded through an Olympus 60X water immersion objective (0.9 NA). Real-time images of changes in the diameter of the vasa recta were captured as a video every second by an attached Rolera XR CCD camera (Qimaging, Surrey, Canada) and recorded using Image Pro Software (Media Cybernetics Inc., Bucks, UK). To establish a baseline vessel diameter, Slices were superfused with PSS alone for ~100s before the following vasoactive compounds were applied: A438079 (Tocris, UK) angiotensin II (Ang-II; Sigma-Aldrich, UK); 2'(3')-O-(4-Benzoylbenzoyl)Adenosine5'-triphosphate (BzATP; Tocris, UK) endothelin-1 (ET-1; Tocris, UK); adenosine 5'-triphosphate (ATP; Sigma-Aldrich, UK); Noradrenaline (NA; Sigma-Aldrich, UK); Bradykinin (BRADY; Sigma-Aldrich, UK); prostaglandin E₂ (PGE₂; Tocris, UK); Indomethacin (Sigma-Aldrich, UK); tyramine (Sigma-Aldrich, UK); (S)-Nitroso-*N*-acetylpenicillamine (SNAP; Tocris, UK); along with PSS only control superfusion experiments. Proinflammatory cytokines tumour necrosis factor- α (TNF- α ; Bio-Techne Ltd, UK), and interleukin 1 β (IL-1 β ; Bio-Techne Ltd, UK) were also applied (see Table 1.1 for concentrations). To demonstrate the responsive potential of the slices, PSS control experiments were subsequently followed by perfusion with ET-1; a response with ET-1 but not PSS would demonstrate the reason why no change in vessel diameter could be measured is due to lack of agonist in PSS.

Concentrations used were those that had previously been established in the rat live slice kidney preparation (Crawford et al., 2011; Crawford et al., 2012; Kennedy-Lydon et al., 2015); unpublished data (Data provided by Kirsti Daylor) see **Table 2.1** for concentrations used. All compounds were made up in PSS, oxygenated with 95% O₂/5% CO₂, with: Ang-II, ET-1, ATP, NA, Indomethacin, and tyramine used to evoke vasoconstriction; and PGE₂, BK, SNAP used to evoke vasodilation. Cytokines IL-1 β and TNF- α were also applied to kidney slices to determine how pericytes responded to these compounds. Initially slices were superfused for ~100s with PSS alone to establish the baseline for the vasa recta capillary, after which kidney slices were superfused with vasoactive compounds for ~250s, cytokines were superfused for ~600s, to match exposures times experiments previously performed in the SD model. After application of agonist, slices were superfused again with PSS to assess reversibility of pericyte-mediated changes in vessel diameter, with at least 10 minutes of a washout with PSS in all experiments. Time-series analysis of the change in vasa recta diameter was conducted using FIJI public domain software (Schindelin et al., 2012). For each experiment, a pericyte site and a non-pericyte site were identified along vasa recta capillaries, and the diameter at both sites were measured (D) every 5s for the entirety of the experiment, with each vessel acting as its own control. The average of the first 5 measurements of vasa recta width were used as the baseline

diameter (D_b) and normalised to be 100%. Every subsequent diameter measurement was expressed as a percentage change of the original baseline diameter (**Equation 2.2**). Due to limitations of resolving very small changes in vessel diameter in the images obtained, only changes in vasa recta vessel diameter greater than 5% of the baseline value were considered a response to the agonist applied, and only changes in vessel diameter greater than 5% were to be included in statistical analysis as described in **section 2.6**. A vessel was considered to have returned to baseline if it returned to within 5% of the resting diameter. This threshold was set as there is a limit with which the tissue can be resolved by the microscope and the corresponding pixel size measurable on-screen for analysis. It was calculated that 10 μm is approximately 47 pixels (Crawford et al., 2012). At least 3 replicates of experiments where the change in vessel diameter was >5% were taken.

$$\% \Delta \text{ vessel diameter} = \left(\frac{\text{Measured diameter } (D)}{\text{Mean baseline diameter } (D_b)} \right) * 100$$

$$D_b - \% \Delta \text{ vessel diameter} = \% \text{ constriction or dilation}$$

Equation 2.2 Calculation of the percentage change in vessel diameter

2.5 Immunohistochemical staining of Sprague-Dawley and C57BL/6J kidney slices with pericyte and macrophage markers.

Prior to use of these antibodies (Ab) in murine and rodent kidney sections for quantitative experimentation, the optimised dosage of these Ab needed calculating. The dilutions presented in table 2.2 were those found to be ideal for staining the 200- μm thick kidney sections. After which, initial exploratory experiments were conducted to assess suitability of multiple macrophage ($M\Phi$) markers; CD68 (rabbit: 1:100, AB125212; Abcam, Cambridge, UK), CD163 (mouse; 1:100, MCA342GA, Bio-Rad Laboratories, Oxford, UK), F4/80 (rat; 1:1000, MCA497R, Bio-Rad Laboratories, Oxford, UK), and the pericyte marker platelet derived growth factor receptor- β (PDGFR- β ; rabbit, 1:500; AB_2783647; kindly donated by William Stallcup, Sanford-Burnham Medical Research Institute) for use in the kidney slice preparations. NG2 was not included in these exploratory experiments as it has previously been used for renal pericytes (Crawford et al., 2012), but staining of PDGFR- β in the renal medulla has not yet been visually characterized. NG2 is also considered an identifier of a sub-population of pericytes (Stark et al., 2012), notably residing along arteriolar capillaries (Murfee et al., 2005; Stefanska et al., 2015); PDGFR- β is considered a pan pericyte marker, and, like NG2 (Smirkin et al., 2009; Prazeres et al., 2017) has reported co-

expression of MΦ identifying markers (Inaba et al., 1993). Anti-PDGFR-β was used in conjunction with Alexa Fluor-488 conjugated IB₄ determine locale along the IB₄-labelled vasculature.

To ascertain the basal cellular spatial relationships and any degree of co-staining between pericytes and resident MΦ in both C57 and SD: anti-NG2 and anti-PDGFR-β to stain for pericytes in both SD (Crawford et al., 2012) and C57; anti-F4/80 was used to stain residential MΦ in C57; and anti-CD163 was used to stain residential MΦ in SD, having both been used to characterise these cells in the respective species previously (Hume, and Gordon, 1983; Kaissling, and Le Hir, 1994), and previously reported overlap in these markers in the CNS (Balabanov et al., 1996; Yamazaki et al., 2017; Komuro et al., 2017). Slices were also stained with Hoechst 33342 (Hoechst; Invitrogen Ltd. UK), to accurately quantify and elucidate any overlap between pericyte and MΦ cells by correlation of their blue nuclei in images.

Table 2.2 Antibody dilutions table.

Antibody	Dilution	Reference	Antibody	Dilution	Reference
1 ⁰¹ Rabbit-α-NG2	1:200	AB5320; Merck-Millipore	1 ⁰ Rabbit-α-PDGFR-β	1:500	AB_2783647 Dr William Stallcup
1 ⁰ Rabbit-α-CD68	1:100	AB125212; Abcam	1 ⁰ Rat-α-F4/80	1:1000	MCA497R; Bio-Rad Laboratories
1 ⁰ Mouse-α-CD163	1:100	MCA342GA; Bio-Rad Laboratories	2 ⁰ Donkey-α-Rabbit conjugated Alexa-555	1:200	A-31572; Invitrogen Ltd.
2 ⁰² Donkey-α-Rat conjugated Alexa-488	1:200	A-21208; Invitrogen Ltd.	2 ⁰ Donkey-α-Mouse conjugated Alexa-488	1:200	A-21202; Invitrogen Ltd.
Alexa Fluor 488-conjugated isolectin B ₄	1:10	i21411, Invitrogen Ltd.			

¹⁰ = Primary antibody ²⁰ = Secondary antibody

For the basal characteristics of healthy tissue, fresh live kidney slices from C57 and SD were incubated with 5 μM Hoechst made in PSS, bubbled with 95% O₂/ 5% CO₂,

for 20-minutes. After incubations, slices were washed with PSS for three 5-minute intervals, and then subsequently fixed for 15-minutes with 4% paraformaldehyde (PFA) made in 0.1 M phosphate buffered saline (PBS, Sigma-Aldrich Ltd.). Post fixation, immunohistochemical staining was conducted as described in **Section 2.3**, with the respective primary antibody concentrations as listed above in **Table 2.2**. For the MΦ: to probe the anti-CD163, donkey-anti-mouse Alexa Fluor-488 (donkey, 1:200, A-21202, Invitrogen Ltd.) secondary antibody was used; to probe the anti-F4/80, donkey-anti-rat Alexa Fluor-488 (donkey, 1:200, A-21208, Invitrogen) secondary antibody was used; and to probe the anti-CD68, donkey-anti-rabbit Alexa Fluor-555 secondary antibody was used, which was also used to probe NG2 and PDGFR-β as described in **Section 2.3**.

Given reported low cell numbers of CD163⁺ MΦ in the rat (Kaissling, and Le Hir, 1994), and the possible dormant state of residential immune cells, SD and C57 slices were also incubated in pro-inflammatory cytokines TNF-α and IL-1β (R&D Systems, Abingdon Science Park) at a concentration of 10 ng/mL, made in PSS, to activate the MΦ, and possibly pericytes with MΦ functions. These slices were incubated for 4 hours with either; TNF-α, IL-1β, or PSS alone for 4 hours. In the experimental group of tissue slices that were incubated with inflammatory compounds as described above, these tissue slices were incubated with 5 μM Hoechst 33342 for the last 20-minutes of that incubation, prior to processing as described above in **section 2.2**.

and were excited and detected as described above in **section 2.3**. 33342 excited and detected as described in **section 2.2**. At least four regions of interest (ROI) were randomly selected for both the IM and OM, after which 10 μm deep z-stacks were acquired, with an optical plane area of 214.21 μm x 214.21 μm per slice of the stack, each plane 1 μm apart.

As measurement per μm² would overlook stereology of pericytes and MΦ for this analysis, the acquisition of a z-stack and reconstruction of the 3-D distribution allows for morphological heterogeneity in the cell counts. In a 2-D image the ratio of large nuclear profiles to small nuclear profiles in sections almost certainly does not equate to the actual ratio in the three-dimensional tissue (Bertram, 2001). ROI were determined by showing presence of both positively labelled MΦ and pericytes as these were my cells of interest, and ≥ 35 pericytes per ROI in the OM and ≥ 10 pericytes in the IM, due to differences in regional pericyte density, and influences of stimulation on pericyte densities (Crawford et al., 2012). ROI were determined by pericytes as the object of study. This number of pericytes allows for 200 counting events per animal in the OM and IM combined which ensures observed variation within a group is

dominated by the biological variation between experiments and not by the variation due to stereological sampling (Weibel et al., 2007; Bertram, 2001). Only whole cells were included in analysis, as determined by a non-bisected Hoechst 33342⁺ cell nuclei in frame. This depth of render balanced resolution of the structural and spatial arrangements of both pericytes and MΦ in the medulla, without influencing the fluorophores fluorescent signal.

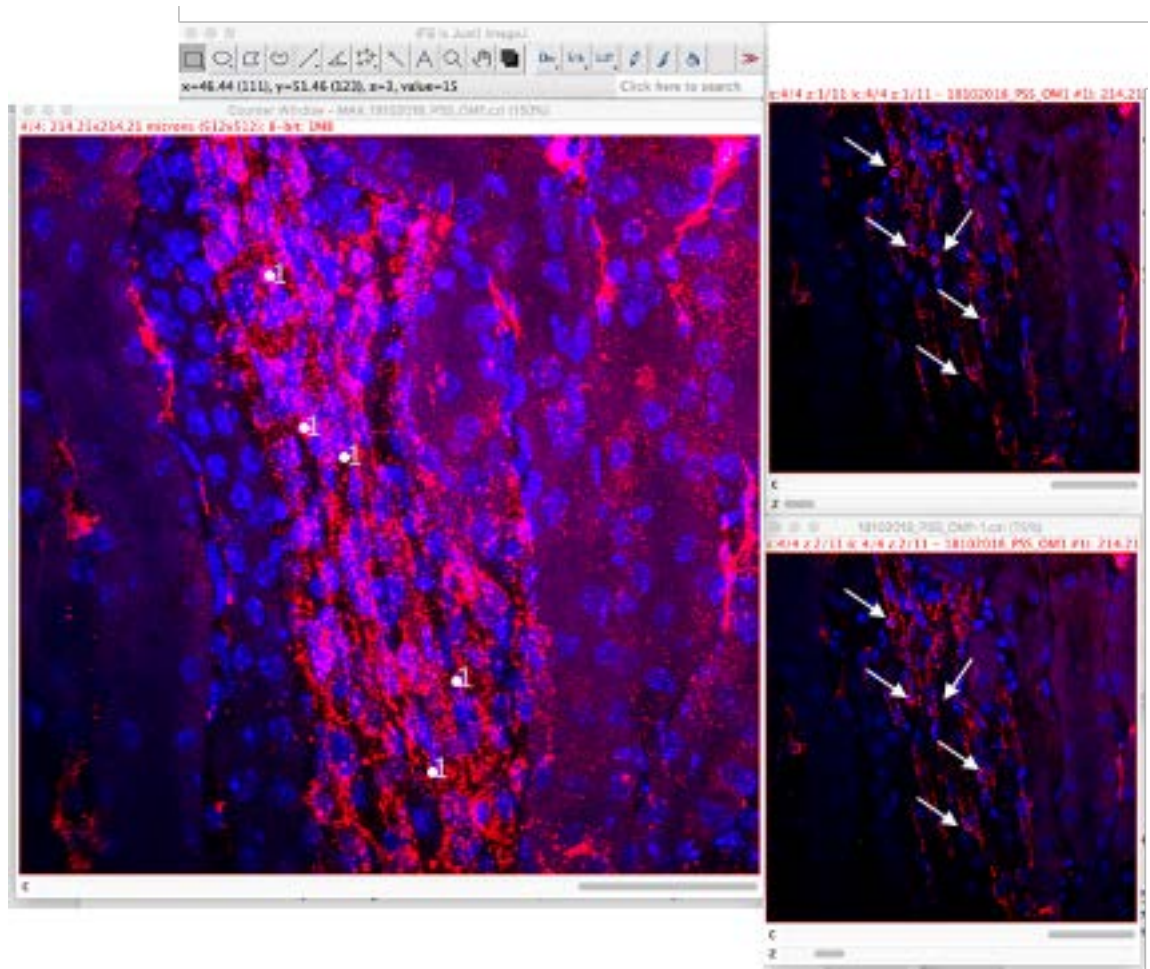


Figure 2.1 Distribution of NG2⁺ pericytes in a region of interest (ROI) from mouse tissue. Images are a representative confocal acquired ROI from murine tissue incubated for 4-hours in control physiological saline solution (PSS), fluorescently showing anti-neural-gial-2 (NG2; a;red) and Hoechst 33342 (H342;blue) fluorescence. On the left is the maximal intensity z-projection where cell counts were performed. Individual cell bodies can be identified by NG2⁺ immunofluorescence surrounding a Hoechst 33342⁺ nucleus, indicated by numbers in the reconstruction (left) and white arrows in the non-reconstructed images (right). As can be seen in the non-reconstructed images, pericytes occur across multiple planes and as such these were used in tandem to ensure accurate cell counts. 52 pericytes were counted for this ROI projection, though for clarity only 5 are shown.

Images acquired were processed off-line using FIJI software (Schindelin et al., 2012). In both SD and C57 for NG2⁺ experiments, dual channel images were used to quantify the number of pericytes or MΦ cells present individually, determined by red or green

staining surrounding a Hoechst 33342 (blue) stained nucleus from maximal intensity reconstructed z-stacks, so cell counts were not duplicate (**Figure 2.1**). As F4/80⁺-labelled MΦ were abundant and clearly defined these were counted in the same manner as NG2⁺-labelled pericytes, whilst CD163⁺ MΦ were scarce and did not require such extensive counting. After cell counts, tri-channel images were used to determine if any nuclei were positive for both red and green staining to establish if co-expression of receptors around the same nuclei occurred and therefore demonstrate co-labelling. For examples of co-labelling see **Figure 3.9**.

In the mouse, but not the rat spatial distance between between F4/80⁺-labelled and NG2⁺-labelled cell bodies. Subsequently, the percentage of the total F4/80⁺-labelled and NG2⁺-labelled cells per render that had cell-cell contact was calculated. Use of spectrally separated fluorophores for MΦ and pericytes allowed detection of independent cell populations as well as co-labelling. Cell-cell contact was defined as non-co-labelled, “oppositely” labelled Hoechst 33342⁺ nuclei that had no measurable space between the fluorescent soma, no pseudopodia or pericyte processes. The 10 μm depths of field of the renders allowed for greater resolution of this phenomena and allowed distinguishing of true contacts from instances in which pericytes and MΦ co-localized in the x-y plane but were in fact separated in the z dimension (**Figure 3.3** and **Figure 5.5** and **5.6**). For cells not in direct cell-cell contact, minimal distance between oppositely labelled soma were measured. This distance was measured in the same slice of the z-stack render where both the NG2⁺ and F4/80⁺ cells soma were visible. Distance was calculated with both the NG2⁺-labelled pericytes as the loci of measurement, and F4/80⁺-labelled MΦ as the loci of measurement because distances may vary as vascular-resident NG2⁺ pericytes, unlike F4/80⁺ MΦ, are not motile in control conditions.

NG2⁺ pericyte density per 100μ², and pericyte size for both PDGFR-β and NG2⁺ pericytes was calculated as described above in **section 2.3**. vasa recta diameter encircled by PDGFR-β⁺ or NG2⁺ pericytes was measured as described in **section 2.3**. For PDGFR-β⁺ experiments, maximal intensity z-stacks of the 10 μm-deep z-projections (214.21 μm x 214.21 μm) were reconstructed in order to calculate the percentage of the render area positive (%area) for PDGFR-β to quantify these pericytes, as reported in the literature previously (Ikeda et al., 2018; Craggs et al., 2015). NG2⁺ density has also been calculated this way (Nakano et al., 2017; Hesp et al., 2017), so for comparison between the two pericyte markers this was another way NG2⁺-pericyte density was calculated. The %area is not the same as an objective cell count and is a limitation of this method for quantification, and inter-sample variability of staining influences results, as observed in **section 3.3.4**. This technique is not as

readily reproducible, objective, nor comparable with studies that provide a cell count. However, there was no practical way of counting PDGFR- β^+ cells given the expansive nature of PDGFR- β staining (**Figure 3.1** and **5.1**), and has been reported as a difficulty for this marker previously (Floege et al., 2008). The use of the %area was deemed necessary here. All other measurements taken for PDGFR- β^+ pericytes and experiments involving this marker were the same as described above. Limitations to this method of quantification are further discussed in **section 3.4.1**.

2.6 Statistics

Values are presented as the mean \pm standard error mean (SEM), *n* numbers are presented as the number of animals used then the number of kidney slices. The number of animals, not slices, was used for calculation of the SEM. At least 3 animals were used per final series of experiments. SEM, not confidence intervals (CI) were used as *n* numbers of animals, not slices, were used to calculate the SEM. SEM falls as *n* increases, yet in this study *n* values were small and thus SEM here would not erroneously imply a small spread of data. Statistical significance was calculated using a two-tailed Student's t-test, paired or unpaired when relevant. For statistical analysis between differing concentrations of the same vasoactive agent used in the murine functional experiments, a one-way ANOVA with post-hoc Bonferroni correction. For statistical analysis between IL-1 β -stimulated, TNF- α -stimulated, and PSS control experiments, a one-way ANOVA with post-hoc Dunnett's tests were performed to compare treatment groups. Values were calculated using GraphPad PRISM 5.0 software (La Jolla, California). A value of $p < 0.05$ was considered statistically significant.

3 A RODENT LIVE KIDNEY SLICE MODEL TO INVESTIGATE THE MULTIFUNCTIONAL NATURE OF RENAL PERICYTES.

3.1 Introduction

Pericytes are a vascular-resident cell present throughout all tissues, and are responsible for providing structural support to the microvasculature and regulating capillary blood flow (Shaw et al., 2018), at the microcirculatory level. Functional evidence from isolated outer medullary descending vasa recta (OMDVR) (Silldorff et al., 1995; Pallone et al., 2000; Pallone, and Silldorff, 2001), and more recently the “live” rodent kidney slice technique (Crawford et al., 2011; Crawford et al., 2012), provides compelling evidence of renal pericytes responding to locally synthesized vasoactive agents, and can thereby independently regulate medullary blood flow (MBF). Loss of pericytes leads to renal dysfunction (Kramann et al., 2017), and their role in MBF regulation shows how integral pericytes are in maintaining homeostasis in the kidney.

However, emerging evidence suggests the quiescent activity of pericytes goes beyond haemodynamic regulation and can vary in an organ specific manner (for more detail see **Chapter 1 Section 1.2.2**). Yet, recent work has shown a cross-organ and cross-species, interactive role for pericytes in the innate immune system (Proebstl et al., 2012; Stark et al., 2012; Hung et al., 2017; Balabanov et al., 1996; Schreiner, 1992; Winau et al., 2007; Yang et al., 2016; Navarro et al., 2016). The perivascular position of pericytes is of strategic advantage for surveillance in both the intra- and extravascular space, as well as co-ordinating the immune response (**chapter 1 section 1.3**) (Navarro et al., 2016; Alon, and Nourshargh, 2013). In rats, humans, and mice inflammation is co-ordinated at the DVR (Kielar et al., 2005; Ysebaert et al., 2004), this pericyte multifunctionality is a cross species behaviour in the kidney (Liu et al., 2018; Xavier et al., 2017) (see **Chapter 1 section 1.4** for limitations).

This trans-species trend in function suggests a conserved activity of pericytes, much like pericyte-mediated regulation of vasa recta diameter (Sendeski et al., 2013). However, some early findings demonstrating immunoactivity of pericytes have been contested, highlighting the importance of accurate identification of cell types (Krueger, and Bechmann, 2010). There are multiple reasons why confusion exists over which populations of cell, residential macrophage (M Φ) or pericytes, are responsible for immunoactivity (see **chapter 1 section 1.3.3**). Much data on immunoactivity has been generated *in vitro* (**section 1.3**). *Ex vivo* analysis of extracted cell suspensions oversimplifies both M Φ and pericyte populations, and does not reflect their *in vivo*

morphology, distribution (Gordon, and Plüddemann, 2017; Gordon et al., 2014) or functionality (Stapor et al., 2014). Results can be further confounded by overlapping expression of classical resident M Φ markers CD68 (Rustenhoven et al., 2016) and CD163 (Balabanov et al., 1996; Honda et al., 1990), and commonly used pericyte markers NG2 (Moransard et al., 2011; Komuro et al., 2017) and PDGFR- β (Inaba et al., 1993; de Parseval et al., 1993). Objective cell quantification and immunohistochemical techniques are ideally used together to determine cell populations.

The use of the rodent “live” kidney slice model is beneficial for studying cellular diversity, and by preserving the renal architecture cellular communications are maintained (Stribos et al., 2016), and show exclusively residential M Φ with no source of circulating leukocytes (Stribos et al., 2016). The rodent slices in this technique are 200 μ m thick (Peppiatt-Wildman et al., 2012), which will allow for visualisation of the complex arrangement of renal M Φ and pericytes, and how that may change over time within the same animal; multiple slices mean an animal can act as its own time-point control. Immunohistochemical analysis of α -SMA expressing pericytes encouraged investigations into pericytes contractile capabilities, identifying renal pericytes co-expressing M Φ receptors, with consideration for the notable pericyte morphology (Attwell et al., 2016), may encourage more accurate investigation in pericyte multifunctionality.

As such, the primary aim here is to determine if the rodent kidney slice model is suitable for investigations into the multifunctional nature of renal pericytes, by i) validating the use of anti-PDGFR- β , -CD68, and -CD163 as identifying markers of pericytes and M Φ in the live slice preparation, ii) co-immunostaining with antibodies that reportedly identify both pericytes (anti-NG2 and anti-PDGFR- β) and M Φ (anti-CD68 and anti-CD163), and iii) seeing if co-expression is either basally present, or can be induced by emulating pro-inflammatory environments using TNF- α and IL-1 β , cytokines previously shown to encourage immune activities of pericytes (Proebstl et al., 2012; Pieper et al., 2013; Nehmé, and Edelman, 2008).

3.2 Methods:

Intact live kidney slices from Sprague-Dawley rats were obtained as described in the general methodology chapter and processed as described in **chapter 2 section 2.1**.

3.2.1 Immunohistochemical staining of Sprague-Dawley kidney slices.

See **Chapter 2** for more detail, but in brief, initial exploratory immunohistochemical experiments to identify whether antibodies are appropriate markers for identifying residential cell types were performed. Anti-CD68 (rabbit, 1:100; Abcam) and anti-CD163 (mouse; 1:100; Bio-Rad), were used to determine the presence of M Φ cells in the rodent kidney slices. To assess suitability of anti-PDGFR- β as a pericyte marker in the rodent slice preparation, immunohistochemical experiments were performed using Alexa Fluor 488-conjugated IB₄ (Invitrogen) to label capillaries and anti-PDGFR- β (rabbit, 1:500; William Stallcup) used to label associated pericytes. Markers were deemed suitable if positive immunofluorescence was identified combined with appropriate morphology.

For subsequent co-expression experiments, slices were incubated with anti-CD163 to identify M Φ and either anti-PDGFR- β or anti-NG2 (1:200, Merck-Millipore) to identify pericytes. Nuclear stain Hoechst 33342 5 μ M (Invitrogen) was included for positive identification for a cell body to enable identification of any overlap between the nuclei of pericyte and M Φ cells by correlation of their blue nuclei in images. Inclusion of rodent M Φ marker anti-CD163 was to also provide clarity as to whether anti-NG2 and anti-PDGFR- β exclusively stain renal pericytes and not M Φ . Experiments where kidney slices were fixed with 4% paraformaldehyde (PFA) immediately post Hoechst 33342 incubation were performed to see if under homeostatic conditions any co-expression of pericyte and macrophage markers occurred. These tissues that were freshly slices were classified as the “0-hour” experimental group. To stimulate co-expression of M Φ and pericyte markers, slices were stimulated with pro-inflammatory cytokines TNF- α and IL-1 β . The PSS controls in the cytokine stimulation experiments are referred to as the “4-hour” control.

Kidney slices were incubated in Hoechst 33342, and then washed with PSS, slices were then fixed in 4% PFA then washed in 0.1 M phosphate buffered saline (PBS).

Tissue then underwent permeabilisation in 0.1% Triton X-100, and a step to block non-specific antibody binding with 10% donkey serum solution, before an overnight incubation with primary antibodies. Subsequently, slices were washed with 0.1 M PBS and the primary antibodies were probed with fluorescent secondary antibodies donkey-anti-rabbit Alexa Fluor 555 (donkey, 1:200; Invitrogen), and donkey-anti-mouse Alexa Fluor 488 (donkey, 1:200; Invitrogen). Slices were then washed a final time using PBS, then mounted using Citifluor (Agar Scientific) and stored at 4°C in the dark. Unless otherwise specified, reagents are from Sigma-Aldrich.

Tissue sections stimulated with pro-inflammatory cytokines TNF- α , and IL-1 β (10 ng/mL; R&D Systems) were incubated for 4 hours prior to be processed as described above. Cytokine stimulations have a corresponding “4-hour” PSS-time control. Data acquisition and analysis was conducted as described in **chapter 2 section 2.5**.

3.2.2 Statistics.

All data is presented as mean values \pm standard error mean (SEM), *n* numbers are presented as the number of animals used, then the number of kidney slices. The SEM is calculated with the number of animals used in the IHC experiments. Statistical significance was calculated using a two-tailed Student's unpaired t-test for superfusion and “0 hour” PSS background experiments, and a one-way ANOVA with post-hoc Dunnett's test was used for cytokine-stimulated and control tissue that was incubated for 4-hours. Values were calculated using GraphPad PRISM 5.0 software (La Jolla, California). A value of $p < 0.05$ was considered statistically significant.

3.3 Results:

3.3.1 Vasa recta pericytes are identifiable via immunohistochemical staining with PDGFR- β .

The suitability of anti-PDGFR- β for labelling vasa recta pericytes was determined by the presence of Alexa-555 2° fluorescence (used to probe anti-PDGFR- β) adjacent to IB₄ labelled vasa recta capillaries, and by brightfield images used to confirm morphology. A positive pericyte identification required PDGFR- β ⁺ cells to present the notable morphology (**Figure 3.1(aii-iii)**); namely large, round cell bodies (Armulik et al., 2005) with branched cytoplasmic processes (Smith et al., 2012; Peppiatt-Wildman,

2013). PDGFR- β^+ -labelled cells were extensive throughout the rodent kidney, present in all regions, and closely associated with IB₄ stained vessels (**Figure 3.1(a)**). In the cortex, comparative to NG2, there is extensive expression throughout the interstitial zone of the cortical labyrinth, and from mesangial cells of the glomerular tuft. It is reportedly not expressed by smooth muscle cells of the arteries or podocytes in healthy tissue (Floege et al., 2008), corroborated by observations here (n=1 animal and 2 slices; **Figure 3.1(ai)**). Use of PDGFR- β in murine tissue concurrently (**section 5.3.2**) showed comparable staining and as such it was deemed that further validation of PDGFR- β was not needed and this antibody could be used for further study. Capillaries were distinguished based on linearity, as the medullary capillary plexus is extensively tortuous (Ren et al., 2014), whereas vasa recta capillaries are organised into straight vascular bundles (Pallone et al., 1998b). In the medulla, it is greatly expressed on pericytes around the vasa recta (**Figure 3.1(aii-iii)**).

These cells have a preponderance in the renal medulla, and it is likely not all the cells positively identified with PDGFR- β fluorescent stain are pericytes. Yet, on the vascular bundles PDGFR- β^+ -labelled pericytes show the notable large soma and “bump-on-a-log” pericyte-identifying morphology (Peppiatt et al., 2006). It is important to note, however, in the inner medulla anti-PDGFR- β stains interstitial fibroblasts (**Figure 3.1(c)**), as demonstrated by their “rung on a ladder” elongated morphology (Kriz, and Kaissling, 2013), yet these are still distinguishable from true pericytes. Interestingly, unlike with NG2⁺ pericytes, PDGFR- β^+ pericytes are occasionally paired along the vasa recta capillaries (**Figure 3.1(b)**) and PDGFR- β^+ -labelling does not reduce deep into the inner medulla (IM). Direct like-for-like comparisons of PDGFR- β^+ and NG2⁺ pericytes are presented below in **section 3.3.3**.

3.3.2 CD68 and CD163 expression is regionally specific in rodent kidney slices.

In this study, known rodent residential macrophage (M Φ) receptors CD68 and CD163 were targeted for their expression by both rat and human M Φ (Lee et al., 2008), as well as reported presence on pericytes (Balabanov et al., 1996; Pieper et al., 2014). Prior to co-labelling experiments with pericyte markers anti-NG2 and anti-PDGFR- β , these antibodies were trialled alone to determine their proximity to the medullary vasculature as no comment has previously been made for regional presence of CD163⁺ or CD68⁺ M Φ in a slice preparation. Usefulness for potential future identification of perivascular cells co-expressing M Φ and pericyte proteins could first be assessed by using the morphology and both the regional and perivascular location

of CD68⁺-fluorescently labelled or CD163⁺-fluorescently labelled cells. If no medullary presence of these markers were present, it is unlikely rodent vasa recta pericytes would express these cell surface proteins.

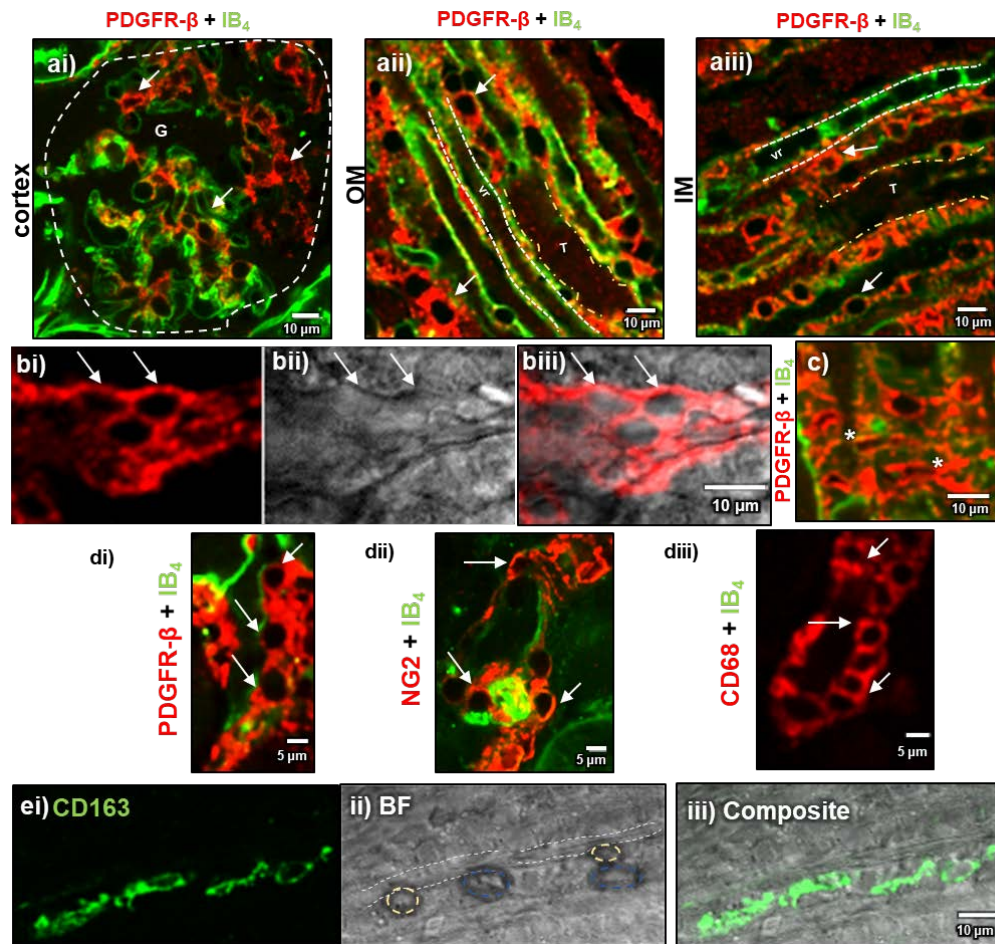


Figure 3.1 Platelet derived growth factor receptor- β (PDGFR- β)⁺, CD68⁺, and CD163⁺ positive staining in the Sprague-Dawley rat.

Representative regional images of PDGFR- β ⁺ staining (*red*) in the (ai) cortex, (aii) outer medulla (OM), and (aiii) inner medulla (IM) along IB₄⁺ capillaries. PDGFR- β ⁺ cells are extensively present throughout the rodent kidney. (b) PDGFR- β ⁺ pericytes were occasionally paired along vasa recta capillaries. (bi) PDGFR- β alone, (bii) bright field (BF), and (biii) composite image (biii; n = 2 animals and 5 slices). (c) Shows IM PDGFR- β ⁺ cells that have “rung-on-a-ladder” fibroblast morphology (*) (Kriz, and Kaissling, 2013). White arrow heads indicate pericyte and mesangial cell bodies, determined by glomerular or medullary location (diii) CD68 (*red*; n=1 animal and 3 slices) staining was perivascular and localised to arterioles, with comparable morphology to PDGFR- β ⁺ (di), and neural-gial 2⁺ (dii; NG2⁺; *red*; n=4 animals and 9 slices). (ei-iii) Representative images of CD163⁺ macrophage (M Φ ; *green*; highlighted with blue dashed circles). When present, CD163⁺ M Φ were closely apposite the vasculature (white dashed lines) and pericytes (yellow dashed circles). (ei) CD163, (eii) BF and (eiii) composite image (n=1 animal, and 1 slice). Structures (dashed lines); G = glomerulus, vr = vasa recta, T = tubule. Scale bars are 5 μ m or 10 μ m.

After preliminary experiments with anti-CD68 it was observed there were few cells positively expressing this receptor all of which were found in the cortex of the slice, perivascular to the arterioles as shown in **Figure 3.1(diii)**, Morphological and location-

dependent discrimination meant anti-CD68 was not used in subsequent experiments, not fitting criteria set out in the above paragraph (n=1 animal, and 1 slice). As murine experiments with CD68 were performed concurrently, and showed only cortical staining in a similar fashion (**Figure 5.2(c)**) CD68 is reported as a pan-M Φ marker (Davies et al., 2013), but also used to quantify infiltrating M Φ (Rubio-Navarro et al., 2016; Ysebaert et al., 2004; Mattson et al., 2006). In the context of this experimental model, there are no means by which infiltrating M Φ can be recruited as there are no circulating leukocytes (Stribos et al., 2016). Any circulating cells in the vasculature are likely to have been washed out during the slicing procedure as evidenced by the complete absence of red blood cells in the capillary in **Figure 3.1(e)**. Positively stained CD68 cells were morphologically similar to NG2⁺ and PDGFR- β ⁺ fluorescently labelled cells surrounding the arterioles (**Figure 3.1(d)**). However, data suggests these arteriolar cells form a complete muscular wall (Gattone et al., 1984; Molema, and Aird, 2012), and are therefore not spatially separated pericytes (Attwell et al., 2016). Summatively, morphological and location-dependent discrimination excluded CD68 from subsequent experiments.

Initial experiments with anti-CD163, like anti-CD68, showed expression by few cells (n=1 slice, 1 animal), yet CD163⁺ fluorescently-labelled cells were present primarily in the renal medulla, closely apposite the vasculature (**Figure 3.1(e)**). Some of these CD163⁺ M Φ had comparable large, ovoid cell bodies, as determined by bright-field images (**Figure 3.1(eii)** and **Figure 3.2(a-b), (d)**), to the pericytes identified residing along the vasa recta capillaries. The non-ovoid CD163⁺ M Φ were fusiform, with short processes (**Figure 3.2(c-e)**; images in **Figure 3.2** taken from the control 0-hour PSS experiments). Unlike pericytes, the CD163⁺ M Φ shape was spread along the vessel, it did not resemble staining shown in **Figure 3.2** for PDGFR- β ⁺ pericytes, or for NG2-identified pericytes (**Figure 3.3**; taken from the control 0-hour PSS experiments).

The CD163⁺ M Φ were interspersed throughout tissue sections, with cell bodies separated by microns in the z-plane. As such, to visualise the medullary CD163⁺ M Φ z-stack acquisition was deemed necessary for more accurate identification of co-labelling of cell soma with pericyte markers and CD163, and the spatial relationship between CD163⁺ M Φ and pericytes. A 2D rendition could also deceptively show co-staining when in-fact the cells reside side-by-side in the optical plane, as well as an underestimation of their total cell number, hence the need for a deeper render. Adding the third dimension, in the form of a 10 μ m-deep z-stack would enable accurate determination of co-expression around a Hoechst 33342-identified nuclei as CD163⁺ was sparse this better reflected their presence in the interstitium, illustrated in **Figure**

3.3. Given the proximity the vasculature of the CD163-identified MΦ, and residence in the medulla, anti-CD163 was used to co-stain with anti-NG2 and anti-PDGFR-β.

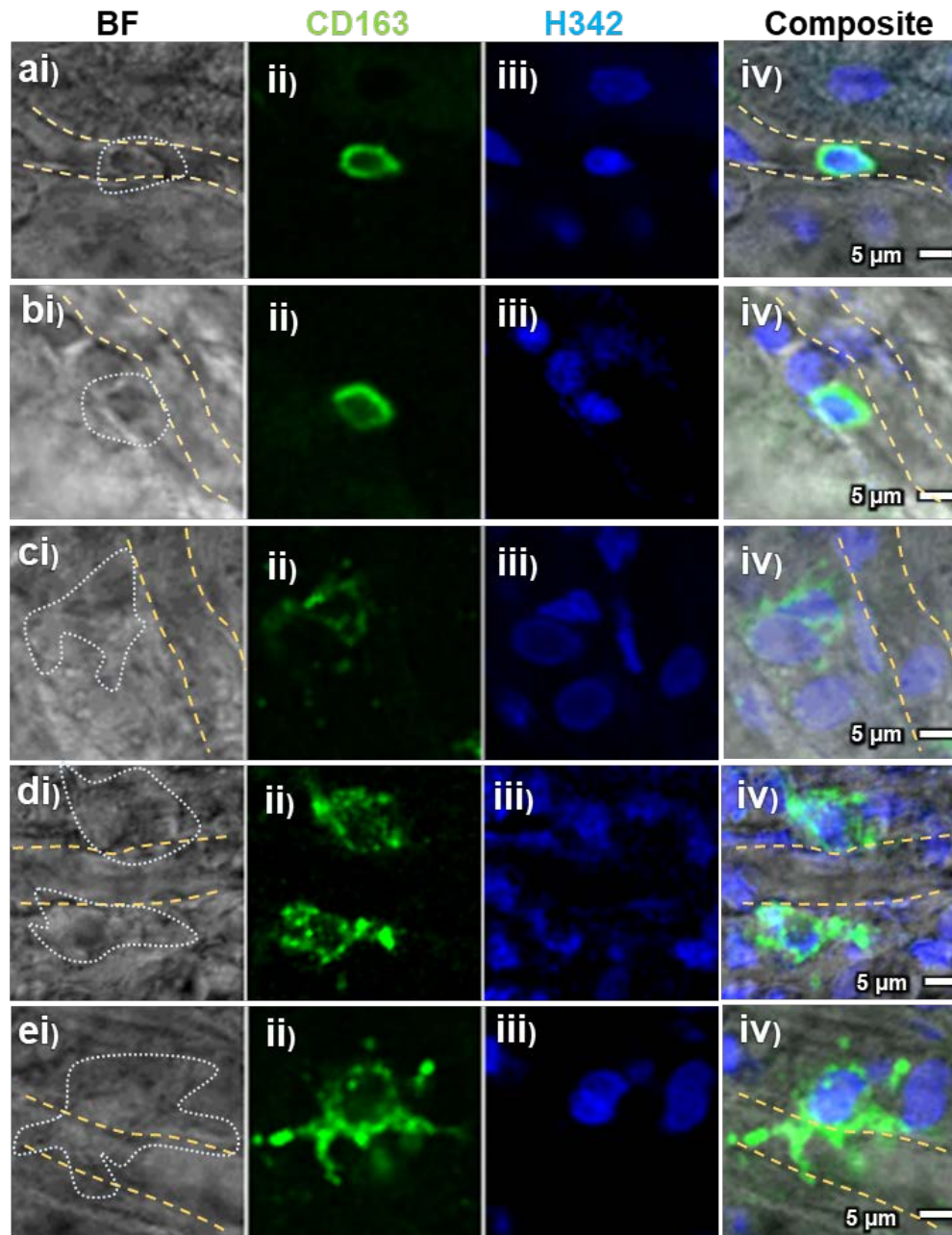


Figure 3.2 Morphologies of CD163⁺ macrophage (MΦ).

Images show renal CD163⁺ MΦ morphology, with brightfield (BF; *i*), CD163 (*green*; *ii*), Hoechst 33342 (H342; *blue*; *iii*) channels and the corresponding composite (*iv*) shown (**a-e**). CD163⁺ MΦ typically had ovoid morphology with no ramifications (**a-b**) or fusiform with short processes (**c-e**). Proximity to the vasa recta capillaries (yellow dashed lines) is demonstrated for MΦ (light blue dashed lines) in the BF. In BF Scale bars = 5 μm. n=3 animals, 18 slices.

3.3.3 PDGFR- β ⁺ pericytes are larger and more abundant than NG2⁺ pericytes.

Rodent kidney slices were co-immunostained with either: anti-NG2, anti-CD163 and Hoechst 33342; or anti-PDGFR- β , anti-CD163, and Hoechst 33342, to investigate any co-labelling of pericyte-identifying and M Φ -identifying markers around individual Hoechst 33342⁺ nuclei, and the spatial relationship between these cell-types. In other tissues the abundance of PDGFR- β -labelled and NG2-labelled pericytes vary dependent to where upon the vascular tree they reside (Murfee et al., 2005; Dore-duffy, and Esen, 2018); in the kidney this was established as approximately 3:1 PDGFR- β ⁺ to NG2⁺ pericytes (LeBleu et al., 2013). Anti-PDGFR- β had not been used as a pericyte identifying marker with the slice technique, so PDGFR- β ⁺ pericyte density, along with the pericyte size and the diameters of the vasa recta vessels on which they reside, were calculated, as staining with these antibodies outlines the

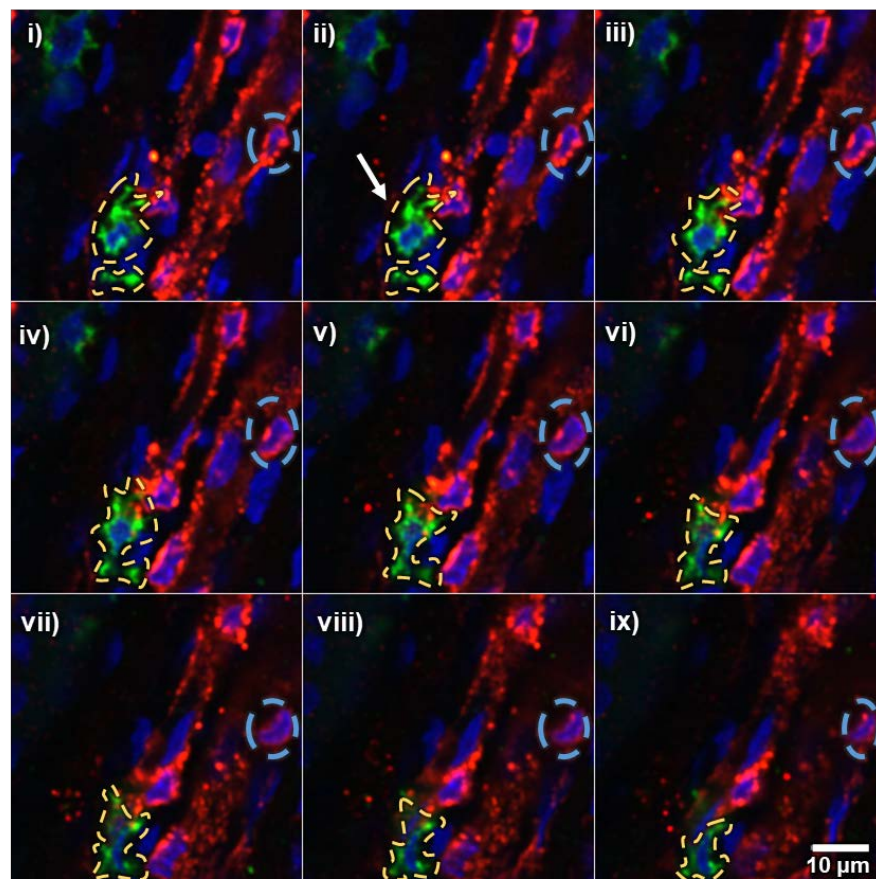


Figure 3.3 Features of neural-glia-2 (NG2)⁺ pericyte and CD163⁺ macrophage (M Φ) distribution.

Images (i-ix) are a composite montage of an 8 μ m section from a 10 μ m z-projection of fluorescent staining with anti-NG2 (*red*), anti-CD163 (*green*), and Hoechst 33342 (H342; *blue*). Pericyte cell bodies are highlighted with blue dashed circles, whilst M Φ are highlighted with yellow dashes around the entirety of the cell. White arrow indicates M Φ cell body, only present in the first 4 images. Of note is the regular, round morphology of pericytes throughout the render compared with the ramified, M Φ spread. n= 3 animals and 9. Scale bars are 10 μ m.

shape of the capillaries (Minocha et al., 2015). NG2⁺ pericyte density for rat kidney slices has been characterised as the number of NG2⁺-fluorescently labelled cell bodies per 100 μm^2 , and here in the rat was quantified to be 11.9 ± 0.9 cells per 100 μm^2 in the outer medulla (OM; **Table 3.1**), significantly greater than in the rat IM (7.2 ± 0.6 cells per 100 μm^2 , $p < 0.0001$; $n = 3$ animals and 9 slices; **Table 3.1**), non-significantly different with what was previously reported (Crawford et al., 2012).

As seen in **Section 3.3.1**, PDGFR- β^+ -labelling is not wholly pericyte-specific and made accurate cell quantification impractical. Therefore, PDGFR- β^+ and NG2⁺ pericyte density was calculated as described in **section 2.5**, the percentage of the area in the ROI occupied by positive immunolabelling. In healthy kidney sections, PDGFR- β^+ density was significantly greater in the OM than the IM ($32.6\pm 1.2\%$, vs $21.7\pm 1.2\%$, $p < 0.0001$; $n = 3$ animals and 9 slices), and significantly greater than the NG2⁺ density in both the OM ($10.1\pm 1.0\%$, $p < 0.0001$; **Figure 3.4(ei)**) and IM ($4.8\pm 0.6\%$, $p < 0.0001$; **Figure 3.4(ei)**) as might be expected from previous reports on PDGFR- β ; NG2 density in the kidney (LeBleu et al., 2013), and the expansive nature of PDGFR- β fluorescent labelling.

Table 3.1 Characteristics of platelet derived growth factor receptor- β (PDGFR- β^+) and neural-glial 2 (NG2)⁺ pericytes in the renal medulla.

	PDGFR- β		NG2	
	OM ¹	IM ²	OM	IM
Pericyte Density				
Area ³	$32.6\pm 1.2^{***}$	$21.7\pm 1.2^{***\$}$	10.1 ± 1.0	$4.8\pm 0.6^{\$}$
# ⁴	N/A		11.9 ± 0.9	$7.2\pm 0.6^{\#}$
Pericyte size, μm				
Height	5.6 ± 0.2	5.2 ± 0.3	$4.8\pm 0.2^{**}$	$4.3\pm 0.2^{**}$
Width	6.8 ± 0.3	6.2 ± 0.4	7.2 ± 0.3	6.8 ± 0.3
Vessel diameter, μm				
P ⁵ site	7.9 ± 0.3		$7.2\pm 0.2^*$	
NP ⁶ site	$10.0\pm 0.3\%$		$9.0\pm 0.2\%^*$	

Data presented are the mean \pm SEM. $n = 3$ animals and 9 slices, ≥ 200 pericytes per animal

¹OM= outer medulla, ²IM = inner medulla

³Area calculated as the average percentage of area occupied with fluorescent stain per 10 μm deep ($214.2 \mu\text{m}^2$) z-projection, ⁴# = Number of cells per 100 μm^2

⁵P = Pericyte, ⁶NP= non-pericyte

* $p < 0.05$; ** $p < 0.01$; and *** $p < 0.0001$ between NG2⁺ and PDGFR- β^+ pericytes

$\%$ $p < 0.001$ P vs NP.

$\$$ $p < 0.01$; $\#$ $p < 0.0001$ between the OM and IM.

Pericyte soma size was quantified as describe in **section 2.4**. PDGFR- β^+ pericytes, identified by positive fluorescent labelling and BF morphology and location on vasa recta capillaries, are significantly larger in height than NG2⁺ pericytes in the OM ($5.6\pm 0.2 \mu\text{m}$ vs $4.8\pm 0.2 \mu\text{m}$, $p < 0.01$; **Table 3.1**), and in the IM ($5.2\pm 0.3 \mu\text{m}$ vs $4.3\pm 0.2 \mu\text{m}$, $p < 0.01$; **Table 3.1**). However, there is no significant difference between PDGFR-

β^+ and NG2⁺ pericyte width in the OM ($6.8 \pm 0.3 \mu\text{m}$ vs $7.2 \pm 0.3 \mu\text{m}$, $p > 0.05$), or IM ($6.2 \pm 0.4 \mu\text{m}$ vs $6.8 \pm 0.3 \mu\text{m}$, $p > 0.05$). NG2⁺ pericyte characteristics here are consistent published NG2 pericyte characteristics (Crawford et al., 2012). Considering pericyte markers separately, there were no significant differences found between the OM and IM pericyte size for either stain ($p > 0.05$).

Considering pericyte markers separately with regards to vasa recta diameter; pericyte sites, the site where the pericyte soma resides, were significantly narrower than non-pericyte sites, the section of vessel without pericyte cell coverage. The average vessel diameter covered with NG2⁺-labelled pericytes reside was $7.2 \pm 0.2 \mu\text{m}$ at pericyte sites, and $9.0 \pm 0.2 \mu\text{m}$ at non-pericyte sites ($p < 0.001$; **Figure 3.4(eii)**, **Table 3.1**). For PDGFR- β^+ pericyte covered vasa recta, the average pericyte site diameter was $7.9 \pm 0.3 \mu\text{m}$, significantly narrower than non-pericyte sites ($10.0 \pm 0.3 \mu\text{m}$; $p < 0.001$; **Figure 3.4(eii)**; **Table 3.1**). The average vessel diameter measured for NG2⁺ pericyte covered vessels was significantly narrower than PDGFR- β^+ pericyte covered vessels at both pericyte sites ($p < 0.005$) and non-pericyte sites ($p < 0.05$; **Figure 3.4(eii)**; **Table 3.1**).

3.3.4 In control tissue, few CD163⁺ macrophages are present spatially close to vasa recta NG2⁺ and PDGFR- β^+ pericytes.

CD163⁺ M Φ were scarce in healthy rodent kidney slices, which has been previously reported (Kaissling, and Le Hir, 1994). As such, determining the regions of interest (ROI) was limited to, where possible, the definite presence of CD163 staining in order to investigate co-labelling and pericyte-M Φ spatial relationships and, the following data may overestimate CD163⁺ M Φ presence in the rat kidney (**Table 3.2**). When present, CD163⁺ cells were primarily located in the renal medulla, with no significant differences observed between the outer medulla (OM; **Figure 3.4(a), (c)**), and inner medulla (IM; **Figure 3.4(b), (d)**) and associated with the vasculature, interwoven throughout the tissue (**Figure 3.3**). The CD163⁺ M Φ present had two distinctive morphologies: very round without ramifications, or fusiform with processes (**Figure 3.2**). CD163⁺ M Φ reportedly have large cell bodies (Kaissling, and Le Hir, 1994), yet a degree of variation was observed, with the ovular CD163⁺ M Φ (**Figure 3.1(e)** and **Figure 3.2(a-b), (d)**) larger than fusiform CD163⁺ M Φ (**Figure 3.2(c)&(e)**).

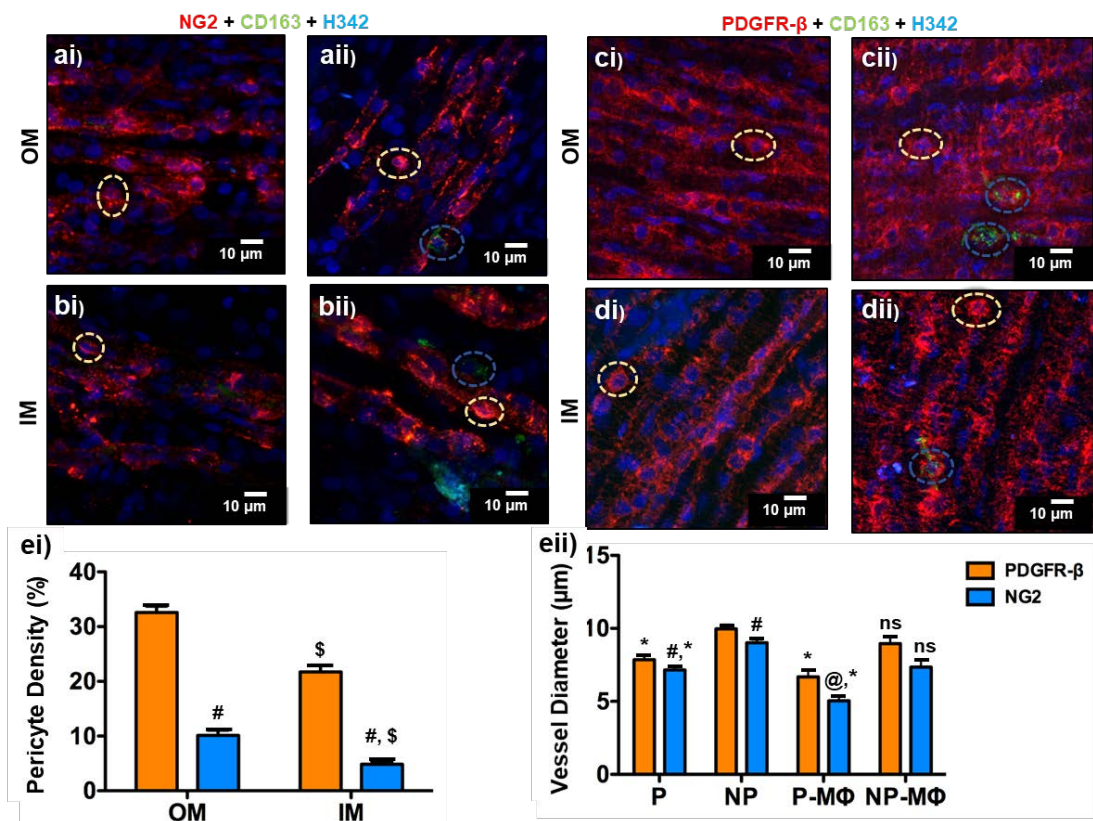


Figure 3.4 Both platelet derived growth factor receptor- β (PDGFR- β)⁺ vessel diameter, and fluorescent staining is significantly greater than neural-gial-2 (NG2)⁺ staining in the outer and inner medulla.

(a-d) are representative maximal intensity z-projections of 10 μm deep z-stack, confocal acquired images of outer (OM;a,c) and inner medullary (IM;b,d) staining with NG2 (ai-ii, bi-ii;red) or PDGFR-beta (a-iii-iv, b-iii-iv; red), CD163 (green), and Hoechst 33342 (H342; blue). Yellow dashed circles highlight pericyte cell bodies, as determined by H342 and either NG2⁺ or PDGFR- β ⁺ staining, whilst blue dashed circles indicate CD163⁺ M Φ . The respective pericyte densities, determined by the percentage of the reconstructed render occupied by positive staining for PDGFR- β (orange bar) and NG2 (blue bar) can be seen in (ei) The average vasa recta diameter at a pericyte site (P) or non-pericyte site (NP), and comparative pericyte sites with (M Φ) or without CD163⁺ M Φ contact can be seen in (eii) All bar graph values represent means \pm SEM. Scale bars = 5 or 10 μm . n= 3 animals, and 9 slices. [§] p<0.001 OM vs IM; # p<0.01, @ p<0.001, and & p<0.001 PDGFR- β vs NG2; * p<0.05 for P vs NP; ^{n.s} p>0.05.

In rodent kidney sections CD163⁺ M Φ were present, yet infrequent such that it was not possible to acquire images with CD163⁺ M Φ present in every render. However, as a subjective metric from all z-stacks acquired, when present there were 1-4 cells per acquisition in ~41% of OM renders from PDGFR- β experiments in the OM, and ~46% of IM renders; and ~46% of OM renders from NG2 experiments, and 58% of IM renders. This is not a true density of M Φ , and values are approximations only for ROI identified as described in **Section 2.5** and is a limitation of this study. On average, the number of CD163⁺ cells present were not significantly different between the IM and OM of NG2 (0.6 \pm 0.5 cells in the OM, 0.8 \pm 0.5 in the IM, p>0.05; **Table 3.2**) or PDGFR- β (0.7 \pm 0.6

cells in the OM, 0.7 ± 0.5 in the IM, $p > 0.05$; **Table 3.2**) groups. The averaging above likely overestimates their abundance in healthy tissue sections due to the infrequency of CD163⁺ MΦ and is not a cellular density.

Table 3.2 Characteristics of renal platelet derived growth factor receptor-β (PDGFR-β)⁺ and neural-gial 2 (NG2)⁺ pericytes in contact with CD163⁺ macrophages (MΦ).

	PDGFR-β		NG2	
	OM ¹	IM ²	OM	IM
Number of CD163⁺ MΦ				
	0.7±0.6	0.7±0.5	0.6±0.5	0.8±0.5
Pericyte size, μm				
Height	5.4±0.4*	4.7±0.5	4.3±0.2	4.1±0.2
Width	6.8±0.4	5.9±0.8	7.0±0.7	6.6±0.4
Vessel diameter, μm				
P ³ site	6.7±0.4 [§]		5.0±0.3 ^{**%}	
NP ⁴ site	9.0±0.5		7.3±0.5 ^{**%}	

Data presented are the mean±SEM. n = 3 animals and 9 slices, ≥ 200 pericytes per animal. The number of CD163⁺ MΦ (CD163⁺ MΦ (#)) are calculated as the average number of cells in the regions of interest identified here. This is not a cellular density.

¹OM= outer medulla, ²IM = inner medulla, ³P = Pericyte, ⁴NP= non-pericyte

* p<0.05; **p<0.01 for comparisons between NG2⁺ and PDGFR-β⁺ pericytes

[§]p<0.05; [%]p<0.001 for comparisons between values presented here and corresponding values in **Table 3.1**.

PDGFR-β⁺ fluorescent labelling was extensive and showed a sustained association with CD163⁺ MΦ, when present (**Figure 3.4(c-d)**), and as such direct measurements were not calculated for the spatial relationship between cell-types. In the NG2-labelled tissue, NG2 staining was not so prolific and cell soma are clearly distinguishable so the spatial relationship could be calculated specifically regarding the cell soma. Distance between NG2⁺ pericytes and CD163⁺ MΦ was measured in the same slice of the z-stack render, with the locus of measurement being CD163⁺ MΦ, where both the NG2⁺ and CD163⁺ cell soma were visible. Subsequently, the percentage of the total CD163⁺-labelled cells per render that had cell-cell contact was calculated. This was not performed with NG2⁺ pericytes as the focus of measurement due to limited numbers of MΦ.

There was approximately 75% contact between CD163⁺ MΦ and NG2⁺ pericytes in the OM, with cells 34.1 ± 5.4 μm apart if not in contact on average; and approximately 73% of CD163⁺ MΦ had contact in the IM, with cells 41.3 ± 13.3 μm apart, on average, when not in contact (**Figure 3.5**). In a solitary cell mathematical model (Francis, and Palsson, 1997), and whole *drosophila* wing sections (Bollenbach et al., 2008); as a realistic *in vivo* estimation, local cytokine signalling has been calculated to span a maximal effective distance of ~200-250 μm, or ~20-25 cell diameters, within 10-30-minutes (Francis, and Palsson, 1997; Bollenbach et al., 2008). This means communication is

possible between these separate M Φ and NG2⁺ pericytes. Both distance and the degree of contact were not significantly different for the OM or the IM (>0.05; **Figure 3.5**).

3.3.5 Pericytes in contact with CD163⁺ macrophages are constricted in healthy tissue.

As shown in Section 3.3.3, vasa recta diameter was significantly narrower at pericyte sites the non-pericyte sites, for PDGFR- β ⁺ and NG2⁺ pericyte covered vessels. Given the extent of M Φ -pericyte contact, characteristics of vasa recta diameter and pericyte soma with CD163⁺ M Φ contact were measured to determine if M Φ -pericyte contact had any influence on pericyte characteristics. It is not solely the pericyte cell body that is involved in communications, but pericyte processes that extend along the vasculature allow direct chemical communications between pericytes and neighbouring cells (Armulik et al., 2011). Their lack of inclusion here (and in **chapter 5**) is a limitation of this study as it understates any potential involvement the process may have in pericyte-M Φ communications or process-mediated communications. It may also mean the degree of pericyte-M Φ contact is greater than stated here. However, given the difficulty in discriminating between the pericyte soma associated with individual processes (**section 4.3.2**) versus the clarity of cell-cell contact (**Figure 3.3, 5.5, and 5.6**) their involvement was not commented upon.

Vasa recta where pericytes were in direct cellular-contact with CD163⁺ M Φ were significantly constricted at the pericyte sites comparative to those pericyte sites with no M Φ contact; 5.0 \pm 0.3 μ m at NG2⁺ pericyte sites (vs 7.2 \pm 0.2 μ m, p <0.001; **Figure 3.4(eii); Table 3.2**) and 6.7 \pm 0.4 μ m at PDGFR- β ⁺ pericyte sites (vs 7.9 \pm 0.3 μ m, p <0.05; **Figure 3.4(eii); Table 3.2**). There was a significant difference (p <0.001) between the corresponding non-pericyte sites for NG2⁺ pericyte covered vessels (7.3 \pm 0.5 μ m vs 9.0 \pm 0.2 μ m; **Figure 3.4(eii); Table 3.2**), but not for PDGFR- β ⁺ pericyte covered vessels (9.0 \pm 0.5 μ m vs 10.0 \pm 0.3 μ m; p >0.05; **Figure 3.4(eii); Table 3.2**).

No statistically significant differences in pericyte soma size were measured irrespective of M Φ contact. PDGFR- β ⁺ pericytes in contact with CD163⁺ M Φ were: 5.4 \pm 0.4 μ m (vs 5.6 \pm 0.2 μ m, p >0.05) in height, and 6.8 \pm 0.4 μ m (vs 6.8 \pm 0.3 μ m, p >0.05;) wide in the OM; and 4.7 \pm 0.5 μ m (vs 5.2 \pm 0.3 μ m, p >0.05) in height, and 5.9 \pm 0.8 μ m (vs 6.2 \pm 0.4 μ m) wide in the IM (**Table 3.2**). NG2⁺ pericytes in contact with CD163⁺ M Φ were: 4.3 \pm 0.2 μ m (vs 4.8 \pm 0.2 μ m; p >0.05) in height, and 7.0 \pm 0.7 μ m (vs 7.2 \pm 0.3 μ m,

$p > 0.05$) wide in the OM; and $4.1 \pm 0.2 \mu\text{m}$ (vs $4.3 \pm 0.2 \mu\text{m}$, $p > 0.05$) in height, and $6.6 \pm 0.4 \mu\text{m}$ ($6.8 \pm 0.3 \mu\text{m}$, $p > 0.05$; **Table 3.2**) wide in the IM. In the OM, NG2⁺ pericytes in contact with CD163⁺ MΦ were significantly smaller ($p < 0.05$) than their PDGFR-β counterparts (**Table 3.2**).

3.3.6 Exposure of live tissue to cytokines, and duration of incubation in control tissue sections, influences CD163⁺ macrophage presence in the renal medulla.

CD163 is considered to label mature resident MΦ, whilst some resident monocytes are considered dormant (Fabriek et al., 2005a; Polfliet et al., 2006). Maturation of MΦ occurs with cytokine stimulation. As pericytes have shown to acquire immune activity and upregulate expression of immune receptors upon stimulation with cytokines (Matsumoto et al., 2014; Takata et al., 2011; Pieper et al., 2014). The primary aim of cytokine stimulation of rat kidney slices here was to observe if NG2⁺-labelled or PDGFR-β⁺-labelled medullary pericytes were “dormant” and express MΦ markers when activated in an emulated inflammatory state. No co-labelling of MΦ-identifying and pericyte-identifying markers occurred in the 0-hour experiments yet did in stimulated PDGFR-β tissue. This is discussed below in **section 3.3.10**.

Slices that were kept in PSS control solution ($n = 3$ animals and 3 slices for both NG2 and PDGFR-β experiments) or incubated with either TNF-α (10 ng/mL; $n = 3$ animals and 5 slices for both NG2 and PDGFR-β experiments) or IL-1β (10 ng/mL, $n = 3$ animals and 5 slices for both NG2 and PDGFR-β experiments) for 4-hours had an increased presence of CD163⁺ MΦ. In the PSS time-matched control conditions after 4-hours, there were 1-3 MΦ in approximately 70% of renders in the OM (an average of 1.3 ± 0.3 MΦ, and 2.1 ± 0.6 MΦ in NG2 and PDGFR-β experiments respectively; **Table 3.3**), and 80% of renders from the IM (an average of 1.8 ± 0.4 MΦ, and 2.6 ± 0.5 MΦ in NG2 and PDGFR-β experiments respectively; **Table 3.3**). This represented a 1.5-fold increase in CD163⁺ MΦ presence in NG2 experiments, and 1.7-fold increase in PDGFR-β experiments under control conditions at 4-hours compared to the 0-hour PSS experiments. An important note is that whilst MΦ were present at a frequency that enabled selection of 3-4 ROI in cytokine stimulated tissue, the image acquisition area was still limited to where there was CD163⁺ fluorescent stain and as such, as discussed in Section 3.3.4, values here likely overestimate CD163⁺ MΦ presence in the renal medulla.

Table 3.3 CD163⁺ Macrophage (MΦ), platelet derived growth factor receptor-β (PDGFR-β)⁺, and neural-gial-2 (NG2)⁺ pericyte quantification after TNF-α and IL-1β stimulation.

	PDGFR-β			NG2		
	PSS	TNF-α	IL-1β	PSS	TNF-α	IL-1β
Number of CD163⁺ MΦ						
OM ¹	2.1±0.6	3.4±0.5	4.4±0.6*	1.3±0.3	3.4±0.4*	3.7±0.6**
IM ²	2.6±0.5	3.1±0.4	3.6±0.5	1.8±0.4	4.9±0.8*	3.8±0.5
Normalised CD163⁺ MΦ numbers, %						
OM	100.0±29.7	164.0±23.5	209.0±30.4*	100.0±25.8	257.9±27.9*	296.3±42.6**
IM	100.0±17.4	119.7±14.9	139.4±17.5	100.0±23.1	274.7±47.2*	212.4±29.8
Normalised pericyte area density, %						
OM	100.0±13.2	135.0±7.6*	121.6±6.4	100.0±18.8	51.9±3.6**	62.1±8.0*
IM	100.0±6.5	86.5±3.5	75.7±4.1*	100.0±7.9	59.9±4.6	62.1±5.4

Data presented as mean±SEM, n = 3 animals and 3-5 slices, ≥ 200 pericytes per animal.

(%) Values are the percent of the PSS control mean and are calculated as the percent of the 10 μm z-stack (214.2 μm²) occupied with positive stain.

¹OM = Outer medulla, ²IM = Inner medulla.

*p<0.05; **p<0.01 for comparisons between cytokine stimulation and PSS

After cytokine stimulation, the number of CD163⁺ MΦ present in the medullary regions ranged from 1-13 cells per field of view. Upon stimulation of rodent kidney slices with TNF-α, there was a 2.6-2.7-fold increase in the abundance of MΦ in both NG2 (257.9±27.9% in the OM, p<0.05, and 274.7±47.2% in the IM, p<0.05; (**Figure 3.6(d)**); **Table 3.3**) and 1.2-1.6-fold increase in PDGFR-β experiments (164.0±23.9% in the OM, p>0.05, and 119.7±14.9% in the IM, p>0.05; (**Figure 3.7(d)**); **Table 3.3**), although this increase was only significant (p<0.05) for NG2 experiments. Incubations with IL-1β caused 1.2-1.6-fold increase in MΦ in NG2 experiments (286.3±42.6% in the OM, p<0.01, and 212.4±29.8% in the IM, p>0.05; (**Figure 3.6(d)**); **Table 3.3**) and 1.4-2.1-fold increase in PDGFR-β experiments (209.0±30.4% in the OM control, p<0.05, and 139.4±17.5% in the IM, p>0.05; (**Figure 3.7(d)**); **Table 3.3**). In both NG2 and PDGFR-β experiments, the increase of MΦ was only significant in the OM, although there tended to be more MΦ in the IM. The difference between PDGFR-β and NG2 experimental groups likely related to a higher average of MΦ in the PSS 4-hour control in the PDGFR-β group (**Table 3.3**); total cell numbers were low, so the relative increases observed were greater. Direct cell counts can be seen in **Table 3.3**. Together these show pro-inflammatory cytokines activate dormant MΦ in the renal medulla, as does the slicing procedure itself given the increase in occurrence of CD163⁺ MΦ observed in the 4-hour PSS time-matched control sections. See above section regarding CD163⁺ cell number (**section 3.3.4**).

3.3.6.1 Cytokine stimulation did not influence contact between CD163⁺ macrophage and NG2⁺ pericytes.

As discussed below, cytokine stimulation significantly reduces NG2⁺-pericyte density so it is possible that the emulated pro-inflammatory environment encourages increased MΦ-pericyte communications but cannot be commented upon further here. Cytokine stimulation did not significantly influence the degree of CD163⁺ MΦ-NG2⁺ pericyte cell-cell contact with direct cellular-contact (**Figure 3.5(i)**), nor alter the distance of MΦ to the nearest NG2⁺ pericyte when not in contact from the time-matched PSS control in the IM. However, in the time-matched 4-hour PSS control OM values showed a significant 4.5-fold reduction in distance between MΦ and NG2⁺ pericytes comparative to the 0-hour PSS experiment $7.5 \pm 3.4 \mu\text{m}$ ($34.10 \pm 5.4 \mu\text{m}$; $p < 0.01$; **Figure 3.5(ii)**), although the percentage of OM CD163⁺ MΦ with NG2⁺ pericyte cellular-contact did not significantly change ($p > 0.05$).

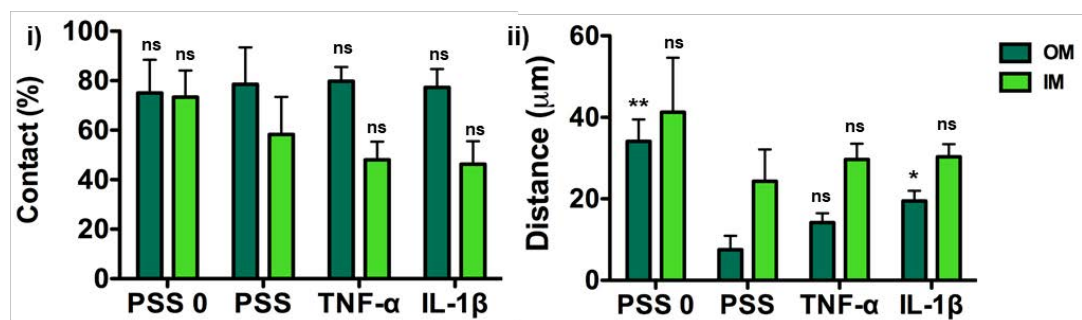


Figure 3.5 The effect of pro-inflammatory cytokines TNF-α and IL-1β on the spatial arrangement of neural-glia-2 (NG2)⁺ pericytes and CD163⁺ macrophages (MΦ).

In (i) bars represent the average percentage of total CD163⁺ MΦ present with NG2⁺ pericyte contact per 10 μm deep z-stack (214.2 μm²) (Contact %), in the outer (OM; dark green) and inner medulla (IM; light green). (ii) shows the corresponding distance for CD163⁺ MΦ without direct cell contact with an NG2⁺ pericyte to the nearest NG2⁺ pericyte. “PSS 0” are values from the basal experiments, “PSS” is data from the time-matched 4-hour PSS control. Data presented as mean ± SEM. * $p < 0.05$, ** $p < 0.01$, ns $p > 0.05$ when compared with “PSS”. $n = 3$ animals and 5 slices for TNF-α and IL-1β treatment groups, and $n = 3$ animals and 3 slices for PSS treatment group.

In the 4-hour PSS control, $78.0 \pm 14.9\%$ of OM CD163⁺ MΦ had direct contact with an NG2⁺ pericyte, and when not in contact MΦ were $7.5 \pm 3.4 \mu\text{m}$ apart on average. After TNF-α stimulation, $79.8 \pm 5.8\%$ of OM MΦ had contact with an NG2⁺ pericyte (**Figure 3.5(i)**), and $77.3 \pm 7.4\%$ of OM MΦ had contact with a pericyte upon IL-1β stimulation (**Figure 3.5(i)**). The corresponding distance between OM CD163⁺ MΦ and NG2⁺-labelled pericytes that did not have contact was a non-significant 1.9-fold increase with

TNF- α ($14.2 \pm 2.9 \mu\text{m}$; $p > 0.05$; **Figure 3.5(ii)**), yet after IL-1 β incubation it was a significant increase with cells 2.6-times further apart ($19.5 \pm 2.5 \mu\text{m}$; $p < 0.05$; **Figure 3.5(ii)**).

The degree of CD163⁺ M Φ -NG2⁺ pericyte contact in the OM tended to be greater than that observed in the IM, and the corresponding distance between cells not in contact tended to be larger in the IM than the OM, across all treatment groups. However, within the measurements taken from the IM, there was no significant difference ($p > 0.05$) in any of the treatment groups. The percentage of CD163⁺ M Φ in contact with an NG2⁺ pericyte was; $58.3 \pm 15.1\%$ in PSS, $48.1 \pm 17.3\%$ in TNF- α , and $46.32 \pm 9.2\%$ in IL-1 β , although there was an approximately 1.2-fold reduction in direct cellular-contact after cytokine stimulation (**Figure 3.5(i)**). Whilst not significantly reduced, there tended to be a higher degree of IM CD163⁺ M Φ -NG2⁺ pericyte contact in the 0-hour PSS control comparative to the time-matched 4-hour PSS treatment group ($73.3 \pm 10.8\%$; $p > 0.05$; **Figure 3.5(i)**).

The corresponding distances between of IM CD163⁺ M Φ not in contact with an NG2⁺ pericyte was also not significantly different ($p > 0.05$). In the time-matched PSS control, IM CD163⁺ M Φ were, on average, $24.2 \pm 7.8 \mu\text{m}$ apart from NG2⁺ pericytes (**Figure 3.5(ii)**). Upon TNF- α and IL-1 β stimulation this distance between cells was approximately 1.3-times greater at $30.6 \pm 3.8 \mu\text{m}$ ($p > 0.05$) and $30.3 \pm 3.1 \mu\text{m}$ ($p > 0.05$) respectively (**Figure 3.5(ii)**). In the 4-hour PSS time-matched control, the distance between CD163⁺ M Φ and NG2⁺ pericytes was, on average, approximately halved in the IM after 4-hours comparative to the 0-hour PSS experiments ($24.2 \pm 7.8 \mu\text{m}$ vs $41.3 \pm 13.3 \mu\text{m}$), although this change was not significant ($p > 0.05$; **Figure 3.5(ii)**).

The CD163⁺ M Φ -NG2⁺ pericyte close spatial arrangement, as discussed above in **section 3.3.4**, means that cell-cell signalling is possible within the distances measured. Cell-cell contact forms part of neutrophil-pericyte communication (Wang et al., 2012) and the high degree of contact between M Φ and pericytes, whilst CD163⁺ total cell numbers are low, is suggestive of communication between these cell types. It also suggests that such communication is a feature of CD163⁺ M Φ activities regardless of pro-inflammatory states, seeing as there was not a significant difference in the degree of contact in any experimental group.

3.3.7 Cytokine stimulation differentially altered PDGFR- β^+ and NG2 $^+$ -labelled pericyte densities.

In kidney slices exposed only to control PSS solution, there were 14.5 ± 5.0 NG2 $^+$ -labelled pericytes per $100 \mu\text{m}^2$ in the OM, and 8.9 ± 1.3 pericytes per $100 \mu\text{m}^2$ in the IM. Cytokine stimulation significantly reduced NG2 $^+$ pericyte density in both the OM and IM. Stimulation of kidney slices with TNF- α resulted in a significant 48% reduction of pericyte density versus the time-matched control in the OM (7.5 ± 1.2 pericytes per $100 \mu\text{m}^2$, $p < 0.01$), and 40% in the IM (5.3 ± 1.0 pericytes per $100 \mu\text{m}^2$, $p < 0.001$; **Figure 3.6(c)**; **Table 3.3**). Stimulation with IL-1 β caused less of a reduction in NG2 $^+$ pericyte density, yet it was still a significant decrease of 38% in the OM (8.9 ± 2.7 pericytes per $100 \mu\text{m}^2$, $p < 0.05$), and 38% in the IM (5.5 ± 1.1 pericytes per $100 \mu\text{m}^2$, $p < 0.001$; **Figure 3.6(c)**; **Table 3.3**).

Interestingly, when NG2 $^+$ pericyte density was calculated as the percentage area of the render occupied by positive fluorescent stain, as described in **section 3.3.3**, there was a non-significant reduction ($p > 0.05$) in the OM after incubation with either TNF- α ($6.2 \pm 0.9\%$) or IL-1 β ($8.1 \pm 0.9\%$) compared with the time-matched PSS control ($9.2 \pm 1.6\%$; $p > 0.05$). In the IM, TNF- α stimulation caused a non-significant reduction in NG2 $^+$ pericyte density ($3.2 \pm 0.5\%$ vs 4.7% density in PSS; $p > 0.05$), yet IL-1 β significantly reduced the IM NG2 $^+$ pericyte density by 40% ($2.8 \pm 0.3\%$; $p < 0.05$). This could be suggestive of a localised reduction of NG2 $^+$ pericyte density around the vasa recta capillaries as opposed to an overall reduction of NG2 $^+$ pericytes in the medulla.

Contrastingly, with PDGFR- β experiments there was an apparent reduction of in the area occupied by PDGFR- β^+ fluorescent labelling in the PSS time-matched control experiments. Comparative to the 0-hour area density of PDGFR- β^+ -labelling in PSS, there was an apparent, significant 45% reduction ($17.6 \pm 2.3\%$; $p < 0.05$) in the OM, and a non-significant reduction of 13% in the IM ($21.7 \pm 1.4\%$; $p > 0.05$) in the 4-hour PSS time-matched experiments. This could possibly relate to observations that CD163 $^+$ M Φ were located near the surface of the tissue in PSS 4-hour experiments demonstrated by the lower density of Hoechst 33342 $^+$ stain (**Figure 3.6(aiii)** and **Figure 3.7(aiii)**). CD163 $^+$ have been reported as a “wound-healing” (Martinez et al., 2011) or “remodelling” phenotype of M Φ (Olmes et al., 2015) so in control sections CD163 $^+$ are potentially migrating to the site of damage caused by preparing the rat kidney slices.

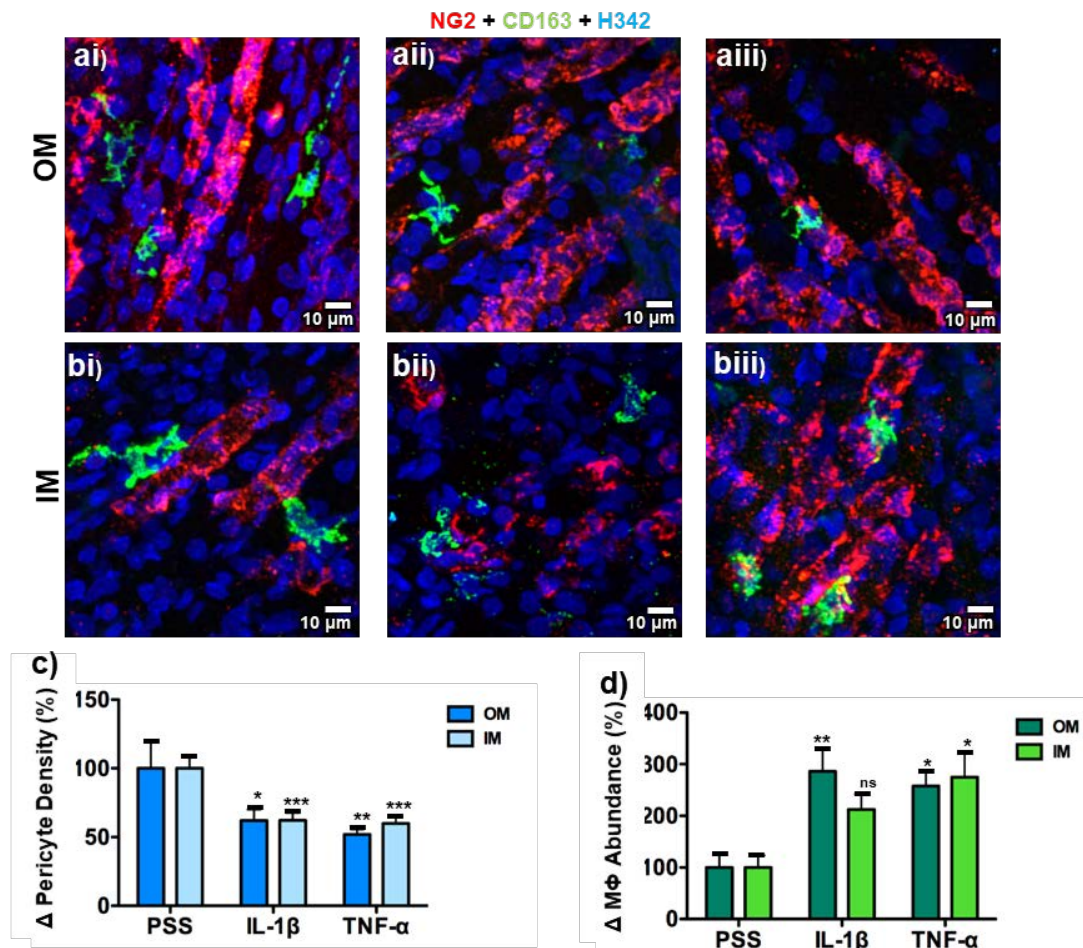


Figure 3.6 Effects of pro-inflammatory cytokine stimulation on CD163⁺ macrophage (MΦ) and neural-gial-2 (NG2)⁺ pericyte density in the outer (OM) and inner (IM) medulla.

Representative reconstructed maximal intensity z-projections of confocal-acquired images in (a-b) showing the effect of stimulation with TNF-α (10 ng/mL; i), IL-1β (10 ng/mL; ii) and the PSS control (iii) on NG2⁺-labelled pericytes (red) CD163⁺-labelled MΦ (green) in the OM (a) and IM (b). Cell nuclei were identified using Hoechst 33342 (H342; blue). The respective changes in pericyte density (c) and the MΦ abundance (d) are presented as the percent change from the PSS control. Data presented as mean±SEM. n= 3 animals and 3 slices for all but NG2 PSS, where n=4 animals and 4 slices. * p<0.05, ** p<0.01, *** p<0.001, ns p>0.05.

Comparatively, in cytokine stimulated tissue sections there was a greater abundance of CD163⁺ MΦ distributed throughout the tissue. Subsequently, changes of PDGFR-β⁺ pericyte density induced by cytokine stimulation presented here may not be representative of actual changes in density. TNF-α stimulated kidney slices showed a significant increase of pericyte density of 1.4-times that of the time-matched control (23.8±1.3%; p<0.05) in the OM, and a 1.2-times reduction of PDGFR-β⁺-labelled pericyte density (18.7±0.8%; p>0.05 **Figure 3.7(c); Table 3.3**) in the IM. With IL-1β treated sections, there was a non-significant 1.2-fold increase in PDGFR-β⁺ pericyte density in the OM (21.4±1.3; p>0.05), and a significant 1.3-fold reduction in the IM (16.4±0.9%; p<0.05; **Figure 3.7(c) Table 3.3**).

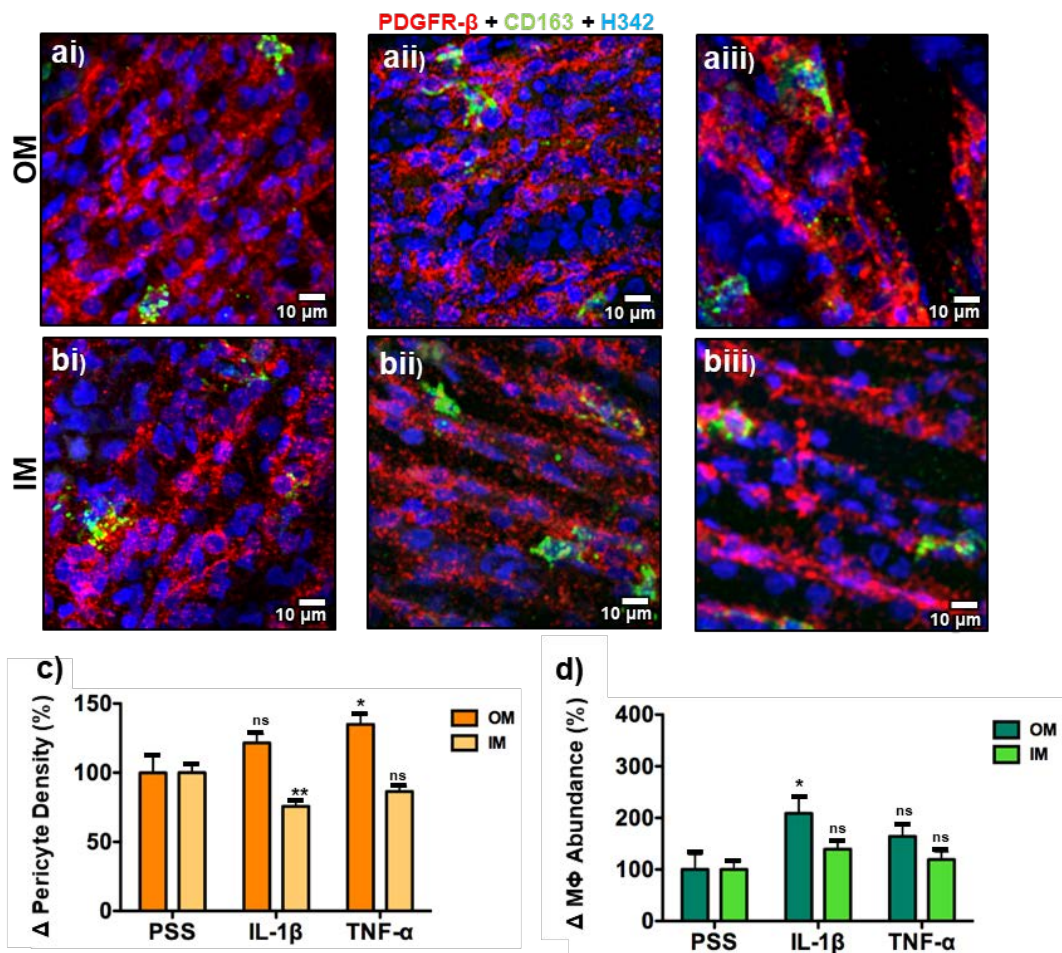


Figure 3.7 Effects of pro-inflammatory cytokine stimulation on CD163⁺ macrophage (MΦ) and platelet derived growth factor receptor-β (PDGFR-β)⁺ pericyte density in the outer (OM) and inner (IM) medulla.

Representative reconstructed maximal intensity z-projections of confocal-acquired images in (a-b) showing the effect of stimulation with TNF-α (10 ng/mL; i), IL-1β (10 ng/mL; ii) and the PSS control (iii) on NG2⁺-labelled pericytes (red) CD163⁺-labelled MΦ (green) in the OM (a) and IM (b). Cell nuclei were identified using Hoechst 33342 (H342; blue). The respective changes in pericyte density (c) and the MΦ abundance (d) are presented as the percent change from the PSS control. Data presented as mean±SEM. n= 3 animals and 3 slices * p<0.05, ** p<0.01, ^{ns} p>0.05.

3.3.8 Cytokine stimulation differentially altered PDGFR-β⁺-labelled and NG2⁺-labelled pericyte covered vasa recta diameters.

From initial experimentation (section 3.3.5), it was observed the vasa recta diameter was significantly narrower at pericyte sites than non-pericyte sites (Table 3.1; p<0.0001), for both PDGFR-β⁺ and NG2⁺ pericytes. Further to this, vasa recta where pericytes had cell-cell contact with CD163⁺ MΦ were constricted to a significantly greater degree than pericytes without MΦ contact (Table 3.2; p<0.0001). Subsequently, after cytokine stimulation, measurements of vasa recta diameter were

also taken from both vessels where pericytes had MΦ contact, and from vessels where pericytes had no MΦ contact in all treatment groups. In time-matched 4-hour PSS control tissue sections, much like the initial experiments, NG2⁺ pericytes with direct cellular contact with CD163⁺ MΦ were significantly more constricted than pericytes without; the average vasa recta diameter was 5.9±0.7 μm at pericyte sites where CD163⁺ MΦ were in contact with NG2⁺ pericytes, significantly narrower than vessels without NG2⁺ pericyte-MΦ contact (7.2±0.3 μm; p<0.05; **Table 3.4**). Vasa recta covered with PDGFR-β⁺ pericytes measured 6.0±0.5 μm in width at pericyte sites in contact with MΦ, compared to 7.5±0.5 μm (p<0.05; **Table 3.4**) at pericyte sites without MΦ contact. No significant difference was measured at non-pericyte sites (p>0.05; **Table 3.4**).

In TNF-α treated tissue sections, when NG2⁺ pericytes had cell-cell contact with CD163⁺ MΦ the pericyte site diameter was significantly narrower than the PSS control pericyte sites with NG2⁺ pericyte-CD163⁺ MΦ contact (5.9±0.7 μm vs 4.8±0.3 μm; p<0.01; **Figure 3.8(i)**), but this was not the case for IL-1β treated sections (5.9±0.5 μm; p>0.05; **Figure 3.8(i)**). There was no significant difference observed in vessel diameters at the corresponding non-pericyte sites, regardless of treatment with TNF-α (8.4±0.6 μm in PSS vs 7.2±0.4 μm; p>0.05) or IL-1β (8.3±0.4 μm; p>0.05). At NG2⁺ pericyte sites without MΦ contact, vessels exposed only to PSS were significantly wider than TNF-α (7.2±0.4 μm vs 5.7±0.2 μm; p<0.01; **Figure 3.8(i)**), and IL-1β (5.9±0.3 μm; p<0.01; **Figure 3.8(i)**) stimulated vessels. Again, there was no significant difference in diameter at the corresponding non-pericyte sites for PSS (8.8±0.6 μm), IL-1β (8.3±0.3 μm; p>0.05) or TNF-α (7.8±0.2 μm; p>0.05) treatment groups. All values shown in **Table 3.4**.

Table 3.4 Effect of TNF-α and IL-1β stimulation, and CD163⁺ macrophage (MΦ) presence on vasa recta diameter encircled by neural-glial-2 (NG2)⁺ or platelet derived growth factor receptor-β (PDGFR-β)⁺ pericytes.

	PDGFR-β				NG2		
	PSS	TNF-α	IL-1β		PSS	TNF-α	IL-1β
CD163⁺ MΦ contact							
P ¹	6.0±0.5 [£]	6.5±0.3	5.6±0.3 [£]		5.9±0.7 [£]	4.8±0.3 [£]	5.9±0.5
NP ²	8.6±0.6	9.1±0.3	8.9±0.4		8.4±0.6	7.2±0.4	8.3±0.4
No CD163⁺ MΦ contact							
P	7.5±0.5	7.1±0.3	6.6±0.4		7.2±0.3	5.7±0.2 ^{**}	5.9±0.3 ^{**}
NP	9.5±0.7	10.0±0.4	10.1±0.4		8.8±0.4	7.8±0.2	8.3±0.3

Data shown as mean±SEM in μm, n = 3 animals and 3-5 slices, ≥ 200 pericytes per animal.

¹P = pericyte site ²NP = non-pericyte site

*p<0.05; **p<0.01 compared with PSS

[£]p<0.05 comparison between MΦ contact and no contact

Interestingly, unlike with NG2⁺ pericyte-covered vasa recta, cytokine stimulation did not significantly influence PDGFR-β⁺ pericyte covered vessel diameter, whilst CD163⁺

MΦ cell-cell contact did. Reportedly renal PDGFR-β⁺/NG2⁻ pericytes do not express contractile protein α-SMA (Wang et al., 2017), so this population may not be contractile. TNF-α stimulated PDGFR-β⁺ pericyte-covered vessels were 7.1±0.3 μm at pericyte sites (vs 7.5±0.5 μm in PSS, p>0.05; **Figure 3.8(ii)**), and IL-1β stimulated vessels were 6.6±0.4 μm (p>0.05; **Figure 3.8(ii)**) at pericyte sites. No significant difference in diameter was seen when comparing data for vessel diameter at non-pericyte sites in PSS (9.5±0.7 μm) with that measured in in TNF-α (10.0±0.4 μm; p>0.05; **Figure 3.8(ii)**), and in IL-1β (10.1±0.4 μm; p>0.05; **Figure 3.8(ii)**). The vessel diameters measured for PDGFR-β⁺ pericyte sites when the corresponding pericyte had CD163⁺ MΦ contact also showed no difference between treatment groups. In the PSS treatment group, the pericyte site with MΦ contact measured 6.0±0.5 μm, non-significantly different from measurements taken from IL-1β stimulated PDGFR-β⁺ pericyte-sites with MΦ contact (5.6±0.3 μm, p>0.05; **Figure 3.8(ii)**), or TNF-α stimulated sections (6.5±0.3 μm, p>0.05; **Figure 3.8(ii)**). There was no significant difference in the corresponding non-pericyte sites between PSS (8.6±0.6 μm), and TNF-α (9.1±0.3 μm; p>0.05) or IL-1β (8.9±0.4 μm; p.0.05; **Figure 3.8(ii)**). Interestingly, when considering the constricted nature of PDGFR-β⁺ pericytes with CD163⁺ cell contact, both PSS (p<0.05; as mentioned above) and IL-1β (p<0.05), but not TNF-α (p>0.05) showed a significant difference between the vasa recta diameters measured for PDGFR-β⁺ pericyte sites with and without CD163⁺ MΦ contact (p>0.05; **Table 3.4**). However, this data from IL-1β may be reflective of NG2⁺/PDGFR-β⁺ pericytes given this measured vessel diameter, and pericyte soma size presented below. All values shown in **Table 3.4**.

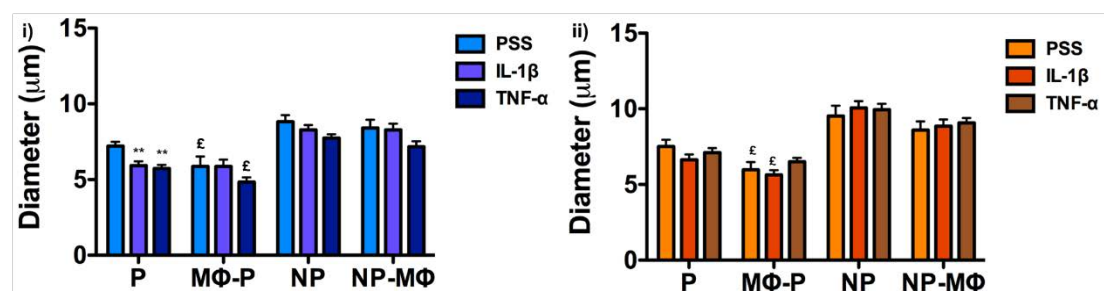


Figure 3.8 The effect of pro-inflammatory cytokines TNF-α and IL-1β and CD163⁺ macrophage (MΦ) presence on neural-glia-2 (NG2)⁺ or platelet derived growth factor receptor-β (PDGFR-β)⁺ pericyte-regulated vasa recta diameter.

(a-b) Show the effect of TNF-α (10 ng/mL; hatched bars) and IL-1β (10 ng/mL; checked bars) on vasa recta diameter, encircled by either PDGFR-β⁺ (a; orange bars) or NG2⁺ (b; blue bars) at a pericyte site (P) and corresponding non-pericyte site (NP). Also shown is the diameter at a pericyte in contact with an MΦ (P-MΦ) and its corresponding non-pericyte site (MΦ-NP). Data presented as mean±SEM. n= 3 animals and 5 slices for TNF-α and IL-1β, and 3 animals and 3 slices for PSS incubations for both NG2 and PDGFR-β. ** p<0.01 for comparison to PSS control; ε p<0.05 for comparison between sites with or without MΦ contact. See colour key for treatment groups.

3.3.9 Cytokine stimulation, but not CD163⁺ macrophage cellular contact, influenced NG2⁺ pericyte soma size.

It was noted in **Section 3.3.3** that whilst direct cellular contact of either PDGFR- β ⁺-labelled or NG2⁺-labelled pericytes with CD163⁺ M Φ influences vasa recta diameter (**Table 3.2**), there was no significant influence on pericyte soma size. However, for consistency, measurements were taken for both pericytes with and without M Φ contact in all treatment groups. In PSS, NG2⁺ pericytes in contact with CD163⁺ M Φ were: 3.8 \pm 0.4 μ m in height, and 5.4 \pm 0.5 μ m wide in the OM; and 3.8 \pm 0.3 μ m by 5.9 \pm 0.8 μ m in the IM. Without M Φ contact, they were 4.4 \pm 0.3 μ m in height by 6.4 \pm 0.4 μ m in width in the OM, and 4.4 \pm 0.2 μ m in height by 7.2 \pm 0.4 μ m in width in the IM (**Table 3.5**).

Table 3.5 Effect of TNF- α and IL-1 β stimulation, and CD163⁺ macrophage (M Φ) presence neural-glia-2 (NG2)⁺ or platelet derived growth factor receptor- β (PDGFR- β)⁺ pericyte soma size.

		PDGFR- β			NG2		
		PSS	TNF- α	IL-1 β	PSS	TNF- α	IL-1 β
CD163⁺ MΦ contact							
OM ¹	H ³	5.4 \pm 0.5	4.9 \pm 0.5	3.8 \pm 0.4*	3.8 \pm 0.4	3.9 \pm 0.2	3.5 \pm 0.3
	W ⁴	6.4 \pm 0.4	6.3 \pm 0.6	6.5 \pm 0.5			
IM ²	H	5.2 \pm 0.7	5.5 \pm 0.3	5.2 \pm 0.3	3.8 \pm 0.3	3.8 \pm 0.2	4.0 \pm 0.3
	W	7.5 \pm 0.3	6.2 \pm 0.4	6.6 \pm 0.4			
No CD163⁺ MΦ contact							
OM	H	5.6 \pm 0.3	5.4 \pm 0.4	4.7 \pm 0.4	4.4 \pm 0.3	3.7 \pm 0.1*	3.6 \pm 0.2**
	W	7.3 \pm 0.4	6.5 \pm 0.4	7.3 \pm 0.4			
IM	H	5.1 \pm 0.4	4.5 \pm 0.4	5.0 \pm 0.3	4.4 \pm 0.2	3.5 \pm 0.1***	3.4 \pm 0.2***
	W	7.0 \pm 0.5	6.5 \pm 0.4	6.7 \pm 0.6			

Data shown as mean \pm SEM in μ m, n = 3 animals and 3-5 slices, \geq 200 pericytes per animal.

¹OM = outer medulla; ²IM = inner medulla

³H = height; ⁴W = width.

*p<0.05; ** p<0.01; *** P<0.001 for comparison with PSS

NG2⁺ pericyte height, but not width, was significantly altered upon exposure to both TNF- α and IL-1 β . However, when NG2⁺ pericytes had cell-cell contact with a M Φ , there was no significant difference in height or width observed between all treatment groups, suggesting that in the 4-hour PSS experiments these NG2⁺ pericytes tended to be smaller in both height and width than those without an adjacent CD163⁺ M Φ .

Stimulation with either TNF- α or IL-1 β caused an approximately 16-18% reduction in NG2⁺ pericyte soma height, with no significant change in width in both the OM and IM (p<0.05). There was no significant difference in pericyte soma width (**Table 3.5**). TNF- α stimulated NG2⁺ pericytes without M Φ contact measured 3.7 \pm 0.1 μ m in height (p<0.05) by 6.6 \pm 0.2 μ m in width (p>0.05) in the OM, and 3.5 \pm 0.1 μ m in height

($p < 0.001$) by $6.1 \pm 0.3 \mu\text{m}$ in width ($p > 0.05$) in the IM (**Table 3.5**). IL-1 β stimulated pericytes without M Φ contact were $3.6 \pm 0.2 \mu\text{m}$ in height ($p < 0.01$) by $6.0 \pm 0.3 \mu\text{m}$ in width ($p > 0.05$) in the OM, and $3.4 \pm 0.2 \mu\text{m}$ in height ($p < 0.001$) by $6.4 \pm 0.4 \mu\text{m}$ in the IM ($p > 0.05$; **Table 3.5**). All other measurements for NG2 $^+$ pericyte soma are in **Table 3.5**.

Much like the 0-hour PSS experiments, there was no difference in size of the time-matched PSS PDGFR- β^+ pericytes with CD163 $^+$ M Φ contact ($5.4 \pm 0.5 \mu\text{m}$ in height, $6.4 \pm 0.4 \mu\text{m}$ wide) or without CD163 $^+$ M Φ contact ($5.6 \pm 0.3 \mu\text{m}$ in height, $7.3 \pm 0.4 \mu\text{m}$ wide, $p > 0.05$; **Table 3.5**) in the OM, or IM ($5.2 \pm 0.7 \mu\text{m}$ in height and $7.5 \pm 0.3 \mu\text{m}$ wide vs $5.1 \pm 0.4 \mu\text{m}$ in height and $7.0 \pm 0.5 \mu\text{m}$ wide, with or without CD163 $^+$ M Φ contact in the IM respectively, $p > 0.05$; **Table 3.5**). Interestingly, unlike with NG2 $^+$ -labelled pericytes, PDGFR- β^+ pericyte soma size was not significantly ($p > 0.05$) influenced by cytokine stimulation, yet IL-1 β stimulated, PDGFR- β^+ pericytes with CD163 $^+$ M Φ contact were approximately 30% smaller in height in the OM ($3.8 \pm 0.4 \mu\text{m}$ vs $5.4 \pm 0.5 \mu\text{m}$; $p < 0.05$) but not the IM ($5.2 \pm 0.3 \mu\text{m}$; $p > 0.05$) with no significant difference in pericyte soma width (**Table 3.5**). TNF- α stimulation caused no significant change in pericyte soma size with or without CD163 $^+$ M Φ cell-cell contact (**Table 3.5**). All other measurements for PDGFR- β^+ pericyte soma are in **Table 3.5**.

Interestingly, as mentioned in the above section, IL-1 β -stimulated PDGFR- β^+ pericytes with M Φ contact were constricted and shown here to be significantly smaller in height. This may reflect an IL-1 β -stimulated CD163 $^+$ M Φ migratory preference to NG2 $^+$ /PDGFR- β^+ pericytes and TNF- α showed no such effect, and this difference was only measured for IL-1 β when M Φ were present. However, as experiments were not conducted with both pericyte markers in tandem, it cannot be commented upon whether these smaller pericytes with M Φ contact are PDGFR- β^+ /NG2 $^+$ or PDGFR- β^+ /NG2 $^-$. Overall, this data suggests that cytokine stimulation with TNF- α and IL-1 β , but not CD163 $^+$ M Φ presence, exerts a cell-surface protein specific reduction in pericyte soma size of NG2 $^+$, but not PDGFR- β^+ pericytes.

3.3.10 Stimulation of kidney slices with pro-inflammatory cytokines TNF- α and IL-1 β does not induce CD163 expression in NG2 $^+$ pericytes but does in few PDGFR- β^+ pericytes.

The primary question that co-immunostaining was utilised to address was “is there any overlap in cellular expression of M Φ -identifying and pericyte-identifying markers?” as has been demonstrated in other studies (Rustenhoven et al., 2016; Balabanov et al.,

1996; Honda et al., 1990; Moransard et al., 2011; Komuro et al., 2017; Inaba et al., 1993; de Parseval et al., 1993) and “does such co-expression co-label perivascular cells in the kidney?”. A positive identification included red pericyte (Alexa-555) and green MΦ (Alexa-488) fluorescent staining around an individual Hoechst 33342⁺-identified cell nuclei. Prior to experimentation, to ensure any potential co-staining observed would not be due to overlap of primary antibodies binding to similar protein sequences, the target sequences of anti-NG2 primary antibody (GENBANK: Q00657), anti-PDGFR-β primary antibody (GENBANK: NP_001139740), and anti-CD163 primary antibody (GENBANK: NP_001101357.1) antibodies were aligned using the UniProt online alignment tool (available at: <https://www.uniprot.org/align/>) to determine sequence homology. After alignment, it was determined that anti-CD163 and anti-NG2 sequence homology was less than 10%, and anti-CD163 and anti-PDGFR-β sequence homology was less than 13%. As such any observations of a Hoechst 33342⁺ cell body co-expressing MΦ and pericyte markers is not likely caused by cross-reactivity of the primary antibodies for pericytes (NG2 and PDGFR-β) or CD163 at the same antigenic sites.

For the purpose of identifying co-staining, 2D images could limit perspective and lead to potential false positives by not providing the opportunity to distinguish 2 cells adjacent to each other in the z-plane. By adding the third dimension in the form of a 10 μm deep z-stack (step size of 1 μm, 212.4 μm²), accurate determination of co-expression of MΦ and pericyte markers around an individual Hoechst 33342⁺ cell nucleus is possible. Another consideration was determination of co-localisation. This method was chosen over a co-localisation assay because both pericytes and MΦ have processes and filopodia, if a computational method to determine co-localisation was employed it would give an overestimation of how frequently this occurs due to physical contact between cells not true co-localisation. A limitation in selecting regions of interest (ROI) was the very limited presence of CD163⁺ MΦ, as described in **Section 3.3.4**; as these MΦ were not evenly distributed throughout the kidney image acquisition was restricted to where there was CD163⁺ cellular presence. For determination of cell type, *i.e.* would these cells be co-labelled pericytes or co-labelled MΦ, pericyte morphology and perivascular location would be used in tandem with co-labelling to determine if it was pericytic expression of MΦ CD163.

In the 0-hour PSS experiments, neither PDGFR-β⁺ nor NG2⁺-labelled pericytes expressed CD163. CD163 is selectively expressed by mature tissue MΦ (Polfliet et al., 2006), so to observe if renal NG2⁺ or PDGFR-β⁺-labelled pericytes were “dormant” monocytes, and could be stimulated to express CD163, kidney slices were subsequently incubated with pro-inflammatory cytokines TNF-α and IL-1β to determine

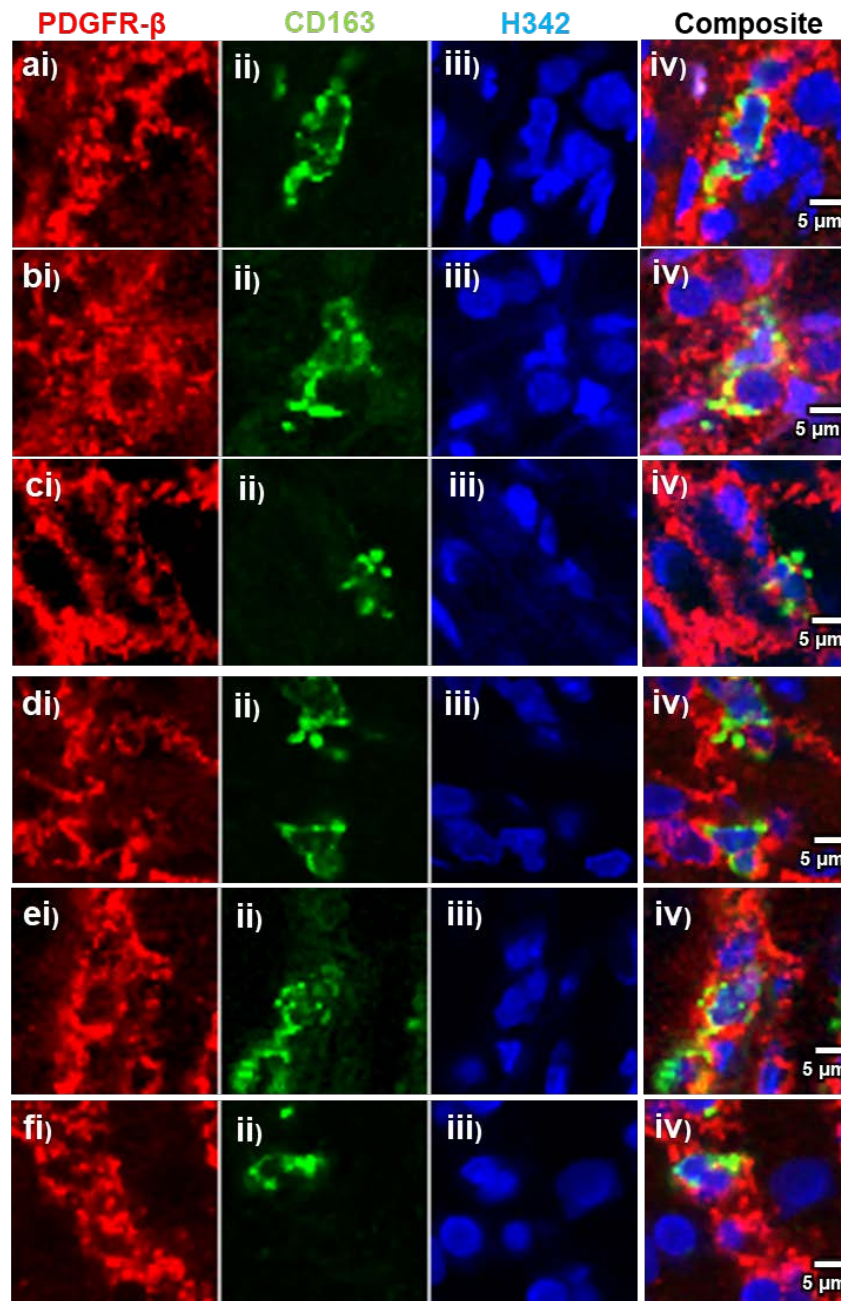


Figure 3.9 Co-expression of platelet derived growth factor receptor- β (PDGFR- β)⁺ with CD163⁺ on vascular resident cells in the renal medulla bearing morphological similarities to PDGFR- β ⁺ pericytes.

Representative images from experiments where tissue was incubated with either TNF- α (a-c) or IL-1 β (d-f), showing positive staining with anti-PDGFR- β (i; red), anti-CD163 (iii; green), and Hoechst 33342 (H342; iv; blue) with the corresponding composite render (iv). Scale bars are 5 μ m.

if this phenomenon may be inducible. Simulation with cytokines could also activate tissue resident immature monocytes for an increased CD163⁺ M Φ cellular presence, better depicting their spatial relationship and cellular interactions with pericyte.

No co-staining of M Φ marker CD163 and pericyte marker NG2 occurred, irrespective of TNF- α or IL-1 β stimulation in either the IM or the OM. Contrastingly to NG2 experiments, there was CD163⁺/PDGFR- β ⁺ co-staining observed after cytokine

stimulation in the medulla of rat kidney sections. Representative images can be seen in **Figure 3.9** for TNF- α (**Figure 3.9(a-c)**) and IL-1 β (**Figure 3.8(d-f)**). Further to this, co-expressing cells bore morphology of pericytes e.g. the “bump-on-a-log” characteristic shape (Peppiatt et al., 2006) (**Figure 3.9(a)**), suggesting that these are pericytes expressing CD163; this morphology is notable different from the morphology of CD163⁺ M Φ presented in **Figure 3.2**.

Whilst a more objective approach would have been fluorescence automated cell sorting (FACS) to accurately identify co-expression of pericyte and M Φ markers on the cell surface. This has been reported as performed in the mouse previously for determining PDGFR- β and CD11_b, co-expression (Xavier et al., 2017), where no co-positive cells were detected. However, what was observed here is that PDGFR- β ⁺/CD163⁺ cells would be a “rare event” i.e. total cell numbers are markedly low, due to their infrequency and as such not readily identifiable using FACS (Rundberg Nilsson et al., 2013; Hedley, and Keeney, 2013), meaning they could be overlooked. However, the data here shows (**Figure 3.9**) that co-expression can be encouraged in a pro-inflammatory environment. Further still, FACS would not provide opportunity to use cellular *in situ* morphology to observe if these are co-labelled pericytes or M Φ . Overall this data suggests that rodent renal PDGFR- β ⁺ pericytes can express M Φ -identifying receptor CD163, bearing pericyte morphology, which may not have been seen using non-immunohistochemical techniques.

3.4 Discussion:

The aim of this study was to determine, using the rodent live slice model, if renal pericytes express M Φ -identifying markers, which could be suggestive of an immune-phenotype. What was found here were morphological and responsive differences between renal neural-glial-2 (NG2)⁺-labelled and platelet derived growth factor receptor- β (PDGFR- β)⁺-labelled pericytes. PDGFR- β ⁺ pericytes were significantly larger than NG2⁺ pericytes, and the vasa recta PDGFR- β ⁺ pericytes covered were significantly wider in diameter. Pericyte populations also had differing responsiveness to pro-inflammatory cytokines TNF- α and IL-1 β , with PDGFR- β ⁺ pericytes being less vaso-responsive in response to stimulation, yet PDGFR- β ⁺ pericytes, not NG2⁺ pericytes, showed co-labelling with CD163. Further still, despite limitations with a small population of CD163⁺ M Φ , data here is suggestive of pericyte-M Φ communication; when correlating vasa recta diameter with incidence of direct cellular-contact between M Φ and pericytes, it was noted that vessels encircled by both PDGFR- β ⁺ and NG2⁺

pericytes were significantly more constricted when in contact with CD163⁺ MΦ, indicating that a cellular communication may be occurring to alter the vessel diameter comparative to when these two cells types did not have cell-cell contact.

3.4.1 PDGFR-β⁺ pericyte covered vasa recta have larger diameters and are more numerous than those covered by NG2⁺ pericytes.

This study considered rodent pericytes expressing the receptor PDGFR-β and the cell surface proteoglycan NG2 as separate populations while investigating any possible differences in their characteristics. Whilst these pericyte-identifying markers have been used to identify functional roles of pericytes in inflammation (Xavier et al., 2017; Lemos et al., 2016; Proebstl et al., 2012) and fibrogenesis (Xavier et al., 2017; Chen et al., 2011; Birbrair et al., 2014), how pericytes with differing cell surface proteins may be functionally and morphologically different remains unclear. Measurements of vasa recta diameter, soma size, and pericyte densities were calculated separately for PDGFR-β⁺-labelled and NG2⁺-labelled pericytes.

The standard approach for calculating medullary NG2⁺ pericyte density is to calculate the cellular density per 100 μm² (Crawford et al., 2012). Yet, the established approach for calculating PDGFR-β⁺ pericyte density is to calculate the percentage of the area positively immunolabelled for this receptor (Ikeda et al., 2018; Craggs et al., 2015). Further to this, PDGFR-β⁺ staining is extensive (**Figure 3.1(a), 3.4(c-d) & 3.7(c-d)**) and meant quantification of cell number would not have been accurate and therefore was not calculated. For direct comparison between pericyte groupings, NG2⁺ pericyte density was calculated was also calculated as %area.

PDGFR-β⁺ is reportedly expressed by all pericytes and by numerous non-pericyte cells (Bergers, and Song, 2005; Díaz-Flores et al., 2009; Chen et al., 2011). Therefore, it would be expected to have a greater percentage of area occupied by staining than that measured for NG2, representing a smaller population of pericytes (Díaz-Flores et al., 2009), restricted to the arteriolar DVR (Pallone et al., 2003b; Murfee et al., 2005). Much like has been previously reported with NG2⁺ pericytes (Crawford et al., 2012), in the rat pericyte “drop off”; the reduction of pericyte density between the OM and IM (Park et al., 1997a); was observed with a significant difference in PDGFR-β⁺ stain (**Figure 3.4(eii)**). Regardless of the method of measurement of NG2⁺ pericyte; per 100 μm², or the corresponding percentage of area occupied by NG2⁺ positive fluorescent staining, there was also significant reduction in density in the IM comparative to the OM (**Figure 3.4e(ii); Table 3.1**).

Given limitations with calculating the PDGFR- β^+ / NG2 $^+$ pericyte density as %area here, these values are not directly comparable with published studies, which tend to be either 2-dimensional calculations of %area (Ikeda et al., 2018; Craggs et al., 2015; Nakano et al., 2017; Hesp et al., 2017), or a direct cell count per 2D ROI (LeBleu et al., 2013). However, the ratio of the amount of staining for anti-NG2 and anti-PDGFR- β correlates with ratios between cell counts for these renal pericytes, and ratios of DVR to AVR. There was a significant difference between the abundance of PDGFR- β^+ -labelled and NG2 $^+$ -labelled pericytes. In both the OM and IM, there were 3-4 fold more PDGFR- β^+ pericytes than NG2 $^+$ pericytes, a ratio that has been previously reported for murine kidneys (LeBleu et al., 2013). Literature suggests NG2 $^+$ pericytes are restricted to the arteriolar end of capillaries (Murfee et al., 2005). Assuming this were true for the kidney, the stark difference in density of NG2 $^+$ and PDGFR- β^+ pericytes could correspond to the ratio of venular ascending (AVR) to arteriolar descending vasa recta (DVR), with a comparable 4-fold difference measured in the rat previously (Holliger et al., 1983). However, as PDGFR- β was also present on other interstitial cells (**Figure 3.1(c)**) the density calculated likely overestimates the total abundance of PDGFR- β^+ pericytes but cannot be commented upon here.

The diameters of vessels of the medullary capillary plexus, whilst also populated with NG2 $^+$ and PDGFR- β^+ pericytes, were not measured because in any given plane of the z-stack renders capillaries had no consistently suitable length of vessel to measure, hence all measurements were from vasa recta capillaries. Rodent vasa recta encircled by PDGFR- β^+ pericytes were approximately 10% larger in diameter than NG2 $^+$ pericyte covered vessels at both the pericyte and non-pericyte sites. It has been previously reported that rodent AVR are approximately 30% larger than the DVR (Holliger et al., 1983), with postcapillary venules known to be larger vessels (Poher, and Sessa, 2014). If the difference in the area of positive fluorescent staining for PDGFR- β and NG2 related to coverage of the AVR by PDGFR- β^+ /NG2 $^-$ pericytes, it could explain why PDGFR- β^+ vasa recta were significantly wider in diameter ($p < 0.05$). It is also possible that the PDGFR- β^+ measurements taken are comprised of both NG2 $^+$ and NG2 $^-$ populations, influencing measurements for PDGFR- β^+ vessels and reflect the lower magnitude of size difference of vessel diameters presented here. Unfortunately, co-staining with both pericyte-identifying markers was not conducted so further commentary cannot be made.

3.4.1.1 Vasa recta PDGFR- β ⁺ pericytes bear morphological differences to NG2⁺ pericytes.

In the rodent ureteric vascular bed pre-capillary arteriolar pericytes and pericytes on the collecting venules (Borysova et al., 2013) bear visual morphological similarity to NG2⁺ (arteriolar) and PDGFR- β ⁺ (venular) pericytes here. Whilst anecdotal, the larger soma of venular pericytes in the ureteric vascular bed reflects observations here of PDGFR- β ⁺ pericyte soma being approximately 20% larger in height than NG2⁺ pericytes, and therefore potentially representing a venular population. Pericyte sizes, when reported, are more often presented as a combined measurement their soma and process coverage over the vasculature (Borysova et al., 2013). In the murine brain, where they measured total cell length (soma and processes), it was found contractile α -SMA⁺ “ensheathing pericytes” (EP) on the pre-capillary arteriole were approximately 1/3rd the size of non-contractile capillary α -SMA⁻ “mesh pericytes” (MP). Further still, the vessels on which EP reside were 30% larger in diameter (Grant et al., 2017). These differences are comparable to those presented here and suggest pericyte function may be inferable from both morphological differences and cell surface protein expression. However, whilst pericyte processes were not measured here it makes direct comparison difficult and is a limitation of this study, pericyte soma size also correlates with these differences.

The likelihood is that the NG2⁺-labelled pericytes also express PDGFR- β as a pan-pericyte marker (Chen et al., 2011), and not co-labelling for these markers is a limitation of this study. Whilst significant differences have been observed, it would be beneficial to measure pericytes that are NG2⁺ and NG2⁻ separately; the average values presented here for PDGFR- β ⁺ pericytes likely contain measurements from both NG2⁺ and NG2⁻ pericytes. These experiments were not conducted because the PDGFR- β and NG2 primary antibodies were both raised in rabbit. The PDGFR- β was kindly donated by William Stallcup, with no other validated alternative anti-NG2 accessible at the time. A future experiment needed is to co-stain with anti-PDGFR- β and anti-NG2 to ascertain whether the morphological differences presented above remain significantly different between PDGFR- β ⁺/NG2⁺ and PDGFR- β ⁺/NG2⁻ pericytes separately. Overall this data, in line with that presented in the literature strongly suggests identifying which morphology belongs to which subtype of pericyte could be another tool for the identification of a known heterogeneous population of cells (Dore-Duffy, and Cleary, 2011; Attwell et al., 2016).

3.4.2 In control kidney tissue there are few CD163⁺ macrophages, which primarily reside in the medulla.

As only MΦ are reportedly perivascular (Lapenna et al., 2018), certain markers that identify multiple immune cell types e.g. MHC-II, were not deemed suitable for use here despite reported pericyte expression (Pieper et al., 2014; Winau et al., 2007). Two separate rodent MΦ-identifying markers were assessed for suitability in the rodent slice model, and whilst both CD68 and CD163 had positive staining, only CD163 was present in the renal medulla and as such this was used for further experimentation. CD68 is considered a pan-MΦ marker (Gordon et al., 2014; Gordon, and Plüddemann, 2017) and is used frequently in the rodent kidney (Rubio-Navarro et al., 2016; Ysebaert et al., 2004; Mattson et al., 2006). However, data here suggests that a more accurate description of CD68 would be of a non-residential MΦ marker given the low occurrence of CD68⁺ MΦ. The restriction to CD68 to arteriolar SMC in the cortex corroborates views of other authors that CD68 expression is an indicator of phagocytic capability instead of MΦ (Beranek, 2005).

In healthy human kidney sections, CD163⁺ MΦ reside apposite the vascular bundles (Colvin, 2019), and an increase in CD163⁺ MΦ correlates with the severity of renal disease in; IgA nephropathy, glomerular sclerosis, and diabetic kidney disease. CD163⁺ MΦ infiltration also correlates with the degree of interstitial fibrosis (O'Reilly et al., 2016; Rubio-Navarro et al., 2016; Olmes et al., 2015; Tang et al., 2019), accumulating at sites where α-SMA⁺ myofibroblasts reside (Ikezumi et al., 2011), suggestive of a highly pathogenic role in human renal disease. Despite the perivascular locale of CD163⁺ MΦ in human kidneys, no current studies have looked at their relationship with pericytes. In the rat, renal CD163⁺ MΦ have previously been noted to be few in number and almost exclusively perivascular (Kaisling, and Le Hir, 1994), which was reflected in observations here; CD163⁺ MΦ maintained a high degree of direct cellular-contact with NG2⁺ pericytes. Interestingly, this remained constant regardless of stimulation with TNF-α or IL-1β with over 70% of MΦ contacting an NG2⁺ pericyte in all treatment groups. In an isolated cell culture model with neutrophils and α-SMA⁻ porcine CNS pericytes, TNF-α stimulation encourages cell-cell contact with an increased adhesion between the two cell types (Pieper, and Galla, 2014), yet in this model, stimulation with the same pro-inflammatory cytokines does not induce a greater degree of cell-cell contact between CD163⁺ MΦs and NG2⁺ pericytes.

The limited presence of CD163⁺ MΦ reported in control tissue sections could relate to numerous factors: the removal of the renal capsule, where many of these MΦ reside

(Kaissling, and Le Hir, 1994); a lack of residential M Φ maturity (Polfliet et al., 2006); CD163 identifying a niche subpopulation of M Φ , M2_c M Φ (Kim et al., 2015b; Chavez-Galan et al., 2015); or the lack of a source of circulating leukocytes to infiltrate into the renal interstitium (Stribos et al., 2016). When present, CD163⁺ M Φ had a varied morphology with regards to size, yet some consistencies in shape were observed with M Φ being ovular or fusiform in shape with processes, reported previously for CD163⁺ M Φ in embryonic rat kidneys (Matsuyama et al., 2018). It would be interesting to probe further if CD163⁺ M Φ morphology relates to subtypes, as it appeared to with pericytes.

3.4.3 CD163⁺ macrophage and pericytes may actively communicate to regulate vasa recta diameter.

Human renal PDGFR- β ⁺ pericytes with cell-cell contact with CD163⁺ M Φ show fibrotic activation, however what specifically occurs remains unclear (Campanholle et al., 2013). Over 70% of M Φ had cell-cell contact with a pericyte, it raised the question of “is there a reason, when present, CD163⁺ M Φ are preferentially next to pericytes? And was there a functional consequence from this association?”. No signalling mechanisms could be elucidated here; whilst immunohistochemistry can identify the location of signalling proteins it would require the inclusion of antibodies against the active proteins or antibodies against phosphorylated amino acids to demonstrate the pathway is active (Svoboda, and Reenstra, 2002). In place of identifying specific signalling pathways, vessel diameter was used as a proxy to determine if there was a physiological outcome from direct cell-cell contact, a mechanism of M Φ communication (Nitta, and Orlando, 2013; Arrevillaga-Boni et al., 2014; Rodriguez et al., 2016). What was found was comparative to pericytes with no M Φ contact, when either PDGFR- β ⁺-labelled or NG2⁺-labelled pericytes were in contact with an M Φ the vasa recta were significantly constricted.

The DVR and AVR have a counter-current arrangement, and it has been proposed that circulating leukocytes migrate out from the circulation at the venular end (NG2⁻) of the capillary bed and their trajectory towards the inflammatory foci is then co-ordinated by the arteriolar (NG2⁺) pericytes (**Figure 1.9**) (Alon, and Nourshargh, 2013). Furthermore, *in vivo* reports in the murine cremaster muscle and ear demonstrated that NG2⁺ pericytes instructed the migration of leukocytes out of the vasculature after TNF- α or IL-1 β stimulation (Proebstl et al., 2012; Stark et al., 2012). Leukocyte and platelet adherence in the postcapillary venules has been proposed to induce constriction of the closely paired arterioles via diffusion of vasoactive mediators in the

mesenteric vascular bed (Harris et al., 2005), authors were unable to determine for what purpose but this would increase chances of leukocyte adherence and subsequent extravasation in the venules by reducing the flow rate (Muller, 2013). In the medulla CD68⁺ infiltrating MΦ accumulate in the AVR post ischaemia-reperfusion injury (Ysebaert et al., 2004), which could potentially result in NG2⁺-pericyte covered DVR vasoconstriction. CD163⁺ MΦ produce TNF-α and IL-1β (Polfliet et al., 2006) and promote leukocyte infiltration (Guo et al., 2018); they could co-ordinate this activity with renal pericytes and induce the subsequent vasoconstriction. Further work is needed to tease out if it is pericyte sites on the AVR or DVR which have constricted when in contact with MΦ. There is an absence of antibodies used to identify these vessels, yet could involve the use of UT-B and plasmalemmal vesicle-1 which have been used previously to identify DVR and AVR respectively in mice and rats (Dantzler et al., 2011; Pannabecker, and Dantzler, 2006; Ko et al., 2010).

Interestingly, CD163⁺ MΦ are reportedly involved in angiogenesis, increasing the permeability of the microvasculature via HIF-1α/VEGF-A signalling and weakening of the endothelial VE-cadherin (Guo et al., 2018), via CD163-dependent cell-cell interactions (Kobori et al., 2018). This would subsequently enable endothelial cell proliferation and generation of the angiogenic sprout (Wallez et al., 2006). However, in an inflammatory bowel disease model, whilst CD163⁺ MΦ depletion improves vasomotor response in the mesenteric arteries *i.e.* reduces the reduces vessel permeability, it does so in an endothelial-independent fashion (Grunz-Borgmann et al., 2019). This suggests it is communications with a non-endothelial vascular cell type that are responsible for this activity, possibly pericytes. Data presented here suggests that this cell-cell communication could be MΦ-pericyte mediated as it was the pericyte site where the vessel diameter was significantly altered, regardless of cytokine stimulation. In the murine cochlear duct pericytes, endothelial cells and MΦ maintain vascular stability of the stria vascularis (Neng et al., 2013), therefore MΦ- pericyte communications could potentially be a homeostatic mechanism in the kidney to regulate vessel diameter.

3.4.4 Stimulation of tissue with TNF-α and IL-1β increase the number of CD163⁺ macrophages in the medulla.

There are contradictory reports regarding the activation of CD163⁺ MΦ by pro-inflammatory cytokines. IL-1β has been shown to upregulate CD163 expression in monocytes (Darrieutort-Laffite et al., 2014; Schenk et al., 2014) whereas TNF-α

suppresses it (Buechler et al., 2000). As the primary focus of this study was pericyte activation, and TNF- α and IL-1 β are known to encourage immune functionality for pericytes (Proebstl et al., 2012; Pieper et al., 2013; Nehmé, and Edelman, 2008) these cytokines were deemed suitable for use in experimentation here. However, it is important to note these values are not objective and the quantification of M Φ here is a limitation of this study. However, selection of ROI was restricted to where both CD163⁺ M Φ and pericytes were present and as such quantification for the ROI were performed.

Following the 4-hour incubations there was an apparent activation of dormant residential monocytes given the semi-quantitative 1.5-fold increase in CD163⁺ M Φ in the time-matched 4-hour PSS experiments comparative to the 0-hour PSS experiments. In precision cut lung slices of Fischer 344, there was an increase 200-1400 pg/mg increase in IL-1 β and TNF- α present, followed by an increase of CD68⁺ M Φ in tissue sections by approximately 1.3-fold in was observed control conditions after a period of 7 days, and that within 3 hours of slice incubation there was a (Behrsing et al., 2013). A comparable upregulation of TNF- α , IL-6, and IL-1 β mRNA was observed in C57BL/6 brain (Schroeter et al., 2003) and both precision cut murine (Poosti et al., 2015) and human (Stribos et al., 2016) kidney slices within 3 hours. TNF- α and IL-1 β stimulation resulted in a 1.2-2.7-fold increase in CD163⁺ M Φ and shows dormant residential M Φ can be activated by TNF- α and IL-1 β to express CD163 (**Figure 3.6 and 3.7**). The degree of M Φ -pericyte contact was higher in the OM than in the IM, regardless of cytokine treatment, despite no significant difference in the total number of CD163⁺ M Φ present in the fields of view between the OM and IM regions (**Table 3.3**), possibly suggesting a regional preference for CD163⁺ M Φ activity with NG2⁺ pericytes but more work is needed. Whilst the data presented regarding the regional differences in CD163 M Φ is not strong, the effect of their presence on vasa recta diameter (**3.4.3**) is an objective quantification and a beneficial finding.

3.4.5 TNF- α and IL-1 β stimulation significantly reduce NG2⁺ pericyte density in both medullary regions.

Following 4-hour incubations with pro-inflammatory cytokines TNF- α and IL-1 β , NG2⁺ pericyte density was significantly reduced. TNF- α and IL-1 β stimulation reduce pericytic expression of α -SMA and PDGFR- β (Persidsky et al., 2016; Jansson et al., 2016), and TNF- α (Tigges et al., 2013) and IL-1 β (Rustenhoven et al., 2018) reportedly activate a proliferatory and migratory pericyte phenotype. It has also been suggested LPS-induced IL-1 β reduces the proliferation of NG2⁺ cells in the rodent brain and also

encourages the shedding of NG2 (Wennström et al., 2014). This raises an interesting question that just because a molecule is no longer expressed by a cell does not necessarily mean that cell is no longer present. In the circumventricular organs salt loading alters pericyte expression of NG2 and PDGFR- β (Morita et al., 2014). This data indicates cell-surface molecule expression is dynamic and influenced by the microenvironment, with shed molecules indicative of activity.

PDGFR- β^+ pericyte density measured in the PSS 4-hour control was significantly less than the TNF- α and IL-1 β treated sections. After 4-hours there was approximately double the number of CD163 $^+$ M Φ in the PDGFR- β PSS 4-hour time-matched experiment compared to the NG2 4-hour PSS control (**Table 3.3**), which may suggest the PDGFR- β PSS experiments were performed in unhealthy tissue sections. As there was doubt with regards to the accuracy of staining in PDGFR- β^+ time-matched control experiments, the effects of cytokine stimulation on the PDGFR- β^+ pericyte density will not be commented upon further. As other measurements could be taken using the bright-field images those measurements were not excluded from the discussion below.

Accumulation of diffuse NG2 protein is correlated with leukocyte infiltration (Moransard et al., 2011), and a reduction in NG2 $^+$ pericyte density correlates with infiltration of immune cells in the murine heart and lung (Zeng et al., 2016). In the SHR kidney a reduction of NG2 $^+$ pericytes correlates with vascular congestion in the vasa recta post-IRI (Crislip et al., 2017), with further evidence showing CD68 $^+$ M Φ and CD28 $^+$ T cells accumulating in the AVR of humans and rats post ischaemic injury (Ysebaert et al., 2004). The constriction and loss of NG2 $^+$ pericytes, or at least loss of the NG2 protein, could lead to destabilisation of the pericyte-endothelial network (You et al., 2014). This cytokine induced reduction of NG2 pericyte density could be a component of enabling extravasation of circulating immune cells, even in the absence of circulating leukocytes as they are not present in the slices (Stribos et al., 2016).

3.4.6 TNF- α and IL-1 β differentially affect PDGFR- β^+ and NG2 $^+$ pericyte contractility and morphology.

In the murine cremaster muscle, α -SMA $^+$ pericytes expressed TNFR1, TNFR2, and IL-1R (Proebstl et al., 2012), and human placental NG2 $^+$ / α -SMA $^+$ pericytes express TNFR1 and various pattern recognition receptors (Stark et al., 2012). Excluding instances of pericyte-M Φ cell contact, in the rat cytokines elicit a significant pericyte-mediated constriction of vasa recta capillaries. However, whether the vessels constricted depended on the expression pattern of the pericyte. Rodent vasa recta covered with NG2 $^+$ pericytes, but not PDGFR- β^+ pericytes, were significantly

constricted after cytokine exposure, specifically at pericyte sites. The lack of contractility of PDGFR- β^+ pericytes in response to IL-1 β exposure may relate to its inhibitory activity of PDGFR- β -induced actin cytoskeleton reorganisation (Sundberg et al., 2009), inhibiting pericyte contractility (Durham et al., 2014). PDGFR- β^+ /NG2 $^-$ pericytes may be a non-contractile population. In the renal medulla NG2 $^+$ /PDGFR- β^+ pericytes express α -SMA (Stefanska et al., 2015) whilst PDGFR- β^+ /NG2 $^-$ pericytes show minimal expression of this contractile protein (Wang et al., 2017) indicating a differential activity of NG2 $^+$ and NG2 $^-$ pericytes. These contractile differences are possibly reflected here in the smaller renal NG2 $^+$ pericyte morphology as RhoGTPases are required for pericyte contractility (Kolyada et al., 2003; Kutcher et al., 2007). Pericytes where these are activated are significantly smaller in size than pericytes where they remain dormant (Kolyada et al., 2003).

Following a similar trend in responsiveness, cytokine stimulation caused a significant reduction in NG2 $^+$ pericyte size whereas no morphological changes were observed with PDGFR- β^+ pericytes. Proebstl *et al* 2012 (Proebstl et al., 2012) reported a morphological change in *in vivo* murine α -SMA $^+$ pericytes upon exposure to TNF- α and IL-1 β , and morphological changes have been reported in cultured rodent lung pericytes (Kerkar et al., 2006), and murine CN2 pericytes *in vitro* (Tigges et al., 2013; Kim et al., 2015a; Persidsky et al., 2016). An expression pattern-dependent difference in pericyte activity is not new, and has been previously reported; PDGFR- β^+ /NG2 $^-$ are fibrogenic whilst PDGFR- β^+ /NG2 $^+$ are not (Stefanska et al., 2015). The evidence here demonstrates NG2 $^+$ pericytes being markedly influenced by pro-inflammatory cytokines and suggests perhaps they are key regulators in the inflammatory process. As described in **section 3.4.1**, as co-staining with PDGFR- β and NG2 was not performed, further commentary on potential subpopulations of pericytes cannot be made. However, these functional differences, in line with the morphological differences, are indicative of subtypes being present. Knowing if residential M Φ preferentially go to PDGFR- β^+ /NG2 $^+$ but not PDGFR- β^+ /NG2 $^-$ pericytes could be informative regarding propagation of the immune response in the renal medulla and warrants further investigation.

3.4.7 A small number of PDGFR- β^+ pericytes were co-labelled with anti-CD163.

Recent evidence has suggested an immune role for renal pericytes (Liu et al., 2018; Xavier et al., 2017; Lemos et al., 2016; Kielar et al., 2005; Ysebaert et al., 2004), but the question of “are these pericytes or perivascular M Φ ” had not been visually probed,

utilising the characteristic pericyte morphology, and potentially confusing activities of differing cell types. Although basally no rodent pericytes expressed CD163, after stimulation with pro-inflammatory cytokines TNF- α and IL-1 β , few cells were positively fluorescently labelled by both anti-CD163 and anti-PDGFR- β , but not with anti-NG2. These cells co-labelled bore morphological similarities to the criteria used for identifying pericytes (Bergers, and Song, 2005), and PDGFR- β reportedly labels human immune cells (Inaba et al., 1993; de Parseval et al., 1993), yet as these PDGFR- β^+ /CD163 $^+$ cells were so infrequent any further commentary is difficult.

Data here is strongly indicative of active communication between renal pericytes and residential CD163 $^+$ M Φ . However, use of a pan-M Φ marker might be more informative. Whilst pericyte-M Φ mediated vasoconstrictions were significant as a measured physiological outcome from cell-cell contact, low CD163 $^+$ cell numbers may not be reflective of the residential M Φ population. Subsequent questions arising from this investigation are is M Φ -pericyte contact a regular occurrence, do these cells communicate in basal conditions, and do pericytes co-express M Φ - identifying markers or do M Φ express pericyte-associated proteins. The scope of anti-CD163 is finite for these questions in rodent kidneys, and would also be limited in murine kidneys (Rubio-Navarro et al., 2016; Bi et al., 2018) despite abundance in the human renal medulla (Colvin, 2019), where it appears to behave as a pan-marker for human renal M Φ .

Ultimately, experiments showed interesting early findings but did not sufficiently address the primary aim of the investigation. As there is a lack of pan-M Φ identifying markers in the rat, this species has limited usefulness in the application here so a more suitable model would be beneficial. Mice are a suitable candidate given numerous studies investigating pericyte immune functionality were conducted in this species (Kovac et al., 2011; Olson, and Soriano, 2011; Xavier et al., 2017; Lemos et al., 2016). Further still, the murine pan-M Φ F4/80 antigen which also has reported co-labelling with NG2 (Komuro et al., 2017; Rajantie et al., 2004; Pieper et al., 2014) which would overcome the issue of using a subpopulation marker.

The establishment and validation of known pericyte behaviours was first characterised in the rodent kidney slice model (Crawford et al., 2012), prior to its use here to investigate renal pericyte multipotency. As such the development of the murine live slice would enable an informed cross-species comparison of models as well as access the murine pan-M Φ marker F4/80 to further address questions regarding the multipotency of renal pericytes. Establishment of the murine model is presented in the next chapter.

4 ESTABLISHMENT OF A MURINE LIVE KIDNEY SLICE MODEL.

4.1 Introduction.

As described in **Section 1.1.3.2**, descending vasa recta (DVR) pericytes are responsible for regulating renal medullary blood flow (MBF) (Silldorff et al., 1995; Crawford et al., 2012; Crawford et al., 2011; Zhang et al., 2005). These studies, and those from other vascular beds (Peppiatt et al., 2006; Almaça et al., 2018; Hall et al., 2014) characterised pericytes upon: NG2-expression; morphology; vascular residence; and their contractile responses upon exposure to a panel of vasoactive agonists including angiotensin-II (Ang-II), endothelin-1 (ET-1), and noradrenaline (NA) (Crawford et al., 2012; Almaça et al., 2018; Peppiatt et al., 2006). Whilst all NG2⁺ pericytes are considered to co-express PDGFR- β (Dore-duffy, and Esen, 2018), in the renal medulla NG2⁺/PDGFR- β ⁺ pericytes express α -SMA (Stefanska et al., 2015) whereas NG2⁻/PDGFR- β ⁺ pericytes show minimal expression of this contractile protein (Wang et al., 2017). With the expression of NG2 restricted to the arteriolar end of the vascular bed (Murfee et al., 2005) together these support the notion that the pericyte subpopulations which regulate MBF are likely NG2⁺. Renal NG2⁺ pericyte morphology, regional distribution, and vasoactivity has been characterised for the rodent kidney slice model (Crawford et al., 2012). The functional and morphological features of murine renal pericytes have yet to be characterised.

However, the translation of models between species is not quite so straightforward. Data generated in differing rat and mouse models are often used to corroborate findings with the assumption that physiology is similar, if not equivalent, between rats and mice (Downs, 2011). However species-related differences in pathogenesis (Natoli et al., 2013; Ellenbroek, and Youn, 2016), and the use of inconsistent experimental methods and poorly characterised models (Steven et al., 2017), can make interpretation of data difficult. C57BL/6J are known to be resistant to hypertension (Neuhofer, and Beck, 2005; Hartner et al., 2003). In isolated tissue preparations from the liver (Zhao et al., 2009), mesentery (Hedemann et al., 2004), and abdominal aorta (Russell, and Watts, 2000) the vasoactive response of C57BL/6J mouse tissue comparative to Sprague-Dawley rat tissue is markedly reduced when all experimental parameters, aside from the species used, are identical. As a characteristic example, with systemic administration of exogenous Ang-II, in mice the duration of the pressor response was 25% less than in the rat, and the magnitude of the response *i.e.* the degree of vasoconstriction, was up to 50% lower in the mouse, depending on the Ang-II concentration (Cholewa et al., 2005).

Chapter 3, whilst showing interesting pre-liminary findings with regards to pericyte-multipotency, was limited in usefulness for addressing the question “do renal pericytes show potential for multipotency”, so a more suitable model is needed. Establishment of a murine model would enable the use of the pan-macrophage identifying antigen F4/80, which is extensively expressed in murine kidneys (Hume, and Gordon, 1983) and has reported pericyte and macrophage (MΦ) expression (Discussed in **section 1.3.3**). There is also a definitive benefit to having the same model developed in multiple species, looking for trends in behaviour whilst being knowledgeable on their respective differences (Cunningham, 2002; Boswell et al., 2014), offering predictive validity of the model in a translatable fashion (Denayer et al., 2014). Application of vasoactive agents to murine kidney slices should demonstrate the known responsive differences between C57BL/6J mice and SD rats, reflected by the vasoactivity of murine pericytes.

As such, the aim of this chapter is to; i) Use the anti-NG2 antibody in the mouse, that was used in the rat, to identify pericytes on IB₄-labelled vasa recta capillaries, as was performed in the original rat model iii) characterise the murine NG2⁺-labelled pericytes distribution and morphology objectively, and iii) characterise the responsiveness to vasoactive agents used to initially to validate the rodent kidney slice model (Crawford et al., 2012), and thus translate the rat live slice kidney preparation into a viable C57BL/6J murine kidney slice model.

4.2 Methods.

Experiments using animals were conducted in accordance with UK Home Office Scientific Procedures Act (1986).

4.2.1 C57BL/6J tissue slicing.

Murine kidneys were retrieved, prepared and sliced as described in **Chapter 2 Section 2.1**. Prior to experimentation slices were kept in a slice hold chamber kept for up to 4 hours in a holding chamber containing PSS bubbled with 95% O₂/ 5% CO₂ at room temperature (25°C).

4.2.2 Viability of C57BL/6J live kidney slices.

See **Chapter 2 section 2.2**, but in brief; to determine the viability of the murine kidney slices, incubations were conducted with 5 μ M Hoechst 33342 (Hoechst, Sigma-Aldrich, UK), and 20 μ M propidium iodide (PI, Sigma-Aldrich, UK), in bubbled (95% O₂/5% CO₂) PSS. Post incubation slices were washed three times in PSS (95% O₂/5% CO₂) for 5-minutes, then fixed with 4% paraformaldehyde (PFA; Sigma-Aldrich, UK) for 15-minutes. After fixation, slices were washed with 0.1 M phosphate buffered saline (PBS, Sigma-Aldrich) and mounted using Citifluor (Agar Scientific Ltd, Essex, UK). Slices were imaged using a Zeiss LSM 800 confocal microscope (Carl Zeiss Ltd, Welwyn Garden City, UK) and analysed using FIJI, a public domain software (Schindelin et al., 2012), to calculate the ratio of live:dead cells using the cell counter plugin, and **Equation 2.1**.

4.2.3 Determination of C57BL/6J NG2⁺ pericyte density and pericyte characteristics.

For more detail please see **Chapter 2 section 2.3**, but in brief; prior to fixation, live kidney slices were incubated with 50 μ g/mL Alexa Fluor-488-conjugated isolectin B₄ (IB₄; Invitrogen Ltd), prepared in bubbled (95% O₂/5% CO₂) PSS for 45-minutes. Subsequently, slices were washed with PSS for 15-minutes, followed by a 15-minute fixation period using 4% PFA. Fixed slices were washed three times for 10-minutes with 0.1 M PBS, before permeabilisation with 0.1% Triton X-100 (Sigma-Aldrich, Dorset, UK) made in 0.1 M PBS, and blocked with 10% donkey serum (Sigma-Aldrich, Dorset, UK). Post blocking, slices were incubated with anti-nerual-gial (NG2) rabbit polyclonal primary antibody (Ab; Millipore UK Ltd, Watford, UK) to identify pericytes for 16-hours overnight. This Ab was then probed with an Alexa Fluor 555-conjugated donkey-anti-rabbit secondary Ab (Invitrogen Ltd) for 2-hours, washed with PBS and then mounted using Citifluor. Slices were kept at 4°C in the dark prior to imaging using a Carl Zeiss LSM 880 confocal microscope (Carl Zeiss Ltd, Oberkochen, Germany) as described in **Chapter 2, section 2.2**. Measurements taken are listed in **Chapter 2, section 2.3**.

4.2.4 Functional experiments and video analysis

Differential interference contrast (DIC) images of pericytes on subsurface vasa recta capillaries and their functional responses were conducted and measured as described in **Chapter 2 section 2.4**. The vasoactive agents that were chosen are important endogenous mediators of MBF (Neuhofer, and Beck, 2005; Pallone, and Silldorff, 2001; Cowley et al., 1995), and trialled in the rat (Crawford et al., 2012; Crawford et al., 2011). These agents were adenosine 5'-triphosphate (ATP; Sigma-Aldrich, Dorset, UK); angiotensin II (Ang-II; Sigma-Aldrich, Dorset, UK.); endothelin-1 (ET-1; Tocris, Bristol, UK); bradykinin (BK; Sigma-Aldrich, Dorset, UK); prostaglandin E₂ (PGE₂; Tocris, Bristol, UK); noradrenaline (NA; Tocris, Bristol, UK); 3'-O-(4-Benzoyl)benzoyl adenosine5'-triphosphate (BzATP ;Sigma-Aldrich, Dorset, UK); S-Nitroso-N-Acetyl-D,L-Penicillamine (SNAP, Tocris, Bristol, UK); Indomethacin (Sigma-Aldrich); and Tyramine (Sigma-Aldrich). Control superfusion experiments with PSS alone, followed by exposure to 10 nM ET-1. Concentrations used can be seen in **Table 2.1 in Chapter 2**. Time-Series was conducted using FIJI software as previously described (Crawford et al., 2012). In brief, measurements were taken from an identified pericyte and non-pericyte site every 5s for the duration of the experiment. Each capillary acted as its own control. The first 5 measurements were used to determine the baseline diameter, and represented the resting value, expressed as 100%. All subsequent measurements are expressed as a percentage of this resting value.

4.2.5 Statistics

For all experiments, statistical analysis was conducted using GraphPad PRISM 5.0 software (La Jolla, California) using a Student's *t*-test, paired or unpaired where relevant. ANOVA and Bonferroni post-hoc tests were used to compare responses when tissue was exposed to differing concentrations of the same agonist if they elicited a vasoactive response. A value of $p < 0.05$ was considered significant. All experiments where the change in vessel diameter is $< 5\%$ of the baseline diameter were considered non-significant and discounted from statistical analysis. Values are expressed as mean \pm SEM. SEM is calculated with animal number. Sample size (*n*) represents the number of pericytes (with 1 pericyte site and non-pericyte site per live kidney slice), as variation in response was found between pericytes and not animals (Crawford et al., 2011).

4.3 Results

4.3.1 C57BL/6J kidney slices are viable, with pericytes clearly identifiable.

The slicing depth to expose the entirety of the medulla was approximately 1.7 mm with 3-5 usable slices obtained per pair of murine kidneys. To determine viability of these slices, kidney sections were stained with the fluorophores Hoechst 33342 (H342) and propidium iodide (PI) to calculate the proportion of live (H342): dead (H342 and PI) cells present. From the stained tissue sections, areas of $100\ \mu\text{m}^2$ were analysed and $79.0\pm 2.4\%$ of cells were alive, corresponding to a live: dead cell ratio of 4:1. This reflects observations in the rodent model (Crawford et al., 2012), and from other murine kidney slices (Brähler et al., 2016) (n= 4 animals, and 9 slices).

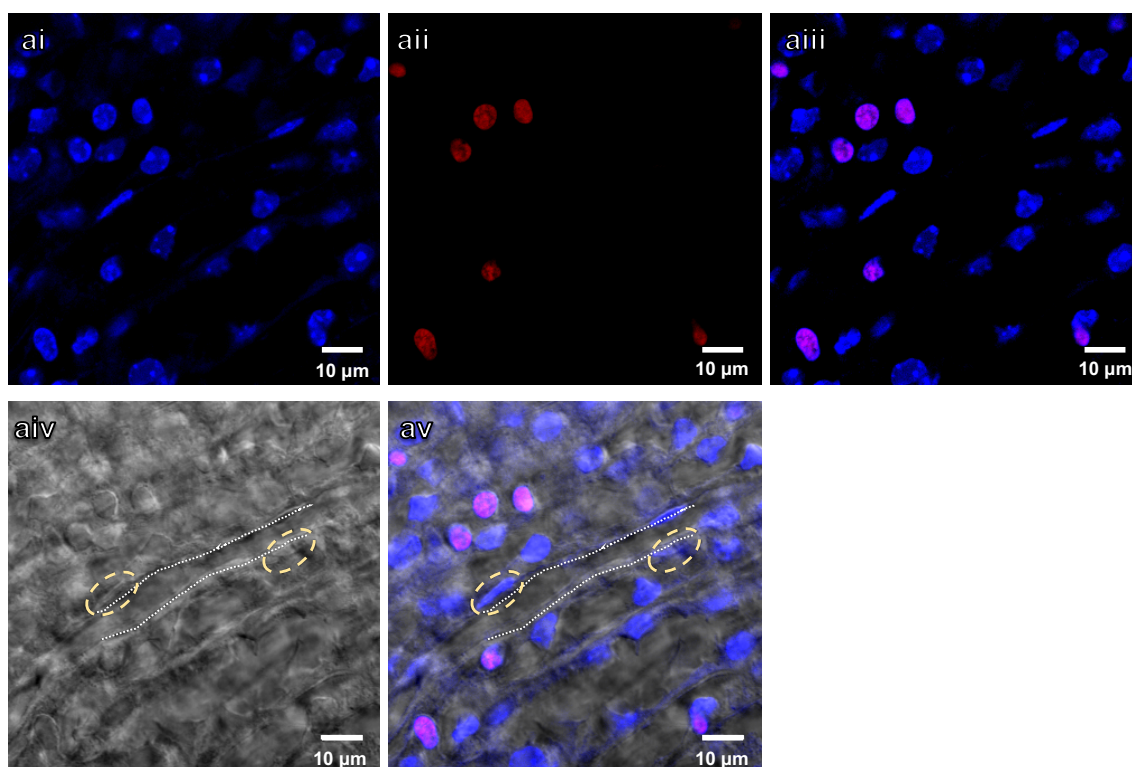


Figure 4.1 Viability of kidney slices from C57BL/6J mice

Live kidney slices were stained with Hoechst 33342 (*blue*) and propidium iodide (PI; *red*) and imaged using confocal microscopy. Hoechst 33342 (**ai**) labelled all nuclei, and PI (**aai**) labelled dead cells, with the composite (**aiii**) of both showing the majority of cells in the field of view are alive. The corresponding DIC image for (**ai-aiii**) shows a vasa recta capillary (**aiv**, white dotted lines) with surrounding pericytes (yellow dashed circle). The composite image of all channels (**av**) shows that the pericytes on this capillary are viable. Scale bars are $10\ \mu\text{m}$ n= 4 animals and 9 slices.

Importantly, from **Figure 4.1(av)**, comprised of a bright field image overlaid with Hoechst and PI fluorescence, it can be seen that not only are the pericytes identifiable via the ‘bump-on-a-long’ morphology (Peppiatt et al., 2006), but that they constitute part of the surviving parenchyma in this preparation, with cells of the tubules and interstitium also viable.

4.3.2 NG2⁺ pericytes are clearly labelled in C57BL/6J kidney slices.

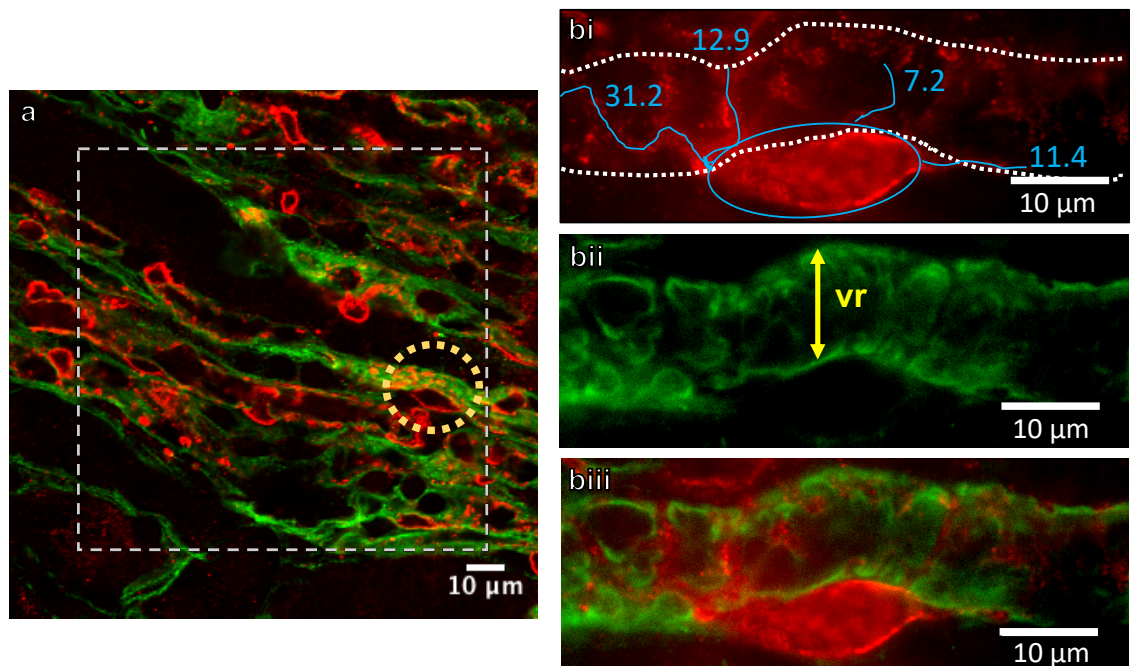


Figure 4.2 Identification of NG2⁺ pericytes in the C57BL/6J renal medulla.

Vasa recta capillaries (*green*) were identified using Alexa-488 conjugated Isolectin-B₄ (IB₄), and pericytes (*red*) with anti-neural-gial 2 (NG2) primary antibody and probed with Alexa-555. Pericyte density was calculated per 100 μm^2 , and a representative image from the renal outer medulla (OM; **a**), as indicated by a white-dashed box. The yellow dashed circle highlights an individual pericyte cell with its processes, which is shown magnified in (**bi-iii**). (**biii**) is the corresponding composite of (**bi**) and (**bii**), which demonstrate identification of the pericyte soma (blue circle), and measurements of pericyte primary processes (blue lines) around the vasa recta wall (μm). The white dashed lines highlight the vasa recta walls. (**bii**) shows the fluorescently labelled IB₄ on the vasa recta (vr), and where a corresponding diameter measurement would be obtained (double ended yellow arrow). All scale bars are 10 μm . n=4 animals and 9 slices.

Pericytes were labelled with anti-NG2, probed with Alexa-555 and co-localised to vasa recta that were stained with Alexa-488- conjugated IB₄ (**Figure 4.2**). Pericyte characteristics were determined by analysis of randomly selected 100 μm^2 regions in both the inner medulla (IM) and outer medulla (OM). Cell bodies and associated

processes were measured, which can be seen emanating from the cell body running both along (longitudinal) and around (circumferential) the abluminal surface of the capillary (**Figure 4.2(biii)**). A summary of murine pericyte characteristics can be seen in **Table 4.1**. For the rest of this section, the pericyte characteristics discussed are specifically for NG2⁺-labelled pericytes.

The average pericyte density per 100 μm^2 in the mouse is 4.3 ± 0.3 in the IM, significantly lower than the 9.4 ± 0.6 pericytes per 100 μm^2 in the OM ($p < 0.0001$; $n = 4$ animals and 8 slices, **Table 4.1**). Comparatively, in the rat the average pericyte density is 9.1 ± 0.5 per 100 μm^2 in the IM and 12.4 ± 1.2 per 100 μm^2 in the OM (Crawford et al., 2012). The distance between pericytes in the mouse was not significantly different between the IM and OM (n ; $p > 0.05$), averaging to be 26.8 ± 1.4 μm apart, and correspondingly almost double the distance than observed in the rat (16.0 ± 1.2 μm ; $p < 0.05$). Correspondingly to the increased distance between pericyte soma, the primary processes protruding from pericytes along the vasa recta (longitudinal) in the mouse were 19.2 ± 0.8 μm , and 9.7 ± 0.6 μm around (circumferential). The longitudinal processes are significantly longer than those in the rat (8.3 ± 0.4 μm , $p < 0.0001$) (Crawford et al., 2012). The primary process lengths measured here would ensure complete coverage of the vasa recta. However, due to difficulties with identifying the end of pericyte processes, measurements of process length were not taken for data in **chapter 3** or **5 (section 3.3.5)**.

Table 4.1 Summary of C57BL/6J NG2⁺ pericyte characteristics.

	OM ¹	IM ²	Average
Pericyte Density			
# ³	9.4 ± 0.6	$4.3\pm 0.3^{***}$	7.3 ± 0.4
Pericyte soma size, μm			
Height	4.9 ± 0.2	4.9 ± 0.2	4.9 ± 0.2
Width	9.0 ± 0.4	9.4 ± 0.4	9.3 ± 0.3
Distance between pericytes on vasa recta, μm			
	24.4 ± 1.8	$28.\pm 2.0$	26.8 ± 1.4
Pericyte processes, μm			
Longitudinal	17.8 ± 1.2	20.4 ± 1.1	19.2 ± 0.8
Circumferential	9.8 ± 1.1	9.7 ± 0.6	9.7 ± 0.6
IB₄-labelled vasa recta diameter, μm			
Pericyte site	6.15 ± 0.3		
Non-pericyte site	$7.9\pm 0.4^{***}$		

Data presented are the mean \pm SEM. $n = 4$ animals and 98 slices, ≥ 200 pericytes per animal.

¹OM = outer medulla, ²IM = inner medulla

³# = Number of cells per 100 μm^2

*** $p < 0.0001$

There was no significant difference in cell body size between the OM or IM (9.0 ± 0.4 μm vs 9.4 ± 0.4 μm in length respectively, $p > 0.05$, **Table 4.1**), and the same size as pericytes in the rat which were 9.0 ± 0.2 μm along ($p > 0.05$). In Chapter 3, SD NG2⁺

pericytes measured $4.6 \pm 0.2 \mu\text{m}$ in height on average, non-significantly different from the mouse here (4.9 ± 0.2 ; $p > 0.05$).

4.3.3 C57BL/6J renal pericytes are functionally responsive, and vasoactive agents affect vasa recta diameter *in situ*.

Vasa recta capillary diameter was measured at a pericyte and corresponding non-pericyte site along the same vasa recta capillary in DIC superfusion experiments. The average resting vessel diameter was calculated as $6.5 \pm 0.2 \mu\text{m}$ at pericyte sites and $8.0 \pm 0.2 \mu\text{m}$ at non-pericyte sites ($p < 0.001$; $n > 40$). This was not significantly different ($p > 0.05$) from values obtained for vasa recta from IB_4 and NG2 experiments; $6.1 \pm 0.3 \mu\text{m}$ at pericyte and $7.0 \pm 0.4 \mu\text{m}$ at non-pericyte sites ($p < 0.001$; **Table 4.1**; $n > 30$ vessel measured), therefore DIC measurements accurately reflect vasa recta capillary diameter. These values are significantly different from those observed in the rat ($7.5 \pm 0.4 \mu\text{m}$ at p and $9.5 \pm 0.4 \mu\text{m}$ at np sites, $p < 0.0001$) (Crawford et al., 2012). For functional experiments, capillary diameter was measured every 5 s before, during, and after superfusion with agonist of choice, and normalised as a percentage of the average “baseline” diameter of the first 120s of the experiment. This was calculated for a paired pericyte and non-pericyte site per experiment, and the values are represented as a percentage change of the original baseline diameter.

To demonstrate that any alterations in vasa recta diameter observed were due to the presence of agonist, PSS control experiments were conducted. These demonstrated that in the absence of an agonist there was no significant alteration in vessel diameter at pericyte sites (change in vessel diameter $< 5\%$ of baseline), and that there was no significant difference between changes at pericyte sites and non-pericyte sites ($2.1 \pm 0.8\%$ at p and $2.0 \pm 1.0\%$ at np sites, $p > 0.05$, $n = 7$ slices and 7 animals). To further validate this finding, that these slices possessed the capability to respond, but were unresponsive due to lack of agonist, after PSS control experiments ET-1 (10 nM) was applied as an additional 1200s experiment. This agonist and concentration were chosen as it demonstrated the highest response rate (67%). An representative trace for a PSS + ET-1 control can be seen in **Figure 4.3(c)**. As can be seen in **Figure 4.3(a-b)** there are two adjacent vessels that are unresponsive during superfusion with PSS alone (**figure 4.3(a)**), yet upon exposure to ET-1 (10 nM; **Figure 4.b(b)**; $n = 7$ slices, and 7 animals) while one vessel does not respond, the adjacent vasa recta capillary forcibly constricts, demonstrating the viability of the kidney slice. This variability of

pericyte responsiveness as has been observed in similar CNS studies and by Crawford *et al* (Peppiatt *et al.*, 2006; Crawford *et al.*, 2012).

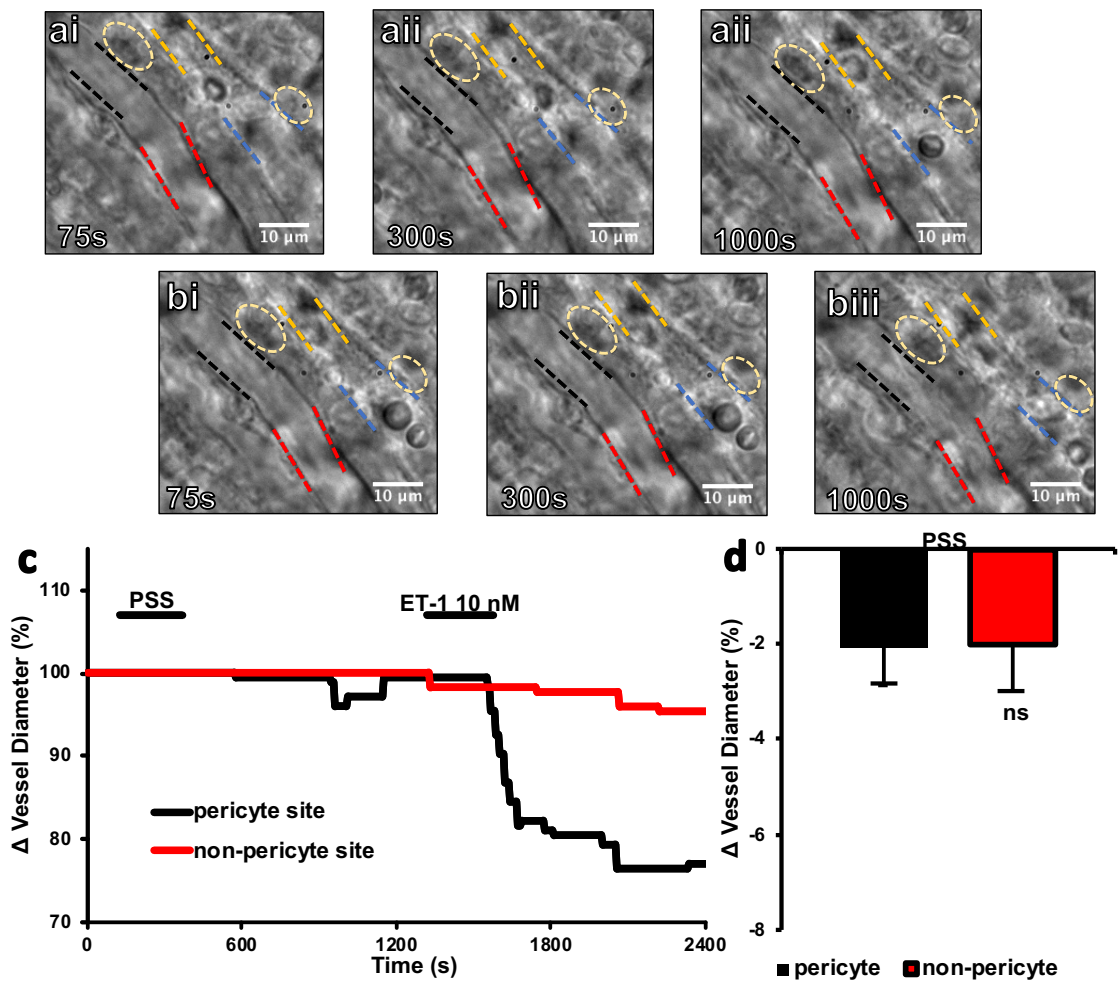


Figure 4.3 Pericytes in the C57BL/6J preparation only constrict in the presence of an agonist.

A standard differential interference contrast (DIC) field of view of *in situ* vasa recta for a time series experiment is shown in (ai-biii). (ai-iii) show a physiological saline solution (PSS) control experiment at: 75s (ai); 300s, where emulated experimental conditions have been replicated with PSS (aii); and 1000s, during a “wash out” period (aiii). Subsequently, (bi-biii) show the same capillary upon exposure to endothelin-1 (ET-1) in an identical setting before (bi), during (bii), and after (biii) at the same time points of the experiment. Pericyte cell bodies are indicated by a yellow dashed circle, pericyte sites by black or blue dashed lines, and non-pericyte sites by red dashed lines. What can be seen is that the vessel in the foreground does not respond in the presence of ET-1 (black and red dashed lines) but the vessel in the background (blue and orange dashed lines) is responsive. (c) In the responsive vessel, measurements were obtained from a pericyte site (c; black line) and corresponding non-pericyte site (red line) every 5s for the first 100s to establish the baseline diameter, then all subsequent measurements were expressed as the percentage change of that width. Experiments were 1200s long, and exposure to PSS is indicated by the 1st black bar (n=4 slices, and 3 animals). Afterwards, endothelin-1 (ET-1; 10 nM, 2nd black bar). The average change in vessel diameter upon exposure to PSS alone is presented in (d) at pericyte (black bar) and non-pericyte (red bar) sites (n=7 slices, and 7 animals). Values presented are mean \pm SEM. Scale bars are 10 μ m.

The overall response rate observed in the rat was, on average, 51% of pericytes (Crawford et al., 2012) whereas in the mouse model the overall average response rate is 30-40%, with individual agonist-induced responses varying from 14-67% depending on the agonist used. Also noted was the majority of vasoactive responses were of a lower magnitude than that observed in the rat This is discussed in greater detail below for each agonist individually (**Section 4.3.3**). On occasions where more than one slice per animal were used for the same experiment, some pericytes were responsive whilst others were not, further demonstrating that responsiveness is dependent upon the pericyte as opposed to the animal. This lower overall response rate and magnitude of responses is likely related to the known resistance of C57BL/6J mice to renal hypertension, and a strain related phenomenon of reduces vascular reactivity (Hartner et al., 2003).

4.3.3.1 Responsiveness of murine pericytes *in situ* to endogenous vasoactive compounds varies from those in the rat.

To characterise the vasoreactivity of the murine kidney slice model, and enable comparison with the rat model, slices were exposed to the same panel of well-known and functionally important vasoactive agents (Neuhofer, and Beck, 2005; Pallone, and Silldorff, 2001), that the Sprague-Dawley model had also been exposed to (Crawford et al., 2012; Crawford et al., 2011; Kennedy-Lydon et al., 2015). Values of pericyte-mediated changes in vessel diameter were not limited to the window of superfusion, as some agonists, such as ET-1, are known to have a lag before any vasoactivity occurs (Potts et al., 2012). Like-for-like concentrations of agonists were initially used on the murine slices, and dependent upon the responsiveness of the murine tissue were adjusted accordingly.

4.3.3.1.1 Angiotensin-II

Upon exposure of naïve vessels to angiotensin-II (Ang-II;100 nM), a significantly greater constriction occurred at pericyte sites ($10.1 \pm 2.6\%$) compared to non-pericyte sites ($3.3 \pm 1.0\%$, $n = 5$ slices and 5 animals, $p < 0.05$; **Figure 4.4(d)**), yet significantly lower than that observed in the rat ($29.3 \pm 4.7\%$ at pericyte sites, $p < 0.05$)(Crawford et al., 2012). As the response rate was moderately low at 100 nM ($\sim 35.7\%$), Ang-II concentration was moderated to determine if response rate could be improved. Ang-II

concentrations of; 1 nM, 10 nm, and 300 nM were assessed. Ang-II at 300 nM significantly reduced vessel diameter by $13.6\pm 2.5\%$ at pericyte sites compared with $3.5\pm 2.0\%$ at non-pericyte sites (n= 8 slices and 8 animals, $p < 0.005$; **Figure 4.4(d)**).

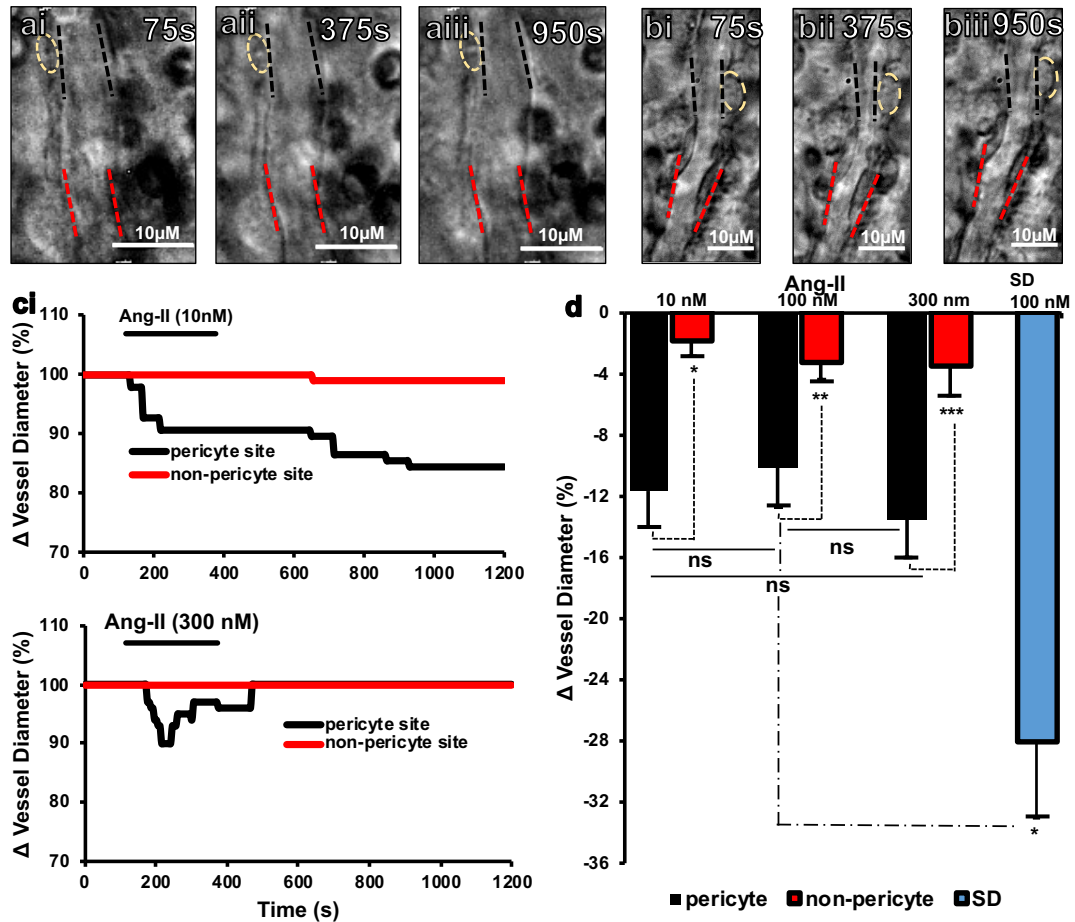


Figure 4.4 Angiotensin-II (Ang-II) evoked constriction of *in situ* vasa recta is of a lower magnitude than in the Sprague-Dawley (SD) model.

Representative differential interference contrast (DIC) images of time-series experiment of superfusion of a vasa recta capillary with either 10 nM (a) or 300 nM (b) of Ang-II: before (i); during exposure to the agonist (ii); and during a washout period from the agonist (iii). Pericyte cell bodies are indicated with yellow dashed circles, and corresponding pericyte (black dashed bars) and non-pericyte sites (red dashed bars) are indicated. 300 nM Ang-II (b) evokes a reversible response during superfusion, but 10 nM (a) evokes a sustained constriction; illustrated by representative traces for 10 nM (ci) and 300 nM (cii). These traces represent the % change over time at a paired pericyte site (black line) and non-pericyte site (red line), exposure to agonist is indicated by a black bar. Average data for superfusion experiments in the C57 with: 10 nM (n=11 slices and 11 animals); 100 nM (n=5 slices and 5 animals); and 300 nM (n=8 slices and 8 animals) of Ang-II show a significantly greater constriction at pericyte sites (black bar) than non-pericyte sites (red bar). The equivalent experiment with 100 nM Ang-II in the Sprague-Dawley rat model (SD; blue bar) shows the pericyte-mediated constriction is more significant in the SD model. The pericyte-mediated constriction was not significantly different between the varying concentrations of Ang-II in the C57 model. Values show mean \pm SEM, * $p < 0.05$, ** $p < 0.001$, *** $p < 0.0001$, ns = $p > 0.05$. Scale bars are 10 μ m.

Despite the magnitude of the vasoconstriction not significantly differing between Ang-II 100 nM or 300 nM ($p>0.05$), 300 nM yielded a higher response rate (60%). Of note is that both these constrictions were reversible; where diameter returned to within 10% of the baseline, as previously defined by Crawford *et al* (Crawford et al., 2012). Ang-II 10 nM also induced a pericyte-mediated constriction, of $12.0\pm 1.3\%$ at p sites (vs $1.8\pm 1.0\%$ at np sites, $p<0.0001$; $n= 11$ slices, and 11 animals), with a 46% response rate. However, this constriction was sustained until the end of the 20-min experimental window, reaching maximal constriction during the washout period (**Figure 4.4(cii)**). Ang-II 1 nM failed to reliably elicit a response ($<15\%$ response rate; $n=8$ slices, and 8 animals used in total).

4.3.3.1.2 Adenosine-5'-triphosphate and noradrenaline.

Superfusion with 100 μ M adenosine-5'-triphosphate (ATP) failed to elicit any vasoactive response ($n=13$ slices and 12 animals), with an average reduction of $1.6\pm 0.6\%$ at pericyte sites and $0.9\pm 0.5\%$ at non-pericyte sites ($p>0.05$). Unlike with Ang-II, where it was response rate needed optimisation from the initial experimental concentration, 100 μ M of ATP elicited no response. Given a reported resistance of the C57 strain to ATP (Donnelly-Roberts et al., 2009), the concentration was increased. 1 mM ATP caused a significant pericyte-mediated constriction ($9.6\pm 1.0\%$ vs $1.1\pm 0.7\%$ at non-pericyte sites; $n= 5$ slices and 5 animals, $p<0.005$; Figure 4.5c). Much like with 100 μ M Ang-II, this response rate was low (31.3%), so for a more reliable model a higher concentration of ATP (2 mM) was tested. This yielded a vasoconstriction that was significantly larger at pericyte sites than non-pericyte sites ($13.4\pm 1.3\%$ vs $1.8\pm 1.3\%$, $n=5$ slices and 5 animals, $p<0.005$; Figure 4.5a-c) and, a significantly larger constriction than that elicited by 1 mM ($p<0.05$). Tissue was more responsive to 2 mM than 1 mM, with a response rate of 45.5%. The magnitude of the pericyte-mediated constrictions elicited by 1 mM and 2 mM ATP were however significantly lower than those elicited by 100 μ M ATP in the rat ($19.4\pm 2.8\%$, $p<0.01$)(Crawford et al., 2011).

Like ATP, the initial concentration Noradrenaline (NA) used in the rodent slice technique (10 nM) was ineffective in the C57 model, with an average constriction of $2.2\pm 0.7\%$ at pericyte sites and 0.8 ± 0.4 at non-pericyte sites measured ($p<0.05$, $n=8$ slices and 8 animals; **Figure 4.5(f)**); not within the $>5\%$ threshold. Subsequently concentrations of 30 nM, 100 nM, and 300 nM were tested, with only 300 nM inducing a vasoactive response. 30 nM ($n = 7$ slices and 7 animals) and 100 nM ($n= 3$ slices and 3 animals) yielded pericyte-mediated constrictions of $1.5\pm 1.0\%$ and $0.6\pm 0.6\%$ at

pericyte sites respectively. NA 300 nM had a low response rate of 36.4%, but elicited an average vasoconstriction of $15.4 \pm 2.7\%$ at pericyte sites, vs $1.3 \pm 0.6\%$ at non-pericyte sites ($p < 0.05$, $n = 4$ slices and 4 animals; **Figure 4.5(c-f)**). Interestingly, upon optimisation of the concentration; the magnitude of response isn't significantly different between species ($20.8 \pm 5.1\%$; $p > 0.05$) (Crawford et al., 2012) but the concentration is 30-times greater (10 nM vs 300 nM).

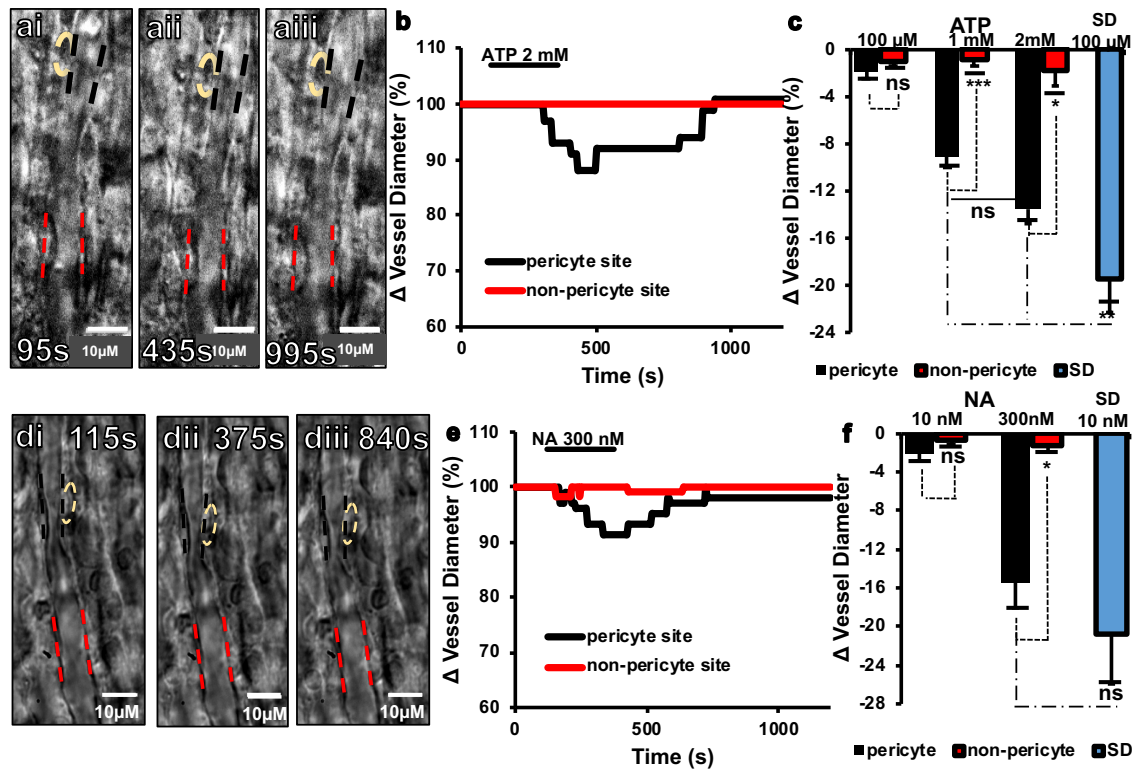


Figure 4.5 Adenosine-5'-triphosphate (ATP) and noradrenaline (NA) needed marked increase in concentration to stimulate vasoactivity of C57BL/6J *in situ* vasa recta capillaries.

Representative differential interference contrast (DIC) images of time-series experiment of superfusion of a vasa recta capillary with either ATP (a) or NA (d) before (i), during exposure to the agonist (ii), and during a washout period from the agonist (iii). Pericyte cell bodies are indicated with a yellow dashed circle, and corresponding pericyte (black dashed bars) and non-pericyte (red dashed bars) sites are indicated. A corresponding representative trace of the % change in diameter over time for ATP (b) and NA (e) at pericyte (black) and non-pericyte (red) sites, with exposure to agonist indicated by a black bar. Average superfusion data for: ATP (c) at concentrations of 100 μM ($n = 13$ slices and 12 animals), 1 mM ($n = 5$ slices and 5 animals), and 2 mM ($n = 5$ slices and 5 animals); and NA (f) at concentrations of 10 nM ($n = 8$ slices and 8 animals) and 300 nM ($n = 7$ slices and 7 animals) show a significantly greater constriction at pericyte sites (black bars) than non-pericyte sites (red bars). The equivalent experiment with 100 μM ATP (c) in the Sprague-Dawley rat model (SD; blue bars) shows the pericyte-mediated constriction is more significant in the SD model but not with 10 nM NA (f). Values are mean \pm SEM. * = $p < 0.05$, * = $p < 0.005$, *** = $p < 0.001$, ns = $p > 0.05$. Scale bars are 10 μm.

4.3.3.1.3 Endothelin-1

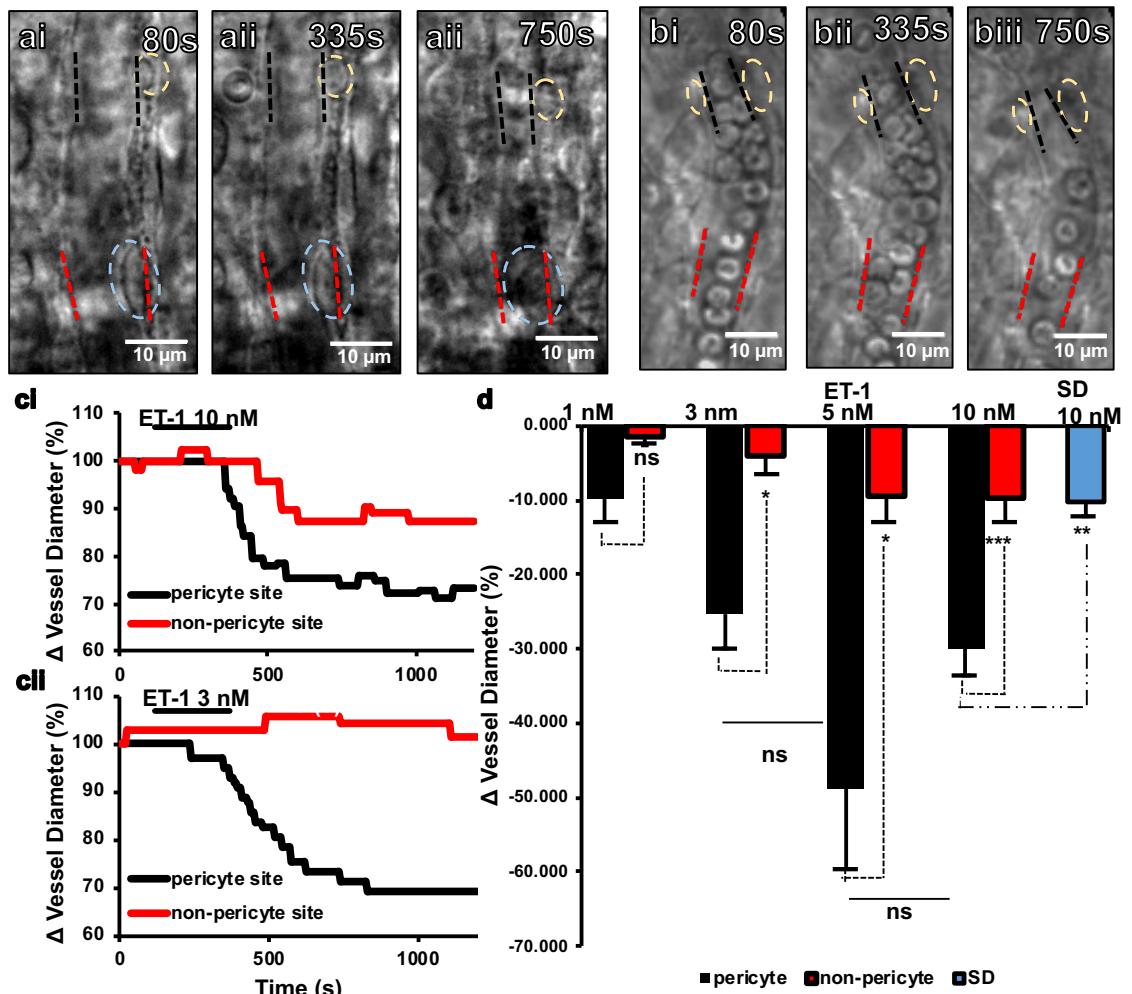


Figure 4.6 Endothelin-1 (ET-1) evoked a significantly greater, pericyte-mediated, constriction in the C57BL/6J mouse.

Representative differential interference contrast (DIC) images of time-series experiment of superfusion of a vasa recta capillary with either 10 nM (a) or 3 nM (d) of ET-1 before (i), during exposure to the agonist (ii), and during a washout period from the agonist (iii). Pericyte cell bodies are indicated with yellow dashed circles, and corresponding pericyte (black dashed bars) and non-pericyte sites (red dashed bars) are indicated. It can be seen with both 10 nM (a) and 3 nM (b) that a vasoactive response begins towards the end of superfusion and is sustained; illustrated by representative traces for 10 nM (ci) and 3 nM (cii). These traces represent the % change over time at a paired pericyte site (black line) and non-pericyte site (red line), exposure to agonist is indicated by a black bar. Average data for superfusion experiments in the C57 with 1 nM (n=4 slices and 4 animals), 3 nM (n=4 slices and 4 animals), 5 nM (n=5 slices and 5 animals), and 10 nM (n=7 slices and 7 animals) of ET-1 show a significantly greater constriction at pericyte sites (black bar) than non-pericyte sites (red bar). The equivalent experiment with 10 nM ET-1 in the Sprague-Dawley rat model (SD; blue bar) shows the pericyte-mediated constriction is more significant in the C57 model. Values are mean±SEM. * = p<0.05, ** = p<0.005, *** = p<0.0001. Scale bars are 10 μm.

ET-1 10 nM significantly decreased vasa recta diameter by 30.0±3.7% at pericyte sites compared to 9.8±3.1% at non-pericyte sites (n= 7 slices and 7 animals, p<0.0001;

Figure 4.6(d)). This is significantly larger (~3 fold) than the vasoconstriction elicited by ET-1 10 nM in the rat (10.3 ± 1.9 , $p < 0.001$) (Crawford et al., 2012). Despite having the highest response rate of any agonist assessed (66.7%), this concentration resulted in severe endothelial swelling (**Figure 4.6(a)**) and so the concentration was lowered for optimisation. ET-1 1 nM, elicited a non-significant response ($12.2 \pm 2.5\%$ at pericyte sites vs $2.0 \pm 1.1\%$ non-pericyte sites, $p > 0.05$, $n = 4$ slices and 4 animals; **Figure 4.6d**). ET-1 5 nM induced a significant, pericyte-mediated constriction of $48.7 \pm 11.0\%$ at pericyte sites (vs $9.4 \pm 3.5\%$ at non-pericyte sites, $p < 0.05$, $n = 5$ slices and 5 animals; **Figure 4.6(d)**) with a lower response rate of 50%. Superfusion with 3 nM ET-1 also induced a significant constriction of $25 \pm 5\%$ at pericyte sites (vs $4.1 \pm 2.5\%$ at non-pericyte sites, $p < 0.05$, $n = 4$ slices and 4 animals), with a pericyte-response rate of 50%. There was no significant difference between the pericyte-mediated constriction at differing concentrations of ET-1 ($p > 0.05$; **Figure 4.6(d)**). For all concentrations, constriction began during the end of drug exposure, with maximal values not observed until approximately 600s after removal and sustained until the end of the 1200s experiment (**Figure 4.6(c)**).

4.3.3.1.4 Prostaglandin E₂ and bradykinin

Prostaglandin E₂ (PGE₂) 10 μ M caused a significant, irreversible dilation that was significantly greater at pericyte sites ($6.5 \pm 0.4\%$) than non-pericyte sites ($0.6 \pm 0.3\%$; $n = 6$ slices and 4 animals, $p < 0.001$; **Figure 4.7(a)**). This pericyte-mediated dilation is not significantly different than that observed in the rat ($8.6 \pm 1.6\%$, $p > 0.05$) (Kennedy-Lydon et al., 2015; Crawford et al., 2012), with a 60% pericyte-response rate. In 2 of the 6 responders, there was an observed constriction before the dilation (**Figure 4.7(b)**). To determine if the concentration of PGE₂ could be further optimised, 1 μ M and 100 μ M were also applied. 1 μ M was ineffective, with an increase in diameter of $4.6 \pm 0.9\%$ at pericyte sites and $1.3 \pm 1.3\%$ at non-pericyte sites ($n = 4$ slices and 2 animals, $p > 0.05$). 100 μ M of PGE₂ induced a significant response, causing an average dilation of $11.0 \pm 3.3\%$ at pericyte-sites and $1.1 \pm 0.5\%$ at non-pericyte sites ($n = 5$ slices and 5 animals, $p < 0.05$), with a 36.4% response rate.

Due to experimental error not noted until post-experimentation and optimisation, a concentration of 10 μ M as opposed to 10 nM was used in the murine model. Bradykinin (BK) 10 μ M failed to elicit a significant response ($n = 10$ slices and 8 animals), so both 1 μ M and 100 μ M were tested. 100 μ M failed to elicit a response in the murine model ($n = 8$ slices and 5 animals), yet 1 μ M ($n = 6$ slices and 6 animals) elicited a significant

pericyte-mediated vasoconstriction of vasa recta capillaries of $13.8 \pm 2.4\%$ compared to non-pericyte sites ($2.4 \pm 0.8\%$, $p < 0.05$), with a response rate of $\sim 50\%$, whereas in the rat a concentration of 10 nM resulted in a pericyte-mediated vasodilation of $8.3 \pm 1.6\%$ (Kennedy-Lydon et al., 2015)

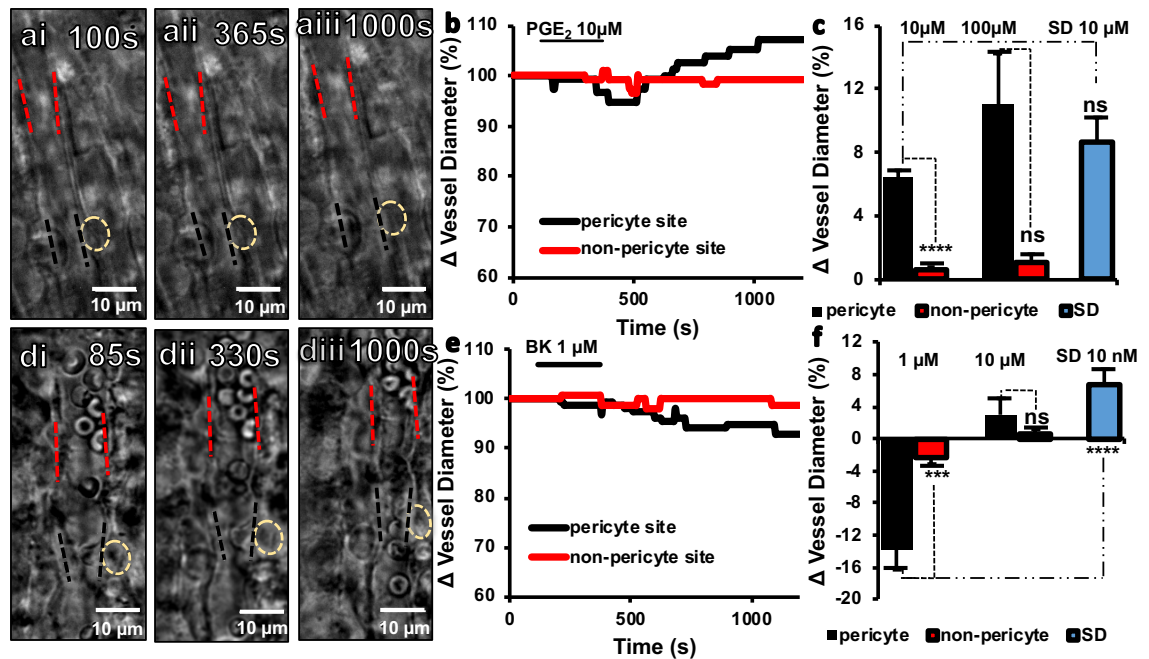


Figure 4.7 Prostaglandin E₂ (PGE₂) and Bradykinin (BK) needed marked increase in concentration to stimulate vasoactivity of C57BL/6J *in situ* vasa recta capillaries.

Representative differential interference contrast (DIC) images of time-series experiment of superfusion of a vasa recta capillary with either PGE₂ (a) or BK (d) before (i), during exposure to the agonist (ii), and during a washout period from the agonist (iii). Pericyte cell bodies are indicated with a yellow dashed circle, and corresponding pericyte (black dashed bars) and non-pericyte (red dashed bars) sites are indicated. A corresponding representative trace of the % change in diameter over time for PGE₂ (b) and BK (e) at pericyte (black) and non-pericyte (red) sites, with exposure to agonist indicated by a black bar. Average superfusion data for: PGE₂ (c) at concentrations of $10 \mu\text{M}$ ($n=6$ slices and 4 animals), and $100 \mu\text{M}$ ($n=5$ slices and 5 animals); and BK (f) at concentrations of $1 \mu\text{M}$ ($n=6$ slices and 6 animals) and $10 \mu\text{M}$ ($n=10$ slices and 8 animals) show a significantly greater constriction at pericyte sites (black bars) than non-pericyte sites (red bars). The equivalent experiment with $10 \mu\text{M}$ PGE₂ (c) in the Sprague-Dawley rat model (SD; blue bars) shows a pericyte-mediated of comparable magnitude in the SD model, but with 10 nM BK (f) a vasodilation is observed, not a pericyte-mediated constriction. Values are mean \pm SEM. *** = $p < 0.005$, **** = $p < 0.0001$ ns = $p > 0.05$. Scale bars are $10 \mu\text{m}$.

4.3.3.2 Superfusion of C57BL/6J slices with exogenous compounds demonstrates pericyte-mediated vasoactivity.

After establishing the behavioural profile of murine vasa recta pericytes in response to endogenous key regulators of blood flow, it was then appropriate to investigate how exogenous compounds would affect pericyte-mediated regulation of *in situ* vasa recta

diameter. To investigate: Tyramine, affecting NA and ATP release from varicosities (Kirkpatrick, and Burnstock, 1994); and Indomethacin, attenuating the local production of PGE₂ were used, as they had been in the rat (Crawford et al., 2012). The NO donor S-Nitroso-N-Acetyl-D,L-Penicillamine (SNAP) was also administered. As the high concentration of ATP required to elicit a response in the mouse is indicative of P2X₇-receptor activation (Donnelly-Roberts et al., 2009), the competitive agonist 3'-O-(4-Benzoyl)benzoyl adenosine5'-triphosphate (BzATP) was superfused for comparison .

Superfusion with SNAP 100 µM elicited a significant pericyte-mediated dilation of 11.4±1.4% at pericyte sites (vs 1.5±0.8% at non-pericyte sites, p<0.0005, n=6 slices and 6 animals) with a 30% response rate, comparable to dilation achieved in the rat (12.6±2.9%, p>0.05; **Figure 4.8(e)**) (Crawford et al., 2012), consequently no optimisation of this agent was performed.

Indomethacin 30 µM elicited a reversible pericyte mediated constriction of 14.4±2.4% (vs 2.4±1.9% at non-pericyte sites, p<0.0005, n=6 slices and 6 animals), with a 38% response rate in the murine kidney slice model. This constriction was not significantly different from the constriction observed in the rat (9.9±0.5%, p>0.05; **Figure 4.8(f)**) (Crawford et al., 2012), correlating with the observations for PGE₂ above (**section 4.3.3.1.4**) that there was no significant differences in the vasoactive response between the species.

Superfusion of murine kidney slices with 10 µM of BzATP resulted in a significantly greater constriction at pericyte sites than non-pericyte sites (9.1±1.7% vs 1.8±0.9% respectively, p<0.005, n= 6 slices and 6 animals; **Figure 4.8(i)**) BzATP is approximately 10-30x more potent than ATP at P2X₇-(Sugiyama et al., 2005; Crawford et al., 2011; Donnelly-Roberts et al., 2009), and this constriction was not significantly different from that elicited by either 1 mM or 2 mM ATP in the mouse (p>0.05). With a response rate of 33%, this is comparable to the response rate observed with 1 mM ATP (**section 4.3.3.1.2**). Much like with ATP, the constriction elicited by BzATP in the mouse is significantly less than that observed in the rat (20.2±2.5%, p<0.0001). Given the expense of BzATP, higher concentrations were not assessed as they were with ATP.

Interestingly, whilst SNAP, BzATP, and indomethacin data correlate with observations in the rat, application of 1 µM tyramine caused a pericyte-mediated dilation. The dilation was significantly greater at pericyte sites than non-pericyte sites (10.7±1.7% and 3.2±1.1% respectively, p<0.005, n= 4 slices and 4 animals), with a 36% response rate, significantly different from the tyramine-evoked constriction (11.9±2.5%, p<0.0001; **Figure 4.8(L)**) observed in the rat (Crawford et al., 2012). Whilst 1 µM

Tyramine induced a pericyte-mediated vasodilation, it has been reported that low concentration ATP is vasodilatory (Crawford et al., 2011). Given the insensitivity to NA observed in the model, it is possible that the neurotransmitter release was such to favour dilation. Superfusion with other concentrations of tyramine were ineffective, not breaching the >5% change in vessel baseline diameter threshold. 100 nM of tyramine elicited a non-significant response (-4.4±2.0% at pericyte sites vs -0.4±0.2% at non-pericyte sites respectively (n=4 slices and 4 animals), as did 10 µM, 30 µM (n>3 slices and 3 animals).

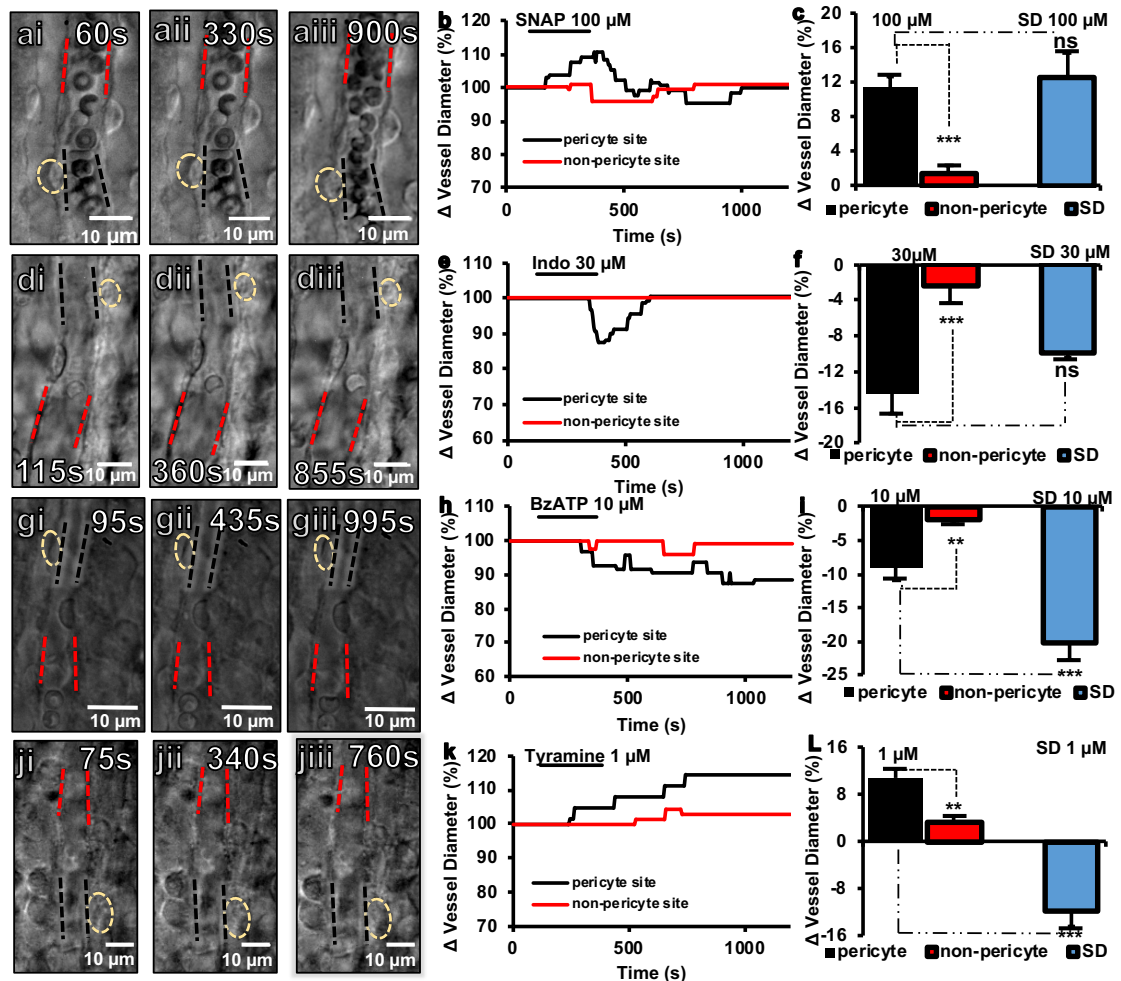


Figure 4.8 Simulating or attenuating the release of endogenous compounds in C57BL/6J kidney slices.

Representative differential interference contrast (DIC) images of time-series experiment of superfusion of a vasa recta capillary with either SNAP 100 µM (a), Indomethacin 30 µM (Indo; d), BzATP 10 µM (g) or Tyramine 1 µM (j) before exposure (i), during exposure to the agonist (ii), and during a washout period from the agonist (iii). Pericyte cell bodies are indicated with a yellow dashed circle, and corresponding pericyte (black dashed bars) and non-pericyte (red dashed bars) sites are indicated. A corresponding representative trace of the % change in diameter over time for SNAP (b), Indo (e), BzATP (h) and Tyramine (k) at pericyte (black) and non-pericyte (red) sites, with exposure to agonist indicated by a black bar. Average superfusion data for C57BL/6J are shown (c,f,i and L) comparative to the Sprague-Dawley (SD; blue bars) model at the corresponding concentrations. Values are mean±SEM. ** = p<0.05, ***=p<0.0001 ns = p>0.05. Scale bars are 10 µm

4.4 Discussion.

As a heterogeneous population of cells, establishing the baseline vasoactive behaviour of murine pericytes, in line with the known vasoactive physiology of the species, was necessary to validate the C57BL/6J (C57) kidney slice model. What has been shown in this chapter is that murine NG2⁺ pericytes have comparable renal distribution and morphology to those of the rat (Crawford et al., 2012), they are vasoactive in response to locally important regulators of blood flow such as Ang-II and PGE₂ (Crawford et al., 2012; Almaça et al., 2018; Peppiatt et al., 2006), and the magnitude of pericyte-mediated regulation of vasa recta diameter reflects the known differences in vascular physiology between C57 mice and Sprague-Dawley (SD) rats (Russell, and Watts, 2000; Cholewa et al., 2005; Hedemann et al., 2004; Zhao et al., 2009). Further still, characterising NG2⁺ pericyte morphological characteristics highlighted other cross-species consistencies in their size and showed the pericyte-mediated regulation of medullary blood flow is a conserved behaviour of renal pericytes across species (Cunningham, 2002; Boswell et al., 2014), and validated the murine as an investigative tool for establishing renal pericyte characteristics with the data generated offering predictive validity in a translatable fashion (Denayer et al., 2014).

4.4.1 C57BL/6J kidney slices are viable.

Upon slicing the C57 kidneys, slicing both together provided 3-5 usable slices whereas the SD model provided approximately 5-6 usable slices per kidney (unpublished data). Given that murine kidneys are approximately 10 times smaller than rat kidneys (Becker, and Hewitson, 2013), this suggests murine kidneys have a larger medulla, possibly facilitating a more concentrated urine (Sands, and Layton, 2009). Further still, the slices obtained were viable with ~79% of cells alive, as was reported in the SD model (Crawford et al., 2012). A different C57BL/6J kidney slice preparation, using the same method of H342 and PI co-labelling, had comparable viability at 90-minutes (Brähler et al., 2016) with another lab assessing ATP content of C57 kidney slices determining they were viable up to 72-hours (Poosti et al., 2015). The window for use of C57 slices was a maximum of 4-hours here and is well within this timeframe of viability.

4.4.2 C57BL/6J NG2⁺ pericyte morphology is comparable to the rat whilst vasa recta capillaries are smaller.

Antibodies against NG2 and IB₄ were used for fluorescent identification and co-localisation of pericytes to vasa recta. Vasa recta capillaries were approximately 13% and 16% smaller in diameter in the mouse than the rat at pericyte sites and non-pericyte sites respectively. Murine red blood cells (RBCs) are 6.0 µm in diameter comparative to rat RBC measuring 6.5 µm in diameter, (Unekawa et al., 2010) hence the capillary diameter also being comparably smaller between species. Much like the rat, a greater density of pericytes in the OM than the IM was observed (**Table 4.1**) (Crawford et al., 2012; Park et al., 1997b). This reduced density in the IM is likely reflective of the reduced density of the DVR (Pallone et al., 2003b; Park et al., 1997a).

There were significantly fewer NG2⁺ pericytes in both the OM and the IM of the C57BL/6J slices comparative to the rat, but pericyte soma were not significantly different in size. There are differences in arrangements of the vasa recta in mice, being more interwoven with medullary tubules in the mouse (Fazan et al., 2002; Kriz, and Kaissling, 2013), which might obfuscate some pericytes. However, given the size difference between rats and mice, with rats being larger (Becker, and Hewitson, 2013) and having a significantly larger vascular volume (Boswell et al., 2014), this lower density is likely reflective of fewer vasa recta overall. It also implies there would be less NG2⁺/α-SMA⁺ DVR pericytes available to constrict, potentially why the response rate was lower in C57 than SD (**section 4.4.2**).

Interestingly, whilst pericyte soma size was not different, murine pericytes had significantly longer longitudinal primary processes than in the rat (**Section 4.3.2**). However, in both species the length of longitudinal processes ensured the endothelium was covered. This could suggest that pericytes ensure vascular stability with their process length supporting the vessel (Bergers, and Song, 2005) with the circumferential processes enacting their contractility (Courtoy, and Boyles, 1983), demonstrated by constrictions and dilations remaining localised to the pericyte soma where these circumferential processes reside and not further along with the longitudinal processes.

Overall, given the difference in process length, this consistency in pericyte soma size could be used as a consistent objective metric for identification of pericytes across species. As there was no difference between OM and IM NG2⁺ pericyte measurements in the mouse, they are not considered separately.

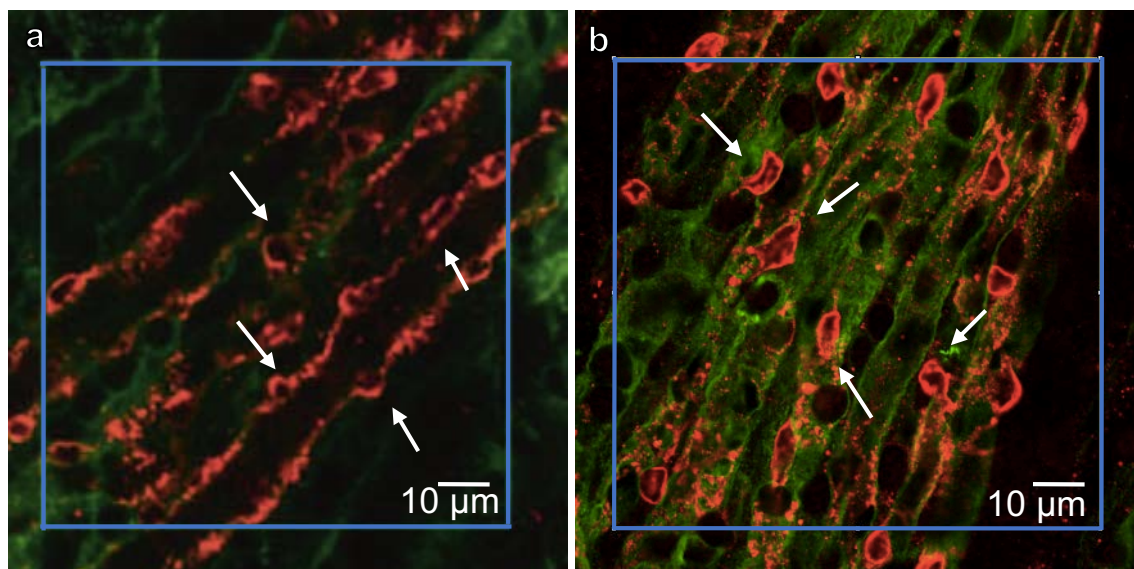


Figure 4.9 Interspecies differences between SD (a) and C57 (b) pericyte density. Vasa recta capillaries were labelled with Alexa-488-conjugated IB 4 (*green*). The cell body (arrows) of pericytes in the renal medulla were labelled with anti-NG2 and Alexa-555-conjugated secondary antibody (*red*). It can be seen there are more pericytes in rodent tissue (a) than murine tissue (b). Image (a) adapted from (Crawford et al., 2012).

4.4.3 C57BL/6J renal pericyte-mediated responsiveness is less frequent than the SD model.

After the murine kidney slices were deemed viable and the structural environment was established, functional experiments were conducted. The vasoactive agents that were chosen are considered to be the most relevant autocrine or paracrine factors modulating medullary O₂ supply (Neuhofer, and Beck, 2005; Pallone, and Silldorff, 2001; Cowley et al., 1995), and had been used in the rat previously (Crawford et al., 2012; Crawford et al., 2011; Kennedy-Lydon et al., 2015). Overall, the observation that not all pericytes respond in the mouse is in line with other models investigating pericyte-mediated regulation of capillary diameter. When reported, rodent pericyte models often demonstrate a moderate response rate; 10-37% of depending on the vasoactive agent and tissue (Kawamura et al., 2003; Peppiatt et al., 2006). A notable difference between the two species for the kidney slice models was the reduced responsiveness of the murine vessels. In the rat, on average, 50-60% of pericytes identified respond to superfusion with vasoactive agents with a significant, measurable response (Crawford et al., 2012). In the mouse, however, even upon optimisation of the concentration, the average response rate is lower at approximately 30-40% of pericytes, and the alterations in vessel diameter are, bar the exception of ET-1, of a lesser magnitude (discussed below in section 4.4.4.5). In the C57BL/6J strain

specifically, it has been observed that they are less prone to hypertension (Hartner et al., 2003), and other vascular models in this strain have shown vasoactivity of a lower magnitude comparative to the SD rat (Russell, and Watts, 2000; Cholewa et al., 2005; Hedemann et al., 2004; Zhao et al., 2009). The alterations of vasa recta diameter measured were localised to the pericyte site in the presence of all of these agents known to endogenously regulate MBF. Whilst it is likely endothelial cells (EdC) might influence vasoactivity (McCarron et al., 2017), if all pericytes were to respond it would not reflect the refined control (Crawford et al., 2012) that is necessary for MBF to be physiologically regulated. The OM tubules are not perfused by capillaries that arise from their parent glomerulus and as such a global change in perfusion would lead to a perfusion-metabolism mismatch (Chou et al., 1990). This reduced response rate in both species also likely reflects that not all pericytes will respond due to their myriad of functions (Harrell et al., 2018), reports of pericyte-mediated vasoactivity from other tissues (Kawamura et al., 2003; Peppiatt et al., 2006), and the additional resistance observed in the mouse due to their known vascular physiology.

4.4.4 C57BL/6J renal pericytes are vasoactive, and contractility reflects known species differences in vascular reactivity

For any model, predictive functionality e.g. the model reliably responding, is a necessary requisite for generating valid data (Astashkina et al., 2012). As such, concentrations were optimised to produce the maximal response possible at the lowest concentration of agonist for a set exposure timeframe. Initial concentrations trialled matched those used in the rat preparation for like-for-like comparisons, which were then adjusted with respect to the measured contractile response and the pericyte response rate in the mouse. Interestingly, for all agonists bar ET-1, the magnitude of the contractile pericyte-mediated response of the C57 model was significantly lower than those even the rat post-optimisation, and reflects reported interspecies differences in isolated liver (Zhao et al., 2009), mesentery (Hedemann et al., 2004), and abdominal aorta (Russell, and Watts, 2000) vascular models, as well as systemically (Billet et al., 2007; Cassis et al., 2004) and in cell culture models (Donnelly-Roberts et al., 2009). However, vasodilatory agents were comparable between the two species.

4.4.4.1 Angiotensin II-mediated constriction of DVR-pericytes is conserved across species.

Angiotensin-II (Ang-II) is a key regulator of MBF (Dickhout et al., 2002; Cowley Jr, and O'Connor, 2013; Fan et al., 2019), with systemic administration resulting in a more pronounced reduction of MBF than cortical perfusion (Fan et al., 2019), and its contractility attenuated within the medulla via mTAL-produced nitric oxide (NO)-mediated tubulovascular feedback to the vasa recta (Dickhout et al., 2002). Whilst Ang-II binding is most significant in the kidney for both rats and mice, SD rat kidneys have approximately double the Ang-II receptor density. Further still, contractile actions of Ang-II are primarily mediated by the AT_{1A} receptor (Billet et al., 2007; Cassis et al., 2004; Rodrigues et al., 2009), yet radiolabelling has shown AT₂ predominates in the murine medulla, with markedly less expression of AT₁ [48]. What AT₁-R are present could have their activity limited by AT₂-R-dependent NO and prostacyclin release (AbdAlla et al., 2001; Russell, and Watts, 2000). Further still, AT₁-R dimerizes with B₂-R and results in a more potent activity of Ang-II in the SD (AbdAlla et al., 2000) which might not occur as readily in the C57 medulla.

Yet, whilst being a key agonist in both species the action of Ang-II is markedly different. *Ex vivo* in the liver and thoracic aorta (Zhao et al., 2009; Russell, and Watts, 2000), and via *in vivo* administration (Cassis et al., 2004; Cholewa et al., 2005) the vascular response of the mouse is reduced compared to the rat. *In vivo*, 10-times the concentration of Ang-II was needed systemically to elicit a modest increase in blood pressure in C57 eliciting approximately 50 % of the reduction of blood pressure measured for the rat (Cholewa et al., 2005; Cassis et al., 2004). This was reflected here in the pericyte-mediated vasoactive response in the kidney. The magnitude of the constriction in the mouse in here for 300 nM was approximately half that of the rat elicited by 100 nM Ang-II, and 2/3^{rds} that elicited by 10 nM Ang-II (Crawford et al., 2012), reflecting the findings in the literature above.

Whilst the constriction measured was not significantly different between 100 nM and 300 nM in C57, the response rate was far more reliable at 60% versus 37%, hence the selection of this concentration as optimal for this preparation. Interestingly, the shape of the 300 nM Ang-II-induced constriction; the rapid onset and gradual return to baseline, matches observations in mice (Ruan et al., 1999; Cassis et al., 2004; Outzen et al., 2015), in the rodent live slice model (Crawford et al., 2012), and in isolated human outer medullary DVR (Sendeski et al., 2013), showing a conserved behaviour

between the animal models and humans upon concentration optimisation, whilst reflecting the reported sensitivities of these different species to Ang-II.

4.4.4.2 Bradykinin is contractile at high concentrations at C57 DVR pericytes.

Whilst still not fully elucidated BK may also play a role in the control of medullary oxygenation, dependent upon the constitutively expressed B₂-R (Kakoki et al., 2007), which is involved in Na⁺/K⁺ homeostasis (Zhang et al., 2018). Blockade of B₂-R selectively reduces MBF without affecting the GFR in rats (Mattson, and Cowley, 1993; Fenoy, and Roman, 1992), whilst perfusion with bradykinin selectively increases MBF in rodent isolated (I) outer medullary DVR, in part due to stimulation of by activity at this receptor (Pallone et al., 1998a; Rhinehart et al., 2002; Pallone et al., 2003b) as well as its effect on local PGE₂ production (Mattson, 2003). Due to conserved similarity between rats and mice in expression of the B₂R (Ma et al., 1994), and BK's known pharmacology it could be assumed that the pericyte-mediated dilatory responses observed in rats would be comparable in mice. Due to experimental error, a concentration of 100-1000-times that used in the SD model (Kennedy-Lydon et al., 2015) was used here and interestingly induced a significant pericyte-mediated vasoconstriction.

On smooth muscle cells, BK is contractile via B₂-R as opposed to dilatory (Wong, 2016), with dilatory functions being endothelium-dependent (Wong, 2016). Activation of B₂-R in the rat leads to afferent arteriolar dilation yet it constricts mesangial cells (Bascands et al., 1994) suggesting BK can be contractile at subpopulations of pericytes in the kidney (Am et al., 2013). However, even though the concentrations are not comparable here this species difference in contractility to BK has been noted previously. In an aortic smooth muscle model, BK caused vasoconstriction in C57 mice (Felipe et al., 2007), whereas in the SD rat model BK produces a vasodilation of aortic smooth muscle at the same concentration (Benetos et al., 1997). Due to experimental error, further comment cannot be made on the interspecies differences in a like-for-like manner. Yet some evidence exists to suggests an indirect mechanism could be responsible for this BK-induced constriction.

In the C57 mouse, 1-10 μM BK-B₂-R signalling, as well as Ang-II-AT₂-R signalling (Wu et al., 2018), inhibits K⁺ channel Kir4.1 and thereby downregulates the sodium-chloride symporter (NCC) on the distal convoluted tubule (DCT) (Zhang et al., 2018), As discussed below in section 4.4.4.6, inhibition of the mTAL Na-K-2Cl results in a

secondary constriction of DVR as a response to reduced metabolic demand (Fan et al., 2019), this may be true for other salt transporters. Further still, there are species related differences to NCC downregulation; acute Ang-II infusion reduces DCT expression of NCC in C57 (Zhao, and Navar, 2008). In SD rats, NCC expression only reduces once acute circulating Ang-II levels fall (Lee et al., 2009). Ang-II activity and BK activity are interrelated (Rodrigues et al., 2009; AbdAlla et al., 2000) and it is therefore possible that BK in murine kidneys would not perform the same as in the rat. As kidney slices retain all the functional architecture of the kidney, it is possible that compensatory mechanisms are activated by BK-stimulation to constrict pericytes on the DVR in response to downregulation of NCC in mice via tubulovascular crosstalk.

4.4.4.3 Adenosine-5'-triphosphate and BzATP suggest DVR pericytes- contractility is mediated at least in part by P2X₇.

ATP is the signalling molecule for the autoregulatory tubuloglomerular feedback mechanism (Peti-Peterdi, and Harris, 2010; Marsh et al., 2019; Bell et al., 2003), with further evidence for autoregulatory activity of purinergic signalling in the medulla, involved in tubulovascular crosstalk between the medullary thick ascending limb (mTAL) and DVR pericytes (Cowley Jr, and O'connor, 2013; Crawford et al., 2011; Crawford et al., 2013; Dickhout et al., 2002). Both rat renal and CNS pericytes have shown to express P2 receptors which are responsible for the vasoactivity of ATP, with both pericyte-mediated constriction and dilation measured (Crawford et al., 2011; Cai et al., 2018; Methner et al., 2019).

The ATP concentration required to elicit a significant response in the mouse was 10-20-fold that of the rat, which has been reported previously (Donnelly-Roberts et al., 2009; Li et al., 2012). Superfusion with 1-2 mM of ATP was required to elicit a response in C57 mouse kidney slices, which has been reported for the C57 brain (Cai et al., 2018) and muscle vasculature (Cai et al., 2018). Conversely, in the SD kidney slice model 100 μ M of ATP was sufficient, with a constriction approximately double the magnitude of the mouse, showing as a species it is more sensitive to ATP-induced vasoconstriction. However, responsiveness to ATP may vary between organs as both C57 (Cai et al., 2018) and SD (Peppiatt et al., 2006) brain preparations responding to 1 mM ATP. However, whilst 100 μ M has shown efficacy in rat pericyte models for the retina and kidney (Sugiyama et al., 2005; Crawford et al., 2011), it is ineffective at C57 pericytes in the pancreas (Almaça et al., 2018), renal pericytes here, and with concentrations of 1-10 mM used in the skeletal muscle and brain (Cai et al., 2018;

Methner et al., 2019), so it is likely the mouse as a species is less responsive to ATP than the rat. Interestingly, in murine muscle fibres, 100 μM of ATP is dilatory whereas in the rat it is contractile (Ziganshina et al., 2019), suggesting a concentration of 100 μM ATP in the kidney slice model may be insufficient to induce a constriction, yet too high a concentration for dilation.

This considered, these concentrations of ATP used to induce constriction in both C57 and SD models are high, for the respective species, which suggests activation of the P2X₇ receptor (P2X₇-R) (Vonend et al., 2005; Donnelly-Roberts et al., 2009; Crawford et al., 2011). The resistance of C57 to ATP-induced contractility, and lower magnitude of response, may reflect the strain specific loss of function mutation in the P2X₇-R (Adriouch et al., 2002), and possibly facilitates some of the species resistance to hypertension (Neuhofer, and Beck, 2005; Hartner et al., 2003). BzATP is 10-30x more potent than ATP at P2X₇-R (Sugiyama et al., 2005; Crawford et al., 2011; Donnelly-Roberts et al., 2009), and this was also reflected in the mouse. The C57 mouse model did not require the concentration of BzATP to be adjusted (10 μM) and the constrictions measured was not significantly different to that obtained by ATP (1-2 mM). BzATP was notably potent in the SD kidney slice model, with detectable pericyte-expression of P2X₇ mRNA (Crawford et al., 2011). With the pericyte-mediated contractility efficacious to superfusion with BzATP in both species, this further suggests DVR pericytes express and can exert contractility through P2X₇-receptor activation.

In vivo, high concentrations of ATP occur in response to extreme cellular damage (North, 2002) so it is possible that ATP-induced constriction is pathological, whereas ATP-induced pericyte-mediated dilation is a homeostatic mechanism that maintain medullary perfusion to the mTAL (Cowley Jr, and O'connor, 2013). Dilation of DVR pericytes in response to low ATP concentrations and the interspecies vasoactive differences to ATP may be further reflected by the murine response to tyramine and NA, discussed in more detail below in **section 4.4.4.4**, but further work is needed to fully understand this.

4.4.4.4 The activity of noradrenaline (NA) and tyramine in the mouse further suggest species-related differences to both NA and ATP

The sympathetic nervous system is involved in the regulation of renovascular resistance by release of ATP and NA (Vonend et al., 2005). Blood flow in the cortex is seemingly more sensitive to NA stimulation than the medulla, primarily due to the α_2

receptor (α_2 -R) presence in the medulla which can attenuate NA-mediated vasoconstriction via α_2 -mediated release of NO (Mattson, 2003; Vonend et al., 2009). However, there is a notable renal medullary presence of varicosities (Yang et al., 1995; Crawford et al., 2012), within 2 μm of NG2⁺ pericytes in the rat kidney (Crawford et al., 2013), suggesting innervation is involved in MBF regulation. Further still, denervation markedly influences MBF more than CBF in the rat, with renal nerve stimulation having a significantly greater impact on MBF (Hermansson et al., 1984). Together these are suggestive of sympathetic involvement in maintaining tonicity of the DVR. However, in line with other vasoconstrictors, the C57 mouse model was resistant to NA.

NA enacts its contractile effects via α_1 -R which have noted differential activity in murine and rodent aorta (Russell, and Watts, 2000), with comparable findings here. To induce a comparable vasoconstriction of vasa recta in the C57 mouse model, 30-times the concentration of NA was required (Crawford et al., 2012). Interestingly the inherent resistance of mice to NA may also relate to architecture of the murine kidney; with $\frac{1}{4}$ of the myelinated nerve presence that is present in the rodent kidney (Fazan et al., 2002). In an isolated-perfused kidney (IPK) preparation in the C57 mouse, a concentration ≥ 300 nM of NA was necessary to cause a resultant reduction in renal perfusion pressure (Vonend et al., 2005), further corroborating the use of 300 nM here.

Interestingly, the efficacy of NA can be related to that of Ang-II, where Ang-II is a secretagogue of NA via neuronal AT₁-R (Bernier, and Perry, 1999; Nakamura et al., 2014; Ma et al., 2001). One study investigating renal sympathetic nerve activity found mice needed 10-times the concentration of NA comparative to Ang-II to achieve the same increase in mean arterial pressure (MAP) (Ma et al., 2001), meaning a concentration with a higher response rate, whilst remaining physiologically relevant, could be 3 μM of NA, but was not trialled here. Interestingly, in the SD rat Ang-II-induced reduction in MBF is more potent than NA, at approximately 1.5-times the magnitude (Bądzyńska, and Sadowski, 2011; Crawford et al., 2012), yet in C57 there was not difference between the NA and Ang-II induced pericyte-mediated vasoconstriction, possibly reflective of differences in AT₁-R expression present in the kidneys between the species.

As mentioned above in section 4.4.4.3, dilation of DVR pericytes in response to low ATP concentrations may be reflected in the C57 mouse model's dilatory, not contractile, response to tyramine. It was noted in the SD mouse model that 1 μM of tyramine seemed to preferentially stimulate ATP release, demonstrated by the effectiveness of P2-antagonist suramin (Crawford et al., 2013). Tyramine stimulates sympathetic nerves to release NA and ATP, and is comparable to the effect of nerve stimulation, which

also produces these co-transmitters (Vonend et al., 2009; Farmer, 1966). The time until maximal change in vasa recta diameter for both species occurred during washout of tyramine (**Figure 4.8(k)**), which likely reflects time taken to release of NA and ATP from varicosities.

In the mouse kidney (Vonend et al., 2005) and other tissues (Burnstock, and Novak, 2012) it has also been observed that in certain conditions ATP, not NA, is the predominant neurotransmitter released. As noted above in section 4.4.4.3, the C57 is notably resistant to ATP, and perhaps whilst stimulation with tyramine evokes comparable ATP release in both species, in the C57 model this is a dilatory physiological concentration. As a dilatory concentration of ATP in the C57 model has yet to be ascertained, further commentary is not possible. However, provides further evidence for purinergic signalling in the regulation of MBF.

4.4.4.5 In the mouse, the DVR pericyte responsiveness to endothelin-1 differs from that described in the literature.

Endothelin-1 (ET-1) is synthesized in the IM by CD and interstitial cells, and a key local mediator of MBF, with a high local concentration in the medulla (Silldorff et al., 1995; Neuhofer, and Beck, 2006). ET-1 is a potent vasoconstrictor of the DVR, noted to cause focal, long lasting constrictions along the capillary (Scherer et al., 2005; Pallone et al., 2003b; Pallone, and Silldorff, 2001), localised to pericyte-sites (Silldorff et al., 1995; Crawford et al., 2012). Interestingly as a potential feed-forward mechanism, ET-1 stimulates production of PGE₂ by medullary interstitial cells (Wilkes et al., 1991) further suggesting there are autoregulatory mechanisms innate to the medulla.

Endothelin pharmacology has been compared between rats, humans and mice (Wiley, and Davenport, 2004), showing similar potency, despite a lesser magnitude of vasoactive response in C57 mice in the aorta (Russell, and Watts, 2000), brain (Horie et al., 2008), and cavernosum (Carneiro et al., 2008) comparative to rats. However, in the kidney slice model, a 10-fold reduction of the concentration in the mouse (10 nM to 1 nM) resulted in a comparable pericyte-mediated vasoconstriction to that measured in the rat for 10 nM; which opposes what the literature would otherwise suggest of the rat exhibiting a larger vasoconstriction. The notable interspecies difference in constriction observed here may relate to overexpression expression of ET-1_A receptors (-R) over ET-1_B-R in the murine DVR, as ET-1_B has demonstrated its vasodilatory properties (Carneiro et al., 2008; Schildroth et al., 2011; Inscho et al., 2005). In the

mouse heart there is a reported 9:1 ratio of ET_{1A}:ET_{1B}, whereas in the rat this ratio is 4:1[69]. The literature suggests ET-1 should have a greater magnitude of response in the rodent kidneys. In afferent arterioles, it was found that both ET_A-R and ET_b-R contribute to vasoconstriction in the rat juxtamedullary vessels (Endlich et al., 1996) whereas in murine AA only ET-1_a-R contributes (Schildroth et al., 2011).

Data acquired from different species demonstrates a conserved contractile profile in response to ET-1, where vessels had a lag in onset of constriction and did not return to baseline diameter within the experimental window, even after washout of ET-1. Much like in this preparation (**Figure 4.6(c)**), porcine microvessels exposed to ET-1 take ~600s to reach maximal contractility and vessels remained constricted (Potts et al., 2012). This sustained constriction in both mice and rats has also been observed hepatically *in vivo*; at >600s post ET-1 injection with portal venous pressure remained elevated (Zhao et al., 2009), and another group who were also looking at pericyte-mediated regulation of IOMDVR observed it took approximately >600-seconds to reach the maximal constriction in the rat (Silldorff et al., 1995), with constriction only moderately reversed 10-minutes once infusion had stopped. Interestingly, in the IOMDVR preparation the constriction measured in response to ET-1 was approximately double the magnitude of the mouse response here, whilst the pericyte-mediated constriction reported by Crawford et al (Crawford et al., 2012) of SD kidney slice DVR pericytes to ET-1 was approximately 4-times smaller than the magnitude of the mouse pericyte-mediated response. In light of the literature and measurements here, it suggests there was error in how the ET-1-mediated vasoconstriction in the original rat model was measured (Crawford et al., 2012), and as such those values are not accurate or in fitting with other vascular models.

4.4.4.6 Prostaglandin E₂, and associated exogenous drugs, have comparable pericyte-mediated activity in both species.

Prostaglandin E₂ (PGE₂) is formed by cyclooxygenases-1 and -2 (COX- 1, COX-2 which are abundantly expressed in the medulla (Kennedy-Lydon et al., 2015), and acts as another key regulator of MBF. PGE₂ has direct and indirect vasoactivity: both directly at DVR pericytes via prostaglandin receptors EP₂ and EP₄ (Silldorff et al., 1995; Meurer et al., 2018); and indirectly by potentiating dilation of peptides like interleukin-1 (IL-1) and atrial natriuretic peptide (ANP), whilst buffering vasoconstriction of antidiuretic hormone (ADH), Ang-II, ET-1 and NA (Silldorff et al., 1995; Neuhofer, and Beck, 2005; Kennedy-Lydon et al., 2015; Wilkes et al., 1991; Mattson, 2003). Without

this complex dilatory-profile PGE₂ could potentially reduce IMBF; in furosemide treated rats and dogs inhibition of the mTAL Na-K-2Cl cotransporter results in a secondary constriction of DVR as a response to reduced metabolic demand (Fan et al., 2019). PGE₂ also inhibits the Na-K-ATPase-mediated NaCl reabsorption in the mTAL and collecting duct (CD) thereby reducing metabolic demand, which could constrict DVR thus reducing MBF (Neuhofer, and Beck, 2006). Thus, PGE₂ can reduce medullary metabolic demand, yet feed-forward mechanisms mean maintenance of medullary perfusion and thus oxygenation.

PGE₂ was not luminally perfused in this study, it needed to penetrate ~50 µm below the slice surface where vasa recta capillaries are visualised, and actual concentration reaching pericytes could not be determined and is possibly lower than the concentration applied. This may suggest DVR pericytes are more resistant to higher concentrations than afferent arterioles (Meurer et al., 2018), which would be important in preserving MBF as stated above. Interestingly, 1 µM the SD (Kennedy-Lydon et al., 2015) and C57 kidney slice models was an ineffective concentration. The magnitude of the response in both species was also not significantly different at 10 µM (Crawford et al., 2012; Kennedy-Lydon et al., 2015), which has been reported for the species in the parenchymal arterioles, with a concentration-dependent vasoactivity of PGE₂ (Dabertrand et al., 2013).

PGE₂ at high concentrations in rodent and murine vascular beds acts as a vasoconstrictor at non-preconstricted arterioles (Dabertrand et al., 2013; Meurer et al., 2018; Ohno et al., 1999). Interestingly, a constriction of the naïve vasa recta was observed with PGE₂ before dilation in some experiments. As can be seen in Figure 4.7(b), PGE₂ 10 µM caused a small constriction during superfusion, and during washout the subsequent vasodilation occurred. This could possibly occur due to dilution of the PGE₂ concentration upon washout. In murine isolated perfused kidneys (IPK), 1 µM/L of PGE₂ cause an increase in renal vascular resistance, where 10 nM/L was dilatory (Meurer et al., 2018), so reduction in the concentration of PGE₂ in the perfusion bath during washout could have resulted in a dilatory concentration.

Correspondingly, perfusion with nonselective COX-inhibitor indomethacin resulted in a pericyte-mediated constriction that was also not significantly different between species (Crawford et al., 2012; Kennedy-Lydon et al., 2015), and this subsequent reduction in MBF could constitute a pathomechanism behind NSAID-induced nephrotoxicity. Given the comparable magnitude of response between the species, which has been observed in other tissues (Dabertrand et al., 2013), data here suggests prostaglandins have comparable vasoactive action in rats and mice. As medullary

PGE₂ both potentiates vasodilators and inhibits vasoconstrictors, there are multiple downstream pathways that may be affected by its inhibition, but are beyond the scope of this study, and is potentially why superfusion in the SD kidney slices with SNAP or bradykinin (BK) did not attenuate indomethacin contractility at DVR pericytes (Kennedy-Lydon et al., 2015)

Further still, there's potential vasodilators have similar efficacy across species as NO-donor S-Nitroso-N-Acetyl-D,L-Penicillamine (SNAP), resulted in a comparable vasodilation at 100 µM. This comparable efficacy of vasodilators suggests potentially mice are protected from renovascular diseases from resistance to vasoconstrictors as opposed to dilatory agents being more effective. An NO-donor having similar efficacy between models, whilst other endogenous agonists do not, is further suggestive of species-difference in both receptor functionalities and/or receptor expression profiles, as NO does not act via a receptor instead diffusing through biological membranes (Mohaupt et al., 1994). Bioavailability of NO in the kidney of each species would need to be established also.

4.4.5 There is benefit to developing and characterising a cross-species model.

As discussed above there are known differences in receptor expression and agonist potencies, and indeed bioavailability that are reflected in the vasoactivity in the two kidney slice models here. These findings further demonstrate there is risk in using a defined experimental model in different species to corroborate findings. This is based on an assumption that behaviour profiles will be equivalent between rats and mice (Downs, 2011). However, it also demonstrates how useful it is to use the same model in different species to observe how functionality might be conserved. Pericyte-mediated regulation of the DVR in mouse and rat is conserved, given the general observation that agonist evoked diameter changes are seen to specifically occur at pericyte sites on vasa recta.

Importantly however, it should be noted that responses measured in the rat are not predictive of what would occur in the mouse version of the same model. Nevertheless, upon assessment of the literature the differences in pericyte-mediated activity observed here reflect what is known about 1) the individual species and 2) how the vasoactive behaviour relates between the species. The C57 mouse vascular reactivity is markedly less pronounced than that measured in the rat (Russell, and Watts, 2000; Cholewa et al., 2005; Hedemann et al., 2004; Zhao et al., 2009), and as such this

reduced responsiveness demonstrates predictive validity of the C57 mouse model. Data here demonstrate the need for important for benchmarking of responses of vessels in each animal model and are indicate these experiments are critical part of validating a mouse live kidney slice model (Denayer et al., 2014). Not only this, the behaviour of the vasculature in the C57 mouse model corroborates other evidence provided for the two models. Notably that the C57 mouse model has reduced vasoactivity comparative to the SD rat.

The aim with animal models is translatability and to generate knowledge around human physiology that is otherwise impractical or unethical to determine. It is important not only to notice differences between species, but to also try and probe why these differences exist and subsequently interpreting data in the context of these species-specific differences in physiology (Cunningham, 2002; Boswell et al., 2014; Martignoni et al., 2006; Radermacher, and Haouzi, 2013). It is also important to consider what is conserved. Mentioned briefly in section 4.4.4.1; humans, rats and mice all show pericyte-mediated contractility in response to Ang-II on the DVR. Upon exposure to the same concentration of Ang-II (10 nM), both rats and human outer medullary DVR reach an approximately 25% constriction at $t = 5$ mins post bolus of Ang-II, and slowly desensitize (Sendeski et al., 2013; Zhang et al., 2004). The magnitude of constriction for a concentration matched concentration of Ang-II (10 nM) was smaller in the SD kidney slice model, with a constriction of $18.0 \pm 2.7\%$ at pericyte sites (Crawford et al., 2012). Whilst the constriction observed in the C57 mouse slices was considerably lower than both SD rats and humans at comparative concentrations, all species show that regulation of DVR diameter is pericyte-mediated and thus a conserved functionality of this cell type. Further still, it may be demonstrative that live kidney slices are a suitable *in situ* in-between model that demonstrates functionality of the vasculature in tissue thus bridging *in vitro* and *in vivo* models (Crawford et al., 2012).

This present study underlines the importance of using companion models across species given the species-related differences in physiology. It also demonstrates how the C57 kidney slice model is: i) representative of the species; ii) representative of known pericyte behaviour (contractile cells that regulate vasa recta diameter) and thus MBF; and iii) the C57 slice model is viable and suitable for further investigations into the multipotency of renal pericytes, as will be addressed in the next chapter.

5 THE USE OF A MURINE LIVE SLICE MODEL TO INVESTIGATE THE MULTIFUNCTIONAL NATURE OF RENAL PERICYTES.

5.1 Introduction

Data presented in Chapter 3 showed CD163⁺ macrophages (MΦ) were spatially close to NG2⁺ and PDGFR-β⁺ pericytes when present, and their cell-cell contact with pericytes induced a constriction of vasa recta capillaries. Further still, in line with reports suggesting that rodent CNS pericytes express the CD163 receptor (Balabanov et al., 1996), after stimulation with pro-inflammatory cytokines TNF-α and IL-1β, few cells were fluorescently labelled with both anti-CD163 and anti-PDGFR-β. Importantly, these cells bore morphological similarities to the criteria used for identifying pericytes (Bergers, and Song, 2005). However, in the Sprague-Dawley (SD) model, anti-CD163 was only able to identify a very small population of resident renal MΦ, as demonstrated by the low number of cells expressing the CD163 receptor in the rat (Kaissling, and Le Hir, 1994) and the mouse (Rubio-Navarro et al., 2016; Bi et al., 2018), despite its abundance in human kidneys (Colvin, 2019). Consequently, these findings may not be generalisable to renal pericytes and would be difficult to further probe using anti-CD163.

Currently in the field, rodent MΦ have few identifying-receptors that would be considered “pan-MΦ”. It is also important that these MΦ markers identify residential populations, as circulating immune cells are not present in tissue slices (Stribos et al., 2016). CD68 is used as a pan-MΦ marker in other models (Damoiseaux et al., 1994; Ysebaert et al., 2004) yet there was no medullary presence, and therefore no pericyte-expression in the rodent kidney slices (**Chapter 3**), despite reported expression on pericytes in other tissues (Rustenhoven et al., 2016; Pieper et al., 2014; Thomas, 1999). The literature has reported pericyte expression of immune receptors can require stimulation, *e.g.* MHC-II has been found expressed by porcine brain capillary pericytes after interferon-γ stimulation (Pieper et al., 2014). Whilst MHC-II is a MΦ marker successfully used in the rat, it is not specific to residential MΦ and is expressed by other immune cells in the interstitium including immature monocytes, lymphocytes, and B-cells (Rimsza et al., 2003; Muhlethaler-Mottet, 1997; Landsman et al., 2009). Therefore, given the lack of a suitable pan-MΦ identifying receptor in the rat, use of the SD model to further investigate the relationship of pericytes and MΦ in the kidney was limited.

In **Chapter 4**, it was established that the murine kidney slice model is a viable tool for the study of pericytes, contractile behaviour of pericytes appeared to be conserved in a species-specific manner. As a model, the mouse is extensively used in the field of immunology (Mestas, and Hughes, 2004), and access to a murine kidney slice model circumvents the issue of a small number of residential identifiable M Φ population in the rat, as was observed in **Chapter 3**. It enables uses of the residential pan-M Φ antigen F4/80, abundantly expressed throughout the murine kidney (Hume, and Gordon, 1983; Cao et al., 2015), and reported co-expression on pericytes (**Section 1.1.3.1**). Therefore, given the F4/80⁺ receptor is considered exclusive to murine M Φ and abundant in the kidney, this allows a more extensive investigation into the pericyte-M Φ relationship than that observed in **Chapter 3**.

Much of the current data on the immune functionality pericytes are generated from murine models (**Section 1.3-4**) This immune activation of renal pericytes is an investigative avenue worth exploring, especially given the novel interaction identified between renal pericytes and CD163⁺ M Φ in this thesis. With the extensive presence of F4/80⁺ M Φ in the medulla (Hume, and Gordon, 1983), a better randomised visualisation of these M Φ with pericytes within the tissue is an advantage over the rat model.

Ultimately, the aim of this chapter is to conduct like-for-like experiments to those performed in the SD rat but using anti-F4/80 to label M Φ . This will enable the characterisation of i) the vasoreactive responsiveness of vasa recta pericytes to short-term stimulation with pro-inflammatory cytokines TNF- α and IL-1 β (acute superfusion experiments), as previously described in the SD rat model **Chapter 4 section 4.2.3**, (Data provided by Kirsti Taylor); ii) determine the influence that M Φ contact has on pericyte characteristics, their spatial relationship, and the possibility of any cells being positive for both pericytic (PDGFR- β and NG2) and M Φ (F4/80) markers, as was observed in **Chapter 3** with the rat; and iii) determine how these characteristics might be influenced by cytokine stimulation with TNF- α and IL-1 β .

5.2 5.2 Methods:

Intact live kidney slices from 9-week-old C57BL/6J mice (Charles River Laboratories, Manston) were obtained and processed as described in **Chapter 2**.

5.2.1 5.2.1 DIC video analysis.

Real time video images were collected of live murine kidney slices superfused with either TNF- α (10 ng/mL; R&D Systems) or IL-1 β (10 ng/mL; R&D Systems) as described in **chapter 2 section 2.5**.

5.2.2 5.2.2 Immunohistochemical experiments.

In brief, initial exploratory immunohistochemical experiments to ascertain appropriate markers for identifying residential M Φ were performed with anti-CD68 (rabbit, 1:100; Abcam) and anti-F4/80 (rat; 1:1000; Bio-Rad), to determine the presence of cells positive for these receptors in the murine kidney slices. Suitability of anti-PDGFR- β was determined as described in **chapter 3 section 3.2.1**

For subsequent co-expression experiments, slices were incubated with anti-F4/80 to identify M Φ and either anti-PDGFR- β or anti-NG2 (1:200, Merck-Millipore) to identify pericytes. Nuclear stain Hoechst 33342 5 μ M (Invitrogen) was included for positive identification for a cell body to accurately quantify and elucidate any overlap between pericyte and M Φ cells by correlation of their blue nuclei in images. Inclusion of rodent M Φ marker anti-F4/80 was to also provide clarity as to whether anti-NG2 and anti-PDGFR- β exclusively stain renal pericytes. Experiments where kidney slices were fixed with 4% paraformaldehyde (PFA) immediately post Hoechst 33342 incubation were performed to see if under homeostatic conditions any co-expression of pericyte and macrophage markers occurred. These tissues that were freshly slices were classified as the "0-hour" experimental group. To stimulate co-expression of M Φ and pericyte markers, slices were stimulated with pro-inflammatory cytokines TNF- α and IL-1 β . The PSS control in the cytokine stimulation experiments are referred to as the "4-hour" control.

Kidney slices were incubated in Hoechst 33342, and then washed with PSS, slices were then fixed in 4% PFA then washed in 0.1 M phosphate buffered saline (PBS). Tissue then underwent permeabilisation in 0.1% Triton X-100, and a step to block non-specific antibody binding with 10% donkey serum solution, before an overnight incubation with primary antibodies. Subsequently, slices were washed with 0.1 M PBS and the primary antibodies were probed with fluorescent secondary antibodies donkey-anti-rabbit Alexa Fluor 555 (donkey, 1:200; Invitrogen), and donkey-anti-rat Alexa Fluor 488 (donkey, 1:200; Invitrogen). Slices were then washed a final time using PBS, then mounted using Citifluor (Agar Scientific) and stored at 4°C in the dark. Unless otherwise specified, reagents are from Sigma-Aldrich.

Tissue sections stimulated with pro-inflammatory cytokines TNF- α , and IL-1 β (10 ng/mL; R&D Systems) were incubated for 4 hours prior to be processed as described above. Cytokine stimulations have a corresponding “4-hour” PSS-time control. Data acquisition and analysis was conducted as described in **chapter 2 section 2.5**.

5.2.3 Statistics

All data is presented as mean values \pm standard error mean (SEM), *n* numbers are presented as the number of animals used, then the number of kidney slices. The SEM is calculated with the number of animals used in the IHC experiments. Statistical significance was calculated using a two-tailed Student’s unpaired t-test for superfusion and “0 hour” PSS background experiments, and a one-way ANOVA with post-hoc Dunnett’s test was used for cytokine-stimulated and control tissue that was incubated for 4-hours. Values were calculated using GraphPad PRISM 5.0 software (La Jolla, California). A value of $p < 0.05$ was considered statistically significant.

5.3 Results:

5.3.1 TNF- α , but not IL-1 β induces a significant pericyte-mediated vasoconstriction of vasa recta.

To assess if pro-inflammatory cytokines have any acute actions on murine pericytes, live kidney slices were superfused with either 10 ng/mL TNF- α or IL-1 β for a time period of 600s, followed by a “wash-out” period of approximately 600s frames to determine whether any cytokine-induced changes in vessel diameter were reversible. These experiments have previously been conducted in Sprague-Dawley (SD) rats, and data here will be compared against previously obtained data (data provided by Dr. Kirsti Taylor). Exposure of naïve vasa recta capillaries in murine kidney slices to 10 ng/mL of TNF- α resulted in a constriction of vessel diameter that was significantly greater at pericyte sites than non-pericyte sites ($8.9\pm 0.8\%$ vs $2.5\pm 1.2\%$ respectively, $p < 0.05$, $n = 3$ slices and 3 animals; **Figure 5.1(a)**). This was significantly less than the pericyte-mediated constriction previously observed in the SD rat ($-11.9\pm 1.4\%$; $p < 0.0001$). This constriction began during superfusion of the tissue with TNF- α and continued throughout the washout period (**Figure 5.1(b)**), with reversal to baseline observed in only 1/3 experiments. Superfusion with 10 ng/mL IL-1 β failed to elicit any significant change in vasa recta diameter in the murine preparation ($-4.0\pm 0.6\%$ at pericyte sites vs $-3.2\pm 1.3\%$ at non-pericyte sites; $p > 0.05$, $n = 4$ animals, 4 slices; **Figure 5.1(d)**) in the timeframe investigated. Superfusion of SD kidney slices with IL-1 β also failed to elicit any pericyte-mediated alteration of vasa recta diameter ($-2.6\pm 0.8\%$).

5.3.2 PDGFR- β and CD68 expression in the C57BL/6J mouse kidney is similar to that observed in the Sprague-Dawley rat model.

The suitability of anti-PDGFR- β in labelling renal pericytes was determined by the presence of Alexa-555 2 $^{\circ}$ fluorescence (used to probe anti-PDGFR- β) adjacent to IB $_4$ labelled vasa recta capillaries, and by brightfield images used to confirm structures. Data for murine kidney slices show comparable patterns of staining for PDGFR- β (see **section 3.3.1** for description) ($n = 2$ animals, 5 slices; **Figure 5.2(ai-aiii)**). Some PDGFR- β^+ pericytes are seemingly paired (**Figure 5.2(b)**), with adjacent PDGFR- β^+ cells showing pericyte-identifying morphology, the large cell body and association with the vascular wall. PDGFR- β^+ -labelled pericytes are more numerous than those labelled

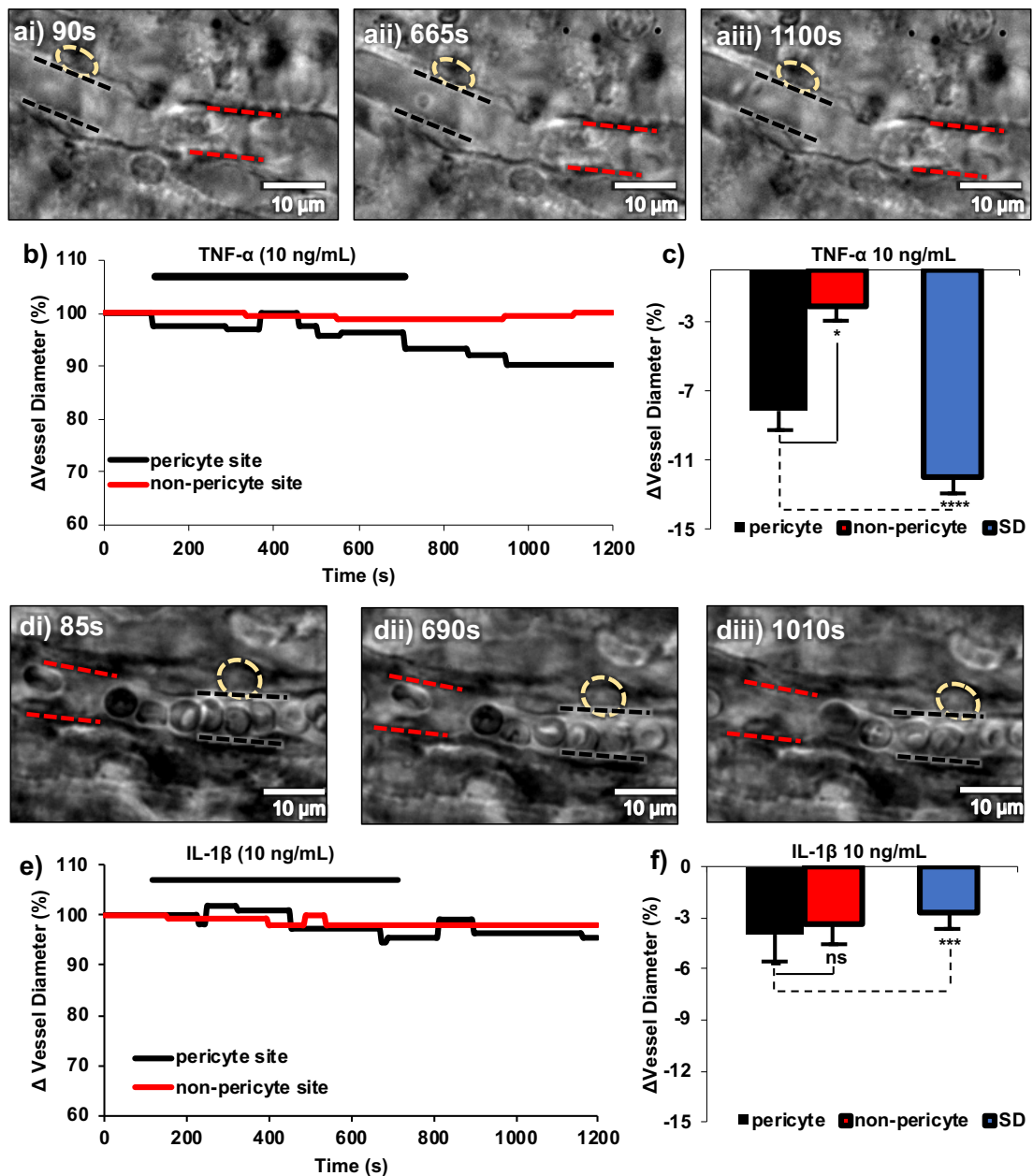


Figure 5.1 Superfusion of C57BL/6J murine kidney slices with TNF- α , but not IL-1 β , caused a pericyte-mediated constriction of vasa recta capillaries.

Representative DIC images of a time-series experiment of superfusion of a vasa recta capillary with TNF- α (a) and IL-1 β (d) (i) before exposure, (ii) during exposure, and (iii) during washout from agonist. Pericytes are indicated with yellow dashed circles, as are a pericyte site (black dashed line) and corresponding non-pericyte site (red dashed line). The percentage change of vessel diameter of both sites was plotted against time (b) at a pericyte (black) and corresponding non-pericyte site (red) site, with exposure to agonist indicated by the black line above the trace. Average data for TNF- α (c; n= 3 animals and 3 slices), and IL-1 β (n=4 animals and 4 slices; f) at concentrations of 10 ng/mL show TNF- α induced a significantly greater constriction at the pericyte site (black bar), whereas IL-1 β was not significantly different from the non-pericyte (red bar) value. The average data for equivalent experiments performed in the Sprague-Dawley (SD) rat are shown by the blue bar and show the pericyte-mediated constriction in response to TNF- α is significantly greater than that observed in the mouse, and that there was no significant pericyte-mediated response to IL- β . * p<0.05, *** p<0.005, **** <0.0001, ^{ns} p>0.05. Scale bars (white) are 10 μ m.

with NG2, yet anti-PDGFR- β does not exclusively label medullary pericytes, as interstitial fibroblasts in the medulla were also identified by immunofluorescence. Unlike NG2⁺ pericytes, PDGFR- β ⁺ labelling does not drop off in the IM, with PDGFR- β ⁺ staining present throughout the entirety of the kidney slices. Direct like-for-like comparisons of pericyte morphological characteristics are presented below in **section 5.3.3**. To exclude interspecies variability, anti-CD68 antibody was also used in the murine model (n=1 animal and 3 slices). CD68 had no presence in the murine medulla, primarily located in the cortex of the slice, around arterioles as shown in **Figure 5.2(c)**. As an infiltrating M Φ marker in the kidney (Mattson et al., 2006), with no recruitment possible, this marker was not used for further study. Again, as described in **section 3.3.2**, the morphology of CD68⁺ M Φ was similar to that of both PDGFR- β and NG2 labelling these cells (**Figure 5.2(c)**).

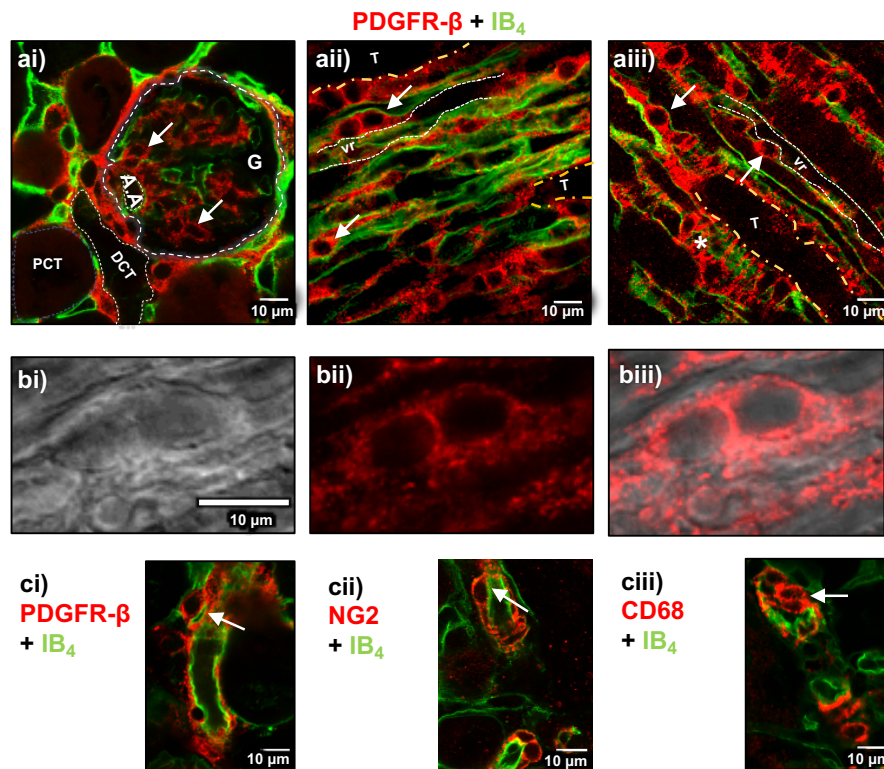


Figure 5.2 Platelet derived growth factor receptor- β (PDGFR- β)⁺ and CD68⁺ positive staining in the C57BL/6J mouse.

PDGFR- β ⁺ (red) pericytes (aii-iii) and mesangial cells (ai) reside along isolectin B4 (IB4; green) stained vasculature, with PDGFR- β ⁺ cells extensively present throughout the rodent kidney. Representative regional images of PDGFR- β ⁺ fluorescent staining in the (ai) cortex, (aii) outer medulla (OM), and (aiii) inner medulla (IM). Observed with PDGFR- β ⁺ pericytes was occasional pairing of cell bodies along vasa recta capillaries, with; (bi) showing the brightfield image of paired cells indicated in (aii), (bii) showing the PDGFR- β ⁺ staining, and the corresponding composite (biii); n = 2 animals and 5 slices). As observed in the Sprague-Dawley rat in chapter 3, when slices were probed with IB4 (green) and anti-CD68 (ciii; red; n=1 animal and 3 slices), staining was perivascular and localised to arterioles in the cortex, with morphology comparable that PDGFR- β ⁺ (ci), and neural-glial 2⁺ (NG2⁺; red; n=4 animals and 9 slices) cell bodies which co-localise to arterioles. Structures are highlighted with dashed lines and are labelled; G = glomerulus, A.A = afferent arteriole, PCT = proximal convoluted tubule, DCT = distal convoluted tubule, T = tubule, vr = vasa recta. White arrow heads indicate pericyte and mesangial cell bodies, whilst the curly blue arrowhead indicates interstitial fibroblasts. Scale bars are 10 μ m.

5.3.3 Vasa recta capillaries where pericytes are in contact with F4/80⁺ macrophages are constricted.

Live murine kidney slices were co-immunostained with either anti-NG2 and anti-F4/80, or anti-PDGFR- β and anti-F4/80, to investigate the spatial relationships between these cell types and to observe if any co-labelling of these receptors on an individual Hoechst 33342⁺ nuclei occurred. For PDGFR- β ⁺ pericyte density, 10 μm deep (214.2 μm^2 ; step size of 1 μm) maximal intensity z-stacks were reconstructed, and density was quantified by the percentage of the area occupied by PDGFR- β ⁺-labelled immunofluorescence. This has been previously reported for quantification of PDGFR- β ⁺ pericyte density in other tissues where immunohistochemical experiments were performed (Ikeda et al., 2018; Craggs et al., 2015). Limitations of this technique are described in **Chapter 2**, and **section 3.4.1**. Whole renders were used irrespective of

Table 5.1 Characteristics of platelet derived growth factor receptor- β (PDGFR- β)⁺ and neural-glial 2 (NG2)⁺ pericytes in the renal medulla.

	PDGFR- β		NG2	
	OM ¹	IM ²	OM	IM
Pericyte Density				
Area ³	20.6 \pm 1.6**	16.0 \pm 1.1%**	10.9 \pm 1.1%	4.7 \pm 0.4
# ⁴	N/A		9.0 \pm 0.6	4.9 \pm 0.3%
Pericyte size, μm				
Height	5.6 \pm 0.2**	5.7 \pm 0.2**	4.5 \pm 0.2	4.0 \pm 0.2
Width	7.6 \pm 0.4	6.8 \pm 0.3 [†]	7.5 \pm 0.3	8.0 \pm 0.4
Vessel diameter, μm				
P ⁵ site	6.7 \pm 0.2%		6.4 \pm 0.2%	
NP ⁶ site	8.9 \pm 0.3**		8.3 \pm 0.2	

Data presented are the mean \pm SEM. n= 3 animals and 9 slices, \geq 200 pericytes per animal

¹OM= outer medulla, ²IM = inner medulla

³Area calculated as the average percentage of area occupied with fluorescent stain per 10 μm deep (214.2 μm^2) z-projection, ⁴# =Number of cells per 100 μm^2

⁵P = Pericyte, ⁶NP= non-pericyte

* p<0.05; **p<0.0001 for comparisons between NG2⁺ and PDGFR- β ⁺ pericytes

% p<0.0001 for comparisons between the OM and IM

the presence of fibroblasts as removal would lead to inaccurate, subjective analysis. For comparison between pericytes, this quantification method was also used for NG2⁺-labelled pericytes, as well per 100 μm^2 as described in **chapter 4**. In healthy tissue sections, PDGFR- β ⁺ labelled pericytes, as determined by their residence on vascular walls, were more abundant in the outer medulla (OM) than the inner medulla (IM; 20.6 \pm 1.6% vs 16.0 \pm 1.1% respectively, p<0.0001, n=3 animals and 9 slices), as were NG2⁺ pericytes (10.9 \pm 1.1% vs 4.7 \pm 0.4% (**Figure 5.3(c)**); 9.0 \pm 0.6 cells/ 100 μm^2 vs 4.9 \pm 0.3 / 100 μm^2 respectively, p<0.0001, n=3 animals and 9 slices; **Table 5.1**. The total PDGFR- β ⁺ presence was significantly larger than NG2⁺ presence in both the OM

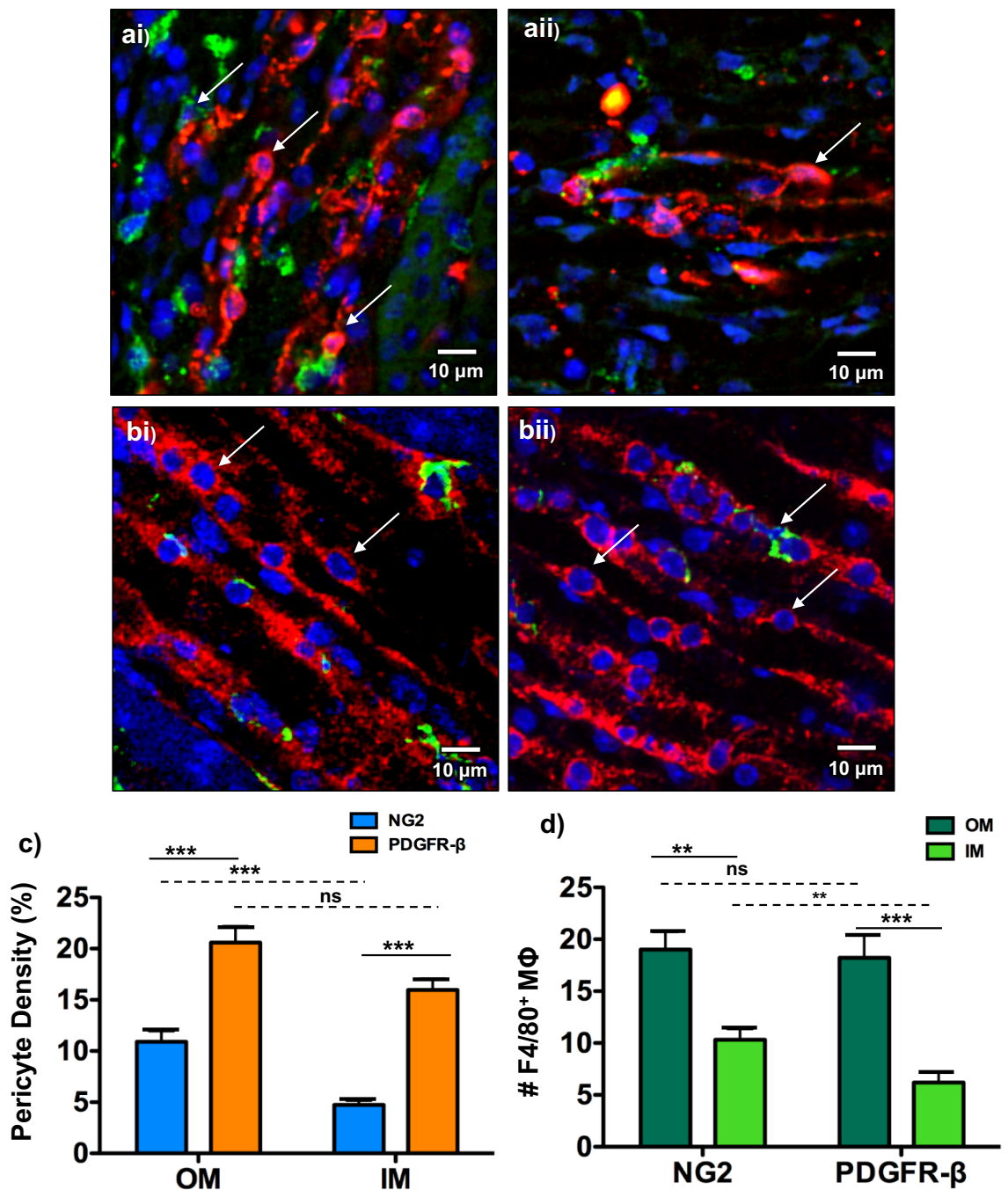


Figure 5.3 The regional densities of pericytes and macrophage (MΦ) in the outer (OM) and inner medulla (IM).

(ai-ii, and bi-ii) are representative confocal acquired images of OM (ai and bi) and IM (aii and bii) fluorescently stained with anti-neural-gliar-2 (NG2; a;red) or anti-platelet derived growth factor receptor-β (PDGFR-β; b;red), anti-F4/80 (green), and Hoechst 33342 (H342;blue). Individual cell bodies can be identified by NG2, PDGFR-β, or F4/80 positive immunofluorescence surround a Hoechst 33342⁺ nucleus, indicated by white arrows. The respective pericyte densities, as determined by the percentage of the render area (10 μm deep, 214.2 μm² standard deviation-projected z-stack) occupied by positive fluorescent staining can be seen in (c) for PDGFR-β⁺-labelled (orange bar) and NG2⁺-labelled (blue bar) pericytes in the OM and IM. The respective cellular density of F4/80⁺ MΦ can be seen in (d). All data presented as mean±SEM. n= 3 animals and 9 slices. ** p<0.0005, *** p<0.0001, ns = p<0.05. Scale bars are 10 μm.

($p < 0.0001$) and IM ($p < 0.0001$). The average number of M Φ present per ROI of the OM was 19.1 ± 1.9 cells, and 10.3 ± 1.1 in the IM in NG2 experiments; and 17.4 ± 2.2 and 6.2 ± 1.0 in PDGFR- β experiments in the OM and IM respectively. The average presence of M Φ in the OM is significantly greater in both NG2 ($p < 0.0005$) and PDGFR- β labelled tissue ($p < 0.0001$) than that in the IM (**Figure 5.3(c)**), which has been reported previously (Hume, and Gordon, 1983; Soos et al., 2006).

Pericyte size measured as described in **section 2.3**. The average size of NG2⁺-labelled pericytes was 4.5 ± 0.2 μm tall and 7.5 ± 0.3 μm wide in the OM, and 4.0 ± 0.2 μm tall and 8.0 ± 0.4 μm wide in the IM, with an average combined size (OM + IM) of 4.3 ± 0.1 μm in height and 7.9 ± 0.3 μm in width. PDGFR- β ⁺-labelled pericytes were 5.6 ± 0.2 μm tall and 7.6 ± 0.4 μm wide in the OM, and 5.7 ± 0.2 μm tall and 6.8 ± 0.3 μm wide in the IM, with an average size of 5.5 ± 0.1 μm in height and 7.2 ± 0.2 μm in width. There were no significant differences found between the OM and IM size for both PDGFR- β ⁺ and NG2⁺ pericytes ($p > 0.05$). PDGFR- β ⁺ pericytes were significantly larger in height ($p < 0.001$) on average and tended to be narrower (significant in the IM; $p < 0.05$).

Table 5.2 Characteristics of renal platelet derived growth factor receptor- β (PDGFR- β)⁺ and neural-gial 2 (NG2)⁺ pericytes in contact with F4/80⁺ macrophages (M Φ).

	PDGFR- β		NG2	
	OM ¹	IM ²	OM	IM
Number of F4/80⁺ MΦ				
	$17.4 \pm 2.2\%$	6.2 ± 1.0	19.1 ± 1.9	10.3 ± 1.1
Pericyte size, μm				
Height	$5.1 \pm 0.2^{***}$	$5.5 \pm 0.2^{***}$	4.0 ± 0.1	3.9 ± 0.2
Width	7.2 ± 0.3	$6.4 \pm 0.3^{**}$	7.5 ± 0.3	8.0 ± 0.4 ,
Vessel diameter, μm				
P ³ site	$5.1 \pm 0.3\%, \#$		$5.1 \pm 0.2\%, \#$	
NP ⁴ site	$8.3 \pm 0.3^*$		7.5 ± 0.3	

Data presented as the mean \pm SEM, n = 3 animals and 9 slices, ≥ 200 pericytes per animal
 The number of F4/80⁺ M Φ are calculated as the number of cells per 10 μm ($214.2 \mu\text{m}^2$) z-stack
¹OM = outer medulla, ²IM = inner medulla, ³P = Pericyte, ⁴NP = non-pericyte
^{*} $p < 0.05$; ^{**} $p < 0.01$; ^{***} $p < 0.0001$ for comparisons between NG2⁺ and PDGFR- β ⁺ pericytes
[£] $p < 0.0005$; [%] $p < 0.0001$ for comparisons between the OM and IM
[#] $p < 0.0001$ for comparisons between values presented here and corresponding values in

Table.5.1

The average vessel diameter covered with NG2⁺-labelled pericytes reside is 6.4 ± 0.2 μm at the site where the pericyte soma resides (termed “pericyte site”), and 8.3 ± 0.2 μm at the section of vessel without pericyte cell coverage (non-pericyte site). Vasa recta covered with PDGFR- β ⁺-labelled pericytes tended to be marginally, although not significantly ($p > 0.05$), wider at pericyte sites (6.7 ± 0.2 μm) and significantly wider at non-pericyte sites (8.9 ± 0.3 μm ; $p < 0.05$) than vasa recta covered with NG2⁺-labelled

pericytes. For vasa recta covered with either PDGFR- β^+ and NG2 $^+$ -labelled pericytes, vessel diameter at pericyte sites was significantly narrower than the vessel width at the corresponding non-pericyte sites ($p < 0.0001$; **Figure 5.4(a): Table 5.1**).

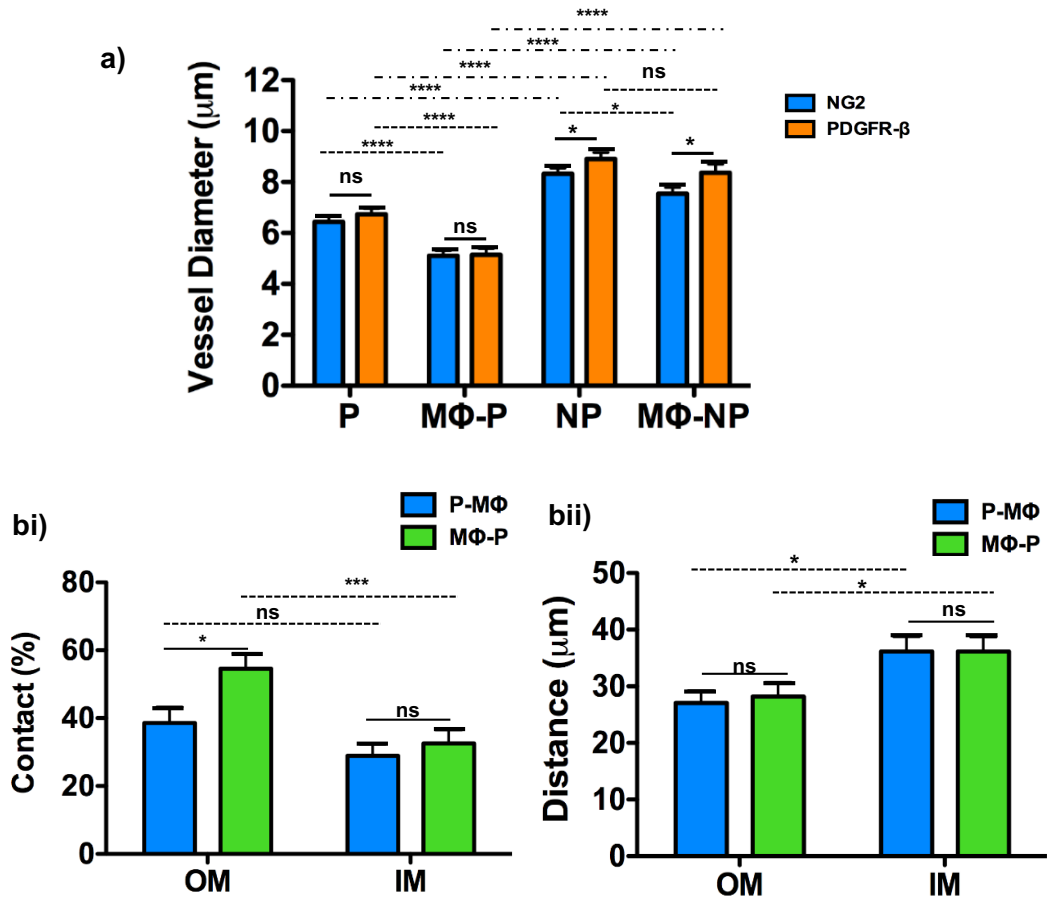


Figure 5.4 The effect of F4/80 $^+$ MΦ on vasa recta diameter and their spatial relationship with neural-glial-2 (NG2) $^+$ pericytes.

Bar chart (a) shows the average vasa recta diameter when encircled by NG2 $^+$ pericytes (blue bar) or PDGFR- β^+ pericytes (orange bar) at a pericyte site (P) and corresponding non-pericyte site (NP), and the average vessel diameter when the pericyte has cell-cell contact with a F4/80 $^+$ MΦ (MΦ-P) with associated non-pericyte site (MΦ-NP). In (bi) bars represent the percentage of total cells present in the render in contact (Contact %) with the locus from either a NG2 $^+$ pericyte (P-MΦ; blue bar) or MΦ (MΦ-P; green bar), in the outer (OM) and inner medulla (IM). (bii) shows the corresponding distance for cells not in contact. Data presented as mean \pm SEM. * $p < 0.05$, *** $p < 0.001$, **** $p < 0.0001$, ^{ns} $p > 0.05$. $n = 3$ animals and 9 slices for both PDGFR- β and NG2.

F4/80 $^+$ -labelled MΦ primarily resided in the interstitial space and were distributed around the vascular and tubular compartments; spread over the outer surfaces of tubular segments and the vasculature, as has been previously reported (Hume, and Gordon, 1983). MΦ morphology is highly heterogenous, with most MΦ ramified; the

filopodia varying from long and spindly to short “hair-like” processes. The interwoven nature of residential MΦ in tissue (Gordon, and Plüddemann, 2017) was observed throughout the planes of renders generated; F4/80⁺-labelled MΦ were present across multiple planes in the 10 μm deep renders. Contrastingly to F4/80⁺-labelled cells, both NG2⁺-labelled pericytes (**Figure 5.5**) and PDGFR-β⁺-labelled pericytes (**Figure 5.6**) were large and ovular in shape, restricted to their perivascular location. The morphology observed is characteristic for MΦ and pericytes respectively, which will be used for determination of any co-staining.

5.3.4 NG2⁺-labelled pericytes and F4/80⁺-labelled macrophages have a close spatial relationship in the OM.

As discussed in **chapter 3, section 3.3.4**, fluorescent PDGFR-β⁺-labelling was also expansive in the mouse. As such, direct quantification of the total cellular abundance of PDGFR-β-labelled cells in the render (10 μm deep z-stack, 214.2 μm²) was not feasible. This extensive PDGFR-β⁺ staining showed a sustained association with MΦ, but direct measurements were not calculated as those would be inaccurate. However, NG2⁺-labelling is less abundant (see **Figure 5.3**) and the degree of cell contact and the corresponding distance between cells not in contact was measured as described in **section 2.5**.

In the OM, on average, 38.6±4.7% of NG2⁺-labelled pericytes in the render had cell-cell contact with an F4/80-labelled MΦ, yet the proportion of F4/80⁺ MΦ with cell contact with NG2⁺-labelled pericytes was on average 54.6±4.5% of the total MΦ present in the field of view, a significantly greater ($p < 0.05$) percentage. In the IM, the average percentage of NG2⁺-labelled pericytes with cell-cell contact with F4/80⁺-labelled MΦ was marginally lower at 28.9±3.5% of pericyte, which was not-significantly different from the average percentage of IM F4/80⁺-labelled MΦ with contact with NG2⁺-labelled pericyte at 32.6±4.0% of F4/80⁺ MΦ ($p > 0.05$; **Figure 5.4(bi)**). The percentage of F4/80⁺-labelled MΦ with NG2⁺-labelled pericyte contact was significantly greater in the OM ($p < 0.05$), but there is no significant difference in the percentage of pericytes with MΦ contact between the OM and IM ($p > 0.05$).

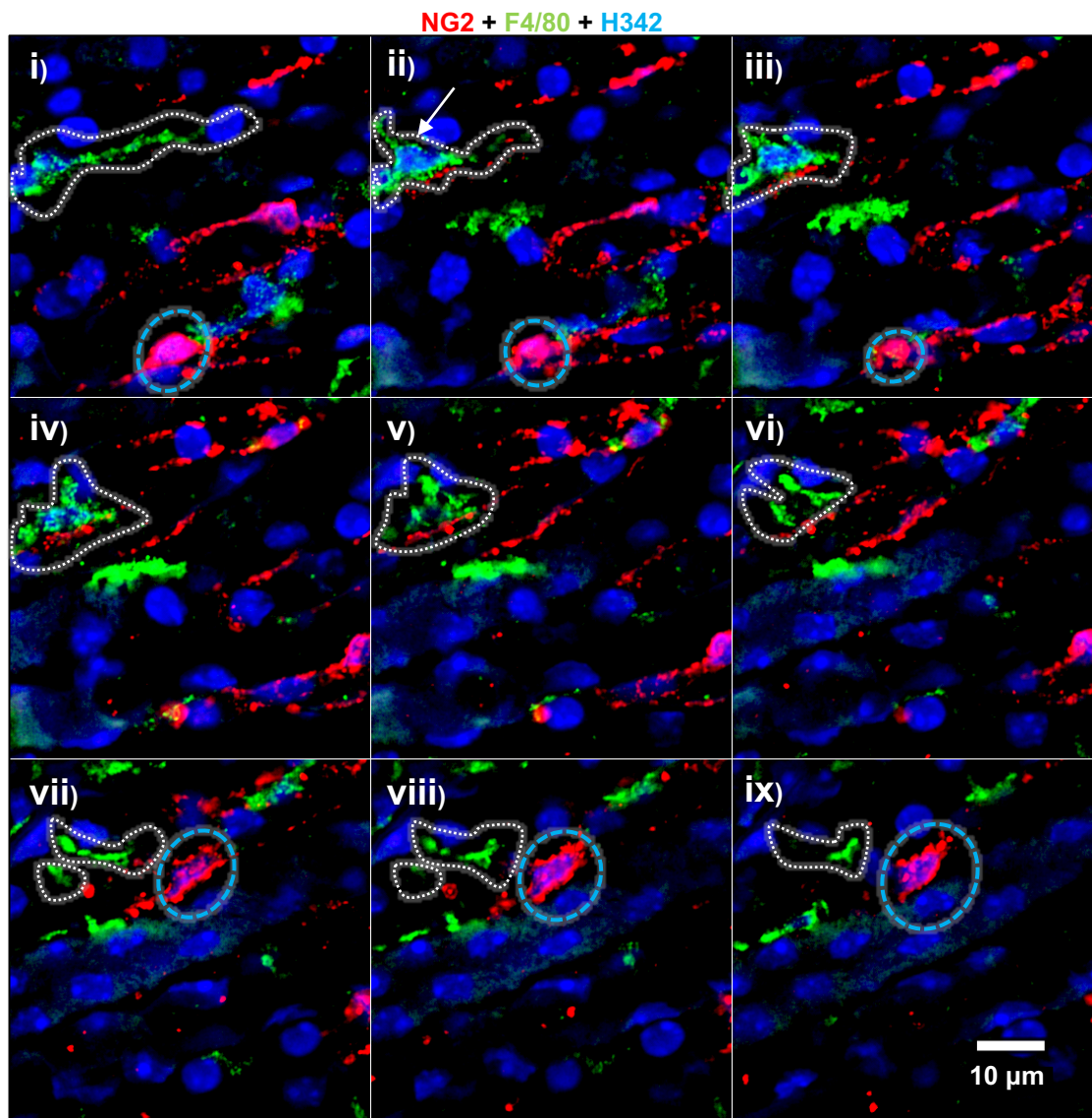


Figure 5.5 Features of neural-glia 2 (NG2)⁺ pericyte and F4/80⁺ macrophage (MΦ) morphology

Images (i-ix) are a composite montage of a section from a 10 µm z-projection (214.2 µm²; 1 µm step size) of fluorescent staining with anti-NG2 (*red*), anti-F4/80 (*green*), and Hoechst 33342 (H342; *blue*). Pericyte cell bodies are highlighted with blue dashed circles, whilst MΦ are highlighted with white dashes around the entirety of the cell. Of note is the regular, round morphology of pericytes throughout the render compared with the ramified, MΦ spread. n = 3 animals and 9. Scale bars are 10 µm.

As stated above, when not in contact, the distance between cell bodies with a differential focus on both MΦ and pericytes was also measured. This measurement was taken between F4/80⁺-labelled and NG2⁺-labelled cell bodies in the same plane of the z-stack and involved focusing on either a NG2⁺ pericyte or F4/80⁺ MΦ, not both for the same measurement, then measuring the distance to the closest “oppositely”-labelled cell body. When not in contact, the average distance between NG2-labelled pericytes (loci of measurement) and F4/80-labelled MΦ in the OM was 27.1±2.1 µm,

and the distance between MΦ (loci of measurement) and pericytes was $28.2 \pm 2.5 \mu\text{m}$ on average ($p > 0.05$). In the IM the average distance was $36.1 \pm 2.6 \mu\text{m}$ with the loci of measurement F4/80⁺-labelled MΦ, and $36.1 \pm 2.6 \mu\text{m}$ for NG2⁺-labelled pericytes ($p > 0.05$; **Figure 5.4(bii)**).

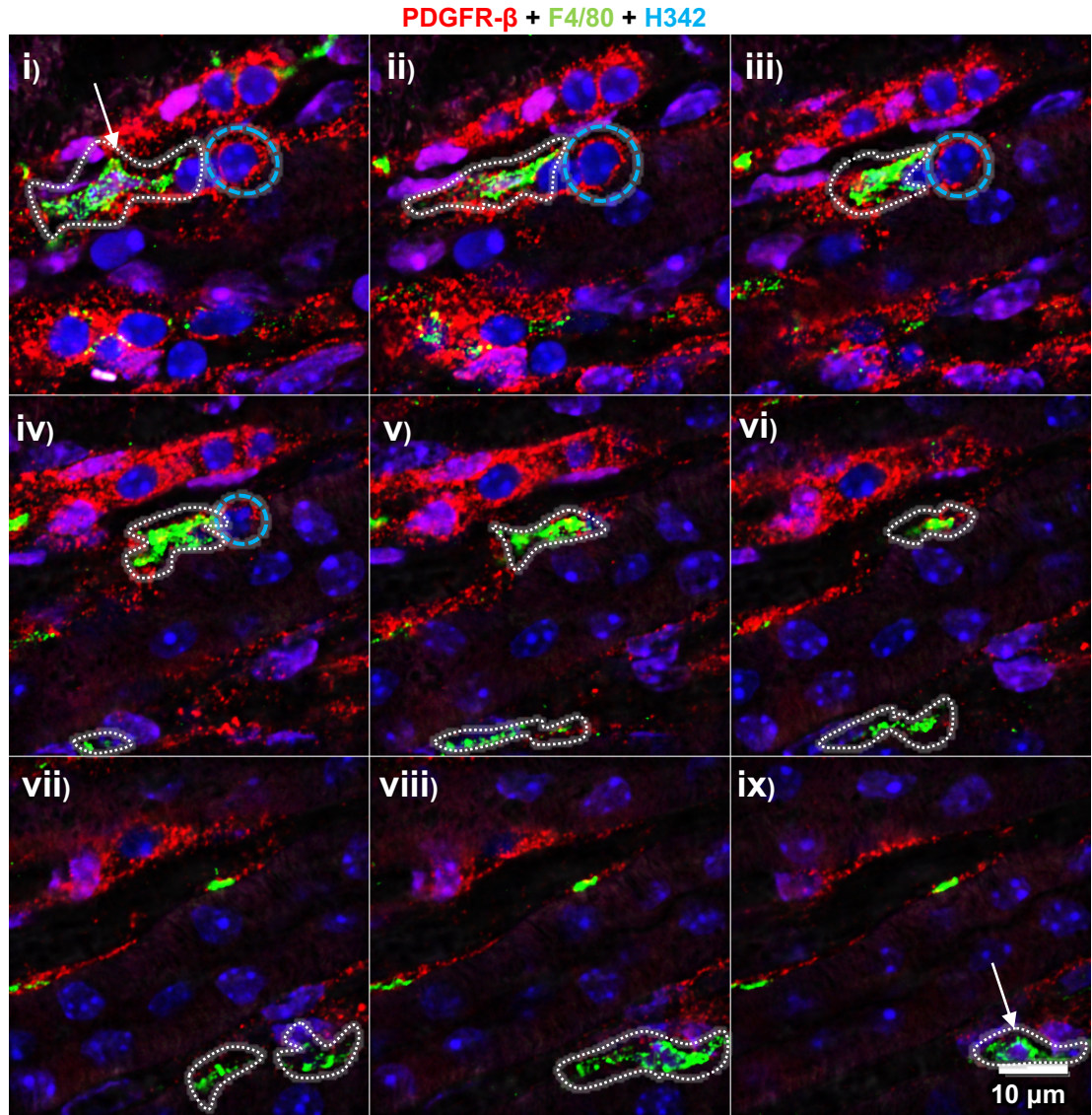


Figure 5.6 Features of platelet derived growth factor receptor-β (PDGFR-β)⁺ pericyte and F4/80⁺ macrophage (MΦ) morphology.

Images (i-ix) are a composite montage of a section from a 10 μm z-projection of fluorescent staining with anti-PDGFR-β (*red*), anti-F4/80 (*green*), and Hoechst 33342 (H342; *blue*). Pericyte cell bodies are highlighted with blue dashed circles, whilst MΦ are highlighted with white dashes around the entirety of the cell. Of note is the regular, round morphology of pericytes throughout the render compared with the ramified, MΦ spread. White arrow indicates MΦ cell body. n = 3 animals and 9. Scale bars are 10 μm.

5.3.5 A small population of cells were positive for both F4/80 and either PDGFR- β or NG2.

Another question co-immunostaining was used to address was co-expression of NG2 or PDGFR- β and F4/80 in murine kidney sections, as described in **chapter 3 section 3.3.10** for the rat, by a Hoechst 33342⁺ identified cell nucleus being positively labelled by both the red pericyte and green M Φ fluorescent stain. Prior to experimentation, to ensure any potential co-staining observed would not be due to overlap of primary antibodies binding to similar protein sequences, the sequences of primary antibodies against anti-NG2 (GENBANK: Q00657), anti-PDGFR- β (GENBANK: NP_001139740) and anti-F4/80 (GENBANK: Q61549-1) were aligned using the UniProt online alignment tool (available at: <https://www.uniprot.org/align/>) to determine sequence homology. After alignment, it was determined that Anti-F4/80 and Anti-NG2 sequence homology was less than 10%, and less than 12% homology between anti-F4/80 and anti-PDGFR- β . As such any observations of a Hoechst 33342⁺ cell body co-expressing M Φ and pericyte markers is not likely caused by cross-reactivity of the primary antibodies at the same antigenic sites.

In Immunostained sections, a small proportion Hoechst 33342⁺ nuclei were seemingly positively labelled by anti-F4/80 immunofluorescence, and either NG2⁺ or PDGFR- β ⁺ immunofluorescence. These cells that appeared to co-express pericyte and M Φ identifying markers had the oval morphology that is characteristic of pericytes and were located along the vasculature as determined by brightfield images (**Figure 5.7**).

An observation of at least one cell co-expressing F4/80⁺-fluorescent labelling with pericyte staining occurred in approximately 35% of NG2 and 57% of PDGFR- β experiments. (**Figure 5.8**). Mentioned in section 5.3.2 of this chapter was an occurrence of paired perivascular PDGFR- β ⁺-labelled cells; co-labelling PDGFR- β and F4/80 occurred within these pairs (**Figure 5.8(c-d)**). Of note is the majority of F4/80⁺ M Φ in the renal medulla did not reside along the vasculature, so these cells co-expressing pericyte and M Φ receptors are a possible sub-population of either M Φ or pericytes. These double positive cells were so infrequent that objective quantification of their occurrence was not possible, however, some residential immune cells are dormant until activation (Fabriek et al., 2005a; Polfliet et al., 2006). Therefore, as in chapter 3, incubations with potent pro-inflammatory cytokines TNF- α and IL-1 β were used to see if it would encourage more cells positive for PDGFR- β or NG2 labelling to also be positively labelled by F4/80 immunofluorescence.

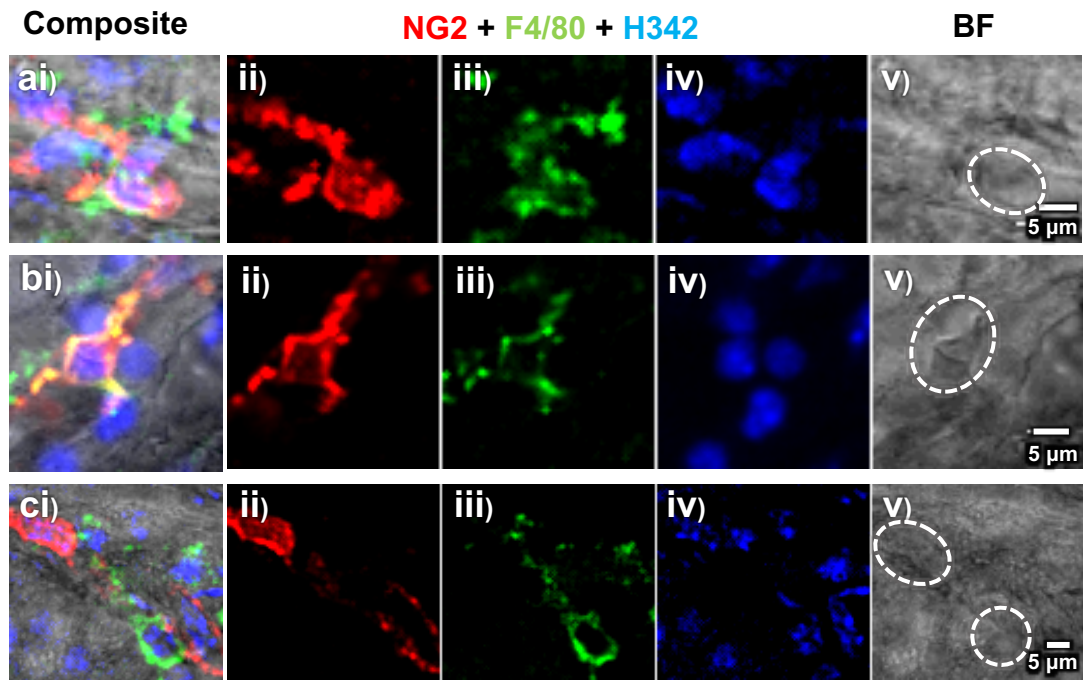


Figure 5.7 Co-expression of neural-glia-2 (NG2) and F4/80 on perivascular cells. (a-c) show representative images of anti-NG2⁺ (red) and anti-F4/80⁺ labelling (green) around Hoechst 33342 (H342; blue) identified nuclei, that bears the morphology characteristic of pericytes. Images labelled with (i) show the composite of; (ii; NG2), (iii; F4/80), (iv; H342), and the bright field image (v; BF). Images in (a-b) show co-labelling of anti-NG2 and anti-F4/80. Images in (c) show a perivascular F4/80⁺, NG2⁻ cell that also demonstrates the characteristic oval morphology of pericytes. Cell bodies in the bright field images are indicated by white dashed circles. Scale bars are 5 μm.

5.3.6 Incubations with cytokines increased the outer medullary (OM) F4/80⁺ macrophages presence and reduced both PDGFR-β⁺ and NG2⁺ pericyte density.

Slices were either incubated in TNF-α (10 ng/mL, n = 3 animals and 3 slices) or IL-1β (10 ng/mL, n = 3 animals and 3 slices), or kept in control PSS conditions (n = 3 animals and 3 slices for PDGFR-β; n = 4 animals and 4 slices for NG2) for 4 hours. In PSS time-matched control experiments, the total number of MΦ present per 10 μm deep render were, on average, 26.5±2.1 in the OM in NG2 experiments, and 24.2±2.6 in PDGFR-β experiments (p>0.05). This was significantly more (p<0.0001) than in the IM, with on average 7.4±1.8 and 8.5±1.4 F4/80⁺-labelled MΦ in NG2 and PDGFR-β⁺ experiments respectively (p>0.05). This is an increase from the baseline cellular abundance of MΦ in the OM, but only significant in NG2 experiments (p<0.05). Representative images can be seen in **Figure 5.9** and **Figure 5.10** for NG2 and PDGFR-β experiments respectively.

Accounting for the increase in the PSS control, in tissue slices that were stimulated with TNF- α , the number of M Φ present increased by 1.4-fold in the OM to $141.8 \pm 12.1\%$ ($p < 0.05$) and $137 \pm 9.0\%$ ($p < 0.05$), and 2.2-fold in the IM to $217.8 \pm 40.0\%$ ($p < 0.05$) in NG2 experiments. Interestingly, there was a non-significant decrease in PDGFR- β experiments $65.3 \pm 15.1\%$ ($p > 0.05$). This stark difference is likely to relate to the regional distribution of PDGFR- β^+ -labelled pericytes compared with NG2 $^+$ -labelled pericytes as described in section 5.3.2; PDGFR- β is present throughout the entirety of the IM whereas there is a known drop-off of NG2 $^+$ pericytes deep in the IM, which limited acquiring renders from the regions where NG2 $^+$ staining is located and increased the odds of M Φ cellular presence being larger as it was closer to the OM.

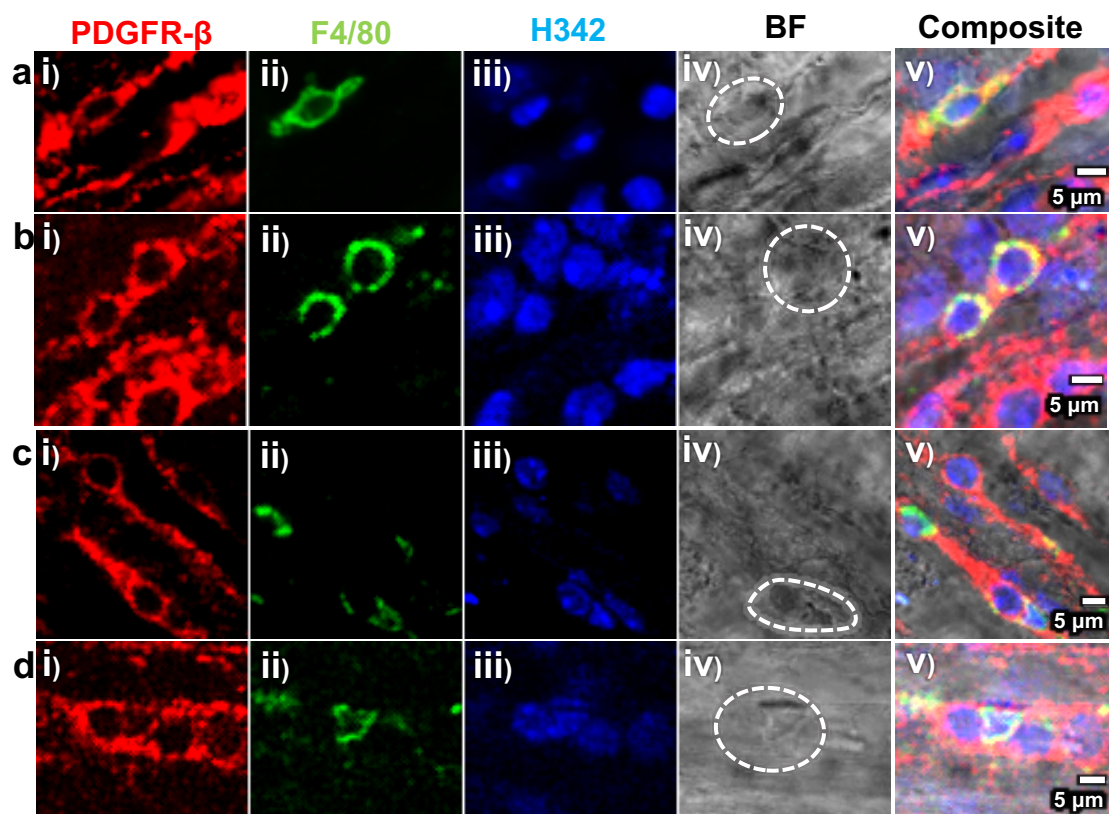


Figure 5.8 Co-expression of platelet derived growth factor receptor- β (PDGFR- β) and F4/80 on perivascular cells.

(a-d) show representative images of anti-PDGFR- β^+ (red; i) and anti-F4/80 $^+$ fluorescent labelling (green; ii) around Hoechst 33342 (H342; blue; iii) identified nuclei, that bears the morphology characteristic of pericytes, seen in the brightfield images (BF; iv). The corresponding composite of the four different channels can be seen in (v). (a-b) Show individual perivascular co-expression of F4/80 and PDGFR- β . (c-d) show co-expression of F4/80 by one cell in a pair of PDGFR- β^+ -labelled pericytes. Cell bodies in the bright field images are indicated by white dashed circles. Scale bars are 5 μ m.

Incubations of kidney slices with IL-1 β resulted in an OM increase of 1.2-1.4 times the number of M Φ than that of the PSS control; corresponding to values that were

123.0±11.1% (ns) and 137.1±7.6% (p<0.05) of those obtained from tissue exposed only to PSS. In the IM a non-significant 1.4-1.6-fold increase was observed, corresponding to 163.6±16.3% (ns) and 136.5±30.3% (ns) of values obtained from the PSS control for NG2 and PDGFR-β respectively (**Table 5.3; Figure 5.9(d) and 5.10(d)** respectively). The presence of MΦ observed here, as in the previous “0 hour” experiments presented in section 5.3.3 and as previously reported (Hume, and Gordon, 1983; Soos et al., 2006), was a significantly larger presence of MΦ in the OM than in the IM for PSS (p<0.0001), TNF-α (p<0.0001), and IL-1β (p<0.001).

Table 5.3 F4/80⁺ Macrophage (MΦ), platelet derived growth factor receptor-β (PDGFR-β)⁺, and neural-glia-2 (NG2)⁺ pericyte quantification after TNF-α and IL-1β stimulation

	PDGFR-β				NG2		
	PSS	TNF-α	IL-1β		PSS	TNF-α	IL-1β
Number of F4/80⁺ MΦ							
OM ¹	24.2±2.6	33.3±2.2*	33.1±1.8*		26.5±2.1	37.6±3.2*	32.6±2.9
IM ²	8.5±1.4	5.6±1.3	11.7±2.6		7.4±1.8	16.1±2.9*	9.4±1.2
Normalised F4/80⁺ MΦ numbers, %							
OM	100±10.8	137.1±9.0*	137.1±7.6*		100±8.1	141.8±12.1*	123.0±11.1
IM	100±16.7	65.3±15.1	136.5±30.3		100±23.9	217.8±40.0*	163.6±16.3
Normalised pericyte area density, %							
OM	100±20.21	81.2±4.6*	77.9±3.1*		100±7.7	63.6±6.3**	69.8±7.8*
IM	100±6.7	107.3±5.4	103.5±3.6		100±7.1	114.7±19.5	99.7±7.8

Data presented as mean±SEM, n= 3 animals and 3-4 slices, ≥ 200 pericytes per animal (%) Values are the percent of the PSS control mean and are calculated as the percent of the 10 μm z-stack (214.2 μm²) occupied with positive stain.

1OM = Outer medulla, 2IM = Inner medulla.

*p<0.05; **p<0.01 for comparisons between cytokine stimulation and PSS.

In kidney sections only exposed to PSS, the average pericyte density measured in the renders for PDGFR-β⁺ was 30.0±2.4% in the OM and 19.3±1.3% in the IM. NG2⁺ pericytes had a density of 20.5±1.8% in the OM and 5.3±0.7% in the IM; pericyte density is significantly greater in the OM for both groups of pericytes (p<0.0001). TNF-α stimulation caused a reduction of pericytes to 81.2±4.6% (p<0.05) of control PDGFR-β⁺ in the OM, but not in the IM (107.3±5.4%; p>0.05; **Figure 5.10(c)**). This reduction of density in the OM was larger with NG2⁺ pericytes (66.6±6.0%; p<0.01; **Figure 5.9(c)**), and also insignificant in the IM (114.7±19.5%; p>0.05, **Table 5.3**). A similar trend was observed with IL-1β, with significant reductions in OM pericytes for both PDGFR-β (77.9±3.1; p<0.05) and NG2 (69.8±7.8%; p<0.05) experiments, but not in the IM (103±3.6% and 99.7±7.8% for PDGFR-β⁺ and NG2⁺ pericytes respectively; p>0.05). These reductions are not significantly different between NG2⁺ or PDGFR-β⁺ pericytes.

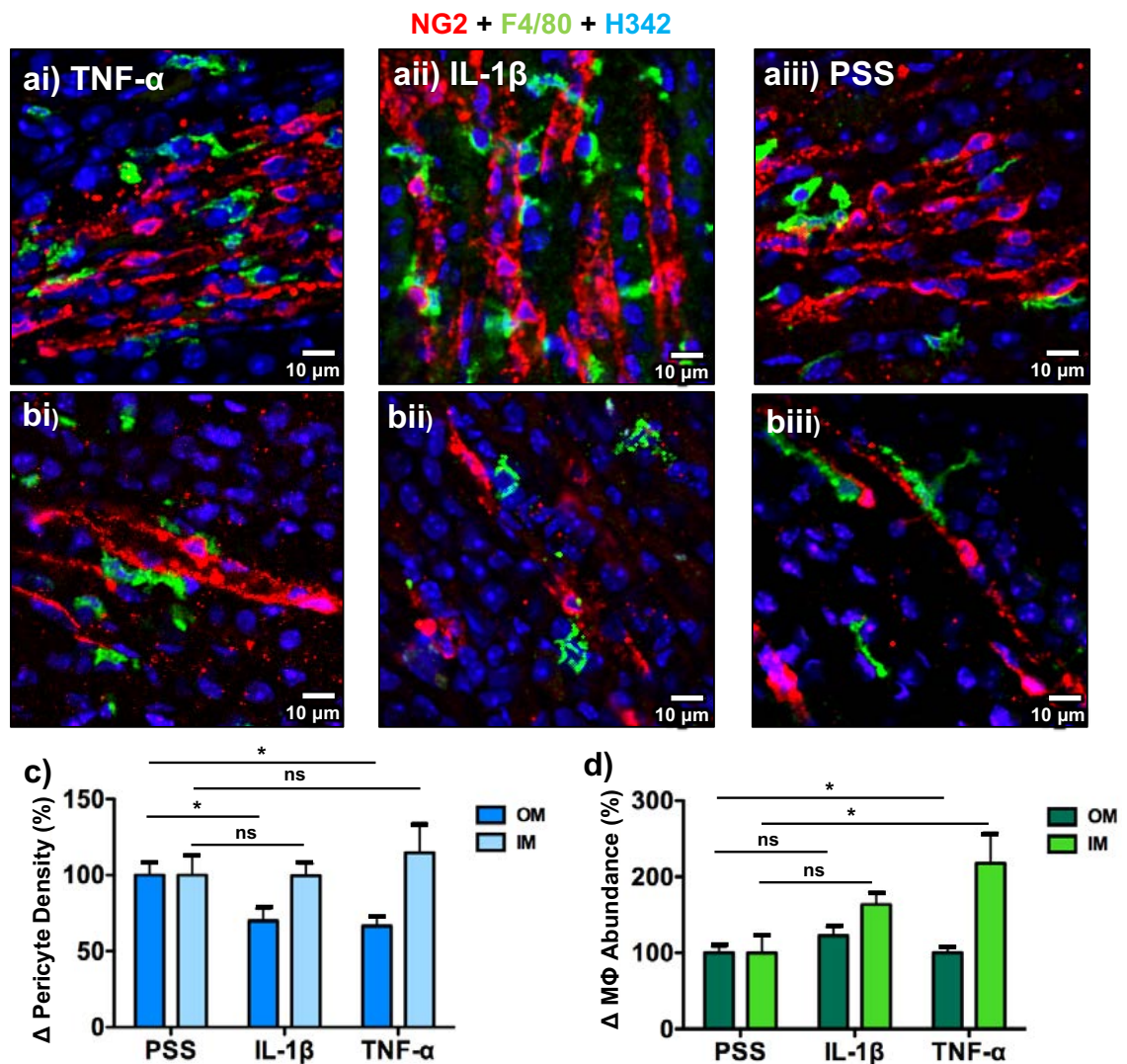


Figure 5.9 Effects of pro-inflammatory cytokine stimulation on F4/80⁺ macrophage (M Φ) and neural-glial 2 (NG2)⁺-labelled pericyte density in the outer (OM) and inner (IM) medulla

Representative confocal-acquired images in (a-b) showing the effect of stimulation with TNF- α (10 ng/mL; i), IL-1 β (10 ng/mL; ii) and the PSS control (iii) on NG2⁺-labelled pericytes (red) F4/80⁺-labelled M Φ (green) in the OM (a) and IM (b). Cell nuclei were identified using Hoechst 33342 (H342; blue). The respective changes in pericyte density (c) and the M Φ abundance (d) are presented as the percent change from the PSS control. Data presented as mean \pm SEM. n= 3 animals and 3 slices for all but NG2 PSS, where n=4 animals and 4 slices. * p<0.05, ^{ns} p>0.05.

Due to the expansive nature of PDGFR- β (Figure 5.1(a)), direct quantification of cell numbers was not feasible or accurate. The standard, as shown above, is to present the percentage of space occupied by positive stain (Ikeda et al., 2018; Craggs et al., 2015). However in the kidney the density of NG2⁺ pericyte cell bodies per 100 μ m² has previously been reported; both in chapter 4 and as published by Crawford *et al* (Crawford et al., 2012). Hence this was also calculated here, along with the total number of cell bodies present in the renders acquired. Total numbers of NG2⁺ pericytes in the renders in PSS were: 53.9 \pm 3.7 cells in the OM, and 12.2 \pm 1.2 in the IM; with

densities per 100 μm^2 of 12.6 ± 1.0 cells in the OM and 4.1 ± 0.3 in the IM. In the OM, TNF- α significantly reduced OM NG2⁺ pericyte vascular bundle density per 100 μm^2 (8.8 ± 1.0 ; $p < 0.05$) and the total quantity to 38.8 ± 3.0 pericytes ($p < 0.05$), but not in the IM (13.1 ± 2.0 total and 3.5 ± 0.5 pericytes per 100 μm^2 ; $p > 0.05$). IL-1 β significantly reduced total NG2⁺ pericyte cell numbers (40.5 ± 5.0 ; $p < 0.05$) in the OM and the pericyte density per 100 μm^2 (9.3 ± 1.1 ; $p < 0.05$). IL-1 β had no significant effect on the IM pericyte densities overall (15.8 ± 1.3) or per 100 μm^2 (4.3 ± 0.4 ; $p > 0.05$).

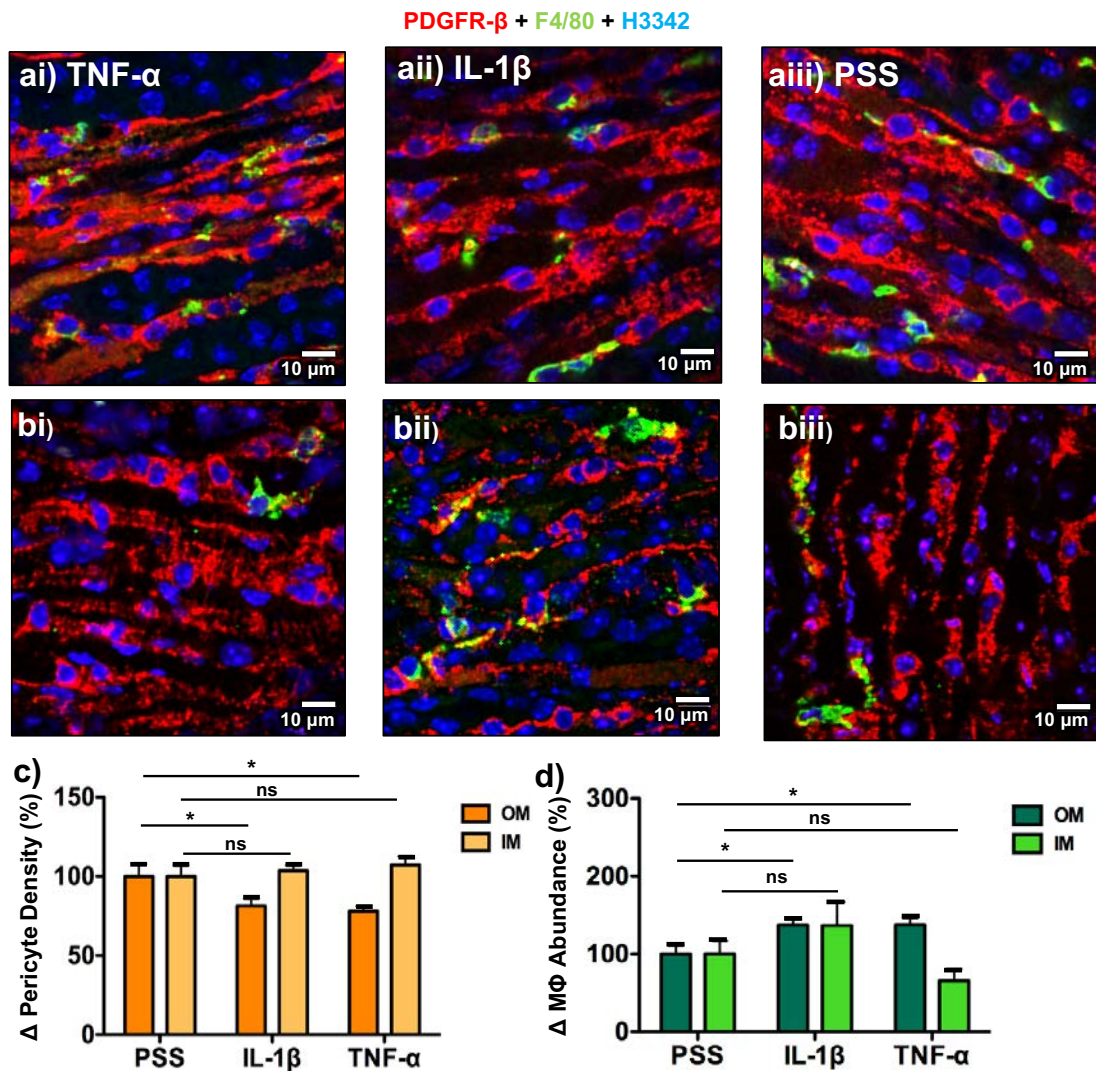


Figure 5.10 Effects of pro-inflammatory cytokine stimulation on F4/80⁺ macrophage (M Φ) and platelet derived growth factor receptor- β (PDGFR- β)⁺-labelled pericyte density in the outer (OM) and inner (IM) medulla.

Representative confocal-acquired images in (a-b) showing the effect of stimulation with TNF- α (10 ng/mL; i), IL-1 β (10 ng/mL; ii) and the PSS control (iii) on PDGFR- β -labelled pericytes (red) F4/80⁺-labelled M Φ (green) in the OM (a) and IM (b). Cell nuclei were identified using Hoechst 33342 (H342; blue). The respective changes in pericyte density (c) and the M Φ abundance (d) are presented as the percent change from the PSS control. Data presented as mean \pm SEM. $n = 3$ animals and 3 slices. * $p < 0.05$, ^{ns} $p > 0.05$.

5.3.7 IL-1 β , not TNF- α , retained F4/80 $^+$ macrophages near NG2 $^+$ pericytes in both the OM and IM.

Due to lack of cell quantification, the percentage of cell-cell F4/80 $^+$ M Φ -PDGFR- β^+ contact was not possible to calculate, nor the distance between those cells without contact, as described in **section 5.3.3**. However, as NG2 $^+$ pericyte cellular density per 10 μm -deep (214.2 μm^2) render was calculated such analysis could be performed in these experiments. Cytokine stimulation significantly increased the percentage of OM NG2 $^+$ pericytes with cell-cell contact to a F4/80 $^+$ M Φ ; 70.9 \pm 2.2% upon treatment with TNF- α ($p < 0.001$), 63.0 \pm 3.2% with IL-1 β ($p < 0.05$), compared with 50.6 \pm 3.7% in slices exposed to PSS. Interestingly, the percentage of NG2 $^+$ pericytes with direct cell-cell contact to F4/80 $^+$ M Φ significantly increased after the incubation time-period of 4-hours in the OM, compared with the “0 hour” PSS experiments showing 38.6 \pm 4.7% of pericytes having contact ($p < 0.05$; **Figure 5.11(ai)**).

Table 5.4 The spatial relationship between F4/80 $^+$ Macrophage (M Φ) and neural-glial-2 (NG2) $^+$ pericytes after TNF- α and IL-1 β stimulation

	Contact				Distance		
	PSS	TNF- α	IL-1 β		PSS	TNF- α	IL-1 β
NG2$^+$ Pericyte–F4/80$^+$ MΦ							
OM ¹	52.6 \pm 3.7 [§]	70.9 \pm 2.2 ^{***}	63.0 \pm 3.2 [*]		100 \pm 10.9	94.4 \pm 8.2	82.7 \pm 10.8
IM ²	24.7 \pm 6.8	35.5 \pm 7.6	25.2 \pm 3.2		100 \pm 9.0	60.8 \pm 11.7 [*]	61.8 \pm 7.6 [*]
F4/80$^+$ MΦ–NG2$^+$ Pericyte							
OM	65.6 \pm 5.1 [§]	58.9 \pm 3.3	59.4 \pm 1.8		100 \pm 9.4	89.7 \pm 7.5	73.2 \pm 4.6 [*]
IM	38.7 \pm 6.7	22.3 \pm 5.3	38.4 \pm 3.6		100 \pm 9.2	89.1 \pm 11.0	60.3 \pm 6.2 ^{**}

Data are shown as mean \pm SEM, n= 3 animals and 3-4 slices, \geq 200 pericytes per animal.

For contact, measurements are shown as the percentage of cells per 10 μm z-stack (214.2 μm^2) with cell-cell contact, %

For distance, values are shown as percentage of the PSS control value, %

¹OM = Outer medulla, ²IM = Inner medulla.

Pericyte-M Φ means the focus of measurement is dependent upon location of the NG2 $^+$ pericyte
M Φ -pericyte means the focus of measurement is dependent upon location of the M Φ

* $p < 0.05$; ** $p < 0.01$; *** $p < 0.001$ for comparison with PSS control

[§] $p < 0.05$ for comparison between OM and IM

There was no such significant increase ($p > 0.05$) in the IM; with 35.5 \pm 7.8% of pericytes with contact upon TNF- α stimulation, and 25.5 \pm 3.2% of pericytes with IL-1 β stimulation, compared to 24.7 \pm 6.8% of pericytes in tissue sections kept in PSS. With regards to the percentage of total M Φ present that were in contact with NG2 $^+$ pericytes, there is no significant difference between cytokine and PSS exposure: 38.7 \pm 6.7%, 22.3 \pm 5.3%, and 38.4 \pm 3.6% in the IM; and 65.6 \pm 5.1%, 58.9 \pm 3.3, and 59.4 \pm 1.8% in the OM for PSS, TNF- α , and IL-1 β exposure respectively in the IM ($p > 0.05$; **Table 5.4**; **Figure 5.11(bi)**). However, whilst not significant, in the OM compared to the 0-hour

PSS experiments, in time-matched 4-hour control there was an approximately 20% increase in the percentage of F4/80⁺ MΦ in contact with NG2⁺ pericytes. The degree of contact for both pericytes to MΦ ($p < 0.0001$), and MΦ to pericytes ($p < 0.0001$) was significantly larger in the OM than the IM.

For those cells not in contact, the distances between them were measured. The loci of measurements were either from a NG2⁺ pericyte cell body, or a F4/80⁺ MΦ cell body to the nearest oppositely labelled cell. The average distance of pericytes to MΦ did not significantly differ in the OM upon cytokine stimulation. In PSS the OM distance from pericytes to the nearest MΦ was $20.9 \pm 2.3 \mu\text{m}$, which TNF- α and IL-1 β stimulation did not significantly reduce ($94.4 \pm 8.2\%$ and $82.7 \pm 10.8\%$ of the PSS control respectively; $p > 0.05$; **Figure 5.11(aii)**). In the IM, upon exposure to PSS only the distance from NG2⁺ pericytes to the nearest F4/80⁺ MΦ was $40.7 \pm 3.7 \mu\text{m}$. TNF- α stimulation reduced this distance 1.6-fold to $60.8 \pm 11.7\%$ ($p < 0.05$) of that observed with PSS alone. This relative change was comparable after stimulation with IL-1 β , reducing the distance to $61.8 \pm 7.6\%$ ($p < 0.05$; **Figure 5.11(aii)**) of that observed in PSS experiments.

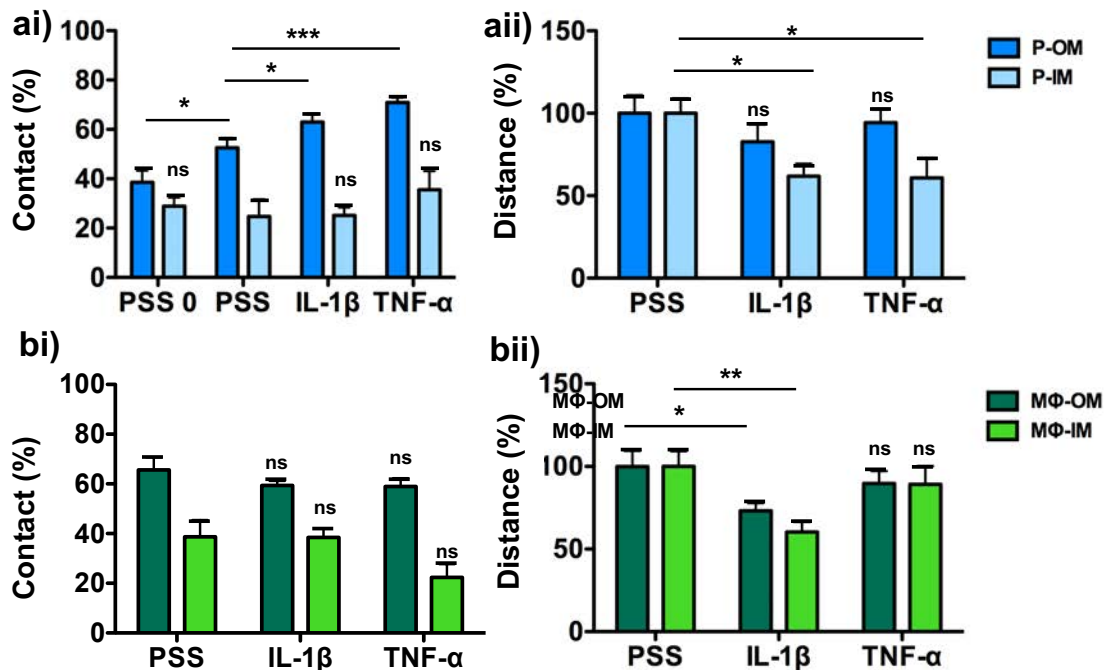


Figure 5.11 The effect of pro-inflammatory cytokines TNF- α and IL-1 β on the spatial arrangement between neural-gial-2 (NG2)⁺ pericytes and F4/80⁺ macrophage (MΦ). In (ai) and (bi) bars represent the average percentage of total cells present with cell-cell contact per 10 μm deep z-stack ($214.2 \mu\text{m}^2$) (Contact %). with the locus from either a NG2⁺ pericyte cell body (ai; blue bars) or F4/80⁺ MΦ cell body (bi; green bars), in the outer (OM) and inner medulla (IM). (aii) and (bii) show the corresponding distance for cells not in contact as a percentage of the distance observed the PSS control (% distance). In (ai) "PSS" is the time-matched control experiment with the cytokine stimulations, "PSS 0" are values taken from slices processed immediately post-slicing. Data presented as mean \pm SEM. * $p < 0.05$, *** $p < 0.001$, ^{ns} $p > 0.05$. $n = 3$ animals and 3 slices for TNF- α and IL-1 β treatment groups, and $n = 4$ animals and 4 slices for PSS treatment group.

The average distance from pericytes to M Φ in PSS was significantly greater in the IM than the OM ($p < 0.0001$), with no regional difference observed for the distance in slices treated with either TNF- α or IL-1 β ($p > 0.05$). With M Φ as the locus, the average distance to the nearest pericyte in the OM was $33.1 \pm 3.1 \mu\text{m}$. TNF- α stimulation did not significantly reduce this distance ($89.7 \pm 7.5\%$; $p > 0.05$), but IL-1 β did to $73.2 \pm 4.6\%$ ($p < 0.05$) of the distance observed in PSS. A similar trend was observed in the IM; on average in slices incubated in PSS, M Φ were $41.1 \pm 3.8 \mu\text{m}$ away from pericytes. TNF- α stimulation did not significantly reduce this distance ($89.1 \pm 11.0\%$; $p > 0.05$), yet IL-1 β stimulation caused a significant reduction in distance from M Φ to pericytes to $60.3 \pm 6.2\%$ of that in PSS ($p < 0.01$; **Figure 5.11(bii)**).

5.3.8

5.3.9 TNF- α - and IL-1 β -induced, pericyte-mediated vasoconstriction, is potentiated by macrophage contact in NG2 $^+$, but not PDGFR- β^+ pericytes

The vasa recta diameter was significantly narrower at pericyte sites than non-pericyte sites (**Table 5.1**; $p < 0.0001$), for both PDGFR- β^+ and NG2 $^+$ pericytes. Further to this, vasa recta where pericytes that had cell-cell contact with F4/80 $^+$ M Φ were significantly constricted, specifically at pericyte sites (**Table 5.2**; $p < 0.0001$). In cytokine treated tissue, vasa recta at both NG2 $^+$ pericyte sites and non-pericyte sites are significantly narrower than in PSS; in TNF- α stimulated tissue pericyte sites measured $5.0 \pm 0.2 \mu\text{m}$, and $7.2 \pm 0.3 \mu\text{m}$ at non-pericyte sites on average ($p < 0.05$ vs $5.6 \pm 0.2 \mu\text{m}$ and $7.9 \pm 0.2 \mu\text{m}$ for vasa recta exposed to PSS at pericyte and non-pericyte sites respectively). Vasa recta exposed to IL-1 β , measured $4.9 \pm 0.2 \mu\text{m}$ and $6.9 \pm 0.2 \mu\text{m}$ at pericyte and non-pericyte sites respectively on average ($p < 0.01$).

There was no significant difference in vasa recta diameters at pericyte sites when M Φ were present. The average vessel diameter measured was $5.2 \pm 0.3 \mu\text{m}$ in PSS alone, $5.3 \pm 0.3 \mu\text{m}$ in TNF- α treated tissue ($p > 0.05$), and $5.6 \pm 0.3 \mu\text{m}$ in IL-1 β treated tissue ($p > 0.05$) at pericyte sites. There was also no significant difference ($p > 0.05$) of vessel diameters at non-pericyte sites when the corresponding pericyte had F4/80 $^+$ M Φ contact which were on average; $7.2 \pm 0.3 \mu\text{m}$ in PSS, $7.2 \pm 0.3 \mu\text{m}$ in TNF- α , and $7.4 \pm 0.3 \mu\text{m}$ in IL-1 β . However, when vessel diameters where pericytes with F4/80 M Φ contact were excluded, TNF- α stimulation caused a significant constriction at PDGFR- β^+ pericyte sites; $5.7 \pm 0.2 \mu\text{m}$ ($p < 0.05$) at the pericyte site and $7.7 \pm 0.3 \mu\text{m}$ ($p > 0.05$) at the corresponding non-pericyte site compared with a capillary diameter of $6.5 \pm 0.2 \mu\text{m}$ at pericyte sites and $8.2 \pm 0.3 \mu\text{m}$ at the corresponding non-pericyte site in PSS incubations.

IL-1 β stimulation did not significantly change vasa recta diameter at pericyte (6.0 \pm 0.2 μ m; p >0.05) or non-pericyte sites (8.2 \pm 0.2 μ m; p >0.05). Both the PDGFR- β ⁺ pericyte site (p <0.0005) and corresponding non-pericyte site (p <0.05) on vasa recta in PSS were significantly narrower when in contact with M Φ , as was the non-pericyte site in IL-1 β (p <0.05) incubations when the PDGFR- β ⁺ had M Φ contact (**Table 5.5; Figure 5.12(b)**). However, in section 5.3.3 it was observed that when pericytes were in direct cellular contact with F4/80⁺ M Φ , vasa recta were significantly narrower, specifically at pericyte sites (**Table 5.2**) suggesting those pericytes were constricted. Subsequently, values were categorised based upon whether the corresponding pericyte had cellular contact with a M Φ .

Table 5.5 Effect of TNF- α and IL-1 β stimulation, and F4/80⁺ macrophage (M Φ) presence on vasa recta diameter encircled by neural-glial-2 (NG2)⁺ or platelet derived growth factor receptor- β (PDGFR- β)⁺ pericytes.

	PDGFR- β				NG2		
	PSS	TNF- α	IL-1 β		PSS	TNF- α	IL-1 β
F4/80⁺ MΦ contact							
P ¹	5.2 \pm 0.3%	5.3 \pm 0.3	5.6 \pm 0.3		4.9 \pm 0.3%	4.7 \pm 0.2	4.4 \pm 0.2@
NP ²	7.2 \pm 0.3 [£]	7.2 \pm 0.3	7.4 \pm 0.3 [£]		7.4 \pm 0.3 [£]	7.0 \pm 0.3	6.3 \pm 0.3* [@]
No F4/80⁺ MΦ contact							
P	6.5 \pm 0.2	5.7 \pm 0.2*	6.0 \pm 0.2		6.2 \pm 0.2	5.3 \pm 0.2*	5.4 \pm 0.3*
NP	8.2 \pm 0.3	7.7 \pm 0.3	8.2 \pm 0.2		8.3 \pm 0.3	7.2 \pm 0.3*	7.5 \pm 0.3

Data shown as mean \pm SEM in μ m, n= 3 animals and 3-4 slices, \geq 200 pericytes per animal.

¹P = pericyte site ²NP = non-pericyte site

* p <0.05 compared with PSS

[£] p <0.05; [@] p <0.005; [%] p <0.0005 comparison between M Φ contact and no contact

When in contact with M Φ , there was no significant difference (p >0.05) in vasa recta diameter at NG2⁺ pericyte sites (4.9 \pm 0.3 μ m, 4.7 \pm 0.2 μ m, and 4.4 \pm 0.2 μ m for PSS, TNF- α , and IL-1 β respectively) between the treatment groups. There was a significant difference in the IL-1 β non-pericyte site diameter compared to that exposed to PSS (6.3 \pm 0.3 μ m vs 7.4 \pm 0.3 μ m; p <0.01), but not with TNF- α (7.0 \pm 0.3; p >0.05). Conversely, when comparing vessel diameter measurements between stimulation groups without F4/80⁺ M Φ contact, there is a significant difference in TNF- α (5.3 \pm 0.2 μ m vs 6.2 \pm 0.2 μ m for PSS; p <0.05) and IL-1 β (5.4 \pm 0.3 μ m; p <0.05) stimulated pericyte sites compared with PSS, and a significant difference in the TNF- α stimulated non-pericyte site (7.2 \pm 0.3 μ m vs 8.3 \pm 0.3 μ m in PSS; p <0.05) but not with IL-1 β (7.5 \pm 0.3 μ m; p >0.05; **Table 5.5; Figure 5.12(a)**). Interestingly, much like was observed in PSS, vasa recta encircled by NG2⁺ pericytes with F4/80⁺ M Φ contact in IL-1 β stimulated tissue are significantly narrower at both the pericyte and non-pericyte site (p <0.005). This did not occur with TNF- α exposure (p >0.05).

On capillaries encircled with PDGFR- β^+ pericytes, there was no significant difference between PSS control and cytokine treated tissue. Diameters measured were on average: 5.7 ± 0.2 μm in PSS, 5.5 ± 0.2 μm ($p>0.05$) and 5.6 ± 0.2 μm ($p>0.05$) for TNF- α and IL-1 β respectively at pericyte sites; and 7.7 ± 0.2 μm in PSS, and 7.5 ± 0.3 μm ($p>0.05$) and 7.8 ± 0.2 ($p>0.05$) for TNF- α and IL-1 β respectively at non-pericyte sites (**Table 5.6**). As with NG2, in **Table 5.2** it can be seen that M Φ presence influences vasa recta diameter at PDGFR- β^+ pericyte sites, so again measurements were divided into with or without F4/80 $^+$ cell contact.

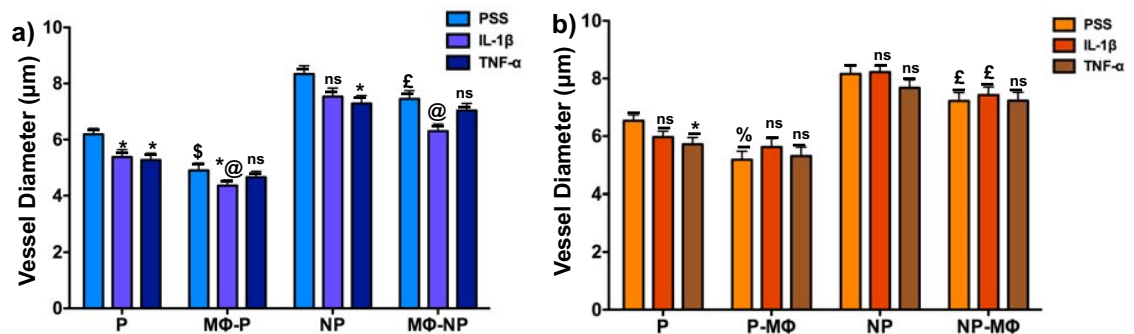


Figure 5.12 The effect of pro-inflammatory cytokines TNF- α and IL-1 β and M Φ presence on vasa recta diameter.

Bar graphs show the effect of TNF- α (hatched bars) and IL-1 β (checked bars) stimulation on the diameter of vasa recta diameter encircled by either platelet derived growth factor receptor- β (PDGFR- β^+ ; **a**; orange bars) or neural-gial-2 (NG2 $^+$; **b**; blue bars) pericytes. Measurements were taken from a pericyte site (P) and corresponding non-pericyte site (NP). Also shown is the capillary diameter at a pericyte site in contact with an F4/80 $^+$ M Φ (P-M Φ) and its corresponding non-pericyte site (M Φ -NP). Data presented as mean \pm SEM. $n=3$ animals and 3 slices for all but the NG2 PSS experiments, where $n=4$ animals and 4 slices. * $p<0.05$, for comparison with PSS; † $p<0.05$; @ $p<0.005$ for comparisons between sites with M Φ contact and no contact; ns $p>0.05$.

There was no significant difference in vasa recta diameters at pericyte sites when M Φ were present. The average vessel diameter measured was 5.2 ± 0.3 μm in PSS alone, 5.3 ± 0.3 μm in TNF- α treated tissue ($p>0.05$), and 5.6 ± 0.3 μm in IL-1 β treated tissue ($p>0.05$) at pericyte sites. There was also no significant difference ($p>0.05$) of vessel diameters at non-pericyte sites when the corresponding pericyte had F4/80 $^+$ M Φ contact which were on average; 7.2 ± 0.3 μm in PSS, 7.2 ± 0.3 μm in TNF- α , and 7.4 ± 0.3 μm in IL-1 β . However, when vessel diameters where pericytes with F4/80 M Φ contact were excluded, TNF- α stimulation caused a significant constriction at PDGFR- β^+ pericyte sites; 5.7 ± 0.2 μm ($p<0.05$) at the pericyte site and 7.7 ± 0.3 μm ($p>0.05$) at the corresponding non-pericyte site compared with a capillary diameter of 6.5 ± 0.2 μm at pericyte sites and 8.2 ± 0.3 μm at the corresponding non-pericyte site in PSS

incubations. IL-1 β stimulation did not significantly change vasa recta diameter at pericyte (6.0 \pm 0.2 μ m; p >0.05) or non-pericyte sites (8.2 \pm 0.2 μ m; p >0.05). Both the PDGFR- β^+ pericyte site (p <0.0005) and corresponding non-pericyte site (p <0.05) on vasa recta in PSS were significantly narrower when in contact with M Φ , as was the non-pericyte site in IL-1 β (p <0.05) incubations when the PDGFR- β^+ had M Φ contact (**Table 5.5; Figure 5.12(b)**)

Table 5.6 Effect of TNF- α and IL-1 β stimulation, and F4/80 $^+$ macrophage (M Φ) presence on neural-glial-2 (NG2) $^+$ or platelet derived growth factor receptor- β (PDGFR- β) $^+$ pericyte soma size.

		PDGFR- β			NG2		
		PSS	TNF- α	IL-1 β	PSS	TNF- α	IL-1 β
F4/80$^+$ MΦ contact							
OM ¹	H ³	4.4 \pm 0.2*	4.8 \pm 0.2	5.0 \pm 0.2	4.4 \pm 0.3	4.6 \pm 0.2	4.3 \pm 0.3
	W ⁴	6.7 \pm 0.4	7.1 \pm 0.3	7.2 \pm 0.3	7.4 \pm 0.4	7.8 \pm 0.5	7.9 \pm 0.3
IM ²	H	5.0 \pm 0.2	4.8 \pm 0.3	4.9 \pm 0.2	4.0 \pm 0.2	3.5 \pm 0.2	3.8 \pm 0.3
	W	6.9 \pm 0.4	6.2 \pm 0.4	7.0 \pm 0.4	6.9 \pm 0.4	6.2 \pm 0.4	7.0 \pm 0.4
No F4/80$^+$ MΦ contact							
OM	H	5.2 \pm 0.2	4.8 \pm 0.1	5.2 \pm 0.2	4.5 \pm 0.2	4.3 \pm 0.3	4.1 \pm 0.2
	W	7.4 \pm 0.3	7.9 \pm 0.3	6.8 \pm 0.4	7.5 \pm 0.3	7.4 \pm 0.5	7.1 \pm 0.3
IM	H	7.4 \pm 0.3	7.9 \pm 0.3	6.8 \pm 0.4	7.5 \pm 0.3	7.4 \pm 0.5	7.1 \pm 0.3
	W	5.9 \pm 0.3	5.8 \pm 0.3	6.5 \pm 0.3	7.9 \pm 0.4	7.2 \pm 0.4	7.2 \pm 0.4

Data shown as mean \pm SEM in μ m, n = 3 animals and 3-4 slices, \geq 200 pericytes per animal.

¹H = height; ²W = width; ³OM = outer medulla; ⁴IM = inner medulla.

* p <0.05 for comparison between pericytes with M Φ contact and pericytes with no M Φ contact.

5.3.10 Presence of F4/80 $^+$ macrophages, not cytokine stimulation has potential to influence PDGFR- β^+ pericyte morphology

In section 5.3.3, it was observed that whilst F4/80 $^+$ M Φ contact caused a pericyte-mediated constriction of vasa recta diameter, this contact did not influence the morphology of the pericyte soma for either PDGFR- β^+ or NG2 $^+$ -labelled pericytes (**Table 5.2**). NG2 $^+$ pericyte morphology was not altered upon to exposure to either TNF- α or IL-1 β (p >0.05), and there was no significant difference, regardless of contact with F4/80 $^+$ M Φ , compared to PSS (p >0.05).

In PSS: NG2 $^+$ pericytes in contact with M Φ were: 4.4 \pm 0.3 μ m in height, and 7.4 \pm 0.4 μ m wide in the OM; and 4.0 \pm 0.2 μ m by 6.9 \pm 0.4 μ m in the IM. Without M Φ contact, they were 4.5 \pm 0.2 μ m in height by 7.5 \pm 0.3 μ m in width in the OM, and 4.2 \pm 0.2 μ m in height by 7.9 \pm 0.4 μ m in width in the IM. With regards to pericytes exposed only to PSS, this lack in morphological difference when M Φ were in contact was observed in the initial experiments for NG2 $^+$ pericytes (**Table 5.2**).

Upon TNF- α stimulation, NG2⁺ pericytes with M Φ contact were; 4.6 \pm 0.2 μ m in height by 7.8 \pm 0.5 μ m in width in the OM, and 3.5 \pm 0.2 μ m in height by 6.2 \pm 0.4 μ m wide in the IM. Pericytes without M Φ contact measured 4.1 \pm 0.2 μ m in height by 7.1 \pm 0.3 μ m in width in the OM, and 3.9 \pm 0.2 μ m in height by 7.2 \pm 0.4 μ m in width in the IM. IL-1 β stimulated NG2⁺ pericytes that also had direct cellular contact with F4/80⁺ M Φ were; 4.3 \pm 0.3 μ m in height by 7.9 \pm 0.3 μ m in width in the OM, and 3.8 \pm 0.3 μ m in height by 7.0 \pm 0.4 μ m in width in the IM. Without this contact, IL-1 β stimulated pericytes were 4.1 \pm 0.2 μ m in height by 7.1 \pm 0.3 μ m in width in the OM, and 4.2 \pm 0.2 μ m by 7.2 \pm 0.4 μ m in the IM.

Cytokine stimulation with either TNF- α or IL-1 β also had no significant effect on PDGFR- β ⁺ pericyte size ($p > 0.05$). However, OM PDGFR- β ⁺ pericytes with M Φ contact in PSS were significantly smaller than those without contact; 4.4 \pm 0.2 μ m in height and 6.7 \pm 0.4 μ m in width with F4/80⁺ M Φ contact, and 5.2 \pm 0.2 μ m in height by 7.4 \pm 0.3 μ m in width without contact (**Figure 5.13**). In the IM there was no significant difference observed with M Φ - PDGFR- β ⁺ pericyte contact in PSS. These pericyte with contact measure 5.0 \pm 0.2 μ m tall by 6.9 \pm 0.4 μ m wide compared to 5.3 \pm 0.2 μ m in height and 5.9 \pm 0.3 μ m in width without M Φ contact. For pericytes exposed only to PSS, this M Φ -related PDGFR- β ⁺ morphological change was a trend observed for pericytes in **section 5.3.3 (Table 5.2)**. However, this reduction in height was not significant in the pilot study ($p > 0.05$), but interestingly is non-significantly different for the height of NG2⁺ OM pericytes. Unfortunately, as experiments were not conducted with both pericyte markers simultaneously, it cannot be commented upon whether these smaller pericytes with M Φ contact are PDGFR- β ⁺/ NG2⁺ or PDGFR- β ⁺/ NG2⁻.

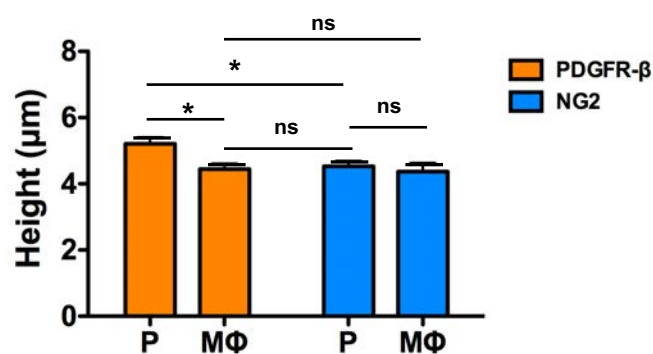


Figure 5.13 Differential effect of F4/80+ macrophage (M Φ) presence on neural-glia-2 (NG2)⁺ or platelet derived growth factor receptor- β (PDGFR- β)⁺ pericytes in the outer medulla (OM).

Bars represent the average height (top-to-bottom) measured for PDGFR- β ⁺-labelled (orange bar) and NG2⁺-labelled (blue bar) pericytes when in direct cellular contact with F4/80⁺-labelled M Φ (M Φ) and without contact with M Φ (P) when exposed only to PSS. Data presented as mean \pm SEM. * $p < 0.05$; ^{ns} $p > 0.05$, $n = 3$ slices and 3 animals for PDGFR- β and $n = 4$ animals and 4 slices for NG2.

With TNF- α stimulation, pericytes in contact with M Φ were 4.8 ± 0.2 μm in height and 7.1 ± 0.3 μm in width in the OM; and 4.8 ± 0.2 μm in height by 6.2 ± 0.4 μm in width in the IM. Pericytes incubated in TNF- α with no direct contact to M Φ , pericytes measured 5.2 ± 0.2 μm in height by 7.4 ± 0.3 μm in width the OM and 4.9 ± 0.3 μm in height by 5.8 ± 0.3 μm in width in the IM. IL-1 β stimulated PDGFR- β^+ pericytes measured 5.0 ± 0.2 μm in height by 7.2 ± 0.3 μm in width the OM, and 4.9 ± 0.2 μm tall and 7.0 ± 0.4 μm wide in the IM when they had direct cellular contact with a F4/80 $^+$ M Φ . IL-1 β stimulated, PDGFR- β^+ pericytes without M Φ contact were 5.2 ± 0.2 μm in height and 6.8 ± 0.4 μm in width in the OM, and 5.1 ± 0.2 μm in height by 6.5 ± 0.3 μm in width in the IM.

5.3.11 Pro-inflammatory cytokine stimulation does not appear to encourage cellular co-expression of F4/80 and NG2 $^+$, but does for F4/80 and PDGFR- β .

In section 5.3.5, it was observed that there was a small population of cells that were seemingly positively labelled for both the M Φ identifying marker anti-F4/80, and either pericyte identifying markers anti-NG2 or anti-PDGFR- β (**Figure 5.7-8**). This co-expression was determined when there was co-staining with both pericyte (red) and M Φ (green) fluorescence localised around an individual Hoechst 33342 $^+$ nucleus. Computational calculation of the degree of co-localisation of fluorescent staining is not feasible in this study as it would likely include cell-cell contact in analysis, overestimating the degree of co-localisation. As described in section 5.3.5, addition of the 3 $^{\text{rd}}$ dimension by acquiring a 10 μm z-stack render ($212.4 \mu\text{m}^2$) enabled exclusion of cells that were merely adjacent to one another in the z-plane from quantification of co-expression. Renders were generated by randomly selecting a ROI in both the OM and IM and co-expression was only assessed after images had been acquired. As F4/80 $^+$ expression is a sign of M Φ maturity (Lee et al., 1985), the aim here of cytokine stimulation of kidney slices was to observe if NG2 $^+$ -labelled or PDGFR- β^+ -labelled pericytes were “dormant” and express M Φ markers when activated in an emulated inflammatory state.

Unlike in experiments presented in section 5.3.5, no co-staining of M Φ marker F4/80 and pericyte marker NG2 occurred, irrespective of TNF- α or IL-1 β stimulation in either the IM or the OM. From observations presented in section 5.3.3, the majority of F4/80 $^+$ M Φ resided in the interstitial space, yet, it was observed here that there was seemingly more perivascular F4/80 $^+$ NG2 $^-$ cells than had been noted previously, having the ovular morphology characteristic of pericytes (**Figure 5.14**). These perivascular F4/80 $^+$ NG2 $^-$ cells reside along capillaries lined with anti-NG2 staining, (**Figure 5.14(b), (e)**).

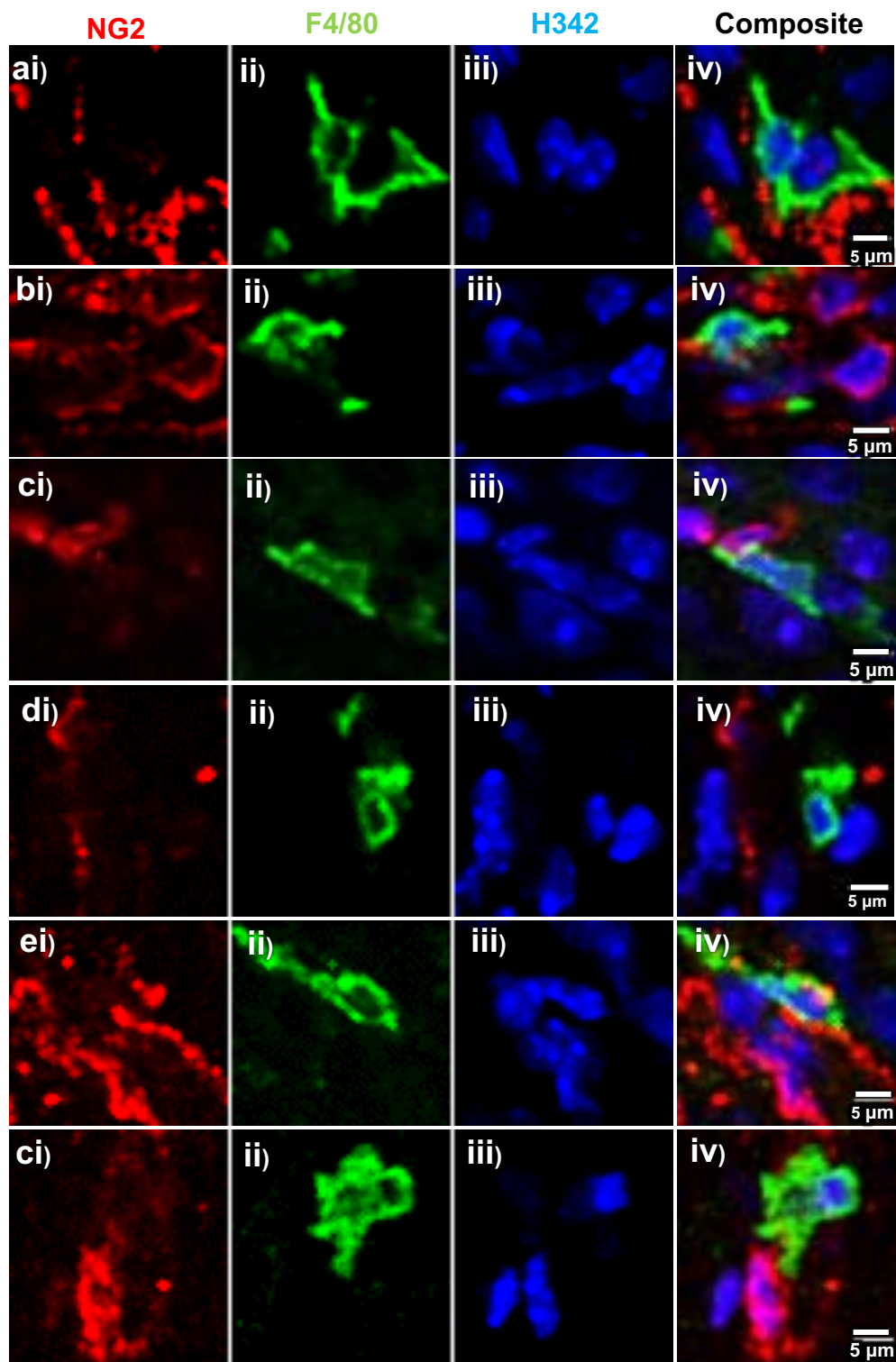


Figure 5.14 Morphology of perivascular neural-glial-2 (NG2)-, F4/80+ cells is comparable to NG2+ pericytes, irrespective of cytokine treatment in the renal medulla. Representative images where tissue was incubated with; PSS (a-b), TNF- α (c-d), and IL-1 β (e-f) showing staining with anti-NG2 (i; red), anti-F4/80 (iii; green), and Hoechst 33342 (H342; iv; blue) with composite render (iv). Scale bars are 5 μ m.

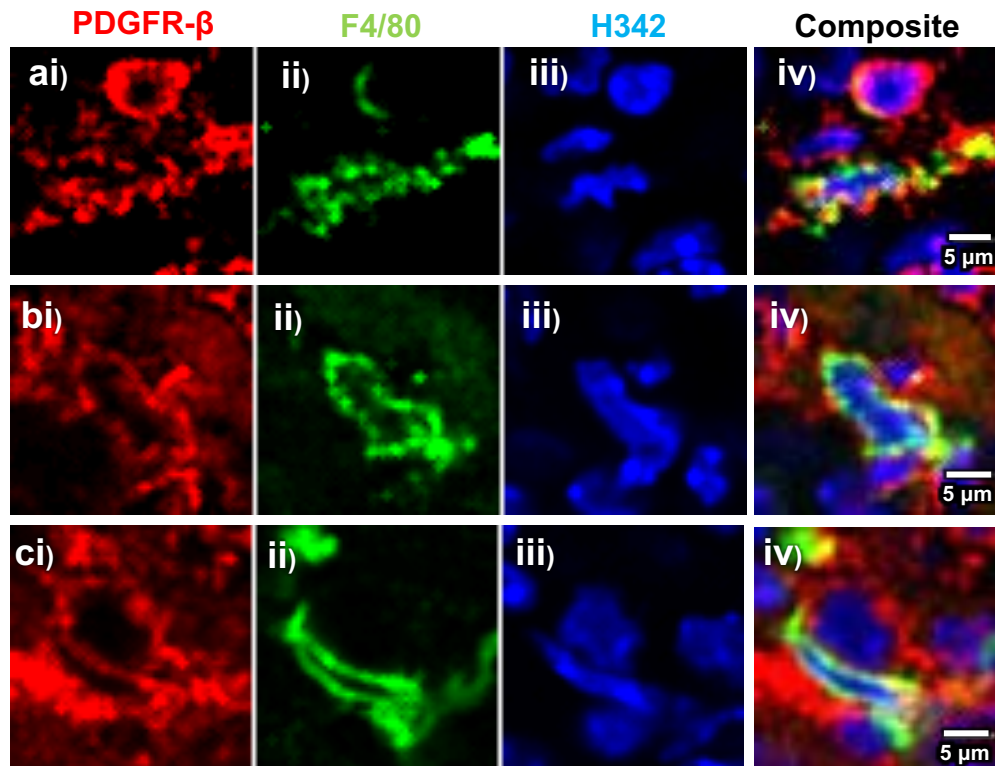


Figure 5.15 Co-expression of platelet derived growth factor receptor- β (PDGFR- β) and F4/80 on non-vascular resident cells in the renal medulla.

Exemplary images from experiments where tissue was incubated with either; PSS (**a-b**), TNF- α (**b**), and IL-1 β (**c**), showing positive staining with anti-PDGFR- β (**i**; *red*), anti-F4/80 (**iii**; *green*), and Hoechst 33342 (H342; **iv**; *blue*) with the corresponding composite render (**iv**). Scale bars are 5 μ m.

Contrastingly to NG2 experiments, there was frequent F4/80⁺/PDGFR- β ⁺ co-staining observed, also independent of cytokine stimulation in both the IM and OM. Representative images can be seen in **Figure 5.16**. Given the nature of this study it was not possible to determine if there was an increase in the quantity of these cells, however, they appeared in more of the renders acquired than in section 5.3.5. Further to this, also observed were F4/80⁺, PDGFR- β ⁺ cells that were not co-localised to a vasa recta capillary and also lacked the distinct morphology of a pericytes *e.g.* the “bump-on-a-log” characteristic shape (Peppiatt et al., 2006) (**Figure 5.15**), suggesting that these may be F4/80⁺, PDGFR- β ⁺ M Φ as opposed to pericytes. However, further experimentation would be needed to definitively say cells co-expressing these receptors were pericytes or M Φ .

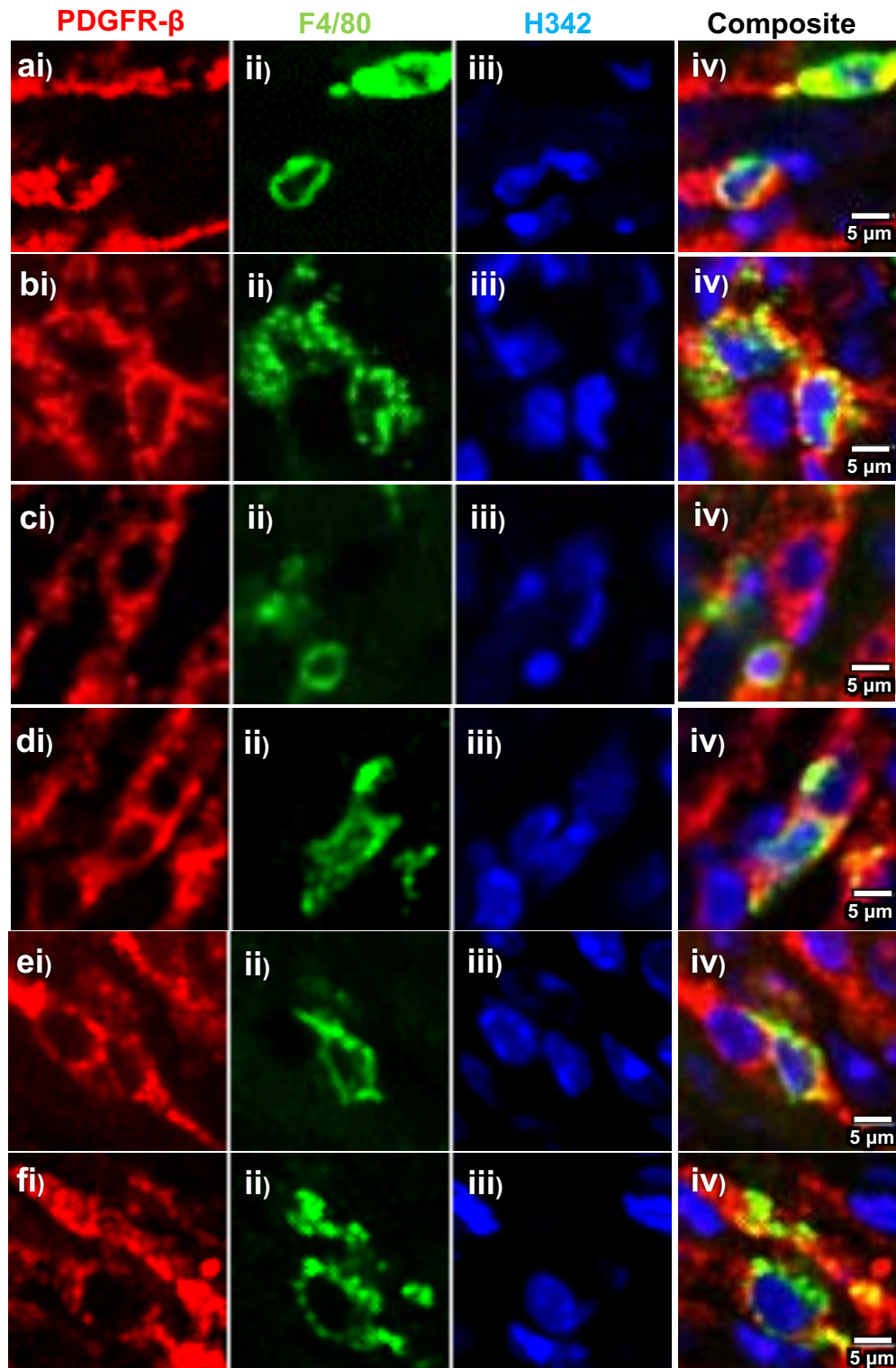


Figure 5.16 Co-expression of platelet derived growth factor receptor- β (PDGFR- β)⁺ with F4/80⁺ on vascular resident cells in the renal medulla bearing morphological similarities to PDGFR- β ⁺ pericytes.

Representative images from experiments where tissue was incubated with either; PSS (**a-b**), TNF- α (**c-d**), and IL-1 β (**e-f**), showing positive staining with anti-PDGFR- β (**i**; *red*), anti-F4/80 (**iii**; *green*), and Hoechst 33342 (H342; **iv**; *blue*) with the corresponding composite render (**iv**). Scale bars are 5 μ m.

5.4 Discussion

The aim of this study was to repeat those experiments conducted in the rat kidney slice model in chapter 3, using the novel murine live kidney slice model, developed in chapter 4, to bypass the issue of a small population of residential CD163⁺ MΦ observed in experiments in rats. It was found that murine PDGFR-β⁺ and NG2⁺ pericytes show different characteristics and responsiveness, much like was observed with rat tissue (**Chapter 3**). Further still, vessels covered by PDGFR-β⁺ and NG2⁺ pericytes with MΦ-pericyte cell-cell contact were significantly constricted at the pericyte site compared to vessels without such cell-cell contact, suggesting a conserved consequence of residential MΦ-pericyte interaction across species is vasa recta constriction.

Ultimately, the primary question of co-immunostaining aimed to address was “is there any overlap in cellular expression of MΦ-identifying and pericyte-identifying markers in renal perivascular cells?”. There were a small number of CD163⁺/PDGFR-β⁺ pericytes in rat tissue (**Chapter 3 Figure 3.9**) after stimulation with TNF-α and IL-1β. What was observed in the mouse is cells with both MΦ (**Figure 5.15**) and pericyte (**Figure 5.16**) morphology co-label with PDGFR-β and the F4/80 antigen consistently, regardless of cytokine stimulation. Those cells that are co-labelled with pericyte morphology are likely pericytes and suggests renal PDGFR-β⁺ pericytes are multifunctional, yet both NG2⁺ and PDGFR-β⁺ pericytes interact with residential MΦ.

5.4.1 5.4.1 Murine PDGFR-β⁺ pericyte covered vasa recta have larger diameters and are more numerous than those covered by NG2⁺ pericytes.

In both rat (**Chapter 3**) and murine kidney slices, the morphological difference, regional variation in pericyte densities, and the diameters of vasa recta on which of NG2⁺ and PDGFR-β⁺ pericytes reside are seemingly conserved across species. Please see **Chapter 3 section 3.4.1-3.4.1.1** for detailed discussion, as it applies to the murine kidney slices.

5.4.2 5.4.2 F4/80⁺ macrophages and pericytes may actively communicate to regulate vasa recta diameter.

Prior to investigating the multifunctional nature of renal pericytes, it was necessary to identify whether perivascular cells that are positive for pericyte identifying markers NG2 and PDGFR- β also positively labelled for F4/80. There is a reported overlap in all the pericyte and M Φ -identifying markers, including F4/80 (Prazeres et al., 2017), NG2 (Moransard et al., 2011), and PDGFR- β (Inaba et al., 1993; de Parseval et al., 1993), used in this study. Only M Φ are reportedly perivascular, so other immune cell populations are unlikely to overlap with pericytes and therefore not considered. Brightfield images and cell morphologies were used for categorising cells as pericytes and M Φ in tandem with immunolabelling. Co-labelling is discussed below in **section 5.4.7**. Limitations with how M Φ and pericyte densities were calculated and the subsequent generalisability have been discussed in **section 3.4.1**.

This study corroborates current knowledge for renal F4/80⁺ M Φ distribution in healthy tissue, these M Φ are interwoven throughout the interstitium and reside primarily in the OM, concentrated by the medullary rays (Hume, and Gordon, 1983; Berry et al., 2017; Kielar et al., 2005). The morphology of these interstitial F4/80⁺ M Φ is highly heterogenous and ramified comparative to the ovoid, regular morphology of the pericyte soma (**Figure 5.3-5.4**). It has been suggested that F4/80^{hi} M Φ in the kidney are involved with the maintenance and restoration of tissue homeostasis (George et al., 2017), and their proximity to the medullary rays suggests active communication with cells of the microvasculature. This is supported by observations here that, on average, of the total number F4/80⁺ M Φ present in OM ROI, over 50% have direct contact with NG2⁺-labelled pericytes. With NG2⁺ pericytes as the loci of measurement, this was significantly less at approximately 39% of pericytes in the renders having cellular contact with M Φ . When not in contact, cells were on average 30 μ m apart, well within the maximal spatial limits for effective paracrine signalling (**chapter 3 section 3.3.4**) (Francis, and Palsson, 1997; Bollenbach et al., 2008). Data published by another group has shown in the absence of PDGFR- β ⁺ pericytes, the immune response is not propagated in the kidney by tubular injury (Lemos et al., 2016), suggesting active communication between pericytes and immune cells is required to trigger immune responses. Please see **chapter 3 section 3.4.3** for detailed discussion on the implications of M Φ -pericyte contact to facilitate the immune response.

5.4.3 The differential acute activity of TNF- α and IL-1 β appears to be conserved between mice and rats, whilst reflecting species differences.

Much like in the rat, acute superfusion of murine kidney slices with TNF- α elicited a pericyte-mediated vasoconstriction, and IL-1 β failed to elicit any vasoactive response (rodent data provided by Kirsti Taylor). In the rat TNF- α induce a significantly greater vasoconstriction, approximately 30% larger than that measured in the mouse and further reflects a reduced magnitude of responsiveness of the C57BL/6J vasculature (Russell, and Watts, 2000). Whilst TNF- α has previously been shown to reduce renal blood flow and GFR in the murine kidney in an acute setting (Shahid et al., 2008), species differences in cytokine profiles may also influence the responses observed. In a cerebral ischaemia model in the SD rat there is a rapid, strong induction of TNF- α and IL-1 β mRNA comparative to the weaker, delayed but protracted response in C57BL/6J mice to the same injury model (Schroeter et al., 2003). It is possible that longer exposure time to lower concentrations of TNF- α would have greater efficacy as it would better mimic the murine inflammatory response.

IL-1 β activity reportedly peaks at 4-hours, whereas TNF- α has a reduced latency period (Proebstl et al., 2012) meaning the acute nature of the superfusion experiments could offer an alternate explanation as to why no constriction was observed with short-term exposure IL-1 β in the slice preparations. However, unlike TNF- α , IL-1 β has limited evidence for being directly vasoactive in the kidney and other tissues, instead seeming to augment the vasoactive response of other agonists. In hypertensive rats, endothelium denuded aortic rings incubated in IL-1 β had a potentiated contractile response to phenylephrine (Dorrance, 2007). In a similar fashion, IL- β reduced the potency of vasoconstriction in rat cremaster arteriole to noradrenaline whereas TNF- α alone induced a vasodilation (Baudry et al., 1996). Together this suggests observations in both models are reflective of the different responses observed between the species in response to various cytokines, whilst reflecting the differential short-term vasoactivity of TNF- α and IL-1 β .

5.4.3.1 In the mouse, TNF- α and IL-1 β differentially affect PDGFR- β^+ and NG2 $^+$ pericyte contractility, whilst not affecting the morphology of either.

Following 4-hour incubations in the murine model with both cytokines, a significant pericyte-mediated constriction of vasa recta capillaries was elicited in comparison to

the time-matched PSS control in which no pericyte-mediated change in vasa recta diameter was measured, as described in **section 3.4.6**. Interestingly, as observed in the rat, whether murine vasa recta constricted depended on the surface protein expression of the pericyte. Vasa recta covered with NG2⁺ pericytes were significantly constricted, specifically at pericyte sites yet PDGFR-β⁺ pericytes show minimal cytokine-induced contractility in both the mouse and rat kidney slices.

Interestingly, unlike in the rat TNF-α and IL-1β stimulation did not affect murine NG2⁺ or PDGFR-β⁺ pericyte soma size. The rodent cytokine stimulated renal NG2⁺ pericytes were approximately 20% smaller in soma height, as discussed in **section 3.4.6**. It is that process length was not measured here and is a limitation of this study (**section 3.3.5**). *In vitro* pericytes do not have the dynamic morphology of pericytes *in situ*, and the morphological change reported by Proebstl *et al* (Proebstl et al., 2012) in murine pericytes may not have involve a change in soma size. Conversely here in the murine kidney slices there may have been a reduction in total NG2⁺ glycoprotein coverage over the vessel as the total area covered by pericytes reduces as they constrict (Kolyada et al., 2003), which would correlate with a total morphological change. As there is no universal consensus on measuring pericyte size, comparison is difficult. Yet, observations here reflect further interspecies functional differences in PDGFR-β⁺ and NG2⁺ pericytes, whilst illustrating a conserved behaviour with the differential activity of cytokines on NG2⁺ and PDGFR-β⁺ pericytes and their associated vessels. This is discussed in more detail in **chapter 3 section 3.4.6**

5.4.4 Dormant monocytes when activated migrate towards NG2⁺ pericytes in the outer medulla.

Unlike in **chapter 3** with the rat having few CD163⁺ MΦ present, F4/80⁺ MΦ in the mouse were abundant and as such the spatial relationship was readily quantifiable, though limited (**section 3.4.1**). F4/80⁺ MΦ remain motile in the slice preparation whilst NG2⁺ pericytes identified in this technique are vascular resident, so measurements were taken regarding F4/80⁺ MΦ and NG2⁺ pericytes separately to determine if there were differences between the cell types. However, as observed in the rat, a significant increase in the number of F4/80⁺ MΦ was observed in the time-matched PSS control, which needed accounting for when taking measurements from the incubation experiments. Other murine models show that residential MΦ proliferate independently from the recruitment of monocyte precursors (Jenkins et al., 2011), and tissue slices shown a marked upregulation of pro-inflammatory cytokines which would activate

residential monocytes (**section 3.4.4**), reflected in both the murine and rodent kidney slices with an increase in the number of M Φ within 4 hours.

Accounting for the approximately 25% increase of M Φ observed in the PSS 4-hour control, TNF- α and IL-1 β stimulate maturation of F4/80⁺ M Φ from a local monocyte precursor population, given there is no source of circulating leukocytes (Stribos et al., 2016). Interestingly, in the inner medulla (IM) for PDGFR- β and NG2 experiments, the average number of M Φ quantified after stimulation of TNF- α were starkly different. These discrepancies in the IM are likely from the NG2⁺ pericyte drop-off (Shaw et al., 2018) limiting the available ROI selection to the upper portion of the IM where M Φ cell numbers are likely higher from proximity to the outer medulla (OM). Conversely, PDGFR- β ⁺ stain is expressed throughout the entirety of the IM resulting in sections of the lower portions of the IM being randomly selected as the ROI and is subsequently a flaw in the methodology. This does suggest the regional differences persist past the OM/IM border and that there may be further regional differences in cell behaviour throughout the kidney.

In the OM, cytokine stimulation increased M Φ cell number and decreased pericyte density and correspondingly the total number of pericytes present in the field of view. Migration of residential F4/80⁺ M Φ specifically to the vascular bundles has been observed post IRI (Kielar et al., 2005), and shown in **Figure 5.11**, this likely reflects F4/80⁺ M Φ migrating to NG2⁺ pericytes. For the percentage of F4/80⁺ M Φ with cell-cell contact with NG2⁺ pericytes to remain constant at 4-hours of incubation across all treatment groups, the newly activated monocytes would need to be migrating towards the NG2⁺ pericytes to maintain the degree of contact as the total cell numbers change. This is corroborated by the significant increase in the percentage NG2⁺ pericytes with cell-cell contact with an F4/80⁺ M Φ , despite the significant reduction in pericyte density by both cytokines. It is interesting to note even in the absence of cytokine stimulation, the percentage of OM NG2⁺ pericytes with cell-cell contact to an F4/80⁺ M Φ in PSS at 4-hours increased by 36%, whilst M Φ cell number only increased by 25%. Together this suggests newly mature M Φ migrate towards OM NG2⁺ pericytes, indicating that immune activity may be co-ordinated here.

5.4.5 IL-1 β , but not TNF- α , significantly influences distances between NG2⁺ pericytes and F4/80⁺ macrophages.

Interestingly, IL-1 β , but not TNF- α , consistently reduced the distance between M Φ and NG2⁺ pericytes in both the OM and IM. In a matrigel plug model of sterile inflammation, it was observed post-hypoxia that whilst IL-1 α was responsible for the recruitment of neutrophils, IL-1 β was responsible for recruitment and retention of residential CD11b⁺, Ly6C^{dull}, F4/80^{hi} M Φ (Rider et al., 2011), suggesting that in the murine kidney slice model that IL-1 β retained M Φ in close proximity to the vasculature. IL-1 β triggers this recruitment of M Φ via the MyD88 pathway (Babcock et al., 2008) and it has recently been demonstrated that activation of PDGFR- β ⁺ pericyte MyD88 signalling amplifies inflammation (Leaf et al., 2016), suggesting IL-1 β -mediated M Φ recruitment could be coordinated via pericytes. Conversely, data suggests that TNF- α recruits circulating monocytes; in the CNS of MCMV-infected neonatal mice, TNF- α neutralising Ab significantly reduced infiltration of Ly6C⁺ CCR2⁺ monocytes (Seleme et al., 2017). These reported differences in the roles of TNF- α and IL-1 β may explain the differences observed here in the murine slice preparation, with IL-1 β encouraging retention of F4/80⁺ M Φ near NG2⁺ pericytes.

5.4.6 The pericyte-mediated constriction of vasa recta capillaries induced by macrophages may be orchestrated by NG2⁺ not NG2⁻ pericytes.

The cellular contact between pericytes and M Φ could have been an artefact from their respective high densities in the murine OM. However, much like in the rat, when murine renal pericytes had cell-cell contact with M Φ the vasa recta were significantly constricted at the pericyte site, comparative to vessels where pericytes had no M Φ contact, suggesting communication is occurring between M Φ and pericytes. This also demonstrates a cross-species physiological outcome from contact between these cell types. Interestingly, unlike in the initial exploratory experiments, after the 4-hour incubation period OM PDGFR- β ⁺ pericytes, but not NG2⁺ pericytes, in PSS that had cell-cell contact with an F4/80⁺ M Φ had significantly smaller cell bodies. This event did not occur with rodent PDGFR- β ⁺ pericytes in **chapter 3**. Conversely, rodent NG2⁺ pericytes with CD163⁺ M Φ contact in PSS were significantly smaller than those without contact, whereas murine NG2⁺ pericyte soma were not significantly different either way.

PDGFR- β^+ soma measurements when in contact with M Φ were not significantly different in size for those of NG2 $^+$ pericyte soma, whilst PDGFR- β^+ pericytes without M Φ contact were significantly larger than those in contact. Given the size discrepancy that was not noted in the initial exploratory experiments, these PDGFR- β^+ pericytes with M Φ contact are potentially PDGFR- β^+ /NG2 $^+$. In control PSS conditions at 4-hours over half of the NG2 $^+$ pericytes in the renders were in direct cellular contact with M Φ compared to just over 1/3rd in tissue immediately fixed at "0-hours", with over 60% of M Φ in contact with NG2 $^+$ cells. This increase in the number of NG2 $^+$ pericytes with M Φ contact could possibly explain why this difference was not observed in initial experimentation but it was after 4-hours; the odds of randomly selecting an NG2 $^+$ /PDGFR- β^+ pericyte were much greater because the degree of NG2 $^+$ -F4/80 $^+$ cell-cell contact was significantly increased (**Figure 5.11**). If true, this could further imply that F4/80 $^+$ M Φ preferentially migrate to the NG2 $^+$ /PDGFR- β^+ pericytes of the DVR upon activation. In the mesentery, the corresponding paired arteriole constricts upon PMN and platelet adhesion in the venule (Harris et al., 2005). Data here may suggest there are potentially differing reasons why arteriolar NG2 $^+$ and venular PDGFR- β^+ are encouraged to constrict with F4/80 $^+$ M Φ contact. Arteriolar constriction may be necessary to allow for the adhesion of PMN, which could then encourage dilation at the venular end of the capillary bed.

Alternatively, this constriction of venular NG2 $^-$ /PDGFR- β^+ pericyte populated capillaries could be a functional requirement allowing circulating polymorphonuclear leukocytes (PMN) to extravasate out of venular NG2 $^-$ capillaries. Circulating leukocytes move passively in the bloodstream, swept along by the laminar flow of blood. In postcapillary venules at sites of inflammation, local reduction in the flow of blood increases the chances that leukocytes will make contact with the endothelial cells lining the vessel (Muller, 2013). In tumour cells direct cellular contact with residential M Φ activates the RhoA/ROCK pathway (Roh-Johnson et al., 2014), whilst activated PMN encourage relaxation of the pericyte actin-myosin system when there is direct cell-cell contact between the cell types, communicating via inhibition of the RhoA/ROCK signalling pathway (Wang et al., 2012), leading to vasodilation. In this model there is no source of circulating PMN (Stribos et al., 2016), and lack of such cell-cell contact with PDGFR- β^+ pericytes could have resulted in these vessels remaining constricted. As mentioned in **chapter 3**, pericytes where Rho GTPases are activated are smaller in size (Kolyada et al., 2003) so these may be PDGFR- β^+ /NG2 $^-$ pericytes with this signalling pathway activated. Alluded to above in **section 5.4.1**, experiments for co-labelling tissue sections with anti-PDGFR- β and anti-NG2 were not performed at any point in this study and has shown to be a limitation due to the lack of clarity.

5.4.7 A small population of cells co-label with anti-PDGFR- β and anti-F4/80, with both pericyte and macrophage morphology

Interestingly in the kidney it has been previously reported that co-expression of PDGFR- β and M Φ markers does not occur, whilst having a close spatial relationship (Ferland-McCollough et al., 2016), as discussed in **Chapter 1 section 1.4.1.1**. However, these pericytes were co-labelled with more niche identifying markers and subsequently expression did not wholly co-localise with PDGFR- β , meaning the populations of cells identified here were likely excluded from analysis. Observed here was a very small population of perivascular cells positive for either NG2 or PDGFR- β fluorescent labelling also appeared to co-express the F4/80 antigen, with staining surrounding a Hoechst 33342⁺ cell nuclei showing the characteristic ovoid morphology of pericytes. This occurred more frequently with PDGFR- β ⁺ pericytes than NG2⁺ pericytes however, these populations were too small to accurately quantify. Pericytes may only acquire an inflammatory phenotype in a pathological setting, so tissue slices were exposed to pro-inflammatory cytokines TNF- α and IL-1 β to see if co-expression of F4/80 and NG2 or PDGFR- β increased in frequency of occurrence.

The importance of assessing co-labelling of pericyte and M Φ -identifying markers is described in section 5.4.2. Whilst data presented here showed limited evidence for co-expression of NG2 and F4/80, PDGFR- β ⁺ and F4/80 fluorescent staining was consistently found to regularly identify the same cell, as determined by the presence of a Hoechst 33342-identified cell nucleus, regardless of cytokine treatment. Unlike with NG2 experiments where no co-labelling was observed at 4 hours, the occurrences of apparent PDGFR- β and F4/80 double-labelled cells increased. Interestingly, and shown in Figure 5.15-16, the morphology of these cells varies between varied like M Φ , and the ovoid soma typical of pericytes. PDGFR- β is reportedly expressed on an array of haematopoietic cells, including both murine (Inaba et al., 1993) and human (de Parseval et al., 1993) M Φ , along with T-cells (Daynes et al., 1991) and NK cells (Gersuk et al., 1991), despite not co-localising with CD11_b in the mouse (Chen et al., 2011). The morphological differences observed between the “pericyte-like” and “M Φ -like” PDGFR- β ⁺/F4/80⁺ cells is suggestive that there may be differing populations that co-express these receptors, and further distinction is necessary.

In summary, the use of a murine live kidney slice model has provided compelling evidence to suggest that residential F4/80⁺ M Φ and both NG2⁺ and PDGFR- β ⁺ actively communicate, with a regional significance in the OM. This provides compelling

evidence to suggest: i) renal pericytes are multifunctional and actively communicate with residential immune cells; ii) this pericyte-M Φ communication is seemingly conserved cross-species, corroborating data available from the rodent slice preparation presented in **Chapter 3**; iii) a small population of perivascular cells co-express F4/80 and an interstitial population express PDGFR- β ; and iv) A receptor expression-dependent variation in multipotency; renal PDGFR- β^+ pericytes exhibit multifunctionality co-expressing F4/80, a receptor involved in antigen presentation to T-cells (Lin et al., 2005), whilst residential M Φ -pericyte communications are orchestrated by NG2 $^+$ pericytes acting as immune co-ordinators in the renal OM in both rats and mice.

6 GENERAL DISCUSSION

6.1 Pericytes as a multifunctional class of cell?

A reduction in pericyte density is negatively associated with vascular congestion in the renal medulla following ischaemia reperfusion injury (IRI) in SHR, promoting red blood cell congestion in the vasa recta and peritubular capillaries (Crislip et al., 2017). It is the loss of the pericytes (Kramann et al., 2017) which potentiates capillary rarefaction. Further *in situ* evidence from human histological data from CKD biopsies show loss of interstitial capillaries correlates with increased interstitial CD68⁺ MΦ accumulation, with patients with the most reduced capillary density had the most unfavourable outcomes (Eardley et al., 2008). Post ischaemia-reperfusion injury (IRI) CD68⁺ macrophage (MΦ) and CD8⁺ T-cells occlude the AVR after ischaemia get trapped, leading to congestion resulting in no-reflow in both rats and humans (Ysebaert et al., 2004). Together this is indicative that the renal medulla is where the inflammatory response is co-ordinated, with PDGFR-β⁺ pericytes of the vasa recta, not residential MΦ being the source of other pro-inflammatory IL-6 (Kielar et al., 2005; Leaf et al., 2016) being actively involved. The consequence of loss of pericytes and a reduction in capillary density is a disruption of medullary blood flow, renal function and damage to the kidney (Kennedy-Lydon et al., 2013; Peppiatt-Wildman, 2013).

The most extensively researched role of pericytes across tissues is vascular stabilisation and the regulation of blood flow (Lemos et al., 2016; Stapor et al., 2014; Betsholtz et al., 2005; Bergers, and Song, 2005; Díaz-Flores et al., 2009), with involvement in pathophysiology mechanisms; where they can contribute directly to fibrogenesis (Birbrair et al., 2014; Iwaisako et al., 2014; Murray et al., 2017; Rojas et al., 2012; Kramann et al., 2017), tumorigenesis (Huang et al., 2011; You et al., 2014; Lu, and Shenoy, 2017), and irreversibly constrict causing localised ischaemia leading to vessel rarefaction in disease states (Kramann et al., 2017; Hall et al., 2014). Given these extensive homeostatic and pathogenic roles, it is fitting there is plentiful evidence demonstrating pericytes are multifunctional (discussed in **chapter 1 section 1.2.2**). Inflammation is a key feature in the pathogenesis of renal disease, regardless of whether insult is primarily induced by the immune response (Weisheit et al., 2015) and inflammatory pericytes would be heavily implicated in disease (Humphreys et al., 2010; Navarro et al., 2016; Xavier et al., 2017; Sendeski et al., 2013; Crawford et al., 2012; Zhang et al., 2004; Turner, and Pallone, 1997; Silldorff et al., 1995; Yang et al., 1995; Pallone et al., 1998a; Crawford et al., 2011; Kennedy-Lydon et al., 2015; Colvin, 2019) with human, mouse, and rat renal pericytes showing all showing inflammatory

involvement (Leaf et al., 2016; Navarro et al., 2016; Xavier et al., 2017; Crislip et al., 2017), please see sections **1.3-4** for more detail on the current evidence .

However, there is inherent difficulty in determining an activity as being pericyte-mediated (**section 1.3.3.1**). The subsequent aim of this thesis was to assess the validity of the use of the live slice kidney models to further probe the multifunctional capabilities of renal pericytes (**Chapter 3 and 5**). This thesis has provided novel and compelling evidence to support the multifunctionality of renal pericytes.

6.2 Renal pericytes are contractile in a species-specific manner.

The aim with animal models is translatability and to generate knowledge around human physiology that is otherwise impractical or unethical to determine, and subsequently enable the extrapolation of data in the context of known species-specific differences in physiology (Cunningham, 2002; Boswell et al., 2014; Martignoni et al., 2006; Radermacher, and Haouzi, 2013). Pericytes cover the microcirculatory network in all vascularised tissues and possess the machinery to enact a vasoactive response in these vascular beds (Stefanska et al., 2015; Colvin, 2019; Shaw et al., 2018; Peppiatt-Wildman, 2013; Hamilton et al., 2010; Park et al., 1997a; Sendeski et al., 2013; Crawford et al., 2012; Zhang et al., 2004; Turner, and Pallone, 1997; Silldorff et al., 1995; Yang et al., 1995; Pallone et al., 1998a; Crawford et al., 2011; Kennedy-Lydon et al., 2015; Kerkar et al., 2006; Peppiatt et al., 2006; Almaça et al., 2018)

It has been observed that human (Colvin, 2019; Wei et al., 2015) and rodent (Park et al., 1997a) isolated OM DVR (IOMDVR) pericytes express contractile α -SMA and respond to renally synthesized vasoactive agents, including Angiotensin-II and Prostaglandin E₂ (Crawford et al., 2011; Crawford et al., 2012; Kennedy-Lydon et al., 2015; Dickhout et al., 2002; Cowley Jr, and O'connor, 2013; Silldorff et al., 1995; Yang et al., 1995; Pallone et al., 1998a; Turner, and Pallone, 1997; Zhang et al., 2004; Fan et al., 2019; Sendeski et al., 2013). Whilst data shows pericyte contractility is translatable, in identical tissue preparations from the liver (Zhao et al., 2009), mesentery (Hedemann et al., 2004), and abdominal aorta (Russell, and Watts, 2000) the vasoactive response of C57BL/6J mouse is markedly lower than that of the Sprague-Dawley rat, so there are likely species differences in the characteristics of pericyte-mediated vasoactivity. Consequently, establishing the "like-for-like" kidney slice model in the mouse demonstrated exactly this; C57BL/6J mouse vasoactivity is markedly less than that of the Sprague Dawley rat (Russell, and Watts, 2000; Cholewa

et al., 2005; Hedemann et al., 2004; Zhao et al., 2009), and as such the reduced responsiveness and magnitude of response of murine renal pericytes (**section 4.3**) demonstrated predictive validity of the murine model (Denayer et al., 2014), discussed in greater detail in **section 4.4**. Overall, findings in the mouse demonstrated that renal NG2⁺ pericyte morphology and regulation of DVR diameter by pericytes is conserved in mice, rats (Crawford et al., 2012; Zhang et al., 2004; Turner, and Pallone, 1997; Silldorff et al., 1995; Yang et al., 1995; Pallone et al., 1998a; Crawford et al., 2011; Kennedy-Lydon et al., 2015), and humans (Sendeski et al., 2013), and therefore use of the slice models to probe novel renal pericyte characteristics could translate to human tissue.

6.3 The kidney slice models can be used to further investigate the multifunctionality of renal pericytes.

In this study, kidney slice models (Crawford et al., 2012) were useful for investigating specifically residential cell populations (Stribos et al., 2016) whilst maintaining the internal architecture and cell-cell communication pathways reflective of *in vivo* renal behaviour. The use of 200 µm kidney slices also allowed visualisation of the differences in pericyte and MΦ morphology (**Figure 3.3, 5.3 and 5.4**), consideration of cell stereology, and the regional distribution in the kidney. Not only is pericyte morphology characteristic (Attwell et al., 2016) and possibly indicative of function (Kolyada et al., 2003), but MΦ morphology can also indicate functionality or ontogeny (Wang et al., 2013; Lee et al., 2013).

Trans-species conserved cellular distribution, morphological trends, and behaviours suggest conserved activity, leading to better translatability of data from animal models as well as the ability of acknowledging species-specific differences. Knowing such species-specific differences, whilst also elucidating similarities, is beneficial in making an informative model. For example, GABA-A receptor subtype expression varies on T-cells across humans, rats, and mice (Mendu et al., 2012), whilst GABA is immunomodulatory on T-cells across all species (Bjurström et al., 2009). The specific signalling pathways may not be identical, but an overall conserved behaviour across species is a better indication of a translatable finding.

It has been argued that tissue slices are limited in experiment throughput because of the number of capillaries per slice and lack of clarity over signalling pathways (Neuhaus et al., 2017), yet maintaining such involvement of other cells/ pathways

better reflects *in vivo* behaviour; no physiological response is from one single, isolated pathway. When OMDVR are isolated with the adjacent tubular segment pericyte contractility is attenuated (Cowley Jr, and O'connor, 2013). *In vivo*, agonists cause a preferential reduction in IMBF (Fan et al., 2019; Neuhofer, and Beck, 2005; Nakanishi et al., 1995), suggesting a preferential constriction of central DVR, as tubules would communicate with peripheral DVR and moderate their responsiveness, as suggested by the *ex vivo* data. Prior to investigating novel murine pericyte behaviours establishing the baseline characteristics was necessary for the murine kidney slices. The responsiveness of murine pericytes reflected the known species-specific differences in pericyte contractility and thus both slice models accurately model *in vivo* physiology.

Chapter 3 showed an interesting interactive relationship of NG2⁺ and PDGFR-β⁺ pericytes with CD163⁺ MΦ, as well as co-labelling with anti-PDGFR-β and anti-CD163 on cells with pericyte morphology. Yet low numbers of CD163⁺ MΦ, and lack of alternative residential MΦ markers in the rat necessitated the development of a more suitable model to further probe this relationship. Whilst CD163⁺ MΦ numbers are also low in the mouse kidney (Rubio-Navarro et al., 2016; Bi et al., 2018), this species enabled use of the F4/80 antigen, a pan-MΦ marker, that reflects the human cellular distribution of MΦ in the kidney. (Berry et al., 2017; Kielar et al., 2005; Hume, and Gordon, 1983; Colvin, 2019) Further still, F4/80⁺ cells communicate with pericytes (Shi, 2009; Neng et al., 2013) and anti-F4/80 reportedly co-labels pericytes (Yamazaki et al., 2017; Komuro et al., 2017; Rajantie et al., 2004). This was reflected in the murine data (**Chapter 5**) and showed usefulness of the slice models for visualising this behaviour in both species, but further work is needed to expand upon this interaction.

6.4 PDGFR-β⁺ and NG2⁺ pericytes represent different renal populations of pericytes, likely correlating to AVR and DVR coverage.

In other organs like the brain, PDGFR-β⁺ and NG2⁺ co-expression can range from 80-90% (Cuervo et al., 2017; O'Farrel et al., 2017; Hung et al., 2017), whereas in the kidney slices it appears approximately 1/3rd of PDGFR-β⁺ pericytes co-express NG2, in line with published findings of these respective pericyte densities in the kidney (LeBleu et al., 2013; Holliger et al., 1983). It was proposed in **section 3.4.1** that this difference correlates with the respective ratio of AVR:DVR (Holliger et al., 1983) and reflect differences in AVR and DVR pericyte and capillary morphology. The larger size of PDGFR-β⁺ pericytes in both rats and mice may reflect lack of RhoA GTPase-

dependent contractility (Kolyada et al., 2003; Kutcher et al., 2007) which is regulated by NG2 (Binamé et al., 2013; Binamé, 2014). This is supported by lack of contractility of PDGFR- β^+ pericytes to TNF- α and IL-1 β in both rats and mice. The venular pericytes of other tissues reportedly express α -SMA, yet the unique vascular architecture of the vasa recta may mean AVR pericytes do not need to be contractile. Loss of water from the DVR, and the high interstitial osmolality, and a slower perfusion rate of the DVR (Zimmerhackl et al., 1985) results in blood becoming viscous as it descends into the IM, which may itself prevent backflow.

The inter-species discrepancies in PDGFR- β^+ pericyte contractility may have highlighted a preference of NG2 $^+$ pericytes in communicating with residential M Φ . Interestingly, whilst most behaviours were conserved in a species-specific manner, PDGFR- β^+ pericytes showed differences between response between species to TNF- α and IL-1 β . With differing cytokine release profiles (Schroeter et al., 2003), there may be differing activity of TNF- α and IL-1 β between the species. However, all other findings correlated with published data. Instead, in the rat it was only PDGFR- β^+ pericytes with CD163 $^+$ M Φ contact that constricted to IL-1 β , being non-significantly different in size to NG2 $^+$ vessels and pericytes, unlike the other PDGFR- β measurements taken (**Table 3.4 and 3.5**). In the mouse, it was TNF- α that induced a PDGFR- β^+ pericyte-mediated vasoconstriction, with morphology suggesting these pericytes were NG2 $^+$ /PDGFR- β^+ (**Table 5.5**). At the 4-hour time point it was determined that the majority of newly activated F4/80 $^+$ M Φ migrated to NG2 $^+$ pericyte sites. In the comparative PDGFR- β experiments, the PDGFR- β^+ pericytes with F4/80 $^+$ M Φ contact in the PSS group were the same size as NG2 $^+$ pericytes unlike the PDGFR- β^+ pericytes without F4/80 $^+$ M Φ contact. Together this suggests that the contradictory measurements for PDGFR- β in the rat and mouse may reflect PDGFR- β^+ /NG2 $^+$ pericyte behaviour and that residential M Φ -pericyte communications are preferentially co-ordinated in the OM by DVR NG2 $^+$, not AVR NG2 $^-$ pericytes. However, this does need to be confirmed by tri-labelling with α -SMA, PDGFR- β and NG2 and is a future experiment to be conducted.

6.5 Renal pericytes and macrophages seemingly communicate.

Mentioned above in **section 6.3**, preliminary findings in the rat were that CD163 $^+$ M Φ and both NG2 $^+$ and PDGFR- β^+ pericytes were possibly communicating as the net effect of cell-cell contact was that those vasa recta were constricted. This was further reflected by murine data showing pericytes with F4/80 $^+$ M Φ contact were also

constricted. Further still, as mentioned above (**section 6.4**), the increased cell-cell contact observed between NG2⁺ pericytes and MΦ suggests immune co-ordination may be preferentially orchestrated by NG2⁺ pericytes. Pericytes of the kidney recruit inflammatory MΦ (**section 1.4.1**). In line with the data observed here for F4/80⁺ MΦ, it is possible PDGFR-β⁺/NG2⁺ are the population of “recruiter” pericytes in the kidney. This fits with recent work showing arteriolar NG2⁺ pericytes recruit circulating leukocytes (Stark et al., 2012; Proebstl et al., 2012) and instruct their transmigration towards the inflammatory foci post extravasation (Alon, and Nourshargh, 2013). It is possible that the residential MΦ-pericyte communication observed here is an initial step in co-ordinating the recruitment of these immune cells at the DVR, and therefore by NG2⁺ pericytes, and future work needed is to establish both this subpopulation of pericyte and thus the means to identify communication pathways between MΦ and pericytes.

6.6 Macrophages and NG2⁺ pericytes may communicate via RhoA/ROCK signalling.

A limitation of this study is not objectively determining that the pericytes with MΦ contact were not apoptotic (Díaz-Flores et al., 2009; Arroyo, and Iruela-Arispe, 2010), irreversibly-constricted pericytes causing a localised ischaemia being removed by residential MΦ (Neuhaus et al., 2017; Hall et al., 2014). However, the literature strongly suggests that cell-cell interaction is a common key mechanism by which immune cells communicate. Immune cells across tissues are able to communicate via cell-cell contact with their pseudopodium (Kobori et al., 2018; Arrevillaga-Boni et al., 2014) and tunnelling nanotubes (TNT) (Rodriguez et al., 2016; Onfelt et al., 2004; Watkins, and Salter, 2005) enabling the exchange of membrane lipids and particles. Pericytes are also able to communicate via their cytoplasmic process (Armulik et al., 2011), and their lack of inclusion here is another limitation, though it does not discredit the influence of cell-cell contact. In the human kidney MΦ-pericyte contact has a physiological outcome (Dixon et al., 2014), and other renal cell lines show cell-cell communications facilitated by TNT (Rustom et al., 2004). In the brain porcine α-SMA⁻ pericytes-neutrophils perform cell-cell interactions via pericyte-expressed ICAM-1 and TNT projections (Pieper, and Galla, 2014). Further still, the NG2 proteoglycan itself directs cells via direct cellular contact (Binamé et al., 2013; Binamé, 2014; Stark et al., 2012); this data supports the MΦ-pericyte contact seen here being communicative. MΦ cell-cell contact with pericytes induces RhoA GTPase signalling (Roh-Johnson et

al., 2014), with the RhoA/ROCK pathway necessary for PMN infiltration (Rao et al., 2017) and pericyte contractility (Kutcher et al., 2007; Kolyada et al., 2003) and highlights a potential signalling pathway activated by this contact.

The AVR is the site of immune cell extravasation in the kidney (Ysebaert et al., 2004) with vascular bundles showing marked upregulation of adhesion molecules ICAM-1, P-selectin, and MCP-1 within an hour post-IRI (Naruse et al., 2002; Kelly et al., 1994; De Greef et al., 2003). Upregulation of these molecules requires RhoA/ROCK signalling (Rao et al., 2017; Cernuda-Morollón, and Ridley, 2006). The upregulation of these, with a subsequent constriction of DVR NG2⁺ pericytes by MΦ-induced activation of RhoA GTPase could reduce AVR perfusion and enhance leukocyte extravasation after shear-dependent capture by these adhesion molecules (Kolaczowska, and Kubes, 2013; Abtin et al., 2014). Understanding this mechanism could highlight targets against the immune infiltrate and loss of vasa recta pericytes implicated in the progression of renal disease, but further commentary is beyond the scope of this study.

6.7 PDGFR-β co-labels with CD163 and F4/80.

Throughout renal organogenesis most kidney macrophages are perivascular (Munro et al., 2019) and whilst the developmental origin of these co-labelled cells could not be determined here, data has shown developmentally and in adult tissues that subsets of pericytes derive from MΦ (Yamazaki et al., 2017; Dai et al., 2010; Komuro et al., 2017; Rajantie et al., 2004). It is possible that after co-ordinating development of the neovascular tubes (Munro et al., 2019), some of these PVM may differentiate into pericytes. In order for these MΦ-derived pericytes to invest into the endothelial tube they require PDGFR-β expression (Hellström et al., 1999) and MΦ expressing PDGFR-β may represent a population that differentiate into pericytes to maintain vascular homeostasis (Dai et al., 2010). Blockade of PDGFR-β reportedly inhibits recruitment of MΦ, demonstrating the importance of PDGFR-β signalling in inflammation (Chen et al., 2011; Lin et al., 2011), yet it could reflect either PDGFR-β⁺ pericyte-mediated or PDGFR-β⁺ MΦ-mediated recruitment of circulating leukocytes. The F4/80 antigen is not just an identifying marker, it is a functional receptor and its primary role is in antigen presentation to T-cells (Lin et al., 2005); pericytes of the kidney have been shown in humans and mice to be involved in regulation of T-cells (Liu et al., 2018) and could potentially explain pericyte-mediated expression of F4/80.

The overarching question of this thesis was “do renal pericytes show multifunctionality?”, and more specifically, the use of kidney slices in probing the role of renal pericytes in inflammation as demonstrated by other labs in the kidney described above. Interestingly, what was observed in both species was that PDGFR- β^+ cells co-labelled with CD163 and F4/80. Whilst the occurrences of co-labelling were much too scarce to draw conclusions from in the rat with CD163, in the mouse both control and cytokine stimulated tissue demonstrated that anti-F4/80 and anti-PDGFR- β co-labelled the same Hoechst 33342⁺-identified cell nuclei. Further still, cells identified as co-labelled were seemingly different populations; some had morphology of pericytes (**Figure 5.16**), whilst others bore M Φ morphology (**Figure 5.15**). This indicates further work is needed to determine if PDGFR- β^+ pericytes or PDGFR- β^+ M Φ are responsible for the immunogenicity previously reported for renal PDGFR- β^+ pericytes (Xavier et al., 2017; Tanaka et al., 2017). Use of immunohistochemical techniques (IHC) in this study; the brightfield images, as well as the depth of the renders, was what enabled identification of the notable pericyte “bump-on-a-log” morphology (Peppiatt et al., 2006) and subsequent distinction to be made between cells co-labelled with F4/80 and PDGFR- β . This study has explicitly shown that pericyte morphology can enable distinguishing between M Φ and pericytes and will hopefully inform future work to include an IHC component when characterising pericyte multifunctionality.

6.8 Expression of NG2 by macrophage-derived pericytes may occur at a later stage of investment into the endothelial wall.

Described in detail in **Section 1.3.2** is the M Φ origin of subsets of NG2⁺ pericytes and suggests a shared lineage of F4/80⁺ M Φ and a subpopulation of NG2⁺ M Φ -derived pericytes. These M Φ -derived pericytes may not lose their immune-activities, and M Φ expressing PDGFR- β (**Figure 5.15**) may ultimately invest into the endothelium, differentiating into pericytes. As it was PDGFR- β , not NG2, that showed co-labelling reliably with F4/80, this possibly suggests if these F4/80⁺ pericytes were to become NG2⁺ that expression of NG2 by these M Φ derived pericytes may occur later into maturation, outside the 4-hour scope of this study. F4/80⁺ M Φ *in vitro* (Moransard et al., 2011) and in the murine skin (Yamazaki et al., 2017) stimulated by TGF- β are encouraged to express NG2. As inflammation increases the permeability of the vasculature (Arroyo, and Iruela-Arispe, 2010), and can encourage pericytes away from the capillary (Tanaka, and Nangaku, 2013), as TGF- β induces resolution of

inflammation (Gordon, and Martinez, 2010) it may also encourage F4/80⁺ differentiation and investment into the capillary wall, replacing lost pericytes. It was noted that some perivascular F4/80⁺ MΦ had pericyte morphology (**Figure 5.14**), yet at that point in time did not co-express NG2. F4/80 and NG2 expression is dynamic, and as raised in **section 3.4.5**, just because a cell does not in the moment express a molecule does not mean it is unable to or did not previously. Longer experimental timeframes, more time-points in data acquisition or stimulation of murine kidney slices with an anti-inflammatory cytokine like TGF-β may have shown co-labelling of F4/80 and NG2 may have shown alternative findings.

6.9 Future work.

Translatability of animal data to human physiology is a current concern among research communities (Denayer et al., 2014; Rhrissorrakrai et al., 2015), yet discussed and presented in this thesis is the use of trying to ascertain conserved behaviour for translatability. Overall, data here demonstrates the behaviour characterised for renal pericytes in the kidney slice models is reproducible reflecting species differences (discussed extensively in **section 4.4**), whilst showing a conserved role for pericytes regulating MBF. This novel consequence of interaction between residential MΦ and pericytes here is also seemingly conserved across species (**section 6.5**), suggesting that this interaction is orchestrated in the OM by NG2⁺, not NG2⁻. Also in this thesis is that PDGFR-β co-labels with MΦ markers as opposed to NG2, with use of the murine model provided better assessment of such overlap in pericyte and MΦ markers given the very small number of CD163⁺ MΦ in the rat. Expression and distribution of F4/80⁺ MΦ in the mouse is reflective of human CD163 MΦ distribution; the high MΦ density in the OM, and their location primarily apposite the vascular bundles (Colvin, 2019; Hume, and Gordon, 1983)(**Figure 1.10 and 5.5**) as well as a conserved site for co-ordination of the immune response in rats and humans (Ysebaert et al., 2004); the occurrence conserved behaviours across species aids in translatability to humans (Steven et al., 2017).

This thesis provided extensive evidence for direct interaction between pericytes and MΦ, across species, having a physiological outcome. This is a translatable example, as noted in humans is a functional interaction between Mannose Receptor⁺ MΦ and PDGFR-β⁺ pericytes (Dixon et al., 2014). However, the data in **chapter 3 and 5** build upon this interaction to show that these pericytes are constricted upon interaction with

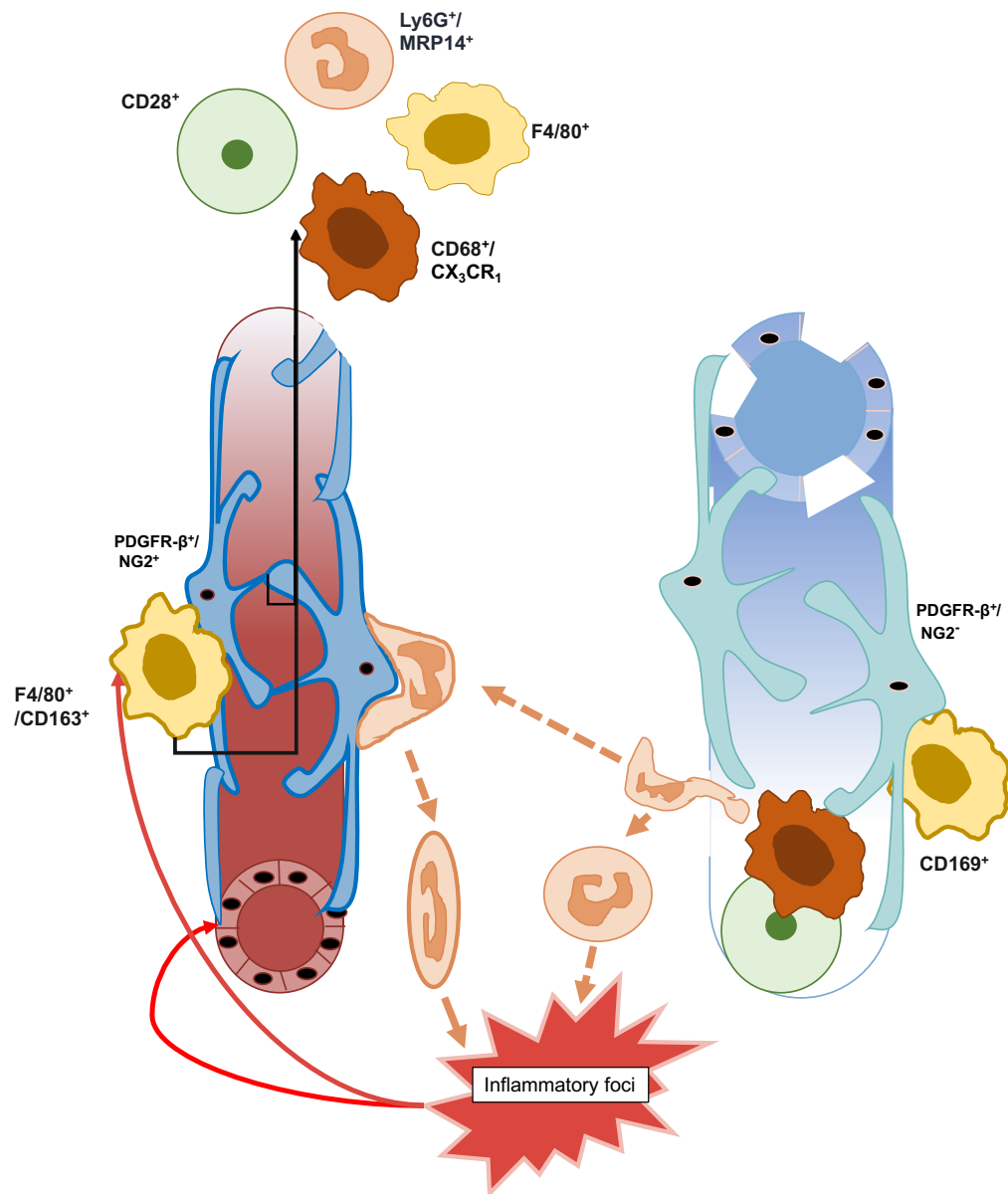


Figure 6.1 Proposed co-ordination of the immune response at the vasa recta capillaries by NG2⁺ and NG2⁻ pericytes.

The inflammatory foci stimulates both residential macrophage (MΦ; *yellow*) and NG2⁺/PDGFR-β⁺ pericytes (*blue*) on the DVR to communicate (dark yellow arrow) secreting pro-inflammatory mediators IL-1β, TNF-α, IL-6, MIF, IL-33 and CCL2 (black arrows) to recruit immune cells including more MΦ, infiltrating MΦ (*orange*), T-cells (*green*) and polymorphonuclear leukocytes (*peach*). Subsequent cell-cell interaction between NG2⁺ pericytes and F4/80⁺ or CD163⁺ MΦ activates RhoA/ROCK signalling resulting in vasoconstriction, and a smaller soma comparative to NG2⁻ pericytes. The recruited immune cells travel along the vasa recta and up a H₂O₂ concentration gradient generated by NG2⁻/PDGFR-β⁺ pericytes (*turquoise*) on the AVR. PMN and other circulating leukocytes migrate out of the AVR via the fenestra in the endothelium (white spaces). The vasoconstriction of DVR NG2⁺ pericytes reduces flow rate to enable adherence, rolling and subsequent extravasation of recruited immune cells. Some immune cells amble to the inflammatory foci (peach dashed arrows), whereas a small population will be instructed by the NG2⁺ pericytes on the DVR expressing ICAM-1, MIF, MAC-1, and LFA-1 (thick border), sensitising them and directing them directly to the inflammation (solid peach arrow) in an NG2-dependent manner. MΦ also express ICAM-1 (thick border) and are necessary for both recruitment (DVR; F4/80⁺ /CD163⁺) and enabling extravasation (AVR; CD169⁺). Gradients indicate a chemotactic gradient on the DVR (red), and expression of matrix proteins α-SMA and Collagen IV as well as H₂O₂ concentration gradient in the AVR (*blue*).

these pericytes and providing insight into this human data and highlights a potential target of future study and a novel cellular mechanism for renal pathology. The vascular reactivity in **chapter 4** builds upon cross-species findings aiding in translatability as the murine and rodent models show a conserved contractility of DVR pericyte that reflects differences in known species gene expression and sensitivity to vasoconstrictors (**section 4.4.3**). For example, the difference in response to Ang-II can be explained by the relative receptor densities. The SD rodent kidney has approximately double the contractile AT₁-R density of the C57BL/6J mouse (Cassis et al., 2004). This difference in magnitude that is species-specific could potentially relate to the capillary size difference (**section 4.3.3**); mice would need to be resistant to hypertensive agents to protect against marked blood pressure increases, which implies human tissue may be more sensitive given the size differences. Investigating and understanding species-specific differences in physiology better aids the translatability of animal data to human disease (**section 1.5**), and data here supports the use of tandem models in answering biological questions. For future study into renal pericyte multifunctionality, for translatability both rodent and murine slice models will be utilised.

This thesis has provided evidence to support the distribution of NG2⁺/NG2⁻ pericytes in the kidney reflection arteriolar and venular locale, but future work identified by this study is a better characterisation NG2⁺ and NG2⁻ pericytes in the kidney, to ascertain for certain the size differences between PDGFR-β⁺ and NG2⁺ correlate with the suggested NG2⁻ population, as well as determining if the ratio of NG2: PDGFR-β does indeed reflect the respective DVR:AVR ratio. Use of UT-B and plasmalemmal vesicle protein 1 (PV-1) which have been used in mouse, rat, and human tissue (Kim, and Pannabecker, 2010; Yuan, and Pannabecker, 2010; Pannabecker, and Dantzler, 2006; Wei et al., 2015) to differentially label DVR and AVR respectively, in tandem with NG2 and PDGFR-β in rat and mouse kidney slices could better determine the vascular location of renal pericyte subpopulations.

Following on from this characterisation of NG2⁺ and NG2⁻ pericytes, another necessary experiment is to perform IHC experiments anti-α-SMA antibodies to determine if indeed the NG2⁻ pericytes do not express this marker. Identifying the NG2⁺/α-SMA⁺ pericytes as the population of pericytes responsible for the MΦ-pericyte contractility observed will allow from their isolation from renal tissue using FACS and therefore their use *in vitro* to investigate the involvement of the RhoA/ROCK signalling pathway. What currently remains unclear is the cellular events leading the instigation of inflammation, though early on both pericytes and MΦ are involved (**section 1.4**). Upregulation of the adhesion molecules necessary for immune cell infiltration requires this pathway (Rao et al., 2017; Cernuda-Morollón, and Ridley, 2006). The irreversible constriction

possibly elicited by MΦ-instigated pericyte RhoA activation could cause acute localised ischaemia, and sustained activation of this pathway could trigger apoptosis (Rao et al., 2017), or their differentiation into myofibroblasts (Shi et al., 2020). This could be the instigator of the notable loss of pericytes, marked immune cell infiltrate, and capillary rarefaction notable in CKD (Eardley et al., 2008; Kramann et al., 2017) and offers a tantalising target to prevent inflammatory damage associated with the progression of kidney disease. It was also help expand upon the co-ordination mechanism proposed in **Figure 6.1**.

Further to this, after ascertaining the arteriolar location of NG2⁺ pericytes by showing they are also α-SMA, the next step is to more accurately determine that the residential MΦ-pericyte interaction is in fact specifically co-ordinated at NG2⁺, not NG2⁻ pericytes tri-staining with F4/80, NG2 and PDGFR-β is necessary, and potential subsequent staining of human tissue sections with PDGFR-β and CD163 for direct comparison. The specific identification of NG2⁺ pericytes as the subpopulation of pericytes responsible for propagation of the immune response would help in elucidating the inflammatory pathway, and may further reflect the known migratory sites of immune cells in rats and humans (Ysebaert et al., 2004), suggesting translatability of the slice models. Of benefit would also be to objectively quantify the co-labelling observed for PDGFR-β, as more work is needed to determine if the PDGFR-β⁺ cells identified in other labs as immunoactive (Xavier et al., 2017; Tanaka et al., 2017) are indeed pericytes and not PDGFR-β⁺ MΦ, especially as co-labelled cells bore both pericyte and MΦ morphology. It has been discussed elsewhere (**section 3.3.5**) but the exclusion of pericyte processes for PDGFR-β⁺ and NG2⁺ is a limitation of this study. Identifying a means of which to quantify pericyte processes accurately and thus their involvement in this MΦ-pericyte interaction could also help answer mechanistic questions behind this interaction.

Establishment of the wild-type (WT) C57BL/6J model also opens up another venue; the use of transgenic (TG) mice. With the background characteristics well established in this thesis (**chapter 4 and 5**), using either NG2 or F4/80 TG mice could be used to investigate the multipotent, not multifunctional nature. Another interesting question raised by this study is, do renal pericytes upregulate NG2 post damage, and why might this occur? In NG2^{null} mice, loss of NG2 reduces repair capabilities of microglia and the proliferative capabilities of pericytes and other NG2-expressing cells including microglia/macrophage (Kucharova et al., 2011). Observed here in both species is that the number of NG2⁺ pericytes per 100 μm² increased by 4-hours. Whilst the NG2⁺ pericytes with F4/80⁺ MΦ contact with may be apoptotic and pre-constricted prior to MΦ presence, CD163⁺ MΦ with cell-cell contact to NG2⁺ pericytes in the rat also

induced a vasoconstriction. CD163⁺ MΦ communicate via their pseudopodia (Kobori et al., 2018) and require direct cell-cell interaction with endothelia to direct vascularization (Kobori et al., 2018). The observed increase in NG2⁺ expression by pericytes, and the conserved contractility observed with both CD163⁺ and F4/80⁺ MΦ-contact suggests that these cells are not apoptotic (Kucharova et al., 2011) and instead that they are potentially proliferatory (Kobori et al., 2018; Hesp et al., 2017) or even angiogenic (Guo et al., 2018; Puranik et al., 2018). Using the superfusion equipment with fluorescence enabled, the real-time activities of the cells in TG mice could be recorded in to measure how their protein expression may change, cellular interaction over time, and potentially their differentiation into other cell types.

Overall, this thesis presents data to support kidney slices accurately modelling *in vivo* vascular physiology and renal pericytes exhibiting multifunctionality, notably in a cell-surface molecule-specific manner that is conserved across species. Whilst more work is necessary to expand upon the above suggestions, this thesis provides a strong supporting argument to the multifunctional, inflammatory nature of renal pericytes. The kidney slice models provide an excellent platform for future experiments in the field. By ascertaining what occurs and the malfunction in the inflammatory renal repair cycle, it could lead to identification of therapeutic targets and interventions to protect patients from the deleterious outcomes that arise from the dysregulation of MBF and the multifunctional activities of renal pericytes.

In conclusion, the data presented in this thesis supports a conserved contractile phenotype of DVR pericytes, that varies in a manner that reflects known species differences. This conserved nature of contractility is also suggestive that the novel observations of communication between renal residential MΦ and NG2⁺ pericytes may also be conserved, in a species-specific manner *i.e.*, human NG2⁺ pericytes may also be constricted when in direct cellular contact with a CD163⁺ MΦ, as was observed in both rats and mice for the respective MΦ markers used in those species. This discussion suggests, with supporting evidence, that this cellular interaction reflects communication between residential MΦ and pericytes in the propagation of the innate immune response (**Figure 6.1**), that is co-ordinated at the level of the medullary vasa recta. The use of live kidney slice models is beneficial in understanding this inflammatory pathway and will hopefully lead to better therapeutic targets to prevent the capillary rarefaction, marked inflammation, and dysregulation of MBF and renal function characteristic of the progression of renal disease.

References

- AbdAlla S, Lothar H, Abdel-tawab AM, Quitterer U: The angiotensin II AT2 receptor is an AT1 receptor antagonist. *J Biol Chem* 2001;276:39721–6.
- AbdAlla S, Lothar H, Quitterer U: AT1-receptor heterodimers show enhanced G-protein activation and altered receptor sequestration. *Nature* 2000;407:94–98.
- Abtin A, Jain R, Mitchell AJ, Roediger B, Brzoska AJ, Tikoo S, et al.: Perivascular macrophages mediate neutrophil recruitment during bacterial skin infection. *Nat Immunol* 2014;15:45–53.
- Adams LD, Geary RL, McManus B, Schwartz SM: A comparison of aorta and vena cava medial message expression by cDNA array analysis identifies a set of 68 consistently differentially expressed genes, all in aortic media. *Circ Res* 2000;87:623–31.
- Adriouch S, Dox C, Welge V, Seman M, Koch-Nolte F, Haag F: Cutting edge: a natural P451L mutation in the cytoplasmic domain impairs the function of the mouse P2X7 receptor. *J Immunol* 2002;169:4108–4112.
- Alarcon-Martinez L, Yilmaz-Ozcan S, Yemisci M, Schallek J, Kılıç K, Can A, et al.: Capillary pericytes express α -smooth muscle actin, which requires prevention of filamentous-actin depolymerization for detection. *Elife* 2018;7:e34861.
- Almaça J, Weitz J, Rodriguez-Diaz R, Pereira E, Caicedo A: The Pericyte of the Pancreatic Islet Regulates Capillary Diameter and Local Blood Flow. *Cell Metab* 2018;27:630-644.e4.
- Alon R, Nourshargh S: Learning in motion: Pericytes instruct migrating innate leukocytes. *Nat Immunol* 2013;14:14–15.
- Am S, Péault P, Jj M: Renal pericytes: Multifunctional cells of the kidneys. *Pflugers Arch Eur J Physiol* 2013;465:767–773.
- Aplin AC, Nicosia RF: Hypoxia paradoxically inhibits the angiogenic response of isolated vessel explants while inducing overexpression of vascular endothelial growth factor. *Angiogenesis* 2016;19:133–46.
- Armulik A, Abramson A, Betsholtz C: Endothelial/Pericyte Interactions. *Circ Res* 2005;97:512–523.
- Armulik A, Genové G, Betsholtz C: Pericytes: Developmental, Physiological, and Pathological Perspectives, Problems, and Promises. *Dev Cell* 2011;21:193–215.
- Arrebillaga-Boni G, Hernández-Ruiz M, Castillo EC, Ortiz-Navarrete V: Intercellular communication through contacts between continuous pseudopodial extensions in a macrophage-like cell line. *Cell Commun Adhes* 2014;21:213–220.

- Arroyo AG, Iruela-Arispe ML: Extracellular matrix, inflammation, and the angiogenic response. *Cardiovasc Res* 2010;86:226–235.
- Astashkina A, Mann B, Grainger DW: Pharmacology & Therapeutics A critical evaluation of in vitro cell culture models for high-throughput drug screening and toxicity. *Pharmacol Ther* 2012;134:82–106.
- Attwell D, Mishra A, Hall CN, O'Farrell FM, Dalkara T: What is a pericyte? *J Cereb Blood Flow Metab* 2016;36:451–455.
- Babcock AA, Toft-Hansen H, Owens T: Signaling through MyD88 regulates leukocyte recruitment after brain injury. *J Immunol* 2008;181:6481–90.
- Bach PH, Vickers AEM, Fisher R, Baumann A, Brittebo E, Carlile DJ, et al.: The use of tissue slices for pharmacotoxicology studies. *Atla* 1996;24:893–923.
- Bądzyńska B, Sadowski J: Moderate Intrarenal Vasoconstriction after High Pressor Doses of Norepinephrine in the Rat: Comparison with Effects of Angiotensin II. *Kidney Blood Press Res* 2011;34:307–310.
- Balabanov R, Washington R, Wagnerova J, Dore-Duffy P: CNS microvascular pericytes express macrophage-like function, cell surface integrin alpha M, and macrophage marker ED-2. *Microvasc Res* 1996;52:127–142.
- Barron L, Gharib SA, Duffield JS: Lung Pericytes and Resident Fibroblasts: Busy Multitaskers. *Am J Pathol* 2016;186:2519–2531.
- Bascands JL, Pecher C, Bompard G, Rakotoarivony J, Tack JL, Girolami JP: Bradykinin-induced in vitro contraction of rat mesangial cells via a B2 receptor type. *Am J Physiol* 1994;267:F871-8.
- Basile D, Anderson M, Sutton T: Pathophysiology of Acute Kidney Injury. *Compr Physiol* 2012;2:1303–1353.
- Baudry N, Rasetti C, Vicaut E: Differences between cytokine effects in the microcirculation of the rat. *Am J Physiol* 1996;271:H1186-92.
- Becker GJ, Hewitson TD: Animal models of chronic kidney disease: useful but not perfect. *Nephrol Dial Transplant* 2013;28:2432–2438.
- Behrsing HP, Furniss MJ, Davis M, Tomaszewski JE, Parchment RE: In vitro exposure of precision-cut lung slices to 2-(4-amino-3-methylphenyl)-5-fluorobenzothiazole lysylamide dihydrochloride (NSC 710305, Phortress) increases inflammatory cytokine content and tissue damage. *Toxicol Sci* 2013;131:470–479.
- Bell PD, Lapointe J-Y, Sabirov R, Hayashi S, Peti-Peterdi J, Manabe K-I, et al.: Macula densa

cell signaling involves ATP release through a maxi anion channel. *Proc Natl Acad Sci U S A* 2003;100:4322–7.

Benetos A, Levy BI, Lacolley P, Taillard F, Duriez M, Safar ME: Role of Angiotensin II and Bradykinin on Aortic Collagen Following Converting Enzyme Inhibition in Spontaneously Hypertensive Rats. *Arterioscler Thromb Vasc Biol* 1997;17:3196–3201.

Beranek JT: CD68 is not a macrophage-specific antigen. *Ann Rheum Dis* 2005;64:342 LP – 344.

Berger M, Bergers G, Arnold B, Hämmerling GJ, Ganss R: Regulator of G-protein signaling-5 induction in pericytes coincides with active vessel remodeling during neovascularization. *Blood* 2005;105:1094–1101.

Bergers G, Song S: The role of pericytes in blood-vessel formation and maintenance. *Neuro Oncol* 2005;7:452–464.

Bernier NJ, Perry SF: Cardiovascular effects of angiotensin-II-mediated adrenaline release in rainbow trout *Oncorhynchus mykiss*. *J Exp Biol* 1999;202:55–66.

Berry MR, Mathews RJ, Ferdinand JR, Jing C, Loudon KW, Wlodek E, et al.: Renal Sodium Gradient Orchestrates a Dynamic Antibacterial Defense Zone. *Cell* 2017;170:860-874.e19.

Bertram JF: Counting in the kidney. *Kidney Int* 2001;59:792–796.

Betsholtz C, Lindblom P, Gerhardt H: Role of pericytes in vascular morphogenesis. *Vascular* 2005;20:115–125.

Bi J, Watanabe H, Fujimura R, Nishida K, Nakamura R, Oshiro S, et al.: A downstream molecule of 1,25-dihydroxyvitamin D₃, alpha-1-acid glycoprotein, protects against mouse model of renal fibrosis. *Sci Rep* 2018;8:1–9.

Billet S, Bardin S, Verp S, Baudrie V, Michaud A, Conchon S, et al.: Gain-of-function mutant of angiotensin II receptor, type 1A, causes hypertension and cardiovascular fibrosis in mice. *J Clin Invest* 2007;117:1914–1925.

Binamé F: Transduction of Extracellular Cues into Cell Polarity: the Role of the Transmembrane Proteoglycan NG2. *Mol Neurobiol* 2014;50:482–493.

Binamé F, Sakry D, Dimou L, Jolivel V, Trotter J: NG2 regulates directional migration of oligodendrocyte precursor cells via Rho GTPases and polarity complex proteins. *J Neurosci* 2013;33:10858–10874.

Birbrair A, Zhang T, Files DC, Mannava S, Smith T, Wang Z-MM, et al.: Type-1 pericytes accumulate after tissue injury and produce collagen in an organ-dependent manner. *Stem*

Cell Res Ther 2014;5:1–18.

Birbrair A, Zhang T, Wang Z, Messi M, Mintz A, Delbono O: Pericytes at the intersection between tissue regeneration and pathology. *Clin Sci* 2015;128:81–93.

Bjurström H, Wang JY, Ericsson I, Bengtsson M, Liu Y, Kumar-Mendu S, et al.: Erratum to “GABA, a natural immunomodulator of T lymphocytes” [*J. Neuroimmunol.* 205 (2008) 44–50] (DOI:10.1016/j.jneuroim.2008.08.017). *J Neuroimmunol* 2009;214:133.

Bollenbach T, Pantazis P, Kicheva A, Bökel C, González-Gaitán M, Jülicher F: Precision of the Dpp gradient. *Development* 2008;135:1137–46.

Borysova L, Wray S, Eisner DA, Burdyga T: How calcium signals in myocytes and pericytes are integrated across in situ microvascular networks and control microvascular tone. *Cell Calcium* 2013;54:163–174.

Boswell CA, Mundo EE, Ulufatu S, Bumbaca D, Cahaya HS, Majidy N, et al.: Comparative physiology of mice and rats: radiometric measurement of vascular parameters in rodent tissues. *Mol Pharm* 2014;11:1591–8.

Brähler S, Yu H, Suleiman H, Krishnan GM, Saunders BT, Kopp JB, et al.: Intravital and Kidney Slice Imaging of Podocyte Membrane Dynamics. *J Am Soc Nephrol* 2016;27:3285–3290.

Brezis M: HYPOXIA OF THE RENAL MEDULLA — ITS IMPLICATIONS FOR DISEASE M. *N Engl J Med* 2005;332:647–655.

Brezis M, Heyman SN, Dinour D, Epstein FH, Rosen S: Role of nitric oxide in renal medullary oxygenation. Studies in isolated and intact rat kidneys. *J Clin Invest* 1991;88:390–5.

Buechler C, Ritter M, Orsó E, Langmann T, Klucken J, Schmitz G: Regulation of scavenger receptor CD163 expression in human monocytes and macrophages by pro- and antiinflammatory stimuli. *J Leukoc Biol* 2000;67:97–103.

Burdyga T, Borysova L: Calcium signalling in pericytes. *J Vasc Res* 2014;51:190–199.

Burnstock G, Novak I: Purinergic signalling in the pancreas in health and disease. *J Endocrinol* 2012;213:123–141.

Cai C, Fordsmann JC, Jensen SH, Gesslein B, Lønstrup M, Hald BO, et al.: Stimulation-induced increases in cerebral blood flow and local capillary vasoconstriction depend on conducted vascular responses. *Proc Natl Acad Sci* 2018;115:E5796–E5804.

Campagnolo P, Cesselli D, Al Haj Zen A, Beltrami AP, Kränkel N, Katare R, et al.: Human adult vena saphena contains perivascular progenitor cells endowed with clonogenic and proangiogenic potential. *Circulation* 2010;121:1735–45.

- Campagnolo P, Katare R, Madeddu P: Realities and misconceptions on the pericytes role in tissue repair. *Regen Med* 2018;13:119–122.
- Campanholle G, Ligresti G, Gharib SA, Duffield JS: Cellular Mechanisms of Tissue Fibrosis. 3. Novel mechanisms of kidney fibrosis. *Am J Physiol Physiol* 2013;304:C591–C603.
- Cao Q, Wang Y, Wang XM, Lu J, Lee VWS, Ye Q, et al.: Renal F4/80+CD11c+ Mononuclear Phagocytes Display Phenotypic and Functional Characteristics of Macrophages in Health and in Adriamycin Nephropathy. *J Am Soc Nephrol* 2015;26:349–363.
- Carneiro FS, Carneiro ZN, Giachini FRC, Lima V V, Nogueira E, Rainey WE, et al.: Murine and rat cavernosal responses to endothelin-1 and urotensin-II Vasoactive Peptide Symposium. *J Am Soc Hypertens* 2008;2:439–447.
- Cassis LA, Huang J, Gong MC, Daugherty A: Role of metabolism and receptor responsiveness in the attenuated responses to Angiotensin II in mice compared to rats. *Regul Pept* 2004;117:107–116.
- Castellano G, Franzin R, Stasi A, Divella C, Sallustio F, Pontrelli P, et al.: Complement activation during ischemia/reperfusion injury induces pericyte-to-myofibroblast transdifferentiation regulating peritubular capillary Lumen Reduction Through pERK Signaling. *Front Immunol* 2018;9:1–17.
- Ceradini DJ, Gurtner GC: Homing to hypoxia: HIF-1 as a mediator of progenitor cell recruitment to injured tissue. *Trends Cardiovasc Med* 2005;15:57–63.
- Cernuda-Morollón E, Ridley AJ: Rho GTPases and leukocyte adhesion receptor expression and function in endothelial cells. *Circ Res* 2006;98:757–767.
- Chavez-Galan L, Olleros ML, Vesin D, Garcia I: Much More than M1 and M2 Macrophages, There are also CD169+ and TCR+ Macrophages. *Front Immunol* 2015;6:1–15.
- Chen Y, Lui VCH, Rooijen N V, Tam PKH: Depletion of intestinal resident macrophages prevents ischaemia reperfusion injury in gut. *Gut* 2004;53:1772–1780.
- Chen YT, Chang FC, Wu CF, Chou YH, Hsu HL, Chiang WC, et al.: Platelet-derived growth factor receptor signaling activates pericyte-myofibroblast transition in obstructive and post-ischemic kidney fibrosis. *Kidney Int* 2011;80:1170–1181.
- Cho H, Kozasa T, Bondjers C, Betsholtz C, Kehrl JH: Pericyte-specific expression of Rgs5: implications for PDGF and EDG receptor signaling during vascular maturation. *FASEB J* 2003;17:440–2.
- Cholewa BC, Meister CJ, Mattson DL: Importance of the renin-angiotensin system in the regulation of arterial blood pressure in conscious mice and rats. *Acta Physiol Scand* 2005;183:309–320.

- Chou SY, Porush JG, Faubert PF: Renal medullary circulation: hormonal control. *Kidney Int* 1990;37:1–13.
- Clements ME, Chaber CJ, Ledbetter SR, Zuk A: Increased Cellular Senescence and Vascular Rarefaction Exacerbate the Progression of Kidney Fibrosis in Aged Mice Following Transient Ischemic Injury. *PLoS One* 2013;8:e70464.
- Colvin RB: Introduction to Renal Pathology; in Lindburg M, Chang A (eds): *Diagnostic Pathology: Kidney Diseases*, ed 3. Quebec, Elsevier, 2019, p 35.
- Courtoy PJ, Boyles J: Fibronectin in the microvasculature: localization in the pericyte-endothelial interstitium. *J Ultrastructure Res* 1983;83:258–273.
- Cowley AW: Renal Medullary Oxidative Stress, Pressure-Natriuresis, and Hypertension. *Hypertension* 2008;52:777–786.
- Cowley AW, Mattson DL, Lu S, Roman RJ: The Renal Medulla and Hypertension. *Hypertension* 1995;25:663–673.
- Cowley Jr AWC, O'connor PM: MEDULLARY THICK ASCENDING LIMB BUFFER VASOCONSTRICTION OF RENAL OUTER-MEDULLARY VASA RECTA IN SALT-RESISTANT BUT NOT SALT-SENSITIVE RATS. *Hypertension* 2013;60:965–972.
- Craggs LJJ, Fenwick R, Oakley AE, Ihara M, Kalaria RN: Immunolocalization of platelet-derived growth factor receptor- β (PDGFR- β) and pericytes in cerebral autosomal dominant arteriopathy with subcortical infarcts and leukoencephalopathy (CADASIL). *Neuropathol Appl Neurobiol* 2015;41:557–570.
- Crawford C, Kennedy-Lydon T, Sprott C, Desai T, Sawbridge L, Munday J, et al.: An intact kidney slice model to investigate vasa recta properties and function in situ. *Nephron - Physiol* 2012;120.
- Crawford C, Kennedy-Lydon TM, Callaghan H, Sprott C, Simmons RL, Sawbridge L, et al.: Extracellular nucleotides affect pericyte-mediated regulation of rat in situ vasa recta diameter. *Acta Physiol (Oxf)* 2011;202:241–51.
- Crawford C, Wildman SSP, Kelly MC, Kennedy-Lydon TM, Peppiatt-Wildman CM: Sympathetic nerve-derived ATP regulates renal medullary vasa recta diameter via pericyte cells: a role for regulating medullary blood flow? *Front Physiol* 2013;4:1–8.
- Crisan M, Chen C-W, Corselli M, Andriolo G, Lazzari L, Péault B: Perivascular Multipotent Progenitor Cells in Human Organs. *Ann N Y Acad Sci* 2009;1176:118–123.
- Crisan M, Corselli M, Chen WCW, Péault B: Perivascular cells for regenerative medicine. *J Cell Mol Med* 2012;16:2851–2860.

- Crisan M, Yap S, Casteilla L, Chen C-W, Corselli M, Park TS, et al.: A Perivascular Origin for Mesenchymal Stem Cells in Multiple Human Organs. *Cell Stem Cell* 2008;3:301–313.
- Crislip GR, O'Connor PM, Wei Q, Sullivan JC, O'Connor PM, Wei Q, et al.: Vasa Recta Pericyte Density is Negatively Associated with Vascular Congestion in the Renal Medulla Following Ischemia Reperfusion in Rats. *Am J Physiol - Ren Physiol* 2017;313:ajprenal.00261.2017.
- Cuervo H, Pereira B, Nadeem T, Lin M, Lee F, Kitajewski J, et al.: PDGFR β -P2A-CreERT2 mice: a genetic tool to target pericytes in angiogenesis. *Angiogenesis* 2017;20:655–662.
- Cunningham ML: A Mouse Is Not a Rat Is Not a Human: Species Differences Exist. *Toxicol Sci* 2002;70:157–158.
- Dabertrand F, Hannah RM, Pearson JM, Hill-Eubanks DC, Brayden JE, Nelson MT: Prostaglandin E₂, a postulated astrocyte-derived neurovascular coupling agent, constricts rather than dilates parenchymal arterioles. *J Cereb Blood Flow Metab* 2013;33:479–482.
- Dai M, Yang Y, Omelchenko I, Nuttall AL, Kachelmeier A, Xiu R, et al.: Bone marrow cell recruitment mediated by inducible nitric oxide synthase/stromal cell-derived factor-1 α signaling repairs the acoustically damaged cochlear blood-labyrinth barrier. *Am J Pathol* 2010;177:3089–3099.
- Damoiseaux JG, Döpp EA, Calame W, Chao D, MacPherson GG, Dijkstra CD: Rat macrophage lysosomal membrane antigen recognized by monoclonal antibody ED1. *Immunology* 1994;83:140–7.
- Dantzler WH, Pannabecker TL, Layton AT, Layton HE: Urine concentrating mechanism in the inner medulla of the mammalian kidney: role of three-dimensional architecture. *Acta Physiol (Oxf)* 2011;202:361–78.
- Darrieutort-Laffite C, Boutet M-A, Chatelais M, Brion R, Blanchard F, Heymann D, et al.: IL-1 β and TNF α Promote Monocyte Viability through the Induction of GM-CSF Expression by Rheumatoid Arthritis Synovial Fibroblasts. *Mediators Inflamm* 2014;2014:1–10.
- Davenport A: The brain and the kidney - Organ cross talk and interactions. *Blood Purif* 2008;26:526–536.
- Davidson A: Mouse kidney development. *StemBook* 2009;
- Davies LC, Jenkins SJ, Allen JE, Taylor PR: Tissue-resident macrophages. *Nat Immunol* 2013;14:986–995.
- Daynes RA, Dowell T, Araneo BA: Platelet-derived growth factor is a potent biologic response modifier of T cells. *J Exp Med* 1991;174:1323–33.

- Denayer T, Stöhrn T, Van Roy M: Animal models in translational medicine: Validation and prediction. *New Horizons Transl Med* 2014;
- Díaz-Flores L, Gutiérrez R, Madrid JF, Varela H, Valladares F, Acosta E, et al.: Pericytes. Morphofunction, interactions and pathology in a quiescent and activated mesenchymal cell niche. *Histol Histopathol* 2009;24:909–969.
- Dickhout JG, Mori T, Cowley AW: Tubulovascular nitric oxide crosstalk: Buffering of angiotensin II-induced medullary vasoconstriction. *Circ Res* 2002;91:487–493.
- Dixon KO, Rossmann L, Kamerling SW a, van Kooten C: Human renal fibroblasts generate dendritic cells with a unique regulatory profile. *Immunol Cell Biol* 2014;92:688–98.
- Donnelly-Roberts DL, Namovic MT, Han P, Jarvis MF: Mammalian P2X7 receptor pharmacology: Comparison of recombinant mouse, rat and human P2X7 receptors. *Br J Pharmacol* 2009;157:1203–1214.
- Dore-Duffy P, Cleary K: Morphology and Properties of Pericytes; in : *Methods in molecular biology* (Clifton, N.J.). 2011, pp 49–68.
- Dore-duffy P, Esen N: The Microvascular Pericyte: Approaches to Isolation, Characterization, and Cultivation; in Birbrair A (ed): *Pericyte Biology - Novel Concepts*. Springer, Cham, 2018, pp 53–65.
- Dorrance AM: Interleukin 1-beta (IL-1beta) enhances contractile responses in endothelium-denuded aorta from hypertensive, but not normotensive, rats. *Vascul Pharmacol* 2007;47:160–5.
- Downs SM: Mouse versus rat: Profound differences in meiotic regulation at the level of the isolated oocyte. *Mol Reprod Dev* 2011;78:778–794.
- Duan L, Zhang X-D, Miao W-Y, Sun Y-J, Xiong G, Wu Q, et al.: PDGFR β Cells Rapidly Relay Inflammatory Signal from the Circulatory System to Neurons via Chemokine CCL2. *Neuron* 2018;100:183-200.e8.
- Duffield JS, Tipping PG, Kipari T, Cailhier JF, Clay S, Lang R, et al.: Conditional ablation of macrophages halts progression of crescentic glomerulonephritis. *Am J Pathol* 2005;167:1207–1219.
- Dulauroy S, Di Carlo SE, Langa F, Eberl G, Peduto L: Lineage tracing and genetic ablation of ADAM12(+) perivascular cells identify a major source of profibrotic cells during acute tissue injury. *Nat Med* 2012;18:1262–70.
- Durham JT, Surks HK, Dulmovits BM, Herman IM: Pericyte contractility controls endothelial cell cycle progression and sprouting: insights into angiogenic switch mechanics. *AJP Cell Physiol* 2014;307:C878–C892.

- Eardley KS, Kubal C, Zehnder D, Quinkler M, Lepenies J, Savage CO, et al.: The role of capillary density, macrophage infiltration and interstitial scarring in the pathogenesis of human chronic kidney disease. *Kidney Int* 2008;74:495–504.
- Elberg G, Guruswamy S, Logan CJ, Chen L, Turman MA: Plasticity of epithelial cells derived from human normal and ADPKD kidneys in primary cultures. *Cell Tissue Res* 2008;331:495–508.
- Ellenbroek B, Youn J: Rodent models in neuroscience research: is it a rat race? *Dis Model Mech* 2016;9:1079–1087.
- Endlich K, Hoffend J, Steinhausen M: Localization of endothelin ETA and ETB receptor-mediated constriction in the renal microcirculation of rats. *J Physiol* 1996;497 (Pt 1:211–8.
- Epstein FH: Oxygen and renal metabolism. *Kidney Int* 1997;51:381–5.
- Evans L, Cowley A: Renal Medullary Circulation. *Colloq Ser Integr Syst Physiol From Mol to Funct* 2015;7:1–104.
- Fabian SL, Penchev RR, St-Jacques B, Rao AN, Sipilä P, West KA, et al.: Hedgehog-Gli pathway activation during kidney fibrosis. *Am J Pathol* 2012;180:1441–53.
- Fabriek BO, Dijkstra CD, van den Berg TK: The macrophage scavenger receptor CD163. *Immunobiology* 2005a;210:153–160.
- Fabriek BO, Van Haastert ES, Galea I, Polfliet MMJ, Döpp ED, Van Den Heuvel MM, et al.: CD163-positive perivascular macrophages in the human CNS express molecules for antigen recognition and presentation. *Glia* 2005b;51:297–305.
- Fan L, Wang S, He X, Gonzalez-Fernandez E, Lechene C, Fan F, et al.: Visualization of the intrarenal distribution of capillary blood flow. *Physiol Rep* 2019;7:1–10.
- Farmer JB: the Biphasic Response of an Isolated Artery To Tyramine. *Br J Pharmacol* 1966;28:340–347.
- Fazan VPS, Ma X, Chapleau MW, Barreira AA: Qualitative and quantitative morphology of renal nerves in C57BL/6J mice. *Anat Rec* 2002;268:399–404.
- Felipe SA, Rodrigues ES, Martin RP, Paiva ACM, Pesquero JB, Shimuta SI: Functional expression of kinin B1 and B2 receptors in mouse abdominal aorta. *Brazilian J Med Biol Res* 2007;40:649–655.
- Fenoy FJ, Roman RJ: Effect of kinin receptor antagonists on renal hemodynamic and natriuretic responses to volume expansion. *Am J Physiol Integr Comp Physiol* 1992;263:R1136–R1140.

- Ferland-McCollough D, Slater S, Richard J, Reni C, Mangialardi G: Pericytes, an overlooked player in vascular pathobiology. *Pharmacol Ther* 2016;
- Floege J, Eitner F, Alpers CE: A New Look at Platelet-Derived Growth Factor in Renal Disease. *J Am Soc Nephrol* 2008;19:12–23.
- Francis K, Palsson BO: By the Relative Time Constants for Cyto⁻Chemokine Secretion. *Engineering* 1997;94:12258–12262.
- Fujimoto T, Singer SJ: Immunocytochemical studies of desmin and vimentin in pericapillary cells of chicken. *J Histochem Cytochem* 1987;35:1105–15.
- Fuxe J, Tabruyn S, Colton K, Zaid H, Adams A, Baluk P, et al.: Pericyte requirement for anti-leak action of angiopoietin-1 and vascular remodeling in sustained inflammation. *Am J Pathol* 2011;178:2897–2909.
- Gattone VH, Luft FC, Evan AP: Renal afferent and efferent arterioles of the rabbit. *Am J Physiol* 1984;247:F219-28.
- George JF, Lever JM, Agarwal A: Mononuclear phagocyte subpopulations in the mouse kidney. *Am J Physiol Renal Physiol* 2017;312:F640–F646.
- Gersuk GM, Westermarck B, Mohabeer AJ, Challita PM, Pattamakom S, Pattengale PK: Inhibition of human natural killer cell activity by platelet-derived growth factor (PDGF). III. Membrane binding studies and differential biological effect of recombinant PDGF isoforms. *Scand J Immunol* 1991;33:521–32.
- Gordon S, Martinez FO: Alternative activation of macrophages: Mechanism and functions. *Immunity* 2010;32:593–604.
- Gordon S, Plüddemann A: Tissue macrophages: heterogeneity and functions. *BMC Biol* 2017;15:53.
- Gordon S, Plüddemann A, Martinez Estrada F: Macrophage heterogeneity in tissues: Phenotypic diversity and functions. *Immunol Rev* 2014;262:36–55.
- Graeber MB, Banati RB, Streit WJ, Kreutzberg GW: Immunophenotypic characterization of rat brain macrophages in culture. *Neurosci Lett* 1989;103:241–246.
- Grant RI, Hartmann DA, Underly RG, Shih AY: Classification of brain pericytes based on cell structure, location, and α -smooth muscle actin content. *bioRxiv* 2017;114777.
- De Greef KE, Ysebaert DK, Persy V, Vercauteren SR, De Broe ME: ICAM-1 expression and leukocyte accumulation in inner stripe of outer medulla in early phase of ischemic compared to HgCl₂-induced ARF. *Kidney Int* 2003;63:1697–1707.

- Grgic I, Krautzberger AM, Hofmeister A, Lalli M, DiRocco DP, Fleig S V., et al.: Translational Profiles of Medullary Myofibroblasts during Kidney Fibrosis. *J Am Soc Nephrol* 2014;25:1979–1990.
- Grunz-Borgmann EL, Jones BW, Boerman EM: Macrophage Depletion Reverses Impaired Sympathetic Vasoconstriction and Sensory Vasodilation of Mesenteric Arteries from IL-10^{-/-} Mice with Inflammatory Bowel Disease; in : *Experimental Biology 2019 Meeting. The FASEB Journal*, 2019, p 523.8.
- Guimarães-Camboa N, Cattaneo P, Sun Y, Moore-Morris T, Gu Y, Dalton ND, et al.: Pericytes of Multiple Organs Do Not Behave as Mesenchymal Stem Cells In Vivo. *Cell Stem Cell* 2017;1–15.
- Guo L, Akahori H, Harari E, Smith SL, Polavarapu R, Karmali V, et al.: CD163⁺ macrophages promote angiogenesis and vascular permeability accompanied by inflammation in atherosclerosis. *J Clin Invest* 2018;128:1106–1124.
- Hall CN, Reynell C, Gesslein B, Hamilton NB, Mishra A, Sutherland BA, et al.: Capillary pericytes regulate cerebral blood flow in health and disease. *Nature* 2014;508:55–60.
- Hall JE: V. The body fluids and kidneys; in : *Guyton and Hall Textbook of Medical Physiology*, ed 12. Elsevier, 2010.
- Hamada A, Torre C, Drancourt M, Ghigo E: Trained Immunity Carried by Non-immune Cells. *Front Microbiol* 2019;9.
- Hamilton NB, Attwell D, Hall CN: Pericyte-mediated regulation of capillary diameter: a component of neurovascular coupling in health and disease. *Front Neuroenergetics* 2010;2.
- Harrell CR, Simovic Markovic B, Fellabaum C, Arsenijevic A, Djonov V, Volarevic V: Molecular mechanisms underlying therapeutic potential of pericytes. *J Biomed Sci* 2018;25:1–12.
- Harris NR, Whatley JR, Carter PR, Specian RD: Venular constriction of submucosal arterioles induced by dextran sodium sulfate. *Inflamm Bowel Dis* 2005;11:806–813.
- Hartmann DA, Underly RG, Grant RI, Watson AN, Lindner V, Shih AY: Pericyte structure and distribution in the cerebral cortex revealed by high-resolution imaging of transgenic mice. *Neurophotonics* 2015;2:041402.
- Hartner A, Cordasic N, Klanke B, Veelken R, Hilgers KF: Strain differences in the development of hypertension and glomerular lesions induced by deoxycorticosterone acetate salt in mice. *Nephrol Dial Transplant* 2003;18:1999–2004.
- He H, Mack JJ, Güç E, Warren CM, Squadrito ML, Kilarski WW, et al.: Perivascular Macrophages Limit Permeability. *Arterioscler Thromb Vasc Biol* 2016;36:2203–2212.

- Hedemann J, Fetscher C, Michel MC: Comparison of noradrenaline and lysosphingolipid-induced vasoconstriction in mouse and rat small mesenteric arteries. *Auton Autacoid Pharmacol* 2004;24:77–85.
- Hedley BD, Keeney M: Technical issues: flow cytometry and rare event analysis. *Int J Lab Hematol* 2013;35:344–350.
- Hellström M, Kalén M, Lindahl P, Abramsson A, Betsholtz C: Role of PDGF-B and PDGFR-beta in recruitment of vascular smooth muscle cells and pericytes during embryonic blood vessel formation in the mouse. *Development* 1999;126:3047–55.
- Henninger DD, Panés J, Eppihimer M, Russell J, Gerritsen M, Anderson DC, et al.: Cytokine-induced VCAM-1 and ICAM-1 expression in different organs of the mouse. *J Immunol* 1997;158:1825–32.
- Hermansson K, Ojteg G, Wolgast M: The cortical and medullary blood flow at different levels of renal nerve activity. *Acta Physiol Scand* 1984;120:161–9.
- Hesp Z, Yoseph R, Suzuki R, Wilson C, Nishiyama A, McTigue D: Proliferating NG2 cell-dependent angiogenesis and scar formation alter axon growth and functional recovery after spinal cord injury in mice. *J Neurosci* 2017;38:3953–16.
- Holliger C, Lemley K V, Schmitt SL, Thomas FC, Robertson CR, Jamison RL: Direct determination of vasa recta blood flow in the rat renal papilla. *Circ Res* 1983;53:401–413.
- Honda H, Kimura H, Rostami A: Demonstration and phenotypic characterization of resident macrophages in rat skeletal muscle. *Immunology* 1990;70:272–7.
- Horie N, Maag A-L, Hamilton SA, Shichinohe H, Bliss TM, Steinberg GK: Mouse model of focal cerebral ischemia using endothelin-1. *J Neurosci Methods* 2008;173:286–290.
- Hosszu KK, Santiago-Schwarz F, Peerschke EIB, Ghebrehiwet B: Evidence that a C1q/C1qR system regulates monocyte-derived dendritic cell differentiation at the interface of innate and acquired immunity. *Innate Immun* 2010;16:115–127.
- Huang F-J, You W, Bonaldo P, Seyfried TN, Pasquale EB, Stallcup WB: PERICYTE DEFICIENCIES LEAD TO ABERRANT TUMOR. *Dev Biol* 2011;344:1035–1046.
- Hume D, Gordon S: Mononuclear phagocyte system of the mouse defined by immunohistochemical localization of antigen F4/80. Identification of resident macrophages in renal medullary and cortical interstitium and the juxtaglomerular complex. *J Exp Med* 1983;157:1704–1709.
- Humphreys BD, Lin S-L, Kobayashi A, Hudson TE, Nowlin BT, Bonventre J V, et al.: Fate tracing reveals the pericyte and not epithelial origin of myofibroblasts in kidney fibrosis. *Am J Pathol* 2010;176:85–97.

- Hung CF, Mittelsteadt KL, Brauer R, McKinney BL, Hallstrand TS, Parks WC, et al.: Lung pericyte-like cells are functional interstitial immune sentinel cells. *Am J Physiol - Lung Cell Mol Physiol* 2017;312:L556–L567.
- Ikeda Y, Sun Z, Ru X, Vandenberghe LH, Humphreys BD: Efficient Gene Transfer to Kidney Mesenchymal Cells Using a Synthetic Adeno-Associated Viral Vector. *J Am Soc Nephrol* 2018;29:ASN.2018040426.
- Ikezumi Y, Suzuki T, Karasawa T, Hasegawa H, Yamada T, Imai N, et al.: Identification of alternatively activated macrophages in new-onset paediatric and adult immunoglobulin A nephropathy: Potential role in mesangial matrix expansion. *Histopathology* 2011;58:198–210.
- Inaba T, Shimano H, Gotoda T, Harada K, Shimada M, Ohsuga JI, et al.: Expression of platelet-derived growth factor β receptor on human monocyte-derived macrophages and effects of platelet-derived growth factor BB dimer on the cellular function. *J Biol Chem* 1993;268:24353–24360.
- Inscho EW, Imig JD, Cook AK, Pollock DM: ETA and ETB receptors differentially modulate afferent and efferent arteriolar responses to endothelin. *Br J Pharmacol* 2005;146:1019–26.
- Iwaisako K, Jiang C, Zhang M, Cong M, Moore-Morris TJ, Park TJ, et al.: Origin of myofibroblasts in the fibrotic liver in mice. *Proc Natl Acad Sci U S A* 2014;111:E3297-305.
- Jansson D, Rustenhoven J, Feng S, Hurley D, Oldfield RL, Bergin PS, et al.: A role for human brain pericytes in neuroinflammation. *J Neuroinflammation* 2014;11:104.
- Jansson D, Scotter EL, Rustenhoven J, Coppieters N, Smyth LCD, Oldfield RL, et al.: Interferon- γ blocks signalling through PDGFR β in human brain pericytes. *J Neuroinflammation* 2016;13:249.
- Jenkins SJ, Ruckerl D, Cook PC, Jones LH, Finkelman FD, van Rooijen N, et al.: Local Macrophage Proliferation, Rather than Recruitment from the Blood, Is a Signature of TH2 Inflammation. *Science (80-)* 2011;332:1284–1288.
- Just A: Mechanisms of renal blood flow autoregulation: Dynamics and contributions. *Am J Physiol - Regul Integr Comp Physiol* 2007;292.
- Kaissling B, Le Hir M: Characterization and distribution of interstitial cell types in the renal cortex of rats. *Kidney Int* 1994;45:709–720.
- Kakoki M, McGarrah RW, Kim H-S, Smithies O: Bradykinin B1 and B2 receptors both have protective roles in renal ischemia/reperfusion injury. *Proc Natl Acad Sci* 2007;104:7576–7581.

- Kang T-Y, Bocci F, Jolly MK, Levine H, Onuchic JN, Levchenko A: Pericytes enable effective angiogenesis in the presence of proinflammatory signals. *Proc Natl Acad Sci U S A* 2019;116:23551–23561.
- Karasawa K, Asano K, Moriyama S, Ushiki M, Monya M, Iida M, et al.: Vascular-Resident CD169-Positive Monocytes and Macrophages Control Neutrophil Accumulation in the Kidney with Ischemia-Reperfusion Injury. *J Am Soc Nephrol* 2015;26:896–906.
- Kawamura H, Sugiyama T, Wu DM, Kobayashi M, Yamanishi S, Katsumura K, et al.: ATP: a vasoactive signal in the pericyte-containing microvasculature of the rat retina. *J Physiol* 2003;551:787–799.
- Kelly KJ, Williams WW, Colvin RB, Bonventre J V.: Antibody to intercellular adhesion molecule 1 protects the kidney against ischemic injury. *Proc Natl Acad Sci U S A* 1994;91:812–816.
- Kennedy-Lydon T, Crawford C, Wildman SS, Peppiatt-Wildman CM: Nonsteroidal anti-inflammatory drugs alter vasa recta diameter via pericytes. *Am J Physiol - Ren Physiol* 2015;309:F648–F657.
- Kennedy-Lydon TM, Crawford C, Wildman SSP, Peppiatt-Wildman CM: Renal pericytes: Regulators of medullary blood flow. *Acta Physiol* 2013;207:212–225.
- Kerkar S, Williams M, Blocksom JM, Wilson RF, Tyburski JG, Steffes CP: TNF- α and IL-1 β Increase Pericyte/Endothelial Cell Co-Culture Permeability. *J Surg Res* 2006;132:40–45.
- Kielar ML, John R, Bennett M, Richardson JA, Shelton JM, Chen L, et al.: Maladaptive role of IL-6 in ischemic acute renal failure. *J Am Soc Nephrol* 2005;16:3315–25.
- Kim J, Chung M, Kim S, Jo DH, Kim JH, Jeon NL: Engineering of a biomimetic pericyte-covered 3D microvascular network. *PLoS One* 2015a;10:1–15.
- Kim J, Pannabecker TL: Two-compartment model of inner medullary vasculature supports dual modes of vasopressin-regulated inner medullary blood flow. *Am J Physiol Renal Physiol* 2010;299:F273–F279.
- Kim MG, Kim SC, Ko YS, Lee HY, Jo SK, Cho W: The role of M2 macrophages in the progression of chronic kidney disease following acute kidney injury. *PLoS One* 2015b;10:1–17.
- Kirkpatrick KA, Burnstock G: Release of endogenous ATP from the vasa deferentia of the rat and guinea pig by the indirect sympathomimetic tyramine. *J Auton Pharmacol* 1994;14:325–335.
- Kisseleva T, Brenner DA: Mechanisms of fibrogenesis. *Exp Biol Med* 2008;233:109–122.
- Ko EA, Song MY, Donthamsetty R, Makino A, Yuan JX-J: Tension measurement in isolated rat

and mouse pulmonary artery. *Drug Discov Today Dis Model* 2010;7:123–130.

Kobori T, Hamasaki S, Kitauro A, Yamazaki Y, Nishinaka T, Niwa A, et al.: Interleukin-18 amplifies macrophage polarization and morphological alteration, leading to excessive angiogenesis. *Front Immunol* 2018;9:334.

Kolaczowska E, Kubes P: Neutrophil recruitment and function in health and inflammation. *Nat Rev Immunol* 2013;13:159–75.

Kolyada AY, Riley KN, Herman IM: Rho GTPase signaling modulates cell shape and contractile phenotype in an isoactin-specific manner. *Am J Physiol Physiol* 2003;285:C1116–C1121.

Komuro I, Ikutani M, Azuma E, Sasahara M, Osawa T, Takatsu K, et al.: A subset of cerebrovascular pericytes originates from mature macrophages in the very early phase of vascular development in CNS. *Sci Rep* 2017;7:1–16.

Kovac A, Erickson MA, Banks WA: Brain microvascular pericytes are immunoactive in culture: cytokine, chemokine, nitric oxide, and LRP-1 expression in response to lipopolysaccharide. *J Neuroinflammation* 2011;8:139.

Kramann R, Schneider RK, DiRocco DP, Machado F, Fleig S, Bondzie PA, et al.: Perivascular Gli1+ progenitors are key contributors to injury-induced organ fibrosis. *Cell Stem Cell* 2015;16:51–66.

Kramann R, Wongboonsin J, Chang-Panesso M, Machado FG, Humphreys BD: Gli1⁺ Pericyte Loss Induces Capillary Rarefaction and Proximal Tubular Injury. *J Am Soc Nephrol* 2017;28:776–784.

Kriz W, Kaissling B: *Structural Organization of the Mammalian Kidney*, 2013.

Krueger M, Bechmann I: CNS pericytes: concepts, misconceptions, and a way out. *Glia* 2010;58:1–10.

Kucharova K, Chang Y, Boor A, Yong VW, Stallcup WB: Reduced inflammation accompanies diminished myelin damage and repair in the NG2 null mouse spinal cord. *J Neuroinflammation* 2011;8:1–13.

Kumar A, D'Souza SS, Moskvina O V., Toh H, Wang B, Zhang J, et al.: Specification and Diversification of Pericytes and Smooth Muscle Cells from Mesenchymal Angioblasts. *Cell Rep* 2017;19:1902–1916.

Kurts C, Panzer U, Anders H-J, Rees AJ: The immune system and kidney disease: basic concepts and clinical implications. *Nat Rev Immunol* 2013;13:738–53.

Kutcher ME, Kolyada AY, Surks HK, Herman IM: Pericyte Rho GTPase mediates both pericyte contractile phenotype and capillary endothelial growth state. *Am J Pathol* 2007;171:693–

701.

- Laitinen L: Griffonia simplicifolia lectins bind specifically to endothelial cells and some epithelial cells in mouse tissues. *Histochem J* 1987;19:225–34.
- Landsman L, Bar-On L, Zerneck A, Kim K-W, Krauthgamer R, Shagdarsuren E, et al.: CX3CR1 is required for monocyte homeostasis and atherogenesis by promoting cell survival. *Blood* 2009;113:963–972.
- Lapenna A, De Palma M, Lewis CE: Perivascular macrophages in health and disease. *Nat Rev Immunol* 2018;18:689–702.
- Leaf IA, Nakagawa S, Johnson BG, Cha JJ, Mittelsteadt K, Guckian KM, et al.: Pericyte MyD88 and IRAK4 control inflammatory and fibrotic responses to tissue injury. *J Clin Invest* 2016;127:1–14.
- LeBleu VS, Taduri G, O'Connell J, Teng Y, Cooke VG, Woda C, et al.: Origin and function of myofibroblasts in kidney fibrosis. *Nat Med* 2013;19:1047–1053.
- Lee CH, Espinosa I, Vrijaldenhoven S, Subramanian S, Montgomery KD, Zhu S, et al.: Prognostic significance of macrophage infiltration in leiomyosarcomas. *Clin Cancer Res* 2008;14:1423–1430.
- Lee DH, Riquier ADM, Yang LE, Leong PKK, Maunsbach AB, McDonough AA: Acute hypertension provokes acute trafficking of distal tubule Na-Cl cotransporter (NCC) to subapical cytoplasmic vesicles. *Am J Physiol Renal Physiol* 2009;296:F810-8.
- Lee H, Stachelek SJ, Tomczyk N, Finley MJ, Composto RJ, Eckmann DM: Correlating macrophage morphology and cytokine production resulting from biomaterial contact. *J Biomed Mater Res Part A* 2013;101A:203–212.
- Lee SH, Starkey PM, Gordon S: Quantitative analysis of total macrophage content in adult mouse tissues. *Immunochemical studies with monoclonal antibody F4/80. J Exp Med* 1985;161:475–89.
- Lemos DR, Marsh G, Huang A, Campanholle G, Aburatani T, Dang L, et al.: Maintenance of vascular integrity by pericytes is essential for normal kidney function. *Am J Physiol Physiol* 2016;311:F1230–F1242.
- Leonhardt KO, Landes RR: Oxygen Tension of the Urine and Renal Structures. *N Engl J Med* 1963;269:115–121.
- Li L, Wu Y, Deng M, Wu G, Ren L: P2X1 receptor-mediated pressor responses in the anesthetized mouse. *Acta Pharm Sin B* 2012;2:459–463.
- Li W, Hsiao H-M, Higashikubo R, Saunders BT, Bharat A, Goldstein DR, et al.: Heart-resident

- CCR2+ macrophages promote neutrophil extravasation through TLR9/MyD88/CXCL5 signaling. *JCI Insight* 2016;1:1–14.
- Lin H-H, Faunce DE, Stacey M, Terajewicz A, Nakamura T, Zhang-Hoover J, et al.: The macrophage F4/80 receptor is required for the induction of antigen-specific efferent regulatory T cells in peripheral tolerance. *J Exp Med* 2005;201:1615–25.
- Lin S-L, Kisseleva T, Brenner D a, Duffield JS: Pericytes and Perivascular Fibroblasts Are the Primary Source of Collagen-Producing Cells in Obstructive Fibrosis of the Kidney. *Am J Pathol* 2008;173:1617–1627.
- Lin SL, Chang FC, Schrimpf C, Chen YT, Wu CF, Wu VC, et al.: Targeting endothelium-pericyte cross talk by inhibiting VEGF receptor signaling attenuates kidney microvascular rarefaction and fibrosis. *Am J Pathol* 2011;178:911–923.
- Liu R, Merola J, Manes TD, Qin L, Tietjen GT, López-Giráldez F, et al.: Interferon- γ converts human microvascular pericytes into negative regulators of alloimmunity through induction of indoleamine 2,3-dioxygenase 1. *JCI Insight* 2018;3.
- Lu J, Shenoy AK: Epithelial-to-pericyte transition in cancer. *Cancers (Basel)* 2017;9:1–13.
- Ma JX, Wang DZ, Chao L, Chao J: Cloning, sequence analysis and expression of the gene encoding the mouse bradykinin B2 receptor. *Gene* 1994;149:283–8.
- Ma X, Abboud FM, Chapleau MW: A novel effect of angiotensin on renal sympathetic nerve activity in mice. *J Hypertens* 2001;19:609–18.
- Marsh DJ, Postnov DD, Sosnovtseva O V., Holstein-Rathlou NH: The nephron-arterial network and its interactions. *Am J Physiol - Ren Physiol* 2019;316:F769–F784.
- Martignoni M, Groothuis GMM, de Kanter R: Species differences between mouse, rat, dog, monkey and human CYP-mediated drug metabolism, inhibition and induction. *Expert Opin Drug Metab Toxicol* 2006;2:875–894.
- Martinez VG, Moestrup SK, Holmskov U, Mollenhauer J, Lozano F: The Conserved Scavenger Receptor Cysteine-Rich Superfamily in Therapy and Diagnosis. *Pharmacol Rev* 2011;63:967–1000.
- Martini FH (University of H at M, Nath JL (Lourdes C, Bartholomew EF: The Urinary System; in Berriman L (ed): *Fundamentals of Anatomy & Physiology*, ed 9th. Pearson Benjamin Cummings, 2012, pp 953–996.
- Masaki T, Chow F, Nikolic-Paterson DJ, Atkins RC, Tesch GH: Heterogeneity of antigen expression explains controversy over glomerular macrophage accumulation in mouse glomerulonephritis. *Nephrol Dial Transplant* 2003;18:178–181.

- Matsumoto J, Takata F, Machida T, Takahashi H, Soejima Y, Funakoshi M, et al.: Tumor necrosis factor- α -stimulated brain pericytes possess a unique cytokine and chemokine release profile and enhance microglial activation. *Neurosci Lett* 2014;578:133–138.
- Matsuyama S, Karim MR, Izawa T, Kuwamura M, Yamate J: Immunohistochemical analyses of the kinetics and distribution of macrophages in the developing rat kidney. *J Toxicol Pathol* 2018;31:207–212.
- Mattson DL: Importance of the renal medullary circulation in the control of sodium excretion and blood pressure. *Am J Physiol Regul Integr Comp Physiol* 2003;284:R13–R27.
- Mattson DL, Cowley Awj: Kinin actions on renal papillary blood flow and sodium excretion. *Hypertension* 1993;21:961–965.
- Mattson DL, James L, Berdan EA, Meister CJ: Immune Suppression Attenuates Hypertension and Renal Disease in the Dahl Salt-Sensitive Rat. *Hypertension* 2006;48:149–156.
- McCarron JG, Lee MD, Wilson C: The Endothelium Solves Problems That Endothelial Cells Do Not Know Exist. *Trends Pharmacol Sci* 2017;38:322–338.
- Mendu SK, Bhandage A, Jin Z, Birnir B: Different subtypes of GABA-A receptors are expressed in human, mouse and rat T lymphocytes. *PLoS One* 2012;7.
- Menzies RI, Unwin RJ, Bailey MA: Renal P2 receptors and hypertension. *Acta Physiol (Oxf)* 2015;213:232–241.
- Mestas J, Hughes CCW: Of Mice and Not Men: Differences between Mouse and Human Immunology. *J Immunol* 2004;172:2731–2738.
- Methner C, Mishra A, Golgotiu K, Li Y, Wei W, Yanez ND, et al.: Pericyte constriction underlies capillary derecruitment during hyperemia in the setting of arterial stenosis. *Am J Physiol - Hear Circ Physiol* 2019;317:H255–H263.
- Meurer M, Ebert K, Schweda F, Höcherl K: The renal vasodilatory effect of prostaglandins is ameliorated in isolated-perfused kidneys of endotoxemic mice. *Pflugers Arch* 2018;
- Minocha S, Valloton D, Brunet I, Eichmann A, Hornung J-P, Lebrand C: NG2 glia are required for vessel network formation during embryonic development. *Elife* 2015;4.
- Mitrou N, Cupples W: Renal Blood Flow Dynamics in Inbred Rat Strains Provides Insight into Autoregulation. *Curr Vasc Pharmacol* 2014;12:801–809.
- Mohaupt MG, Elzie JL, Ahn KY, Clapp WL, Wilcox CS, Kone BC: Differential expression and induction of mRNAs encoding two inducible nitric oxide synthases in rat kidney. *Kidney Int* 1994;46:653–65.

- Molema G, Aird WC: Vascular Heterogeneity in the Kidney. *Semin Nephrol* 2012;32:145–155.
- Montemurro T, Andriolo G, Montelatici E, Weissmann G, Crisan M, Colnaghi MR, et al.: Differentiation and migration properties of human foetal umbilical cord perivascular cells: potential for lung repair. *J Cell Mol Med* 2011;15:796–808.
- Moransard M, Dann A, Staszewski O, Fontana A, Prinz M, Suter T: NG2 expressed by macrophages and oligodendrocyte precursor cells is dispensable in experimental autoimmune encephalomyelitis. *Brain* 2011;134:1315–1330.
- Morita S, Hourai A, Miyata S: Changes in pericytic expression of NG2 and PDGFRB and vascular permeability in the sensory circumventricular organs of adult mouse by osmotic stimulation. *Cell Biochem Funct* 2014;32:51–61.
- Muhlethaler-Mottet A: Expression of MHC class II molecules in different cellular and functional compartments is controlled by differential usage of multiple promoters of the transactivator CIITA. *EMBO J* 1997;16:2851–2860.
- Muller WA: Getting Leucocytes to the sites of inflammation. *Vet Pathol* 2013;50:7–22.
- Munro DA, Wineberg Y, Tarnick J, Vink CS, Li Z, Pridans C, et al.: Macrophages restrict the nephrogenic field and promote endothelial connections during kidney development. *Elife* 2019;8:1–27.
- Munro DAD, Hughes J: The origins and functions of tissue-resident macrophages in kidney development. *Front Physiol* 2017;8.
- Murfee WL, Skalak TC, Peirce SM: Differential arterial/venous expression of NG2 proteoglycan in perivascular cells along microvessels: identifying a venule-specific phenotype. *Microcirculation* 2005;12:151–60.
- Murray IR, Gonzalez ZN, Baily J, Dobie R, Wallace RJ, Mackinnon AC, et al.: Av Integrins on Mesenchymal Cells Regulate Skeletal and Cardiac Muscle Fibrosis. *Nat Commun* 2017;8.
- Nakamura K, Shimizu T, Yanagita T, Nemoto T, Taniuchi K, Shimizu S, et al.: Angiotensin II acting on brain AT1 receptors induces adrenaline secretion and pressor responses in the rat. *Sci Rep* 2014;4:7248.
- Nakanishi K, Mattson DL, Gross V, Roman RJ, Cowley AW: Control of renal medullary blood flow by vasopressin V1 and V2 receptors. *Am J Physiol* 1995;269:R193-200.
- Nakano M, Tamura Y, Yamato M, Kume S, Eguchi A, Takata K, et al.: NG2 glial cells regulate neuroimmunological responses to maintain neuronal function and survival. *Sci Rep* 2017;7:6–7.
- Naruse T, Yuzawa Y, Akahori T, Mizuno M, Maruyama S, Kannagi R, et al.: P-selectin-

dependent macrophage migration into the tubulointerstitium in unilateral ureteral obstruction. *Kidney Int* 2002;62:94–105.

Natoli R, Valter K, Barbosa M, Dahlstrom J, Rutar M, Kent A, et al.: 670nm Photobiomodulation as a Novel Protection against Retinopathy of Prematurity: Evidence from Oxygen Induced Retinopathy Models. *PLoS One* 2013;8:e72135.

Navarro R, Compte M, Álvarez-Vallina L, Sanz L: Immune regulation by pericytes: Modulating innate and adaptive immunity. *Front Immunol* 2016;7:1–10.

Nehls V, Drenckhahn D: Heterogeneity of microvascular pericytes for smooth muscle type alpha-actin. *J Cell Biol* 1991;113:147–154.

Nehmé A, Edelman J: Dexamethasone inhibits high glucose-, TNF- α - And IL-1 β -induced secretion of inflammatory and angiogenic mediators from retinal microvascular pericytes. *Investig Ophthalmol Vis Sci* 2008;49:2030–2038.

Neng L, Zhang F, Kachelmeier A, Shi X: Endothelial Cell, Pericyte, and Perivascular Resident Macrophage-Type Melanocyte Interactions Regulate Cochlear Intrastrial Fluid–Blood Barrier Permeability. *J Assoc Res Otolaryngol* 2013;14:175–185.

Neuhaus AA, Couch Y, Sutherland BA, Buchan AM: Novel method to study pericyte contractility and responses to ischaemia in vitro using electrical impedance. *J Cereb Blood Flow Metab* 2017;37:2013–2024.

Neuhofer W, Beck F-X: Cell Survival in the Hostile Environment of the Renal Medulla. *Annu Rev Physiol* 2005;67:531–555.

Neuhofer W, Beck F-X: Survival in hostile environments: strategies of renal medullary cells. *Physiology (Bethesda)* 2006;21:171–80.

Nicosia RF: The aortic ring model of angiogenesis: A quarter century of search and discovery. *J Cell Mol Med* 2009;13:4113–4136.

Nikolic-Paterson DJ, Wang S, Lan HY: Macrophages promote renal fibrosis through direct and indirect mechanisms. *Kidney Int Suppl* 2014;4:34–38.

Nitta CF, Orlando RA: Crosstalk between Immune Cells and Adipocytes Requires Both Paracrine Factors and Cell Contact to Modify Cytokine Secretion. *PLoS One* 2013;8.

North R a: Molecular physiology of P2X receptors. *Physiol Rev* 2002;82:1013–67.

O'Farrel FM, Mastitskaya S, Hammond-Haley M, Freitas F, Wah WR, Attwell D, et al.: Capillary pericytes mediate coronary no-reflow after myocardial ischaemia. *Elife* 2017;6:1–16.

O'Reilly VP, Wong L, Kennedy C, Elliot LA, O'Meachair S, Coughlan AM, et al.: Urinary Soluble

- CD163 in Active Renal Vasculitis. *J Am Soc Nephrol* 2016;27:2906–2916.
- Ohno, Katori, Majima, Saeki, Boku, Nishiyama, et al.: Dilatation and constriction of rat gastric mucosal microvessels through prostaglandin EP2 and EP3 receptors. *Aliment Pharmacol Ther* 1999;13:1243–1250.
- Olmes G, Büttner-Herold M, Ferrazzi F, Distel L, Amann K, Daniel C: CD163+ M2c-like macrophages predominate in renal biopsies from patients with lupus nephritis. *Arthritis Res Ther* 2015;18:90.
- Olson LE, Soriano P: PDGFR β Signaling Regulates Mural Cell Plasticity and Inhibits Fat Development. *Dev Cell* 2011;20:815–826.
- Onfelt B, Nedvetzki S, Yanagi K, Davis DM: Cutting edge: Membrane nanotubes connect immune cells. *J Immunol* 2004;173:1511–3.
- Orekhov AN, Bobryshev Y V., Chistiakov DA: The complexity of cell composition of the intima of large arteries: Focus on pericyte-like cells. *Cardiovasc Res* 2014;103:438–451.
- Outzen EM, Zaki M, Abdolalizadeh B, Sams A, Boonen HCM, Sheykhzade M: Translational value of mechanical and vasomotor properties of mouse isolated mesenteric resistance-sized arteries. *Pharmacol Res Perspect* 2015;3:e00200.
- Özen I, Deierborg T, Miharada K, Padel T, Englund E, Genové G, et al.: Brain pericytes acquire a microglial phenotype after stroke. *Acta Neuropathol* 2014;128:381–396.
- Pallone TL, Cao C: *Renal Cortical and Medullary Microcirculations: Structure and Function*, 2013.
- Pallone TL, Edwards A, Ma T, Silldorff EP, Verkman AS: Requirement of aquaporin-1 for NaCl-driven water transport across descending vasa recta. *J Clin Invest* 2000;105:215–222.
- Pallone TL, Robertson CR, Jamison RL: Renal medullary microcirculation. *Physiol Rev* 1990;70:885–920.
- Pallone TL, Silldorff EP: Pericyte regulation of renal medullary blood flow. *Exp Nephrol* 2001;9:165–170.
- Pallone TL, Silldorff EP, Cheung JY: Response of isolated rat descending vasa recta to bradykinin. *Am J Physiol Circ Physiol* 1998a;274:H752–H759.
- Pallone TL, Silldorff EP, Turner MR: Intrarenal Blood Flow: Microvascular Anatomy and the Regulation of Medullary Perfusion. *Clin Exp Pharmacol Physiol* 1998b;25:383–392.
- Pallone TL, Turner MR, Edwards A, Jamison RL: Countercurrent exchange in the renal medulla. *Am J Physiol Regul Integr Comp Physiol* 2003a;284:R1153-75.

- Pallone TL, Zhang Z, Rhinehart K: Physiology of the renal medullary microcirculation. *Am J Physiol - Ren Physiol* 2003b;284:F253–F266.
- Palmer BF, Alpern RJ, Seldin DW: Pathophysiology of Sodium Retention and Wastage; in : Seldin and Giebisch's *The Kidney*. Elsevier, 2013, pp 1283–1317.
- Pannabecker TL, Dantzler WH: Three-dimensional architecture of inner medullary vasa recta. *Am J Physiol Renal Physiol* 2006;290:F1355–F1366.
- Paquet-Fifield S, Schlüter H, Li A, Aitken T, Gangatirkar P, Blashki D, et al.: A role for pericytes as microenvironmental regulators of human skin tissue regeneration. *J Clin Invest* 2009;
- Park F, Mattson DL, Roberts LA, Cowley AW: Evidence for the presence of smooth muscle alpha-actin within pericytes of the renal medulla. *Am J Physiol* 1997a;273:R1742-8.
- Park F, Mattson DL, Roberts LA, Cowley AW: Evidence for the presence of smooth muscle alpha-actin within pericytes of the renal medulla. *Am J Physiol* 1997b;273:R1742-8.
- de Parseval N, Fichelson S, Mayeux P, Gisselbrecht S, Sola B: Expression of functional β -platelet-derived growth factor receptors on hematopoietic cell lines. *Cytokine* 1993;5:8–15.
- Peppiatt-Wildman CM: The evolving role of renal pericytes. *Curr Opin Nephrol Hypertens* 2013;22:10–16.
- Peppiatt-Wildman CM, Crawford C, Hall AM: Fluorescence Imaging of Intracellular Calcium Signals in Intact Kidney Tissue. *Nephron Exp Nephrol* 2012;121:e49–e58.
- Peppiatt CM, Howarth C, Mobbs P, Attwell D: Bidirectional control of CNS capillary diameter by pericytes. *Nature* 2006;443:700–4.
- Persidsky Y, Hill J, Zhang M, Dykstra H, Winfield M, Reichenbach NL, et al.: Dysfunction of brain pericytes in chronic neuroinflammation. *J Cereb Blood Flow Metab* 2016;36:794–807.
- Peti-Peterdi J, Harris RC: Macula Densa Sensing and Signaling Mechanisms of Renin Release: Figure 1. *J Am Soc Nephrol* 2010;21:1093–1096.
- Pieper C, Galla HJ: Ultra structure analysis of cell-cell interactions between pericytes and neutrophils in vitro. *Biochem Biophys Res Commun* 2014;445:180–183.
- Pieper C, Marek JJ, Unterberg M, Schwerdtle T, Galla HJ: Brain capillary pericytes contribute to the immune defense in response to cytokines or LPS in vitro. *Brain Res* 2014;1550:1–8.
- Pieper C, Pieloch P, Galla HJ: Pericytes support neutrophil transmigration via interleukin-8

- across a porcine co-culture model of the blood-brain barrier. *Brain Res* 2013;1524:1–11.
- Pober JS, Sessa WC: Inflammation and the blood microvascular system. *Cold Spring Harb Perspect Biol* 2014;7:a016345.
- Pober JS, Tellides G: Participation of blood vessel cells in human adaptive immune responses. *Trends Immunol* 2012;33:49–57.
- Polfliet MMJ, Fabriek BO, Daniëls WP, Dijkstra CD, van den Berg TK: The rat macrophage scavenger receptor CD163: Expression, regulation and role in inflammatory mediator production. *Immunobiology* 2006;211:419–425.
- Poosti F, Pham BT, Oosterhuis D, Poelstra K, van Goor H, Olinga P, et al.: Precision-cut kidney slices (PCKS) to study development of renal fibrosis and efficacy of drug targeting *ex vivo*. *Dis Model Mech* 2015;8:1227–1236.
- Potts LB, Ren Y, Lu G, Kuo E, Ngo E, Kuo L, et al.: Constriction of retinal arterioles to endothelin-1: requisite role of rho kinase independent of protein kinase C and L-type calcium channels. *Invest Ophthalmol Vis Sci* 2012;53:2904–2912.
- Pouly S, Becher B, Blain M, Antel JP: Expression of a homologue of rat NG2 on human microglia. *Glia* 1999;27:259–68.
- Prazeres PHDM, Almeida VM, Lousado L, Andreotti JP, Paiva AE, Santos GSP, et al.: Macrophages Generate Pericytes in the Developing Brain. *Cell Mol Neurobiol* 2017;
- Proebstl D, Voisin M-B, Woodfin A, Whiteford J, D'Acquisto F, Jones GE, et al.: Pericytes support neutrophil subendothelial cell crawling and breaching of venular walls *in vivo*. *J Exp Med* 2012;209:1219–1234.
- Puranik AS, Leaf IA, Jensen MA, Hedayat AF, Saad A, Kim KW, et al.: Kidney-resident macrophages promote a proangiogenic environment in the normal and chronically ischemic mouse kidney. *Sci Rep* 2018;8:1–15.
- Radermacher P, Haouzi P: A mouse is not a rat is not a man : species-specific metabolic responses to sepsis - a nail in the coffin of murine models for critical care research ? *J Software Eng Res Dev* 2013;1:1–5.
- Rajantie I, Ilmonen M, Alminaitte A, Ozerdem U, Alitalo K, Salven P: Adult bone marrow-derived cells recruited during angiogenesis comprise precursors for periendothelial vascular mural cells. *Blood* 2004;104:2084–2086.
- Rao J, Ye Z, Tang H, Wang C, Peng H, Lai W, et al.: The RhoA/ROCK Pathway Ameliorates Adhesion and Inflammatory Infiltration Induced by AGEs in Glomerular Endothelial Cells. *Sci Rep* 2017;7:1–11.

- Ren H, Gu L, Andreasen A, Thomsen JS, Cao L, Christensen EI, et al.: Spatial organization of the vascular bundle and the interbundle region: three-dimensional reconstruction at the inner stripe of the outer medulla in the mouse kidney. *Am J Physiol Physiol* 2014;306:F321–F326.
- Rhinehart K, Zhang Z, Pallone TL: Ca²⁺ signaling and membrane potential in descending vasa recta pericytes and endothelia. *Am J Physiol Physiol* 2002;283:F852–F860.
- Rhrissorrakrai K, Belcastro V, Bilal E, Norel R, Poussin C, Mathis C, et al.: Understanding the limits of animal models as predictors of human biology: Lessons learned from the sbv IMPROVER Species Translation Challenge. *Bioinformatics* 2015;31:471–483.
- Richardson RL, Hausman GJ, Campion DR: Response of pericytes to thermal lesion in the inguinal fat pad of 10-day-old rats. *Acta Anat (Basel)* 1982;114:41–57.
- Rider P, Carmi Y, Guttman O, Braiman A, Cohen I, Voronov E, et al.: IL-1 and IL-1 Recruit Different Myeloid Cells and Promote Different Stages of Sterile Inflammation. *J Immunol* 2011;187:4835–4843.
- Riew T-R, Choi J-H, Kim HL, Jin X, Lee M-Y: PDGFR- β -Positive Perivascular Adventitial Cells Expressing Nestin Contribute to Fibrotic Scar Formation in the Striatum of 3-NP Intoxicated Rats. *Front Mol Neurosci* 2018;11.
- Rimsza L, Roberts R, Miller T, Unger J, LeBlanc M, Braziel R, et al.: Loss of MHC class II gene and protein expression in diffuse large B cell lymphoma is related to decreased tumor immunosurveillance and poor patient survival: A follow-up study to the NIH director's challenge leukemia and lymphoma molecular profiling proje. *Blood* 2003;102:390a-391a.
- Rodrigues ES, Martin RP, Felipe SA, Bader M, Oliveira SM, Shimuta SI: Cross talk between kinin and angiotensin II receptors in mouse abdominal aorta. *Biol Chem* 2009;390:907–913.
- Rodriguez AR, Yu JJ, Navara C, Chambers JP, Guentzel MN, Arulanandam BP: Contribution of Fc ϵ RI-associated vesicles to mast cell-macrophage communication following *Francisella tularensis* infection. *Innate Immun* 2016;22:567–574.
- Roh-Johnson M, Bravo-Cordero JJ, Patsialou A, Sharma VP, Guo P, Liu H, et al.: Macrophage contact induces RhoA GTPase signaling to trigger tumor cell intravasation. *Oncogene* 2014;33:4203–4212.
- Rojas A, Chang F-C, Lin S-L, Duffield JS: The role played by perivascular cells in kidney interstitial injury. *Clin Nephrol* 2012;77:400–408.
- Ruan X, Oliverio MI, Coffman TM, Arendshorst WJ: Renal vascular reactivity in mice: AngII-induced vasoconstriction in AT1A receptor null mice. *J Am Soc Nephrol* 1999;10:2620–30.

- Rubio-Navarro A, Carril M, Padro D, Guerrero-Hue M, Tarín C, Samaniego R, et al.: CD163-macrophages are involved in rhabdomyolysis-induced kidney injury and may be detected by MRI with targeted gold-coated iron oxide nanoparticles. *Theranostics* 2016;6:896–914.
- Rundberg Nilsson A, Bryder D, Pronk CJH: Frequency determination of rare populations by flow cytometry: A hematopoietic stem cell perspective. *Cytom Part A* 2013;83A:721–727.
- Russell A, Watts S: Vascular reactivity of isolated thoracic aorta of the C57BL/6J mouse. *J Pharmacol Exp Ther* 2000;294:598–604.
- Rustenhoven J, Aalderink M, Scotter EL, Oldfield RL, Bergin PS, Mee EW, et al.: TGF-beta1 regulates human brain pericyte inflammatory processes involved in neurovasculature function. *J Neuroinflammation* 2016;13:37.
- Rustenhoven J, Jansson D, Smyth LC, Dragunow M: Brain Pericytes As Mediators of Neuroinflammation. *Trends Pharmacol Sci* 2017;38:291–304.
- Rustenhoven J, Smyth LC, Jansson D, Schweder P, Aalderink M, Scotter EL, et al.: Modelling physiological and pathological conditions to study pericyte biology in brain function and dysfunction. *BMC Neurosci* 2018;19:1–15.
- Rustom A, Saffrich R, Markovic I, Walther P, Gerdes H-H: Nanotubular highways for intercellular organelle transport. *Science* 2004;303:1007–10.
- Sabolic I, Breljak D, Ljubojevic M, Brzica H: Are mice, rats, and rabbits good models for physiological, pharmacological and toxicological studies in humans? *Period Biol* 2011;113:7–16.
- Sands JM, Layton HE: The physiology of urinary concentration: an update. *Semin Nephrol* 2009;29:178–95.
- Sands JM, Layton HE: Advances in Understanding the Urine-Concentrating Mechanism. *Annu Rev Physiol* 2014;76:387–409.
- Sasamura H, Dzau VJ, Pratt RE: Desensitization of angiotensin receptor function. *Kidney Int* 1994;46:1499–1501.
- Sato M, Suzuki S, Senoo H: Hepatic stellate cells: unique characteristics in cell biology and phenotype. *Cell Struct Funct* 2003;28:105–12.
- Saunders WB, Bohnsack BL, Faske JB, Anthis NJ, Bayless KJ, Hirschi KK, et al.: Coregulation of vascular tube stabilization by endothelial cell TIMP-2 and pericyte TIMP-3. *J Cell Biol* 2006;175:179–91.
- Schenk M, Fabri M, Krutzik SR, Lee DJ, Vu DM, Sieling PA, et al.: Interleukin-1 β triggers the differentiation of macrophages with enhanced capacity to present mycobacterial antigen

to T cells. *Immunology* 2014;141:174–180.

Scherer EQ, Arnold W, Wangemann P: Pharmacological reversal of endothelin-1 mediated constriction of the spiral modiolar artery: A potential new treatment for sudden sensorineural hearing loss. *BMC Ear, Nose Throat Disord* 2005;5:1–7.

Schildroth J, Rettig-Zimmermann J, Kalk P, Steege A, Föhling M, Sendeski M, et al.: Endothelin type A and B receptors in the control of afferent and efferent arterioles in mice. *Nephrol Dial Transplant* 2011;26:779–789.

Schindelin J, Arganda-Carreras I, Frise E, Kaynig V, Longair M, Pietzsch T, et al.: Fiji: an open-source platform for biological-image analysis. *Nat Methods* 2012;9:676–82.

Schlondorff D, Banas B: The Mesangial Cell Revisited: No Cell Is an Island. *J Am Soc Nephrol* 2009;20:1179–1187.

Schreiner GF: The mesangial phagocyte and its regulation of contractile cell biology. *J Am Soc Nephrol* 1992;2:S74-82.

Schrimpf C, Xin C, Campanholle G, Gill SE, Stallcup W, Lin S-L, et al.: Pericyte TIMP3 and ADAMTS1 modulate vascular stability after kidney injury. *J Am Soc Nephrol* 2012;23:868–83.

Schroeter M, Küry P, Jander S: Inflammatory gene expression in focal cortical brain ischemia: Differences between rats and mice. *Mol Brain Res* 2003;117:1–7.

Seleme MC, Kosmac K, Jonjic S, Britt WJ: Tumor Necrosis Factor Alpha-Induced Recruitment of Inflammatory Mononuclear Cells Leads to Inflammation and Altered Brain Development in Murine Cytomegalovirus-Infected Newborn Mice. *J Virol* 2017;91.

Sendeski MM, Liu ZZ, Perlewitz A, Busch JF, Ikromov O, Weikert S, et al.: Functional characterization of isolated, perfused outermedullary descending human vasa recta. *Acta Physiol* 2013;208:50–56.

Shahid M, Francis J, Majid D: Tumor necrosis factor- α induces renal vasoconstriction as well as natriuresis in mice. *Am J Physiol - Ren Physiol* 2008;295:F1836–F1844.

Shaw I, Rider S, Mullins J, Hughes J, Péault B: Pericytes in the renal vasculature: Roles in health and disease. *Nat Rev Nephrol* 2018;14:521–534.

Shi X: Cochlear pericyte responses to acoustic trauma and the involvement of hypoxia-inducible factor-1 α and vascular endothelial growth factor. *Am J Pathol* 2009;174:1692–1704.

Shi Z, Wang Q, Zhang Y, Jiang D: Extracellular vesicles produced by bone marrow mesenchymal stem cells attenuate renal fibrosis, in part by inhibiting the RhoA/ROCK

- pathway, in a UUO rat model. *Stem Cell Res Ther* 2020;11:1–21.
- Shih H-M, Wu C-J, Lin S-L: Physiology and pathophysiology of renal erythropoietin-producing cells. *J Formos Med Assoc* 2018;
- Shirley DG, Bailey MA, Wildman SSP, Tam FWK, Unwin RJ: Extracellular Nucleotides and Renal Function; in Alpern R, Caplan M, Orson M (eds): *Seldin and Geibisch's The Kidney*, ed 5th. Elsevier, 2013, pp 511–537.
- Siesky AM, Kamendulis LM, Klaunig JE: Hepatic effects of 2-butoxyethanol in rodents. *Toxicol Sci* 2002;70:252–60.
- Silldorff EP, Yang S, Pallone TL: Prostaglandin E2 abrogates endothelin-induced vasoconstriction in renal outer medullary descending vasa recta of the rat. *J Clin Invest* 1995;95:2734–2740.
- Smirkin A, Matsumoto H, Takahashi H, Inoue A, Tagawa M, Ohue S, et al.: a variety of neuroprotective factors ameliorate ischemic damage of the brain. *J Cereb Blood Flow Metab* 2009;30:603–615.
- Smith SW, Chand S, Savage COSS: Biology of the renal pericyte. *Nephrol Dial Transplant* 2012;27:2149–2155.
- Smith SW, Croft AP, Morris HL, Naylor AJ, Huso DL, Isacke CM, et al.: Genetic Deletion of the Stromal Cell Marker CD248 (Endosialin) Protects against the Development of Renal Fibrosis. *Nephron* 2015;131:265–77.
- Soderblom C, Luo X, Blumenthal E, Bray E, Lyapichev K, Ramos J, et al.: Perivascular Fibroblasts Form the Fibrotic Scar after Contusive Spinal Cord Injury. *J Neurosci* 2013;33:13882–13887.
- Soos TJ, Sims TN, Barisoni L, Lin K, Littman DR, Dustin ML, et al.: CX3CR1+ interstitial dendritic cells form a contiguous network throughout the entire kidney. *Kidney Int* 2006;70:591–596.
- Speyer CL, Steffes CP, Ram JL: Effects of Vasoactive Mediators on the Rat Lung Pericyte: Quantitative Analysis of Contraction on Collagen Lattice Matrices. *Microvasc Res* 1999;57:134–143.
- Stamatiades EG, Tremblay M, Bohm M, Crozet L, Bisht K, Kao D, et al.: Immune Monitoring of Trans-endothelial Transport by Kidney-Resident Macrophages. *Cell* 2016;166:991–1003.
- Stapor PC, Sweat RS, Dashti DC, Betancourt AM, Murfee WL: Pericyte dynamics during angiogenesis: New insights from new identities. *J Vasc Res* 2014;51:163–174.
- Stark K, Eckart A, Haidari S, Tirniceriu A, Lorenz M, von Brühl M-L, et al.: Capillary and

- arteriolar pericytes attract innate leukocytes exiting through venules and “instruct” them with pattern-recognition and motility programs. *Nat Immunol* 2012;14:41–51.
- Stark K, Pekayvaz K, Massberg S: Role of pericytes in vascular immunosurveillance. *Front Biosci (Landmark Ed)* 2018;23:767–781.
- Staruschenko A: Regulation of transport in the connecting tubule and cortical collecting duct. *Compr Physiol* 2012;2:1541–84.
- Stefanska A, Eng D, Kaverina N, Duffield JS, Pippin JW, Rabinovitch P, et al.: Interstitial pericytes decrease in aged mouse kidneys. *Aging (Albany NY)* 2015;7:370–382.
- Stefanska A, Kenyon C, Christian HC, Buckley C, Shaw I, Mullins JJ, et al.: Human kidney pericytes produce renin. *Kidney Int* 2016;90:1251–1261.
- Steven S, Dib M, Roohani S, Kashani F, Münzel T, Daiber A: Time Response of Oxidative/Nitrosative Stress and Inflammation in LPS-Induced Endotoxaemia—A Comparative Study of Mice and Rats. *Int J Mol Sci* 2017;18:2176.
- Stratman AN, Malotte KM, Mahan RD, Davis MJ, Davis GE: Pericyte recruitment during vasculogenic tube assembly stimulates endothelial basement membrane matrix formation. *Blood* 2009;114:5091–101.
- Stribos EGD, Luangmonkong T, Leliveld AM, De Jong IJ, Van Son WJ, Hillebrands JL, et al.: Precision-cut human kidney slices as a model to elucidate the process of renal fibrosis. *Transl Res* 2016;170:8-16.e1.
- Strupler M, Hernest M, Fligny CC, Martin J-L, Tharaux P-L, Schanne-Klein M-C: Second harmonic microscopy to quantify renal interstitial fibrosis and arterial remodeling. *J Biomed Opt* 2008;13:054041.
- Sugiyama T, Kawamura H, Yamanishi S, Kobayashi M, Katsumura K, Puro DG: Regulation of P2X7-induced pore formation and cell death in pericyte-containing retinal microvessels. *Am J Physiol Cell Physiol* 2005;288:C568–C576.
- Sundberg C, Friman T, Hecht LE, Kuhl C, Solomon KR: Two Different PDGF β -Receptor Cohorts in Human Pericytes Mediate Distinct Biological Endpoints. *Am J Pathol* 2009;175:171–189.
- Svoboda KKH, Reenstra WR: Approaches to studying cellular signaling: a primer for morphologists. *Anat Rec* 2002;269:123–39.
- Takata F, Dohgu S, Matsumoto J, Takahashi H, Machida T, Wakigawa T, et al.: Brain pericytes among cells constituting the blood-brain barrier are highly sensitive to tumor necrosis factor- α , releasing matrix metalloproteinase-9 and migrating in vitro. *J Neuroinflammation* 2011;8:106.

- Tanaka S, Tanaka T, Kawakami T, Takano H, Sugahara M, Saito H, et al.: Vascular adhesion protein-1 enhances neutrophil infiltration by generation of hydrogen peroxide in renal ischemia/reperfusion injury. *Kidney Int* 2017;92:154–164.
- Tanaka T, Nangaku M: Angiogenesis and hypoxia in the kidney. *Nat Rev Nephrol* 2013;9:211–222.
- Tang PM, Nikolic-Paterson DJ, Lan H: Macrophages: versatile players in renal inflammation and fibrosis. *Nat Rev Nephrol* 2019;15:144–158.
- Tang W, Zeve D, Suh JM, Bosnakovski D, Kyba M, Hammer RE, et al.: White fat progenitor cells reside in the adipose vasculature. *Science* 2008;322:583–6.
- Thomas WEE: Brain macrophages: on the role of pericytes and perivascular cells. *Brain Res Rev* 1999;31:42–57.
- Tigges U, Boroujerdi A, Welser-Alves J V., Milner R: TNF- α promotes cerebral pericyte remodeling in vitro, via a switch from α 1 to α 2 integrins. *J Neuroinflammation* 2013;10:1–15.
- Tigges U, Hyer EG, Scharf J, Stallcup WB: FGF2-dependent neovascularization of subcutaneous Matrigel plugs is initiated by bone marrow-derived pericytes and macrophages. *Development* 2008;135:523–32.
- Trost A, Lange S, Schroedl F, Bruckner D, Motloch KA, Bogner B, et al.: Brain and Retinal Pericytes: Origin, Function and Role. *Front Cell Neurosci* 2016;10:1–13.
- Turner MR, Pallone TL: Vasopressin constricts outer medullary descending vasa recta isolated from rat kidneys. *Am J Physiol* 1997;272:F147-51.
- Unekawa M, Tomita M, Tomita Y, Toriumi H, Miyaki K, Suzuki N: RBC velocities in single capillaries of mouse and rat brains are the same, despite 10-fold difference in body size. *Brain Res* 2010;1320:69–73.
- Vandamme TF: Use of rodents as models of human diseases. *J Pharm Bioallied Sci* 2014;6:2–9.
- Vickers AEM, Fisher RL: Precision-cut organ slices to investigate target organ injury. *Expert Opin Drug Metab Toxicol* 2005;1:687–699.
- Vonend O, Habbel S, Stegbauer J, Roth J, Hein L, Rump LC: α 2A-Adrenoceptors Regulate Sympathetic Transmitter Release in Mice Kidneys. *Br J Pharmacol* 2009;150:121–127.
- Vonend O, Stegbauer J, Sojka J, Habbel S, Quack I, Robaye B, et al.: Noradrenaline and extracellular nucleotide cotransmission involves activation of vasoconstrictive P2X 1,3- and P2Y 6-like receptors in mouse perfused kidney. *Br J Pharmacol* 2005;145:66–74.

- Wallez Y, Vilgrain I, Huber P: Angiogenesis: The VE-cadherin switch. *Trends Cardiovasc Med* 2006;
- Wang C, Yu X, Cao Q, Wang Y, Zheng G, Tan TK, et al.: Characterization of murine macrophages from bone marrow, spleen and peritoneum. *BMC Immunol* 2013;14:1.
- Wang N, Deng Y, Liu A, Shen N, Wang W, Du X, et al.: Novel Mechanism of the Pericyte-Myofibroblast Transition in Renal Interstitial Fibrosis: Core Fucosylation Regulation. *Sci Rep* 2017;7:1–12.
- Wang S, Cao C, Chen Z, Bankaitis V, Tzima E, Sheibani N, et al.: Pericytes Regulate Vascular Basement Membrane Remodeling and Govern Neutrophil Extravasation during Inflammation. *PLoS One* 2012;7.
- Watkins SC, Salter RD: Functional connectivity between immune cells mediated by tunneling nanotubules. *Immunity* 2005;23:309–18.
- Wei G, Rosen S, Dantzler WH, Pannabecker TL: Architecture of the human renal inner medulla and functional implications. *Am J Physiol - Ren Physiol* 2015;309:F627–F637.
- Weibel ER, Hsia CCW, Ochs M: How much is there really? Why stereology is essential in lung morphometry. *J Appl Physiol* 2007;102:459–467.
- Weinstein AM: Sodium and Chloride Transport: Proximal Nephron; in : Seldin and Giebisch's *The Kidney*, Fifth Edit. Elsevier, 2013, pp 1081–1141.
- Weisheit CK, Engel DR, Kurts C: Dendritic cells and macrophages: Sentinels in the kidney. *Clin J Am Soc Nephrol* 2015;10:1841–1851.
- Wennström M, Janelidze S, Bay-Richter C, Minthon L, Brundin L: Pro-Inflammatory cytokines reduce the proliferation of NG2 cells and increase shedding of NG2 in vivo and in vitro. *PLoS One* 2014;9.
- Wiley KE, Davenport AP: Endothelin receptor pharmacology and function in the mouse: comparison with rat and man. *J Cardiovasc Pharmacol* 2004;44 Suppl 1:S4-6.
- Wilkes BM, Ruston AS, Mento P, Girardi E, Hart D, Vander Molen M, et al.: Characterization of endothelin 1 receptor and signal transduction mechanisms in rat medullary interstitial cells. *Am J Physiol* 1991;260:F579-89.
- Winau F, Hegasy G, Weiskirchen R, Weber S, Cassan C, Sieling PA, et al.: Ito cells are liver-resident antigen-presenting cells for activating T cell responses. *Immunity* 2007;26:117–29.
- Winkler EA, Bell RD, Zlokovic B V: Pericyte-specific expression of PDGF beta receptor in mouse models with normal and deficient PDGF beta receptor signaling. *Mol*

Neurodegener 2010;5:32.

Wong MKS: Bradykinin; in : Handbook of Hormones. Elsevier, 2016, pp 274-e30C-4.

Wu P, Gao Z-X, Duan X-P, Su X-T, Wang M-X, Lin D-H, et al.: AT2R (Angiotensin II Type 2 Receptor)-Mediated Regulation of NCC (Na-Cl Cotransporter) and Renal K Excretion Depends on the K Channel, Kir4.1. Hypertension 2018;71:622–630.

Xavier S, Sahu RK, Landes SG, Yu J, Taylor RP, Ayyadevara S, et al.: Pericyte and immune cells contribute to complement activation in tubulointerstitial fibrosis. Am J Physiol - Ren Physiol 2017;ajprenal.00604.2016.

Yamazaki T, Nalbandian A, Uchida Y, Li W, Arnold TD, Kubota Y, et al.: Tissue Myeloid Progenitors Differentiate into Pericytes through TGF- β Signaling in Developing Skin Vasculature. Cell Rep 2017;18:2991–3004.

Yang S, Silldorff EP, Pallone TL: Effect of norepinephrine and acetylcholine on outer medullary descending vasa recta. Am J Physiol Circ Physiol 1995;269:H710–H716.

Yang Y, Andersson P, Hosaka K, Zhang Y, Cao R, Iwamoto H, et al.: The PDGF-BB-SOX7 axis-modulated IL-33 in pericytes and stromal cells promotes metastasis through tumour-associated macrophages. Nat Commun 2016;7:1–18.

You W-K, Yotsumoto F, Sakimura K, Adams RH, Stallcup WB: NG2 proteoglycan promotes tumor vascularization via integrin-dependent effects on pericyte function. Angiogenesis 2014;17:61–76.

Ysebaert DK, De Greef KE, De Beuf A, Van Rompay ANR, Vercauteren S, Persy VP, et al.: T cells as mediators in renal ischemia/reperfusion injury. Kidney Int 2004;66:491–496.

Yuan J, Pannabecker TL: Architecture of inner medullary descending and ascending vasa recta: Pathways for countercurrent exchange. Am J Physiol - Ren Physiol 2010;299:265–272.

Zeng H, He X, Tuo QH, Liao DF, Zhang GQ, Chen JX: LPS causes pericyte loss and microvascular dysfunction via disruption of Sirt3/angiopoietins/Tie-2 and HIF-2 α /Notch3 pathways. Sci Rep 2016;6:1–13.

Zhang D-D, Gao Z-X, Vio CP, Xiao Y, Wu P, Zhang H, et al.: Bradykinin Stimulates Renal Na⁺ and K⁺ Excretion by Inhibiting the K⁺ Channel (Kir4.1) in the Distal Convolute Tubule. Hypertension 2018;72:361–369.

Zhang Z, Cao C, Lee-Kwon W, Pallone TL: Descending vasa recta pericytes express voltage operated Na⁺ conductance in the rat. J Physiol 2005;567:445–457.

Zhang Z, Rhinehart K, Kwon W, Weinman E, Pallone TL: ANG II signaling in vasa recta

pericytes by PKC and reactive oxygen species. *Am J Physiol Heart Circ Physiol* 2004;287:H773-81.

Zhao D, Navar LG: Acute angiotensin II infusions elicit pressure natriuresis in mice and reduce distal fractional sodium reabsorption. *Hypertens (Dallas, Tex 1979)* 2008;52:137–42.

Zhao Z-S, Shibamoto T, Tsutsumi M, Cui S, Zhang WM, Takano H, et al.: Mouse hepatic portal vasoconstrictive response to vasoconstrictors is much weaker than that in rat. *J Cardiovasc Pharmacol* 2009;54:421–6.

Ziganshina LE, Hoyle CHV, Teplov AY, Gabdrakhmanov AI, Ziganshin BA, Khairullin AE, et al.: The effects of ATP on the contractions of rat and mouse fast skeletal muscle, 2019.

Zimmerhackl B, Robertson CR, Jamison RL: The microcirculation of the renal medulla. *Circ Res* 1985;57:657–667.

Zimmermann KW: Der feinere Bau der Bluteapillaren. *Aus Dem Anat Inst Der Univ Bern* 1923;68:29–109.

Appendix 1:

Posters arising from this thesis

RJ Lilley, RF Barnard, SS Wildman, and CM Peppiatt-Wildman (2016) *Comparison of Agonist-Evoked, Pericyte-Mediated Changes in Vasa Recta Diameter in Mouse and Rat Live Kidney Slice Models*. Pharmacological aspects of microvascular cell-cell signalling and CVS disease 14(2), Oxford, UK September 21st-22nd. Proceedings of the British Pharmacological Society at: <http://www.pa2online.org/abstracts/vol14issue2abst019p.pdf>

R.J.Lilley, S.S. Wildman, C.M. Peppiatt-Wildman (2018) *Identification of a Subpopulation of F4/80+ve, NG2+ve Pericytes on Healthy Murine Vasa Recta*. 11th World Congress for Microcirculation 2018 (WCM2018), Vancouver, BC, Canada September 9th-11th DOI: 10.1111/micc.12524 TUPE036